ANALYSIS AND CORRELATION

OF IGNEOUS CLAST GEOCHEMISTRY AND PETROGRAPHY FROM

FOUR MESOZOIC CONGLOMERATES

A Thesis

submitted in partial fulfillment

of the requirements for the Degree

of

MASTER OF SCIENCE IN GEOLOGY

at the

University of Canterbury.

by

A. A. Dean

University of Canterbury

1993

'Well..... she's looking at pebbles I guess'

(Dr Shelley describes this thesis to Stage 1 students)

ABSTRACT

The Torlesse terrane encompasses three-quarters of the emergent New Zealand micro-continent and much speculation has been made as to the likely source for the detritus of which it is composed. This research concentrates on an examination of the igneous (plutonic and volcanic) clasts from three Torlesse conglomerates, one from the Rakaia terrane of Triassic age, and two from the Pahau terrane, of Early Cretaceous age, to obtain a better understanding of the characteristics of this source terrane.

The Early Cretaceous Ethelton conglomerate comprises predominantly metaluminous I-type and weakly peraluminous evolved I-type granitoids that relate mineralogically and geochemically to the rhyolitic and dacitic volcanic clasts present and are thought to represent one cogenetic suite derived by partial melting of a common igneous source.

The Mount Saul conglomerate contains a predominance of volcanic clasts and a variety of granitoid types. Some volcanic clasts relate to the I-type, and evolved I-type granitoids present. A-type peralkaline to weakly peraluminous volcanic clasts geochemically display a subduction related signature, that reflects source characteristics. A-type magmatism indicates an event unassociated with represented intrusives, either related to anorogenic magmatism or to a change to extensional tectonism.

The predominant granodiorite character and low K content of Lake Hill conglomerate S-type granitoid clasts contrasts with that of the other conglomerates. The dacitic and rhyolitic volcanic clasts examined from Lake Hill exhibit distinctive minerals indicative of I-types and relate to the evolved I-type granitoid clasts also present.

The middle Cretaceous conglomerate located on Pitt Island, Chatham Islands is also examined to provide a comparison to the Torlesse conglomerates and an insight into source characteristics prior to continental separation between New

Zealand and West Antarctica.

The Chatham Islands conglomerate contains a variety of granitoid and volcanic types that are petrographically and geochemically comparable with the Torlesse conglomerates. The granitoid clasts are predominantly leucosyenogranites and leucomonzogranites. The volcanic clasts are rhyolites and dacites. Geochemically I-type, S-type and highly evolved/A-types are identified.

The clasts from all four conglomerates examined exhibit trace element characteristics indicative of subduction-related magmatism. The granite type and highly felsic nature of most clasts indicates intrusion and extrusion occurred along an active continental margin that had attained full crustal thickness. The mineralogy and geochemistry of conglomerate clasts compares favourably with numerous volcano-plutonic continental provinces around the Pacific margin that are believed to represent the former Gondwana margin.

TABLE OF CONTENTS

LIST OF FIGURES

LIST OF APPENDICES

CHAPTER 1

INTRODUCTION

1.1 Objectives and Preliminaries

The Torlesse terrane constitutes approximately two thirds of the New Zealand land area and the majority of the total micro-continent (Figures 1.1a and 1.2). The provenance of Torlesse sediments has been the subject of much debate. However, no consensus of opinion has been achieved to date. The characterization of the source area for the Torlesse terrane during the Mesozoic is the primary aim of this thesis.

The Torlesse terrane comprises Carboniferous to mid/Late Cretaceous sandstone and mudstone and metamorphic equivalents (98%), with subordinate metavolcanics, conglomerate and exotic limestone (2%) (J.D.Bradshaw, pers.comm.). It is predominantly detrital and represents the destruction of an equal volume of continental crust.

The quartzofeldspathic character of the Torlesse is well documented; the stratigraphy, structure and paleontology have been the subject of detailed local and regional study (Bradshaw, 1971; Andrews, 1974; Andrews *et al.*, 1976; Carter *et al.*, 1978; Howell, 1981; MacKinnon, 1983). With the recognition that plate tectonic setting has a significant influence on detrital composition, innovative geochemical techniques have been increasingly applied to sedimentary sequences to

Figure 1.1: a Map of the New Zealand micro-continent with extent delineated by 2000m bathymetric contour.
(after Laird, in press)

b Locality Map indicating conglomerates sampled and spatial relationships.
(after Wood *et al.*, 1989)

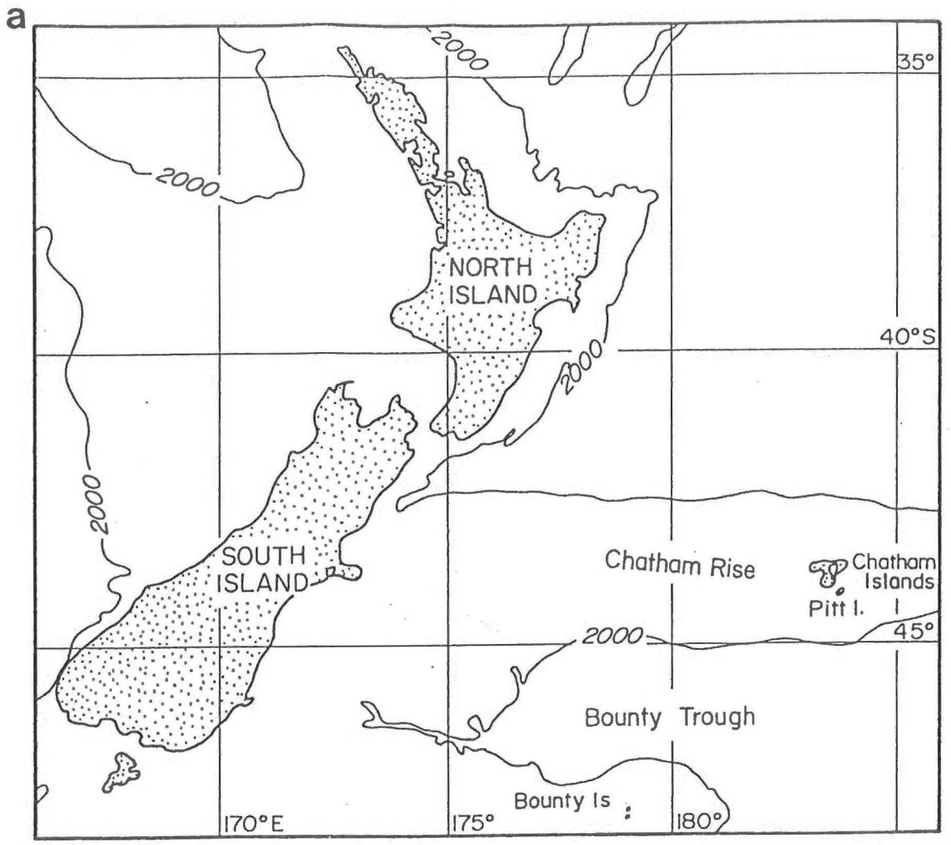

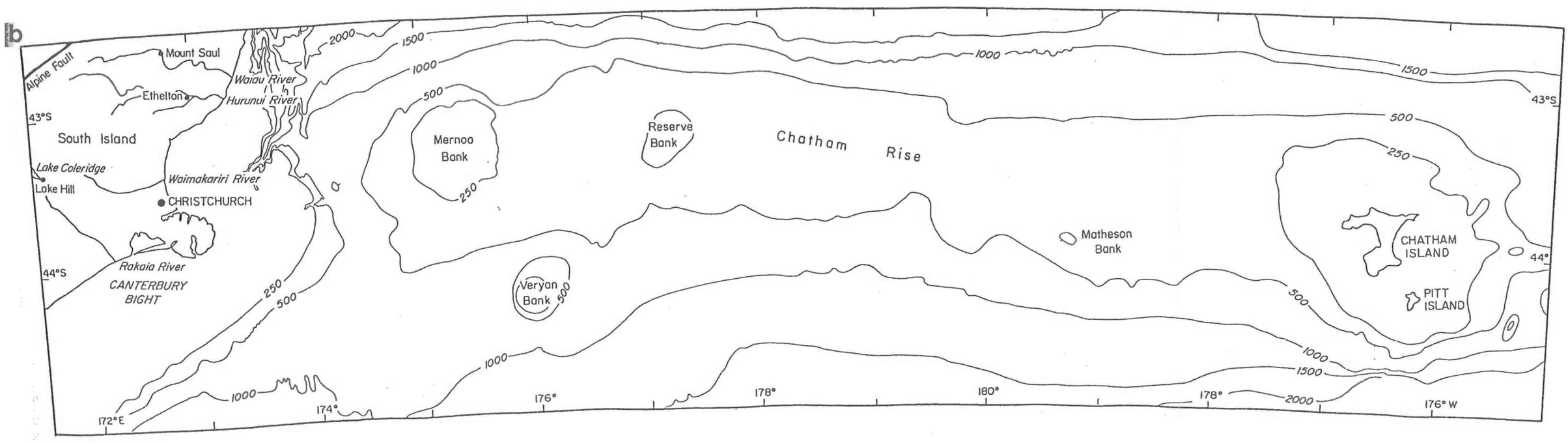

allow the discrimination of provenance (Dickinson, 1974, 1982; Bhatia and Taylor, 1981; Roser and Korsch, 1986, 1988; Roser and Cooper, 1990; Ireland, 1992; Mortimer and Roser, 1992).

Petrographic and geochemical studies of conglomerate clasts can provide direct lithological evidence for correlation with adjacent crustal blocks and can characterize crustal blocks no longer accessible to observation due to displacement, erosion or burial. Detrital conglomerates within the Torlesse terrane, although volumetrically insignificant, are widespread (Figure 1.2) (Andrews *et al.*, 1976).

For this research, petrographic methods and whole rock geochemical analyses have been employed to examine igneous clasts collected from Mesozoic conglomerates at three Canterbury localities, Ethelton, Mount Saul and Lake Hill, and one Chatham Islands locality on Pitt Island (Figure 1.1b). The information accumulated has been utilized to correlate and contrast areas, and to assess possible protoliths. Within the tectonostratigraphic terrane concept of regional geology, the accumulated data allow tighter constraint of Torlesse provenance and improved determination of Mesozoic tectonic setting within the South Island and the Chatham Islands region.

The post-Torlesse Chatham Islands conglomerate was sampled to compare granitoid clasts with those collected from the South Island Torlesse conglomerates, and in addition provided information about igneous source character close to the subsequent continental margin.

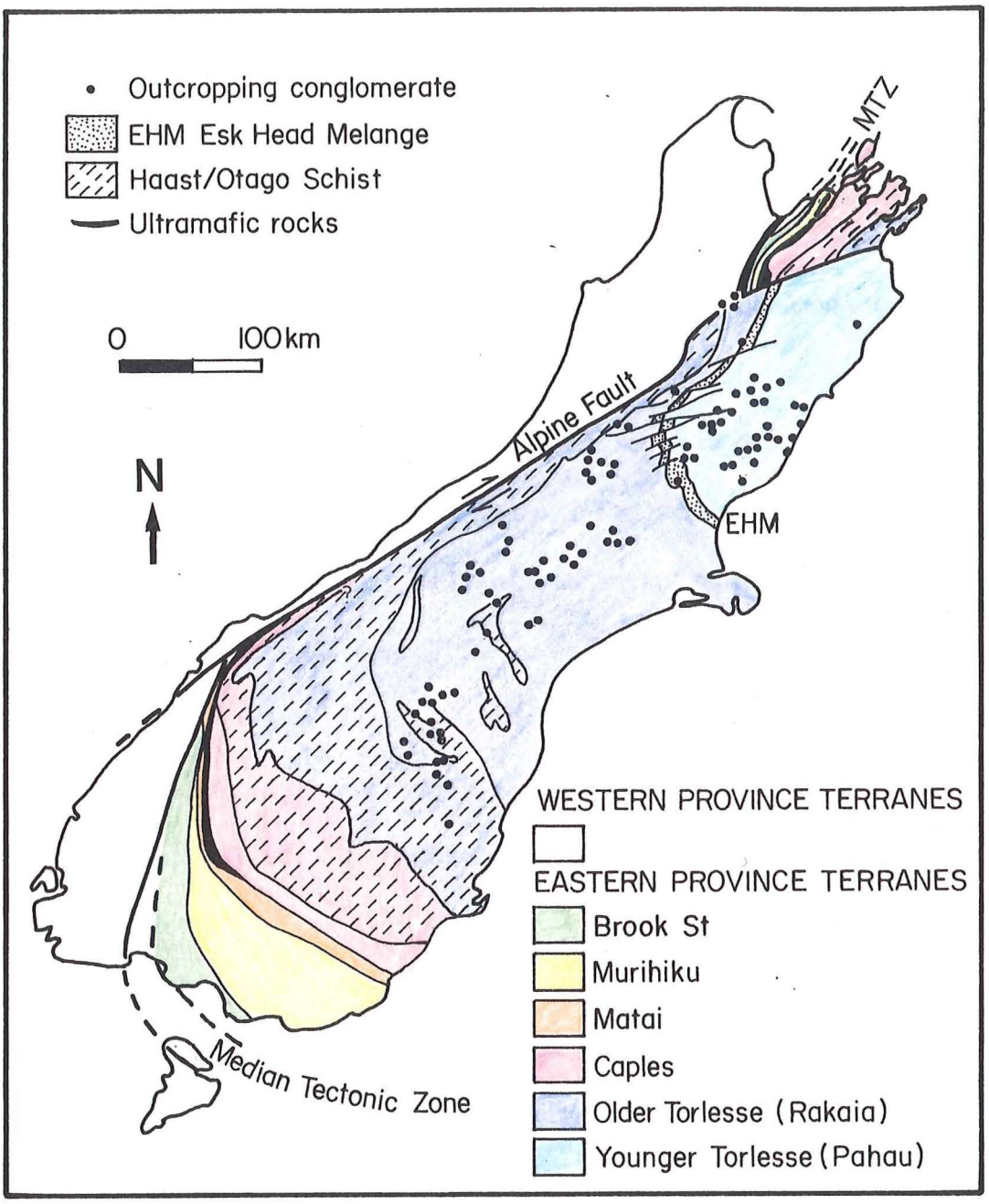

Figure 1.2: Generalized tectonostratigraphic terrane map of the South Island, New Zealand with distribution of the known Torlesse detrital conglomerate outcrops.
(modified from Andrews *et al.*, 1976; Bishop *et al.*, 1985; Frost and Coombs, 1989; Mortimer, 1993)

1.2 Regional Geological Setting and Tectonic Controls

1.2.1 General Characteristics

New Zealand lies across the boundary between the Indo/Australian and Pacific plates in the Southwest Pacific and represents a small emergent part of an extensive plateau of relatively thin, predominately submerged, continental crust. This continental block defines an ~4000 km long segment of the former eastern Gondwana margin rifted from the Australian/Antarctic sector of the supercontinent during the Late Cretaceous (Korsch and Wellman, 1988; Bradshaw, 1989). The 2000m contour has been frequently used to delineate the approximate margins of the New Zealand micro-continent (Figure 1.1a).

The New Zealand basement comprises fault bounded north to northwest trending curvilinear belts which represent a complex composite of terranes divisible into two major provinces:

1. Western Province, comprising early Paleozoic rocks cut by Late Paleozoic and Late Mesozoic granitoids (Landis and Coombs, 1967; Tulloch, 1983; Cooper, 1989).

2. Eastern Province, comprising numerous Late Paleozoic to Late Mesozoic terranes that represent a variety of tectonic settings of predominantly convergent margin origin (arc, fore-arc and accretionary complexes) (Bishop *et al.*, 1985; Bradshaw, 1989).

The two provinces are divided by a complex zone of faulting and intrusion known as the Median Tectonic Zone (MTZ), a fundamental terrane boundary across

which there are no common pre-Cretaceous units (Figure 1.2) (Landis and Coombs, 1967; Bradshaw, 1993).

1.2.2 Eastern Province

When the effects of subsequent Tertiary convergence are removed, the Eastern Province terranes form continuous sub-parallel belts, in many places <5kms in width. Although many contrasting plate tectonic models have been proposed for the present terrane configuration there is general agreement that convergence during the Mesozoic produced the variety of tectonic settings represented by these terranes (Fleming, 1970; Landis and Bishop, 1972; Blake *et al.*, 1974; Coombs, *et al.*, 1976; Carter, *et al.*, 1978; Sporli, 1978; Wood, 1978; Howell, 1980; Bradshaw *et al.*, 1981; Bradshaw, 1989; MacKinnon, 1983). Recent research suggests many Eastern Province terranes are allochthonous (Haston *et al.*, 1989; Frost and Coombs, 1989; Bradshaw, 1993).

1.2.3 Torlesse Terrane

The Torlesse terrane is the largest emergent terrane in New Zealand, coherent on a regional scale but in detail disrupted and highly deformed, representative of an ancient accretionary wedge complex (Bradshaw, 1973; Spörli and Bell, 1976; Spörli, 1978; Dickinson, 1982; Korsch and Wellman, 1988; Bradshaw, 1989). Tectonically controlled fossil zones are recognized within the Torlesse terrane which indicate Carboniferous (exotic limestone mélange) to mid Cretaceous ages (Andrews, et al., 1976).

The true geographical extent of the Torlesse terrane is indeterminable due to continental submergence as a result of post-rifting crustal extension. It is generally accepted that the western margin is a cryptic suture contained within the Haast schist which represents the metamorphosed equivalents of the Torlesse terrane, of felsic igneous provenance and the Caples terrane of predominantly intermediate volcanogenic provenance. The nature of this suture is crucial to Mesozoic tectonostratigraphic reconstructions and has been determined and mapped, both structurally and geochemically, in the Otago schist as a ductilely deformed, low angle thrust fault (Roser and Cooper, 1990; Cox, 1991; Mortimer and Roser, 1992; Mortimer, 1993). To the north, the Torlesse terrane and the unconformably overlying, undeformed, Torlesse-like, Late Cretaceous sediment cover is believed to mark a change in tectonic regime, the culmination of Mesozoic convergence and initiation of extension (Laird, 1981; Bradshaw, 1989). The submerged eastern margin against Pacific oceanic crust is thought to extend along the northern edge of the Chatham Rise, north and to the east of the emergent islands, the Chatham Island Group and the Forty Fours, on which the most eastern outcrops of Torlesse-type lithologies and metamorphosed equivalents are exposed (Figure 1.1a) (Hay *et al.*, 1970; Adams and Robinson, 1977; Andrews *et al.*, 1978; Campbell *et al.*, 1988; Herzer and Wood, 1988; Wood *et al.*, 1989).

In the South Island the Torlesse terrane consists of two subterranes, i.e. similar units of regional extent that are distinguished by age and intensity of deformation. The subterranes are separated by a belt of highly disrupted mélange:

- The Rakaia subterrane comprises older Permian to Triassic sediments

accumulated, folded and amalgamated with the Caples terrane by the Early Jurassic as indicated by the minimum age for the metamorphism which affects both (Adams *et al.*, 1985). The Rakaia subterrane represents a complex accretionary assemblage that was truncated tectonically prior to the amalgamation of the younger Pahau subterrane, or as a result of subsequent juxtapositioning (Bradshaw, 1989).

- The Pahau subterrane comprises younger Late Jurassic to mid Cretaceous sediments which have strong provenance links to the Rakaia subterrane indicating relationship between the two was close. Pahau deformation is consistent with a simple accretionary model. Conglomerates within the Pahau can contain up to 90% older Torlesse detritus (Rakaia), compared with 10-30% recycled material in Triassic conglomerates (MacKinnon, 1983).

- The Esk Head Mélange represents highly deformed Pahau material and slices of the original substrate that became caught up and wedged between the Rakaia and Pahau subterranes with progressive subduction (Silberling *et al.*, 1988).

The differing patterns of deformation inherent in the Rakaia and Pahau subterranes provide evidence that the Mesozoic Rangitata Orogeny was a multiphase event (Bradshaw, 1989).

Various environments of deposition have been suggested from localized sedimentary evidence, including submarine fan, shallow marine, marginal marine, and terrestrial (Andrews, 1974; Andrews *et al.*, 1976; Howell, 1981; Korsch and Wellman, 1988). The volume of the Torlesse terrane is substantial (at least 3.5 x $10^6 km^3$). True thickness is unknown. However, evidence of at least 25kms

thickness is indicated by xenoliths from Mt Somers lavas (Barley, 1987), which implies a normal crustal thickness. Potential source areas must have been of a similar large volume and it has been postulated that the Torlesse terrane formed spatially oceanward of a continental margin with a heterogeneous Andean-like source terrane.

1.2.4 Post Rangitata Orogeny Controls

The convergent margin tectonic regime that juxtaposed the Eastern Province terranes was replaced in the late Early Cretaceous by continental separation and tectonic unroofing along low angle normal faults (detachments) in an extensional regime (Bradshaw, 1989; Tulloch and Kimbrough, 1989). A widespread marine transgression tied to the formation of the new oceans surrounding the New Zealand micro-continent was consequent on the thermal decline of the continental lithosphere following the cessation of extension (Laird, 1981; Bradshaw, 1989).

Differential uplift predominated over subsidence during the early Tertiary and the New Zealand land mass grew to present proportions. The initiation of the present plate boundary, during the Late Oligocene (~25Ma), marked the start of the Kaikoura Orogeny which progresses to the present day (Bradshaw, 1989).

1.3 Methodology

1.3.1 Collection Procedure

A random sample of igneous clasts was collected from two outcrops (Waihere Bay and Parran Dam) of the mid Cretaceous conglomerate exposed on Pitt Island, Chatham Islands during December, 1991. Subsequent random samples were collected on several different occasions during the first four months of 1992 from three Torlesse conglomerates: the Ethelton conglomerate, the Mount Saul/Pahau River conglomerate, both considered Early to mid Cretaceous, within the Pahau sub-terrane, and the Triassic Lake Hill conglomerate, within the Rakaia sub-terrane.

1.3.2 Sample Preparation

Samples from each location were soaked in a weak hydrogen peroxide solution (< 10%) to remove organic matter from the clast surface, then washed in distilled water. Coherent samples of appropriate size and fresh appearance were cut on a diamond bench saw. Clasts were then sorted and subdivided according to an initial provisional hand specimen classification based on textural and mineralogic differences.

A total of 200 samples (approximately fifty from each locality) was selected from the several hundred clasts collected. These were deemed to be representative of the mineralogical and textural variety present. Thin sections were obtained from each of the chosen samples, a percentage of the total being made by hand following

the procedure of Lewis (1984). The mounting epoxy was EPO-TEK 301, which has a specified index of refraction between 1.538 - 1.540.

The remaining central portion of each clast was prepared for whole rock analysis by hydraulic crushing to centimetre size and grinding to a fine powder in a tungsten-carbide lined ringmill. Where possible, weathering rind, obvious alteration products, and quartz and calcite veins were removed prior to crushing and grinding.

Major element analyses required the preparation of glass fusion beads following the general methods outlined by Norrish and Hutton (1969) with modifications after Harvey *et al.* (1973), and Schroeder *et al.* (1980).

Trace element analyses were obtained on 30mm or 50mm pressed powder pellets, prepared by combining powdered rock with either 10-15 drops (for 30mm pellets) or 20-25 drops of 7% aqueous polyvinyl alcohol binder.

1.3.3 Laboratory Procedure

The whole rock major and trace element geochemistry for each area was determined by means of X-ray Fluorescence using the Philips PW 1400 X-ray Spectrometer, with on-line Hewlett Packard 300 computer, at the University of Canterbury. The procedures followed were those outlined in Weaver *et al.* (1990), with calibrations based on recommended values for 30 international standard rocks. Major element analyses (Si, Ti, Al, Fe, Mn, Mg, Ca, Na, K, P) were obtained using a 3Kw Sc-tube. Trace element analyses were obtained using a 3Kw Au-tube

for V, Cr, Ni, Zn, Zr, Nb, Ba, La, Ce and a 3Kw Mo-tube for Ga, Rb, Sr, Y, Pb, Th. Estimates of analytical precision are tabulated in Appendix 2.

1.3.4 Classification of Samples

Classification of samples was accomplished both by petrographic and geochemical methods.

a) Petrographical Classification

Thin sections were examined by transmitted light microscopy to determine the mineralogical composition. Qualitative descriptions were made of the major and accessory mineral phases, textural data and secondary modification features.

Precise quantitative analysis of each thin section was made by point counting (500 points, providing ~95% confidence, based on twice the standard deviation, according to the procedures of Van der Plas and Tobi, 1965). Appendix 3 tabulates the recalculated point count data.

Classification according to modal mineral content was made on the basis of the Quartz - Alkali feldspar - Plagioclase feldspar ternary diagram as prescribed by Le Maitre *et al.*, 1989 (Figure 1.3).

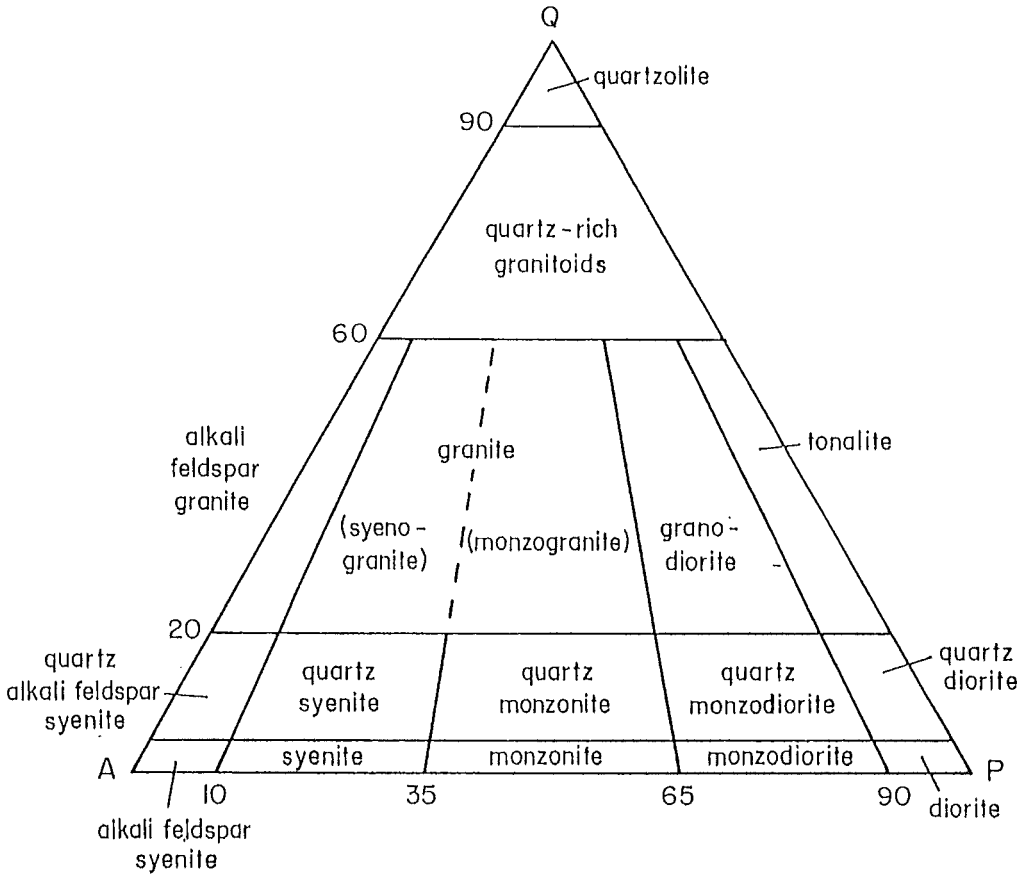

Figure 1.3: Quartz - Alkali Feldspar - Plagioclase ternary diagram. (after Le Maitre, 1989)

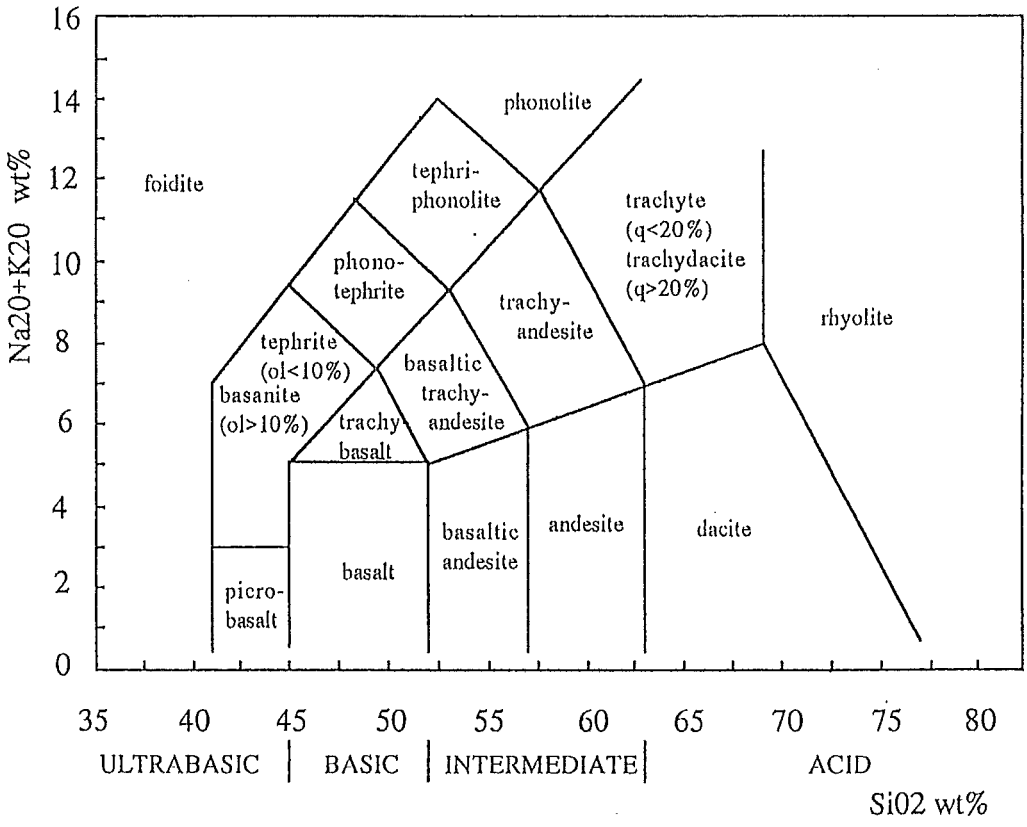

Figure 1.4: Total alkali versus silica (TAS) diagram. (after Le Maitre, 1989)

Samples were grouped according to textural character at the final stage of crystallization, i.e. hypersolvus or subsolvus.

Mineralogy was then considered, with samples subdivided according to the micas present, i.e. biotite only, both biotite and muscovite or muscovite only.

Plagioclase compositions were calculated by the Michel-Lévy method outlined by Shelley (1985), or by comparison of refractive index where {010} could not be identified with confidence (Shelley, 1985).

An accessory mineral common to two localities defied identification by normal optical methods and was analyzed by Electron Microprobe at the University of Otago. A brief analysis is given in Appendix 6.

All locality abbreviations and the arbitrary crystal size determination categories used are listed in Appendix 4.

b) Geochemical Classification

The fine grained nature of the matrix material in the volcanic samples precluded classification by point counting methods as mineral modes could not be determined. Samples were classified according to the Total Alkali Silica diagram (Le Maitre *et al.*, 1989) (Figure 1.4).

Geochemical analysis of plutonic rocks confirmed the validity of names

assigned according to mineral modal values. With the aid of discrimination diagrams correlations between areas and with possible protoliths were established. Any obvious processes of differentiation, the nature of source regions and tectonic environment were determined. The following sections concerning geochemistry will discuss these results.

Geochemical tables, CIPW normative calculations and discrimination diagrams were produced using the PETMIN and NEWPET geochemical software. For the normative calculation, total iron oxide was recalculated using $Fe_2O_3 = 0.3$ FeO. Original geochemical analyses, CIPW normative and normalized anhydrous calculations for each locality are presented in Appendix 1.

Symbols used to define the granitoid/volcanic samples of each area in determination diagrams have been recorded in Appendix 4.

CHAPTER 2

CHATHAM ISLANDS CONGLOMERATE

2.1 Introduction

2.1.1 Locality

The Chatham Islands comprise two main islands, Chatham Island (Rekohu) and Pitt Island (Rangiauria), and several smaller islets located on a shallow bank. They form the emergent part of the continental Chatham Rise submarine plateau that extends due east of Canterbury, South Island, New Zealand for over 1000kms (Figure 1.1).

The general geology of the Chatham Islands (and the Chatham Rise) comprises low grade schistose and greywacke basement unconformably overlain by Cretaceous and Tertiary sediments with interbedded and associated volcanics (Norris, 1964; Adams and Robinson, 1977; Grindley *et al.*, 1977; Herzer and Wood, 1988, 1992; Wood *et al.*, 1989).

The last major tectonic influence evident on the Chatham Rise was extension in the mid/Late Cretaceous that resulted in continental separation between New Zealand and West Antarctica to the east. Structurally, the Chatham Rise/Islands region is dominated by east-west trending half grabens inferred to be the result of incipient rifting associated with the Bounty Trough (Wood and Anderson, 1989;

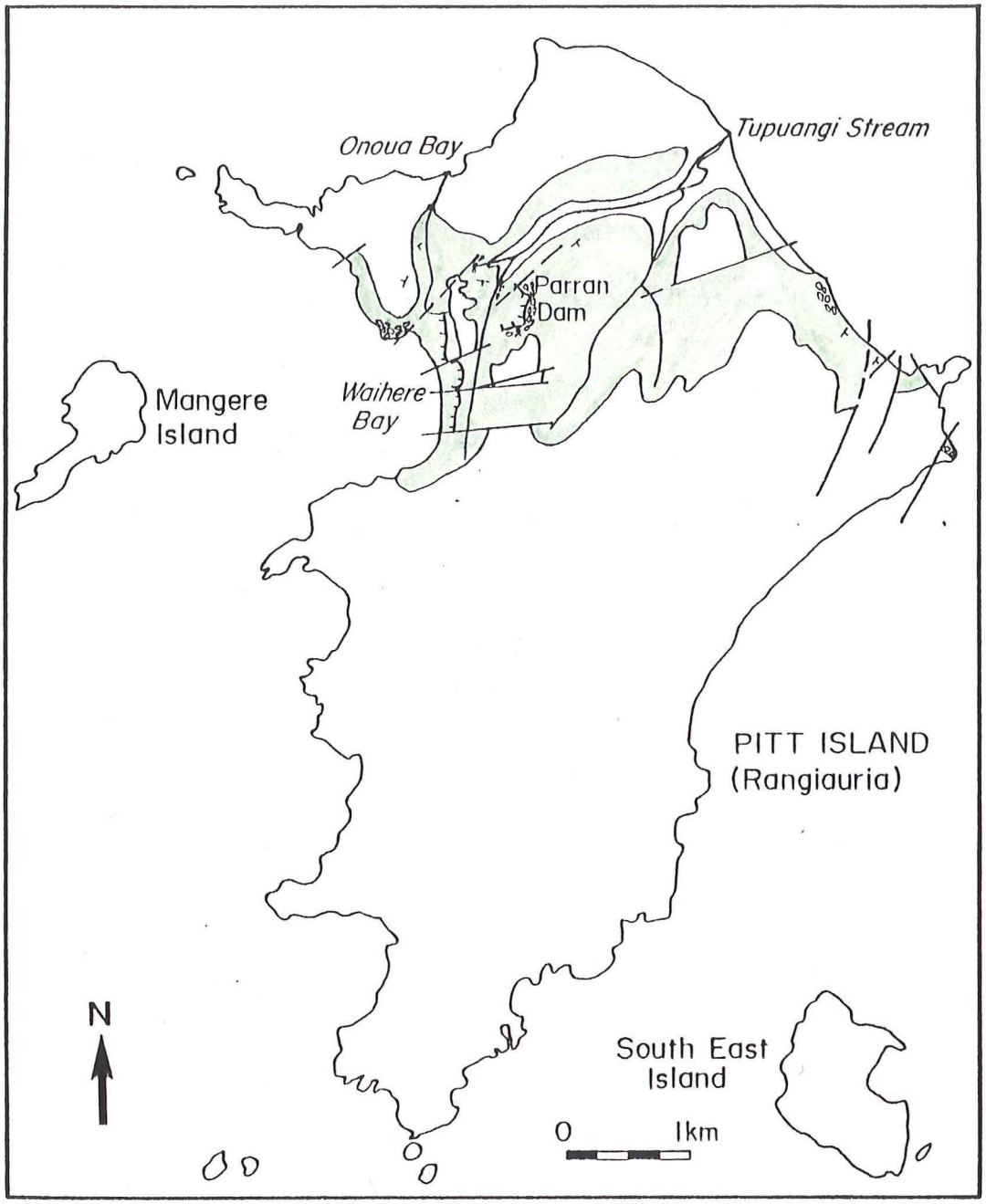

LEGEND

Late Cretaceous, Tertiary, and younger cover rocks — various volcanic, tuffaceous and calcareous formations.

middle Cretaceous — WAIHERE FORMATION massive to well bedded and cross bedded, medium to fine grained sandstone and carbonaceous mudstones with thick channeled, massive to well bedded, conglomerate horizons.

Conglomerate Outcrop

Fault

Figure 2.1: Pitt Island, Chatham Islands with generalized geology illustrating extent of Waihere Bay Formation and conglomerate outcrops. (after Hay *et al.*, 1970; Campbell *et al.*, in press)

Mayes *et al.*, 1990; Herzer and Wood, 1992), or thermal relaxation in response to a halt in convergence during the mid Cretaceous (Bradshaw, 1989). To the east, northeast trending faults, related to the separation of New Zealand from Antarctica, displace the earlier half graben structures (Wood and Anderson, 1989).

The basement Chatham Island Schist/Matarakau Greywacke has been determined as Permian to Triassic in age, equivalent to the Rakaia subterrane of the South Island, New Zealand (Wood and Anderson, 1989; Wood *et al.*, 1989), and an uplift age for the schist of ~162Ma (K-Ar data) is consistent with similar results obtained from the Otago/Haast schists (Adams and Robinson, 1977). Recently T.R. Ireland (unpublished data) has obtained U-Th-Pb SHRIMP ages on individual zircons from the Matarakau Greywacke, which display an age frequency distribution identical with that of the Torlesse Rakaia subterrane sediments. An equivalent to the Pahau subterrane, i.e. Upper Jurassic to Lower Cretaceous rocks with complex deformation, is not apparent on the Chatham Islands or surrounding islets.

Pitt Island lies ~20km to the southeast of Chatham Island across Pitt Strait (Figure 1.1). The polymict conglomerate sampled, outcrops at several localities in the core of a folded and faulted anticline that traverses Pitt Island (Figure 2.1). Palynology indicates a Motuan (mid Cretaceous) age of deposition (Mildenhall, 1977).

At the first sampling locality, the north headland of Waihere Bay (NZMS260, 1:50,000, Chathams Islands, Sheet 2, grid ref.703/212), conglomerate bands ($\leq$3m) dip to the northwest at shallow angles, and have been displaced to the south by east-

Figure 2.2: Waihere Bay, Pitt Island, Chatham Islands
a Waihere Bay headland locality
b Conglomerate band interbedded with sandstone.
Hammer = 33cms.

a

b

west oriented normal faulting (Figure 2.1 and 2.2) (Campbell *et al.*, in press). Inland to the east, ~1.5km from Waihere Bay, is the second sampling area known locally as Parran Dam (NZMS 260,1:50,000, Chathams Islands, Sheet 2, grid ref.723/215) (Figures 2.1 and 2.3). At this locality conglomerate ($\leq$4m) is interbedded with sandstone and the sequence outcrops to form a steep cliff face (Campbell *et al.*, in press) (Figure 2.3). The distinctive topographic expression of the conglomerate allows it to be traced to the east for ~200m (M.G.Laird, pers.comm.). Offshore seismic analysis indicates a major unconformity between underlying basement and the conglomerate, plus considerable unexposed thicknesses of presumably contemporaneous sediments (Herzer and Wood, 1988, 1992).

The depositional environment of the conglomerate at Parran Dam is thought to be fluvial, unlike the exposure at Waihere Bay which displays convincing evidence of marginal marine/tidal influence (Campbell *et al.*, in press).

Early paleocurrent studies indicated a sediment source to the southwest (Hay *et al.*, 1970; Grindley *et al.*, 1977; Campbell *et al.*, 1988). Campbell *et al.* (in press), however, have determined that the various lithofacies that together form the conglomerate have a predominantly north to northeast derivation. The presence of reworked Late Permian pollen and spores within the conglomerate matrix indicates a probable age for source region sediments (Campbell *et al.*, in press). Recently obtained zircon ages from the schist/greywacke are predominantly Permian (~260Ma). The euhedral morphology of the zircons indicates they have only been reworked once, and that the source of detritus for the schist/greywacke contained Permian granitoids (T.R.Ireland, pers.comm.).

Figure 2.3: Parran Dam, Pitt Island, Chatham Islands
a Parran Dam locality
b Bedded conglomerate outcrop.
Hammer = 33cms.

a

b

2.1.2 Previous work

The Pitt Island conglomerate was first mentioned by Hay *et al.* (1970) in a general account of the geological aspects of the Chatham Islands. Hay *et al.* (1970) placed the conglomerate as a discrete basal unit (the Headland Conglomerate) within the Waihere Bay Group, which included all sedimentary and volcaniclastic rocks of Cretaceous age exposed on Pitt Island. Grindley *et al.*(1977) assigned the younger volcaniclastic sediments to the Pitt Island Group. The Waihere Bay Group consisted of the older terrigenous sediments, the Tupuangi Sandstone and the Headland Conglomerate. Campbell *et al.*(1988) considered the conglomerate interformational and part of the Tupuangi Formation. Subsequent work supports this nomenclature and expands the general lithological description of the formation with sedimentological detail (Wood *et al.*, 1989; Campbell *et al.*, in press).

2.2 Petrography

For the purpose of this research the samples collected from the Waihere Bay and Parran Dam localities have been considered together in petrological and geochemical interpretations, despite the fact that they are considered to be different lithofacies and lack detailed correlation across intervening fault blocks.

The recalculated point count data for the Chatham Islands granitoid clasts, presented in Appendix 3, was plotted on the QAP ternary diagram illustrated in Figure 2.4. This enabled initial groupings to be made. The majority of samples plot within the syenogranite or monzogranite fields with some scatter into the granodiorite

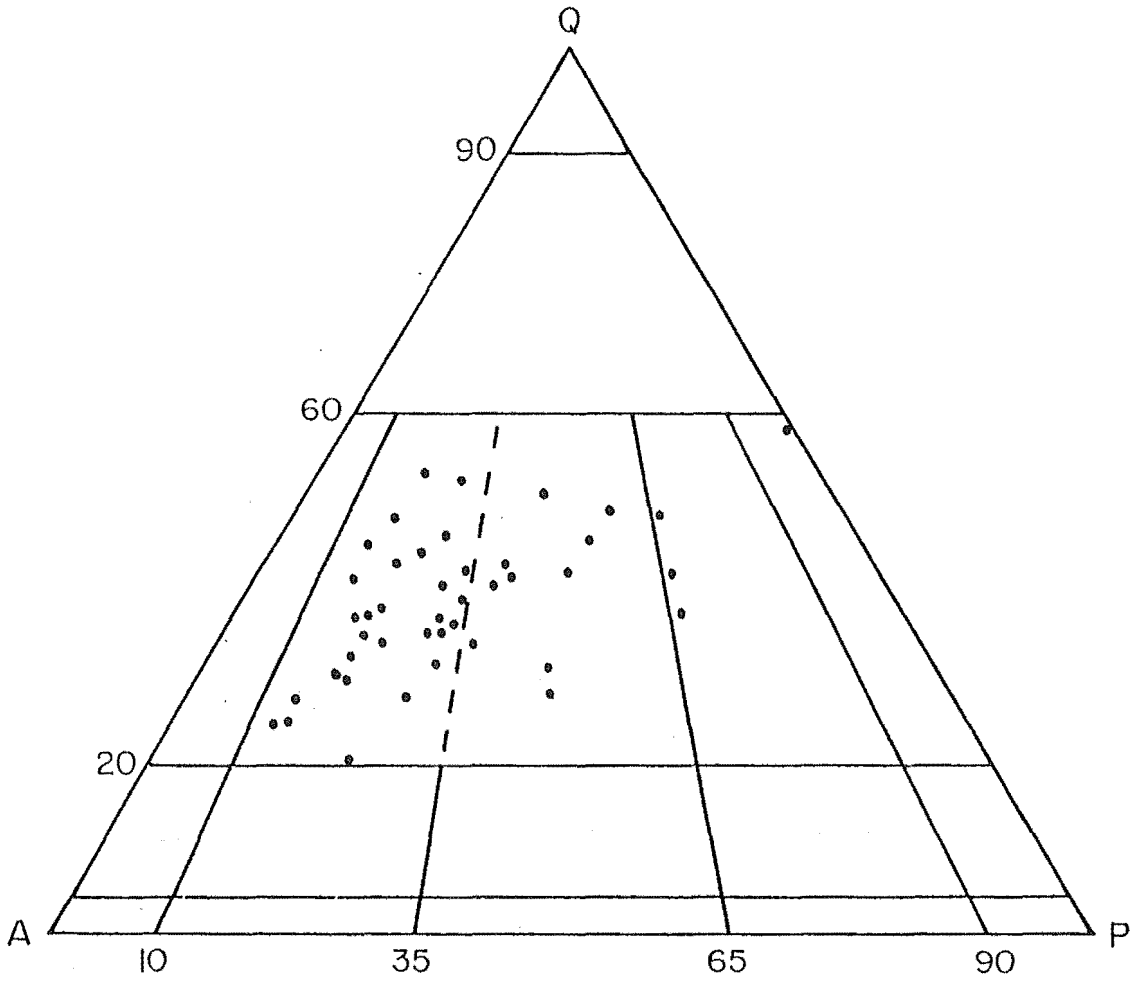

Figure 2.4: Quartz - Alkali Feldspar - Plagioclase ternary diagram illustrating modal distribution for Chatham Island conglomerate granitoid clasts (see Chapter 1, 1.3.4a for definition of fields) (after Le Maitre, 1989).

and tonalite fields.

Using the modal classification as a basis, sections were further subdivided according to mineralogical and textural differences as outlined in Chapter 1, 1.3.4a.

Hypersolvus granitoids are defined as those which crystallized at low water pressure (< 5kbar), as indicated by the presence of a single K/Na feldspar of intermediate composition (often unmixed to mesoperthite). Textural features such as granophyric intergrowth indicate a rapid quenching or freezing of the magma which may be related to loss of volatiles along fractures near the surface or upward movement of magma which intersected the negatively sloped, granite water saturated solidus (Shelley, 1992). Hypersolvus samples frequently display evidence of a prior subsolvus crystallization.

Subsolvus granitoids are defined as those which crystallized at higher water pressure and at greater depth as indicated by the presence of discrete crystals of both alkali feldspar and plagioclase.

2.2.1 Granitoid Clast Descriptions

The Chatham Islands granitoid samples are divisible into nine distinctive mineralogical and textural groups (Figure 2.5):

Group CIG-1:

Subsolvus, holocrystalline, medium to fine grained, equigranular to porphyritic, muscovite biotite leucosyenogranite:

The alkali feldspar is microcline or perthitic orthoclase and is dominant over plagioclase. Plagioclase is sodic oligoclase (An10-20%), often forms very large subhedral crystals (>1cm), and displays albite twinning. Normal zoning of the plagioclase is emphasized by preferential sericitization of the more calcic zones. Refractive index comparisons with quartz inclusions indicate that the core of plagioclase is andesine (An30-40%). The plagioclase has been saussuritized in some sections, with epidote crystals concentrated along cleavages. Myrmekitic intergrowths are found along plagioclase/alkali feldspar grain boundaries. Alkali and plagioclase feldspar display incipient recrystallization around grain boundaries, but inclusions of biotite and quartz within them have a random orientation and remain unaffected by deformation.

Quartz appears as large (>1.5mm) subhedral to anhedral crystals with sutured boundaries and undulatory extinction, and as a well annealed undeformed mosaic of relatively finer grain size.

Minor phases include biotite (pleochroic green/brown, often kinked and chloritized) and muscovite, usually subordinate to and intimately associated with the biotite.

Figure 2.5: Representative photographs of modal, textural, and mineralogical granitoid groups (field of view ~5cms):
a Subsolvus, biotite leucosyenogranite (CIG-2)
b Hypersolvus, biotite leucosyenogranite (CIG-3)
c Subsolvus, foliated, leucomonzogranite (CIG-5)
d Subsolvus, biotite, leucogranodiorite (CIG-8)

a

b

c

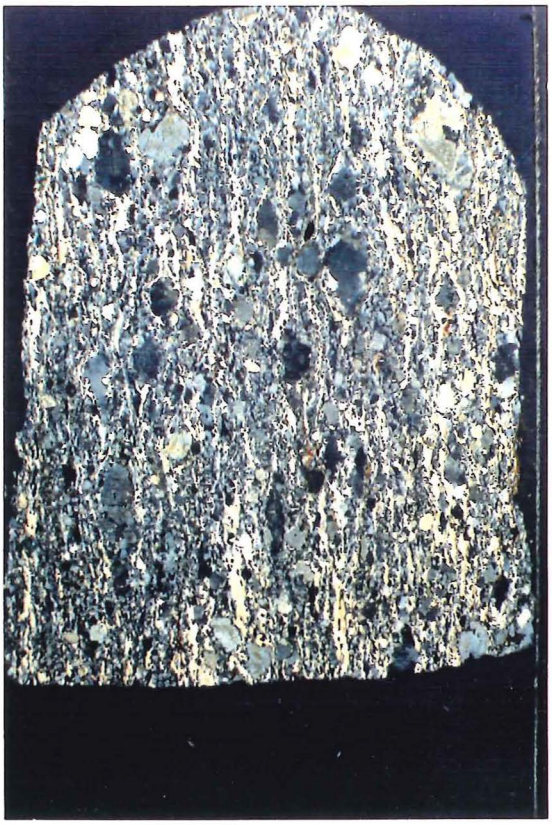

d

Accessory minerals can include euhedral garnet and zircon, and zoned metamict allanite (usually associated with epidote). Opaque Fe/Ti oxides are commonly associated with biotite.

Foliation, where present, is defined by incipient quartz ribbon development and the alignment of muscovite and biotite. A shape and lattice preferred orientation (SPO and LPO) of quartz is evident in some sections.

Group CIG-2:

Subsolvus, holocrystalline, coarse to medium grained, equigranular to porphyritic, biotite leucosyenogranite:

The alkali feldspar is microcline or orthoclase and represents the dominant crystal phase, often rimming plagioclase and quartz. The plagioclase was determined as sodic oligoclase (An10-20%) with more calcic rich cores that are usually distinguished by pronounced sericitization and crystallization of secondary muscovite plates.

Quartz has euhedral to subhedral crystal form in most sections, with deformation limited to undulose extinction and slight suturing of subgrain boundaries.

Biotite is a minor phase, and in most sections is present as large tabular randomly oriented plates.

Zircon and opaque Fe/Ti oxides were the only accessory minerals noted.

In the sections that display a foliation this is defined by an SPO of quartz and alignment of micas. Typical lobate myrmekite is common along alkali feldspar rims.

Group CIG-3:

Hypersolvus, holocrystalline, coarse to medium grained, equigranular to porphyritic, granophyric, biotite leucosyenogranite:

Samples in this group display an original undeformed igneous texture and are typified by interstitial granophyric intergrowths of quartz and alkali feldspar surrounding discrete crystals of plagioclase, alkali feldspar and quartz, indicating a prior subsolvus history (Figure 2.6a). Discrete alkali feldspar is usually microcline and plagioclase is sodic oligoclase (An 10-20%). In some sections mesoperthite predominates (50/50 alkali feldspar and plagioclase).

Quartz forms large, euhedral to subhedral crystals with slight undulatory extinction.

The biotite is large, tabular, partially chloritized, often kinked, and usually associated with opaque Fe/Ti oxides. Dark pleochroic haloes can be seen rimming metamict inclusions of zircon and apatite in some dark brown basal sections. Two biotite populations were commonly noted; large wide tabular plates and small, acicular, thin crystals.

Adcumulate texture was evident, with monomineralic clusters of quartz or alkali feldspar.

Miarolitic cavities are common in most sections, usually lined with euhedral quartz and infilled with a coarser quartz mosaic (Figure 2.6b).

In hypabyssal varieties, phenocrysts are often set in a matrix of coarse felsitic texture that grades into granophyric intergrowth.

Group CIG-4:

Subsolvus, foliated, holocrystalline, medium to fine grained, biotite leucomonzogranite:

The subhedral to anhedral alkali feldspar is orthoclase and microperthitic. The plagioclase is subhedral sodic oligoclase (An10-20%) and displays both primary and deformation albite twinning. Myrmekite is present along alkali feldspar boundaries where bordered by plagioclase.

Quartz ribbon development defines a pervasive foliation, as does the alignment of sheet silicates.

The biotite forms relatively finer crystals, is green/brown pleochroic, and usually partially altered to chlorite. Anhedral opaque Fe/Ti oxides are usually clustered with biotite.

Apatite and zircon are common accessory phases frequently included within quartz and biotite.

Group CIG-5:

Subsolvus, foliated, holocrystalline, medium to fine grained, muscovite biotite leucomonzogranite:

The subhedral to anhedral plagioclase is sodic oligoclase (An10-20%), and has undergone moderate sericitization, as has the alkali feldspar which is anhedral orthoclase.

A well developed foliation is defined by quartz ribbons and the alignment of muscovite and biotite plates around large resistant plagioclase and alkali feldspar, which display only minor recrystallization along grain boundaries. The quartz LPO indicates that c-axes are parallel to the elongation direction. Myrmekite has

developed along alkali feldspar grain boundaries where these border plagioclase crystals and parallel the foliation. The constituent plagioclase frequently displays secondary albite twinning.

Biotite has been altered almost totally to chlorite and is usually associated with opaque Fe/Ti oxides. Muscovite is present as a primary minor phase subordinate to biotite.

Group CIG-6:

Hypersolvus, holocrystalline, medium to fine grained, granophyric, biotite leucomonzogranite:

Granophyric intergrowths of alkali feldspar and quartz dominate the interstitial space between discrete or clustered quartz, mesoperthite, alkali feldspar and plagioclase crystals.

The alkali feldspar has mesoperthite developed around the rim and displays transformation/cross hatch twinning distinctive of microcline. Zoning in the plagioclase has been accentuated by preferential sericitization and saussuritization of the core region, with replacement by muscovite and epidote (Figure 2.6c). The outer rims were identified as albite (An5-10%).

Quartz is subhedral to anhedral and essentially undeformed with symmetrical extinction.

The brown pleochroic biotite is partially chloritized.

Accessory minerals include allanite (metamict) and zircon.

Epidote is abundant as a discrete euhedral to subhedral mineral, and could be primary, or a secondary replacement phase. Interstitial chlorite has replaced mafic minerals that may have been present.

Group CIG-7:

Subsolvus, holocrystalline, coarse to medium grained, equigranular to porphyritic, muscovite leucogranodiorite:

The euhedral to subhedral plagioclase is relatively finer grained and more abundant than quartz and alkali feldspar, and is strongly twinned albite or oligoclase (An5-15%). The anhedral alkali feldspar is perthitic orthoclase. The quartz may exhibit slight undulose extinction but, in general, is undeformed.

Muscovite is the only minor phase and is present throughout sections as large (~2mm), subhedral, randomly oriented, essentially undeformed crystals that frequently enclose euhedral plagioclase (Figure 2.6d).

Accessory euhedral tourmaline and garnet are confined to the finer grained interstitial material. Garnets still exhibit good euhedral form, although partially altered to, and surrounded by, chlorite and opaque Fe/Ti oxides (Figure 2.6e).

Group CIG-8:

Subsolvus, holocrystalline, medium to fine grained, equigranular, biotite leucogranodiorite:

The euhedral to subhedral plagioclase is sodic oligoclase (An10-20%) that usually displays distinct albite twinning. The plagioclase is dominant over the anhedral alkali feldspar, which is microperthitic orthoclase. The quartz is anhedral with slight undulose extinction. Both plagioclase and quartz display adcumulate texture.

Biotite is fine grained, green/brown pleochroic, and associated with opaques.

Accessory phases include euhedral zircon and subhedral to anhedral opaque Fe/Ti oxides.

Figure 2.6: Photomicrographs of thin section features (field of view = ~7mm):

a Granophyric intergrowth of quartz and alkali feldspar surrounding discrete subhedral plagioclase crystals

b Euhedral terminations of quartz, alkali feldspar and plagioclase into a miarolitic cavity lined with euhedral quartz and infilled with a coarse quartz mosaic

c Saussuritization of plagioclase by epidote

d Primary muscovite surrounding euhedral plagioclase

e Euhedral igneous garnet and tourmaline (plane-polarized light)

f Bipyrimidal quartz surrounded by spherulites (key to symbols Appendix 4)

a

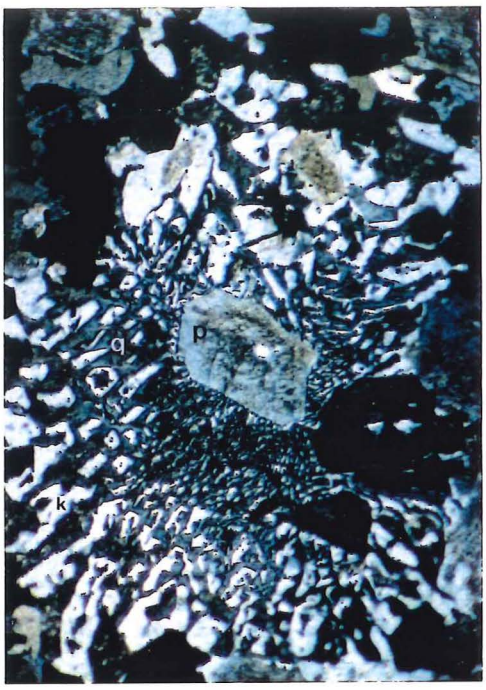

b

c

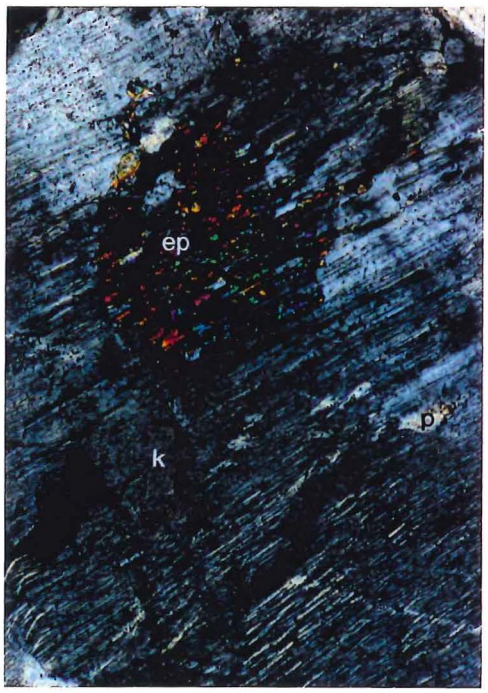

d

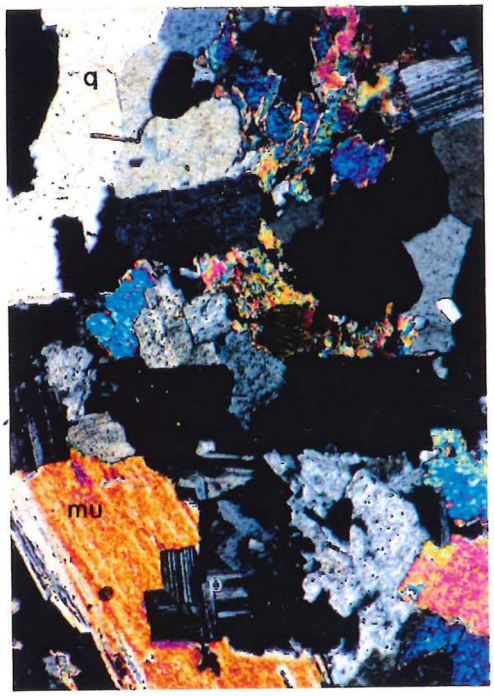

e

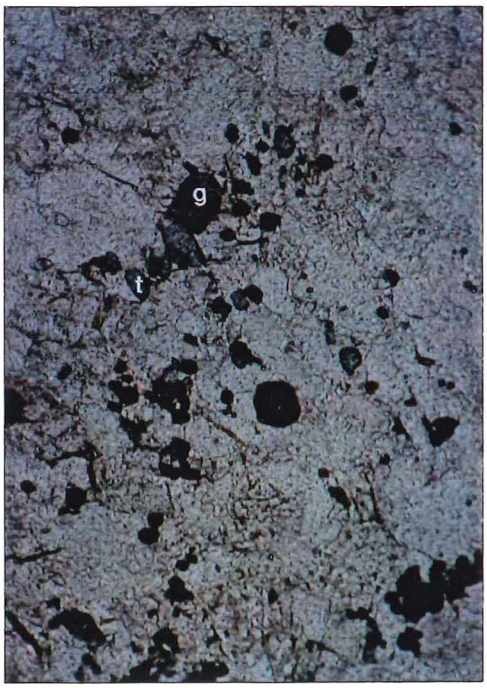

f

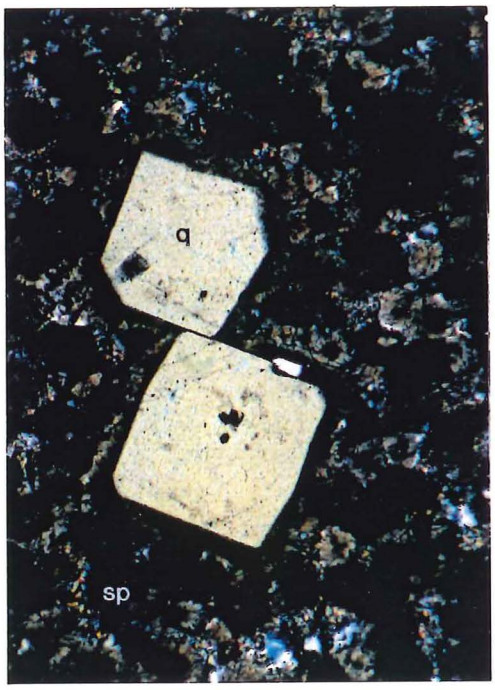

Group CIG-9:

Subsolvus, holocrystalline, medium grained, leucotonalite:

The plagioclase is euhedral to subhedral sericitized sodic oligoclase (An10-15%) that generally has albite and Carlsbad twinning. No alkali feldspar could be identified.

The quartz exhibits subgrain development with sutured grain boundaries, undulatory extinction and incipient SPO, but no LPO indicating moderate deformation. Crystals enclosed in plagioclase display straight extinction.

Accessory phases include euhedral zircon and opaque Fe/Ti oxides, both associated with partially chloritized green/brown biotite.

2.2.2 Volcanic Clast Descriptions

Volcanic clasts sampled from the Chatham Islands are divisible into two fields on the TAS diagram (Figure 2.7) based on geochemistry. The clasts have been grouped and described mineralogically and texturally based on the initial TAS classification (Figure 2.8):

Group CIV-1:

Holocrystalline to hypocrystalline, porphyritic and/or spherulitic rhyolite:

Phenocrysts constitute 10 - 40% of these rocks and often appear fragmented.

Phenocrysts include large (>1cm) euhedral or embayed quartz, typically undeformed with slight undulose extinction (Figure 2.6f). Euhedral to subhedral plagioclase, which is sericitized albite (2V ~90°), and displays "chessboard" albite/pericline twinning. Alkali feldspar, where present, is clear, euhedral sanidine

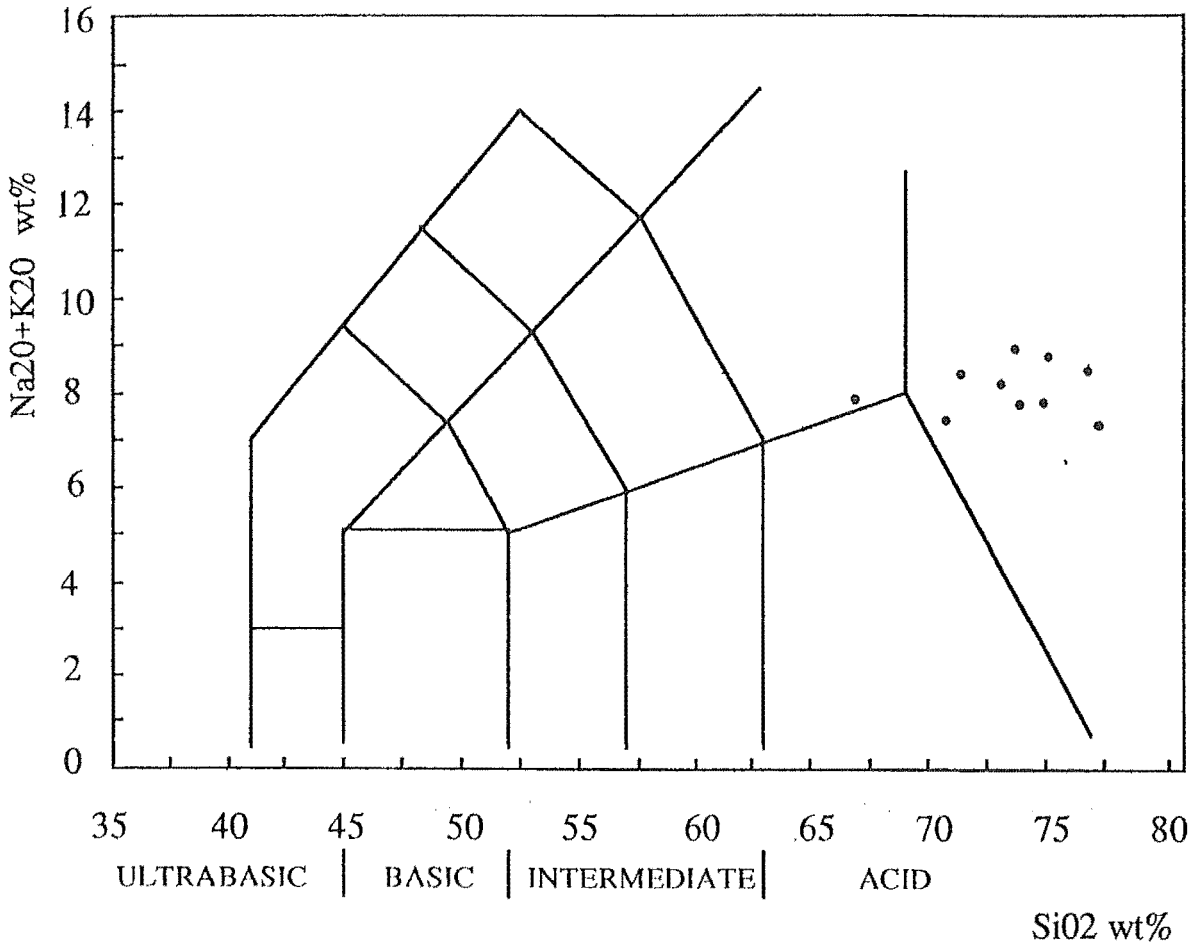

Figure 2.7: TAS classification illustrating distribution for Chatham Islands conglomerate volcanic clasts (after Le Maitre, 1989).

($2V_x$~0-20°) with Carlsbad twinning, and/or anhedral perthite. Phenocrysts are sometimes clustered together to form glomeroporphyritic texture.

Lithic fragments (xenoliths) of volcanic or plutonic origin are common.

Mafic material, both as phenocrysts and in the matrix, has been totally altered to chlorite, epidote, calcite and opaque Fe/Ti oxides. Distinctive pseudomorphs of pyroxene, biotite and amphibole, and others suggestive of olivine were noted.

Mosaics of quartz can fill large (>1cm) elongate vesicles (lithophysae).

The generally felsitic matrix frequently displays flow layering and/or spherulitic texture. Spherulites commonly coarsen outwards into fine granophyric intergrowths of alkali feldspar and quartz. Refractive indices indicate the matrix to be a mixture of quartz and alkali feldspar with varying amounts of plagioclase and minor phases that include biotite and opaque Fe/Ti oxides, plus accessory zircon.

Group CIV-2:

Porphyritic trachydacite:

Phenocrysts are predominantly >0.5cm euhedral to subhedral calcic oligoclase (An25%). Other phenocryst phases include partially chloritized biotite and chlorite/opaque Fe/Ti oxide pseudomorphs with biotite, hornblende and pyroxene euhedral form.

The matrix is a fine grained crystalline mixture of alkali feldspar, quartz and minor plagioclase that has a felsitic texture with flow layering evident around phenocrysts.

Figure 2.8: Representative photographs of volcanic groups (field of view ~5cms):

a Porphyritic rhyolite with euhedral plagioclase and quartz phenocrysts (CIV-1)

b Porphyritic trachydacite with euhedral and fragmented plagioclase phenocrysts (CIV-2)

a

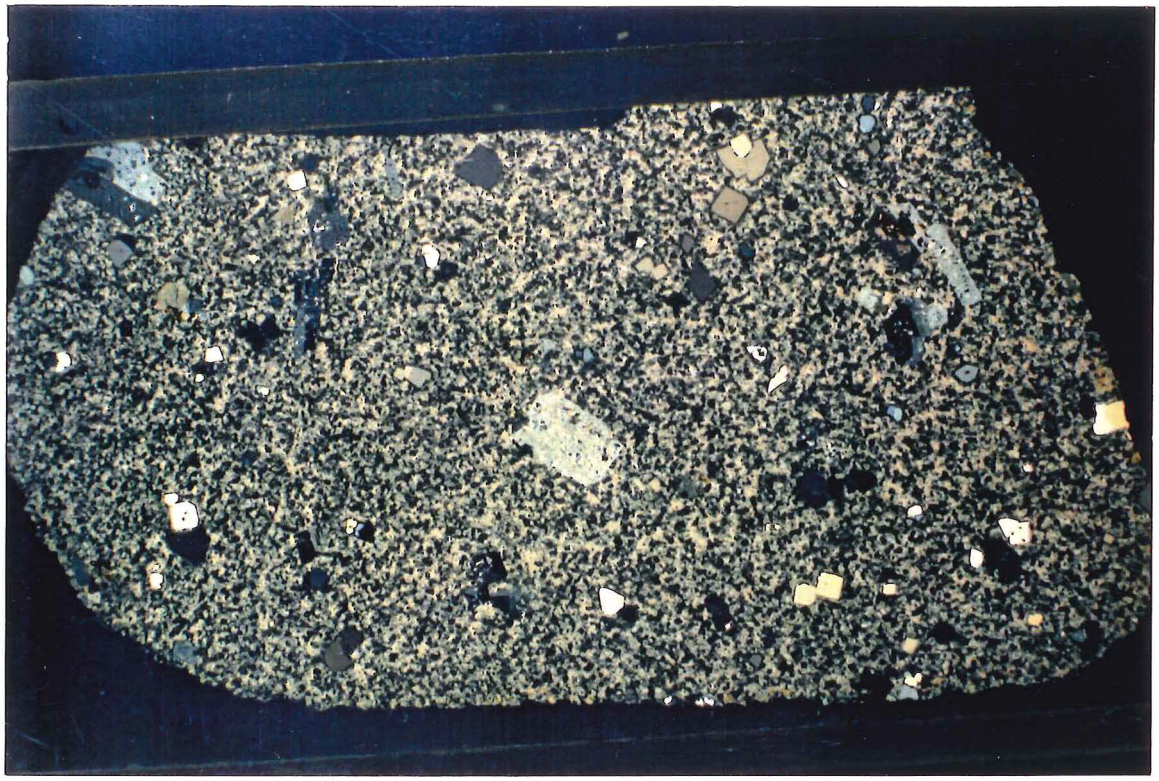

b

2.2.3 Petrological Interpretation

The granitoid groups previously listed and described are combined and compared within the confines of the two distinctive textural categories outlined in Chapter 1, 1.3.4a and previously defined in this chapter.

Chatham Island hypersolvus granitoid samples (groups CIG-3,6) are essentially undeformed with quartz exhibiting only slight undulose extinction. The miarolitic cavities present in some hypersolvus samples indicate emplacement and crystallization at a shallow level associated with the exsolution of a vapour phase due to water saturation.

Hypabyssal forms are evident in the predominantly fine grain size and porphyritic character of many hypersolvus samples, typical of near surface intrusion. This suggests a close relationship between the hypersolvus granitoids and the volcanics (which, by definition, must have undergone final crystallization under hypersolvus conditions).

Most hypersolvus granitoid clasts have evidence of an earlier subsolvus history. The change to hypersolvus conditions is depicted by the presence of interstitial granophyric intergrowths between discrete crystals of quartz, plagioclase and alkali feldspar and the presence of mesoperthite only around the rim of zoned alkali feldspar. In one section (PD2/24011), tabular biotite crystals represented slow crystallization near the solidus whereas acicular biotite in the same section represented rapid crystallization and a large degree of undercooling as a result of

quenching. This change indicates fluctuations in the level of magma and changes in water pressure due to a loss of supercritical fluid and consequent pressure quenching, perhaps due to loss of volatiles as a result of volcanic explosion and/or caldera collapse.

The Chatham Island subsolvus granitoid clasts (groups CIG-1,2,4,5,7,8,9) can be subdivided according to varying degrees of deformation. The subsolvus character is indicated by the presence of both alkali feldspar and plagioclase and the lack of granophyric intergrowths.

Some samples have suffered little deformation with only a slight re-equilibration due to relatively slower cooling (compared with hypersolvus samples), and these rocks display true granitic texture with the development of euhedral, subhedral and anhedral crystal forms.

The majority of subsolvus samples exhibit a pervasive foliation, defined by moderate to well developed quartz ribbons and the alignment of sheet silicates around resistant feldspars, indicative of a dynamic metamorphism (mylonitization). The distinctive LPO recognized, with c-axes parallel to the inferred shearing direction (the extension direction), is characteristic of c slip which is limited to high temperatures ($>650^{\circ}C$) and possibly hydrous conditions (Mainprice *et al.*, 1986). The recrystallization of quartz ribbons and development of gneissic texture in some foliated granitoids indicate a post-intrusive annealing at high temperatures.

That undeformed and foliated subsolvus samples with similar mineralogy are

present may indicate plutons with massive, undeformed centres and foliated margins.

Myrmekite is abundant in many of the deformed subsolvus granitoid samples where it has developed perpendicular to the extension direction. Myrmekite is indicative of high temperature, subsolidus deformation within the amphibolite facies (Simpson and Wintsch, 1989).

Volcanic clasts are primarily classified using geochemical analyses (section 2.2.2). In thin section little mineralogical or textural difference could be determined. However, the absence of quartz as a phenocryst phase was noted in the trachydacite clast. The abundance of lithic fragments, especially those with a high mafic content, is considered a major factor influencing whole rock composition, and therefore type based on geochemistry, for volcanic samples.

The shattered nature of phenocrysts and the presence of volcanic and plutonic lithic fragments (xenoliths) suggests a possible pyroclastic/ignimbritic origin for some of the rhyolite and trachydacite samples. However, no definitive proof of this was obtained.

The matrix material of volcanic samples has undergone devitrification from metastable glass to felsitic or spherulitic texture which suggests ubiquitous undercooling to a high degree, typical of silicic volcanic rocks. Derivation for most of the volcanic samples is considered to be from rhyolite domes. Rhyolite magmas tend to be erupted/extruded either as pyroclastic or, due to their high viscosity, as domes (Shelley, 1992).

Volcanic clast mineralogy was comparable with the granitoid samples and a cogenetic relationship between some members of the two groups is postulated and discussed further in conjunction with the geochemical evidence.

The replacement products chlorite, epidote and calcite were present in most samples, particularly in the volcanics, indicating alteration and fluid interaction at some stage following crystallization. The original position of volcanic and hypabyssal samples would make them more susceptible to weathering and the effects of circulating meteoric water. Veining is present in several samples and semibrittle deformation subsequent to the penetration of fluids is indicated in that many of the veins are bent. Alteration processes that affected samples prior to inclusion in the conglomerate from those affecting them within the conglomerate were difficult to distinguish.

2.3 Geochemistry

2.3.1 Categorization of Granitoids

Classification of granitoids using distinctive major and trace element characteristics supported by mineralogical data to imply source features has been developed in the past decade. White and Chappell (1983) first recognized that granitoids and related volcanic rocks of the Lachlan Fold Belt, southeastern Australia could be grouped according to source rock features using petrographic and chemical data. Primarily distinction is made between rocks derived from igneous (I-type) and sedimentary (S-type) sources. S-types chemically reflect a source that has undergone

at least one weathering cycle at the Earth's surface. Late stage felsic anorogenic (A-type) granitoids were identified as being derived from crust depleted as a result of previous I-type magma production (Collins *et al.*, 1982). Expansion of this classification has occurred with the recognition that further subdivisions could be made within these initial groupings (Whalen *et al.*, 1987; Chappell and White, 1992; Eby, 1990, 1992).

To attempt a similar classification the Aluminium Saturation Indices were determined for each sample from the chemical analyses and are tabulated in Appendix 5. This information was plotted and is displayed in Figure 2.9. No obvious separation occurs between samples. Five clasts (syenogranites from the Waihere Bay and Parran Dam localities) plot within the metaluminous field with an ASI between 0.88 to 1.0 and A/NK <1.25 suggesting an igneous, or I-type character (White and Chappell, 1983; Chappell and White, 1992). Ten clasts have an ASI >1.1 suggesting a metasedimentary source, or S-type character (White and Chappell, 1983; Chappell and White, 1992). The remaining clasts plot between ASI 1.0 and 1.1., within the peraluminous field, and as such provide ambiguous information in terms of I- or S-type classification, i.e. evolved I-types can be weakly peraluminous (with an ASI between 1.0 and 1.1) (Chappell and White, 1992).

The high silica content of the majority of samples, (only two samples have SiO_2 $<70\%$) suggests samples are highly evolved as a result of extensive crystal fractionation, or they are approaching thermal minimum melts ($SiO_2 = 76\%$) representative of source composition (Whalen *et al.*, 1987). In felsic rocks the chemical compositions are similar (ASI's concur) and the distinctive minerals present

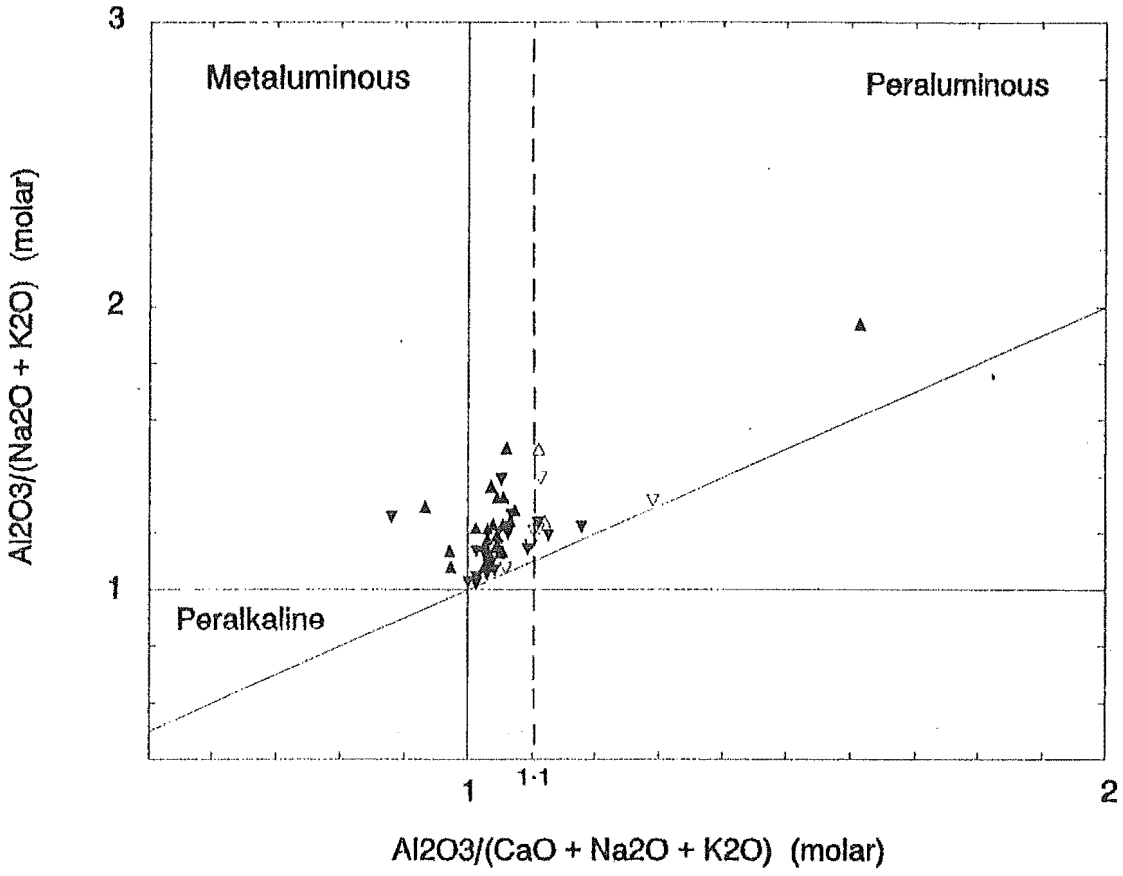

Figure 2.9: Aluminium Saturation Indices plotted for Chatham Islands conglomerate clasts. A/CNK = 1.1 indicates the boundary between highly fractionated I-type/S-types and S-type granitoid/volcanic clasts. (after Maniar and Piccoli, 1989)

in more mafic rocks, i.e. hornblende (I-types) and cordierite (S-types), are not present. Therefore a classification of these rocks into I- or S-types is difficult.

Whalen *et al.* (1987) illustrate that fractionated, felsic I- and S-type granites can have major and trace element values that deviate from the fields used to distinguish average I- and S-types and overlap those considered typical of A-type granites. The common discriminants used are the high field strength elements (HFS) which include Zr, Ce, Nb, Y and Ga, which have relatively low abundances in subduction related magmas. Chatham Islands clasts plot predominantly within the fractionated granite (FG) field in plots of HFS-alkalis or HFS-FeO/MgO (Figures 2.10a and b). In plots of 10000*Ga/Al versus various major and trace elements clasts concentrate outside the defined I- and S-type field, in the A-type field, but separate from the calculated A-type average (Figures 2.11a and b) (Whalen *et al.*,1987).

El Bouseily and El Sokkary (1975) use the Rb-Ba-Sr ternary relationship to define differentiation trends within granitoid suites. When the Chatham Island conglomerate analyses are plotted on the Rb-Ba-Sr ternary diagram a fractionation trend from granodiorite to granite (*sensu stricto*) composition is indicated (Figure 2.12). There is some separation between the trend shown by these samples and that displayed by the relatively more highly evolved samples. This could indicate an I-type suite with evolution toward S-type characteristics, as a consequence of magma evolution, and a separate event with highly evolved or A-type character.

The alkali-lime index (Appendix 4) for Chatham Island clasts was determined

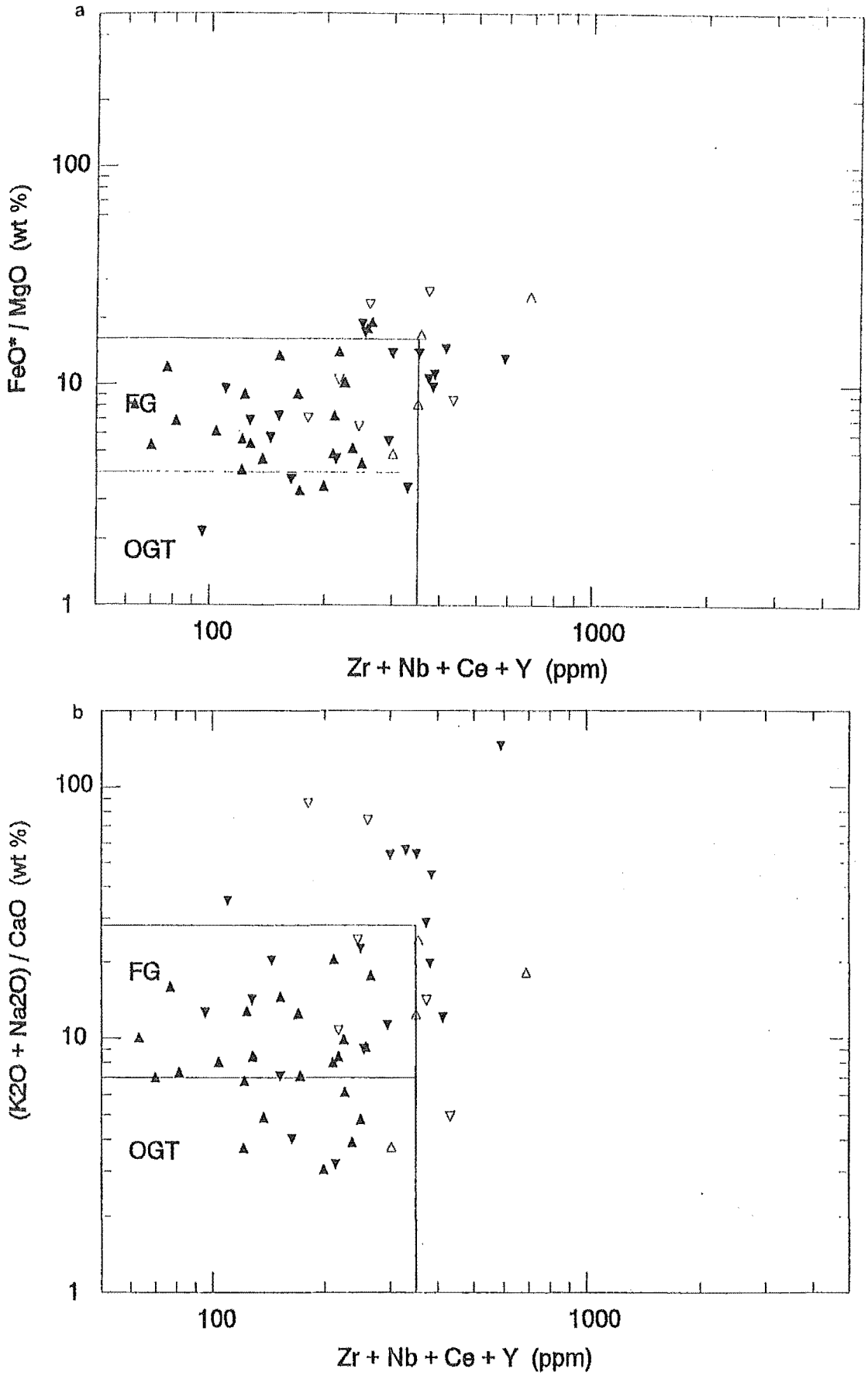

Figure 2.10: High Field Strength trace elements versus major element ratios with fields for fractionated felsic granites (FG), and ordinary granite types (OGT) delineated:
a Zr+Nb+Ce+Y versus FeO*/MgO
b Zr+Nb+Ce+Y versus $(K_2O+Na_2O)/CaO$
(after Whalen *et al.*, 1987)

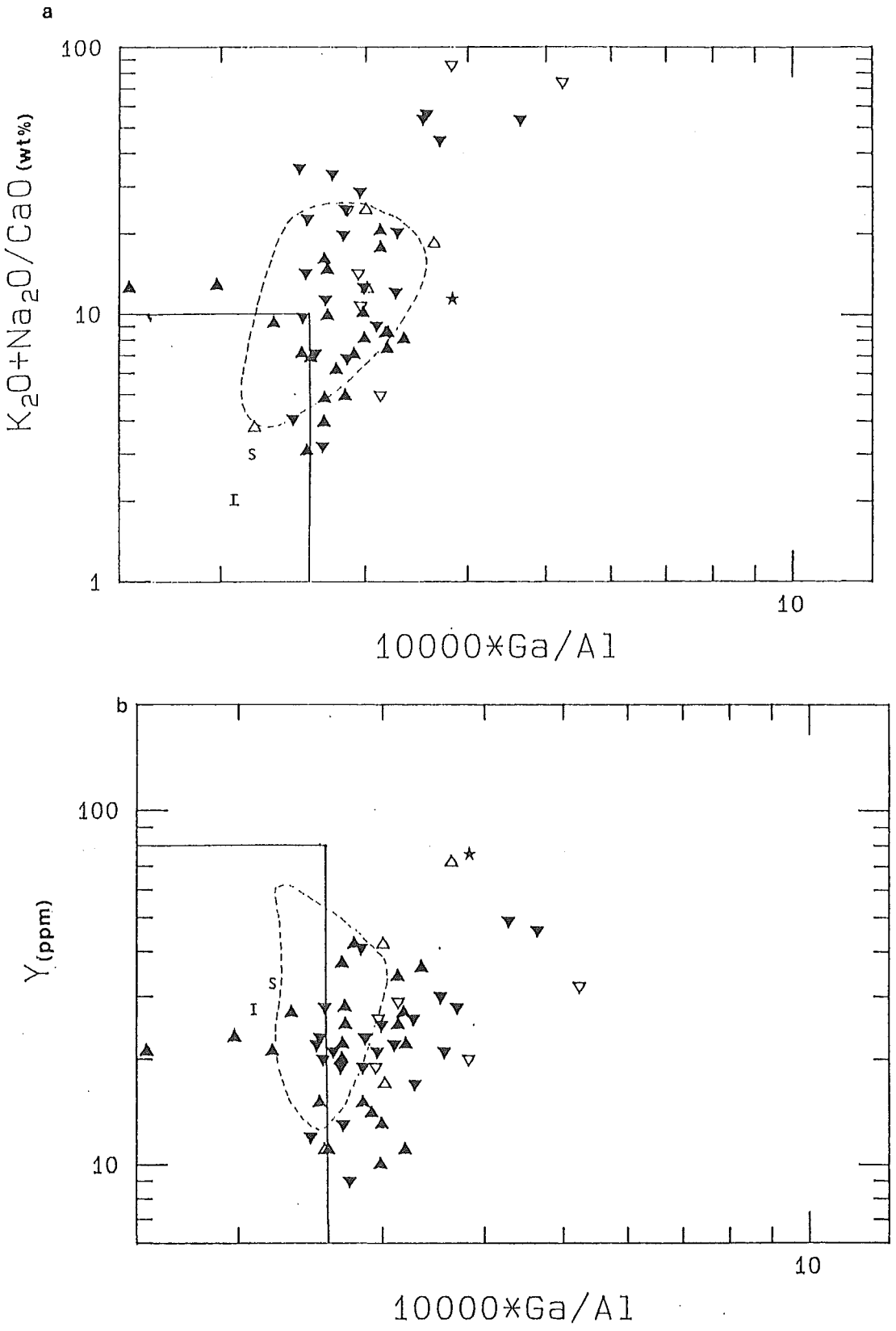

Figure 2.11: Plots of 10000*Ga/Al versus **a** K_2O+Na_2O/CaO and **b** Y illustrating Chatham Islands conglomerate clast distribution. I- and S-type granite field delineated, dashed line represents fractionated granite field, *= calculated average A-type, I = calculated average I-type, S = calculated average S-type.
(after Whalen *et al.*, 1987)

to be between 53 - 58% SiO_2 (Figure 2.13). Under this classification, samples can be considered alkali-calcic to calc-alkaline (Peacock, 1931; Brown, 1982; Maniar and Piccoli, 1989). This extrapolated analysis is supported by the silica-alkalis diagram (Figure 2.14) and the AFM ternary diagram (Figure 2.15). Calc-alkaline samples are considered to be subduction related, whereas the alkali-calcic signature can indicate either compressional or extensional environments (Brown, 1982).

2.3.2 Plutonic/Volcanic Relationship

The eight volcanic clasts are plotted with the granitoids in all discrimination diagrams.

All volcanic clasts are peraluminous with an ASI between 1.02 - 1.31, and generally have higher ASI values than the majority of granitoids. The volcanic clasts have suffered a greater degree of weathering than the granitoids (obvious in the sericitization and saussuritization of feldspars), and the ASI may therefore be an unreliable indicator of source and in this regard is not considered further.

Volcanic clasts tend to parallel the characteristic ranges, diversity and trends exhibited by the less evolved granitoids indicated in the Rb-Ba-Sr ternary diagram (Figure 2.12). The three least fractionated samples are volcanic, a feature recognized in plutonic/volcanic associations where a petrogenetic link has been established; the extrusive phase is early in the development of the magmatic suite, with subsequent evolution of the intrusive magma prior to eventual crystallization (Brown, 1982).

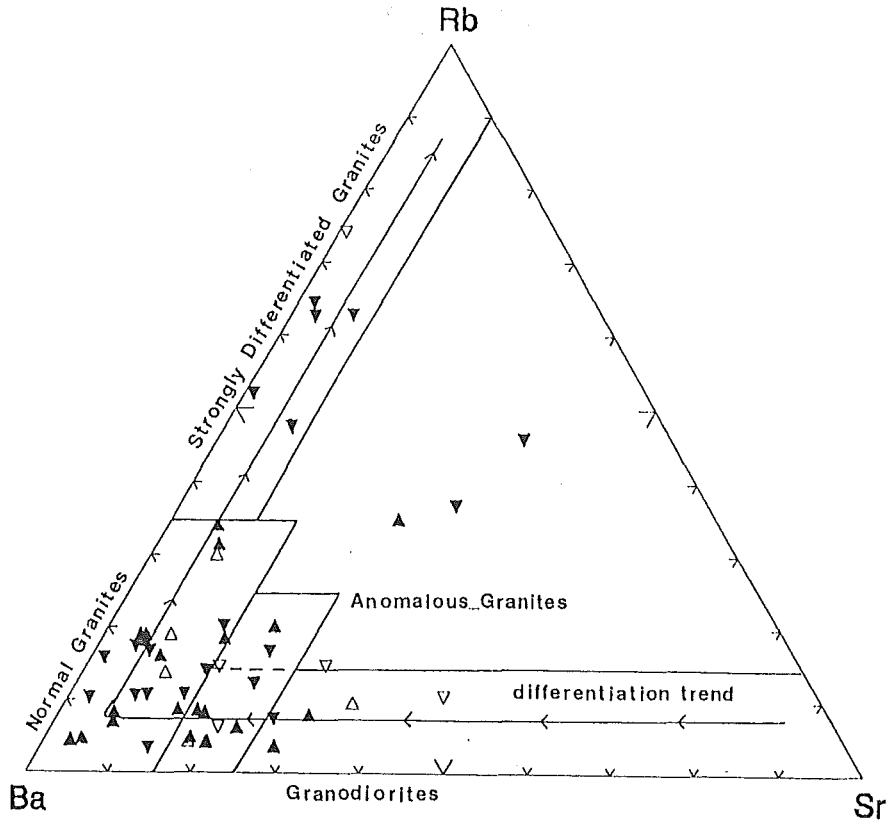

Figure 2.12: Rb-Sr-Ba ternary diagram illustrating the relationship between Chatham Islands conglomerate clasts.
(after El Bouseily and El Sokkary, 1975)

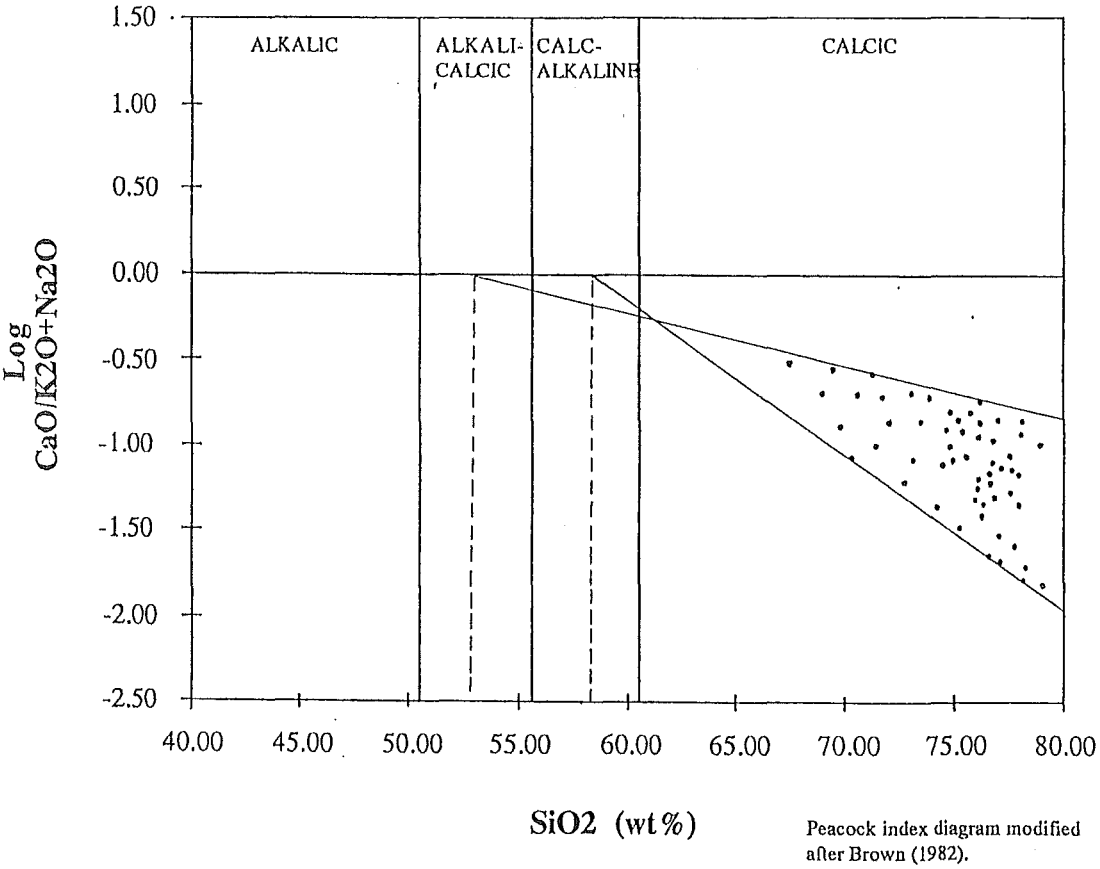

Peacock index diagram modified after Brown (1982).

Figure 2.13: Alkali-lime Index (definition Appendix 4) illustrating extrapolated values for Chatham Islands conglomerate clasts.

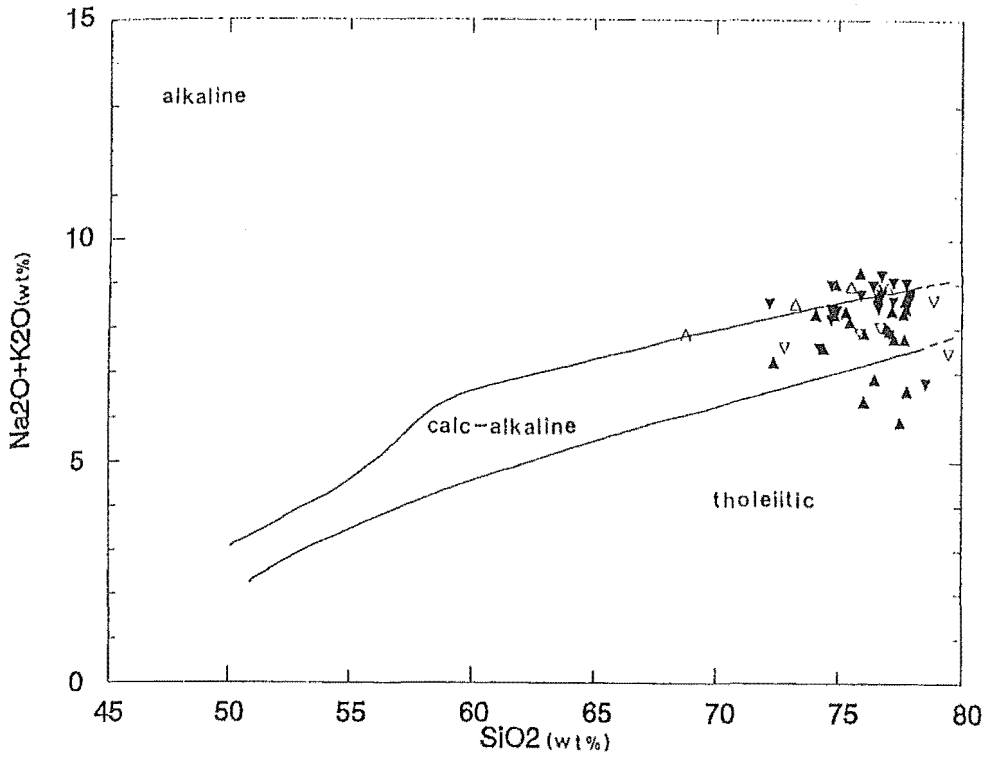

Figure 2.14: Alkali-silica diagram illustrating distribution of Chatham Islands conglomerate clasts between alkaline, calc-alkaline, and tholeiitic fields.
(after Kuno, 1968)

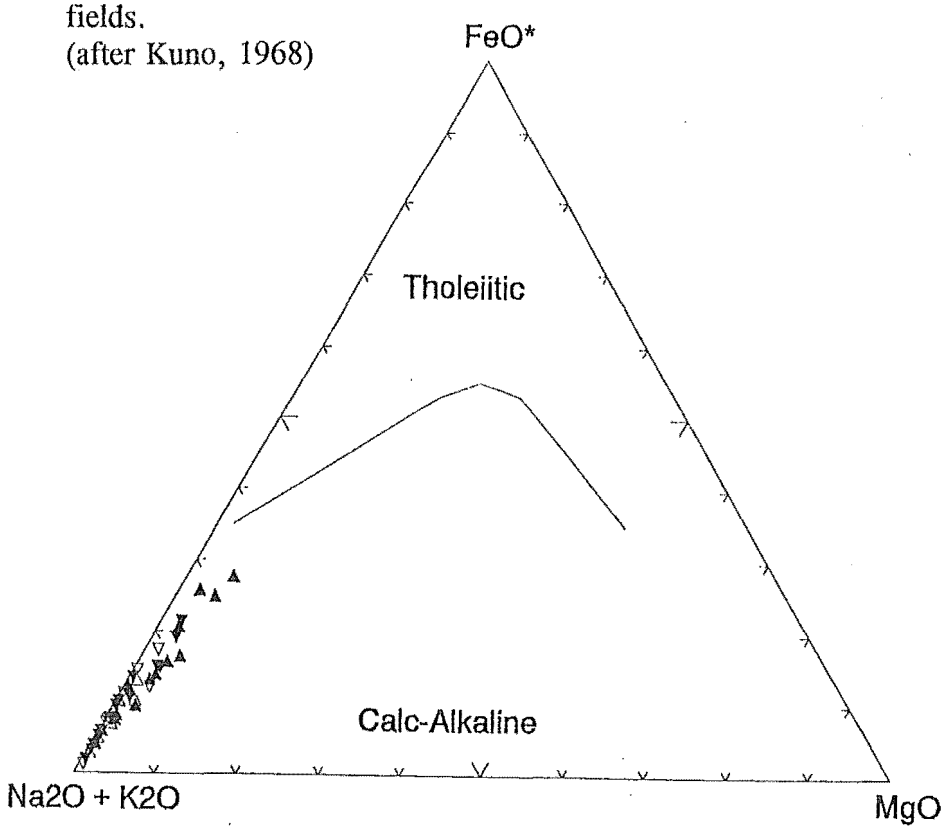

Figure 2.15: AFM (Na_2O+K_2O; Total iron as FeO; MgO) ternary diagram illustrating distribution of Chatham Islands clasts. The dashed line separates tholeiitic and calc-alkaline compositions.
(after Irvine and Baragar, 1971)

Volcanic clasts plot with the main concentration of granitoid clasts that have a K_2O/Na_2O ratio of approximately 1:1, as shown in the K_2O-Na_2O-CaO ternary plot (Figure 2.16). All samples have relatively low CaO which is consistent with their felsic character and restricted compositional range.

Trace element abundance diagrams normalized to primitive mantle (Sun and McDonough,1989) can be used to indicate any gross elemental differences between volcanic and granitoid rocks and to reflect source rock characteristics. Chatham Island clasts, when plotted, display the distinctive spiked patterns indicative of subduction related magmas (Figure 2.17) (Wilson, 1989; Saunders *et al.*, 1991) There is generally a selective enrichment of the incompatible large ion lithophile (LIL) elements (which have high ionic radius/charge ratios and include Rb, K, Sr, Ba, Th, Ce and La), and a low abundance of heavy field strength (HFS) elements (which have low ionic radius/charge ratios and include Ti, P, Zr, Nb, Ga and Y) (Figure 2.17a and b) (Cox *et al.*, 1979). Granitoid and volcanic patterns show a basic similarity indicating comparable sources (Figures 2.17a, b and d). The scatter noted in samples with primary muscovite (± biotite) may indicate varying degrees of crustal contamination or heterogeneous sedimentary source composition (Figure 2.17c). The distinctly high concentration of Nb (65ppm *cf.* with an average of 12ppm) and comparatively low concentrations of Zr, Ce and La noted in one sample (PD14/24086) suggests this granitoid, an S-type (ASI 1.17), had a relatively complex source composition that may not have been influenced by subduction (Harris *et al.*, 1986).

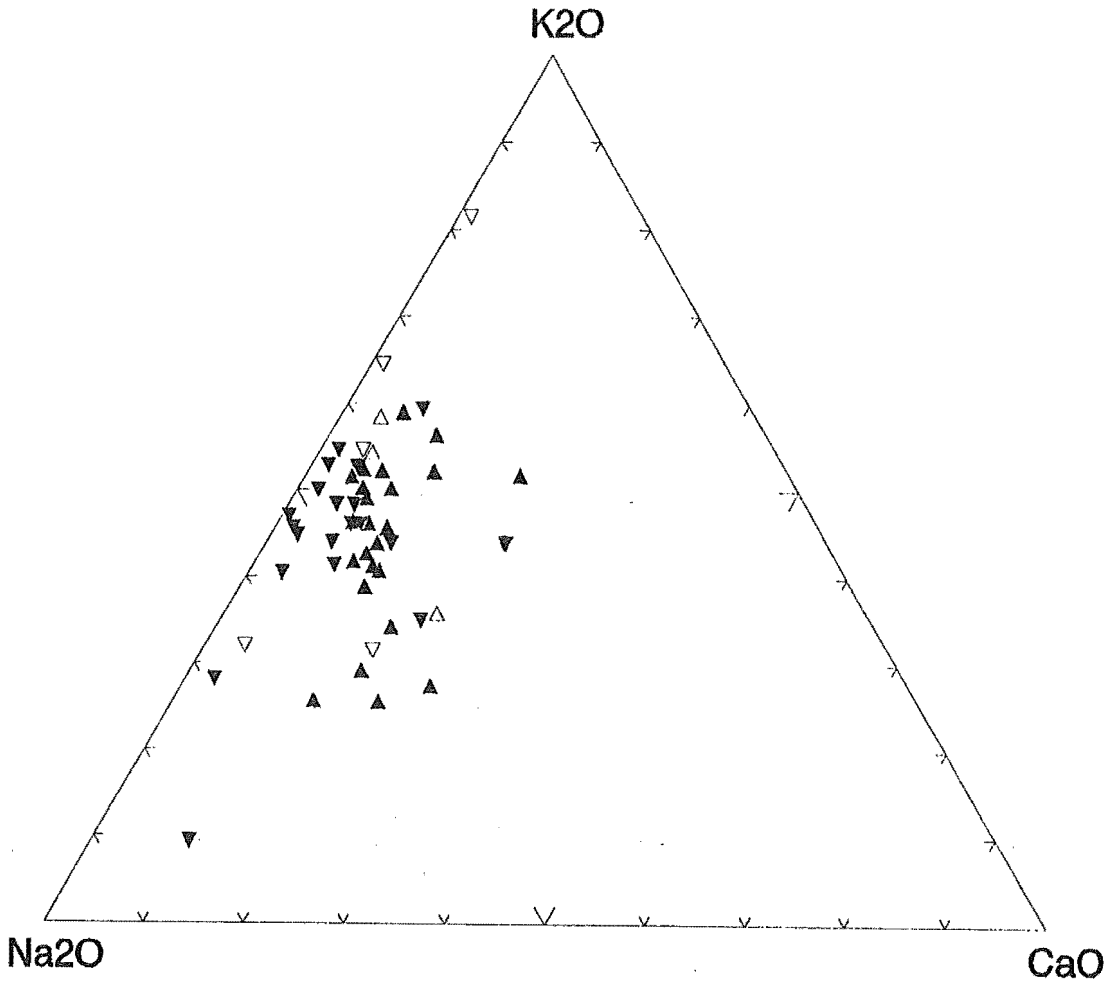

Figure 2.16: K_2O-Na_2O-CaO ternary diagram which illustrates the K_2O/Na_2O ratio, and considers CaO for Chatham Islands conglomerate clasts.

Figure 2.17: Multi-element primitive-mantle-normalized (Sun and McDonough, 1989) abundance diagrams for Chatham Islands conglomerate clasts.
a fractionated granitoids (I-types)
b highly fractionated granitoids (I- or S-types)
c muscovite ($\pm$ biotite) granitoids (S-types)
d volcanic clasts

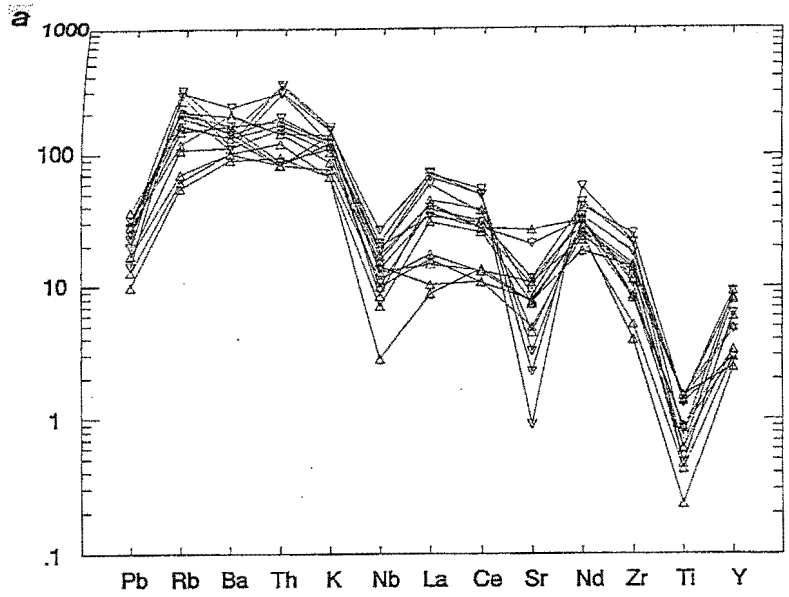
a
1000
100
10
1
.1
Pb Rb Ba Th K Nb La Ce Sr Nd Zr Ti Y

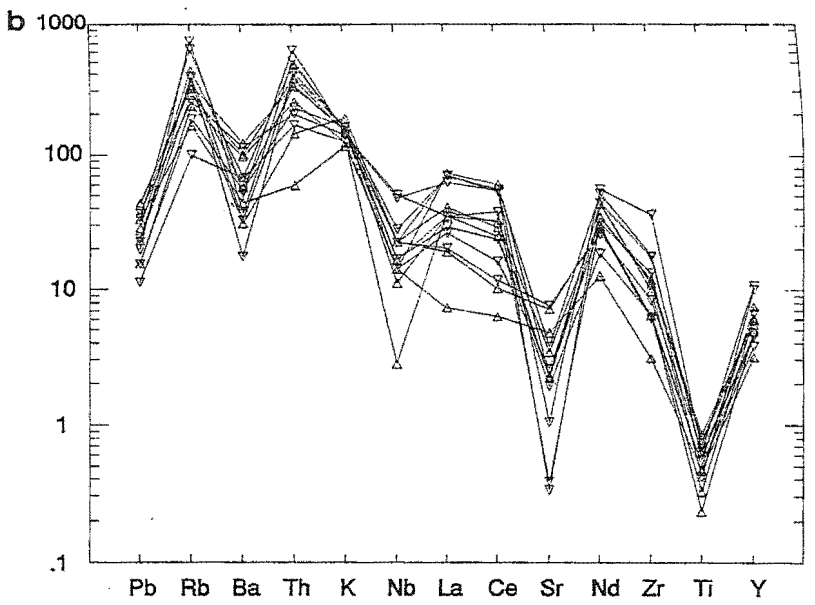
b
1000
100
10
1
.1
Pb Rb Ba Th K Nb La Ce Sr Nd Zr Ti Y

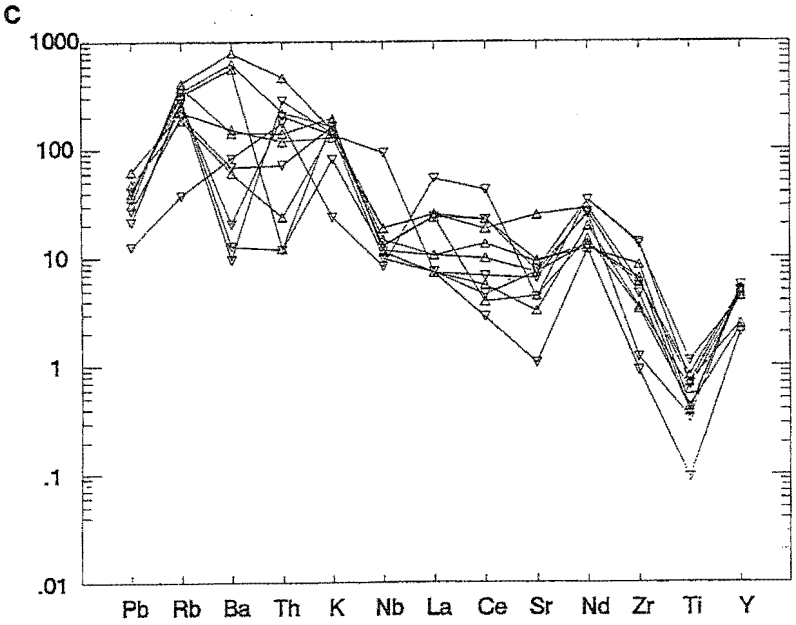
c
1000
100
10
1
.1
.01
Pb Rb Ba Th K Nb La Ce Sr Nd Zr Ti Y

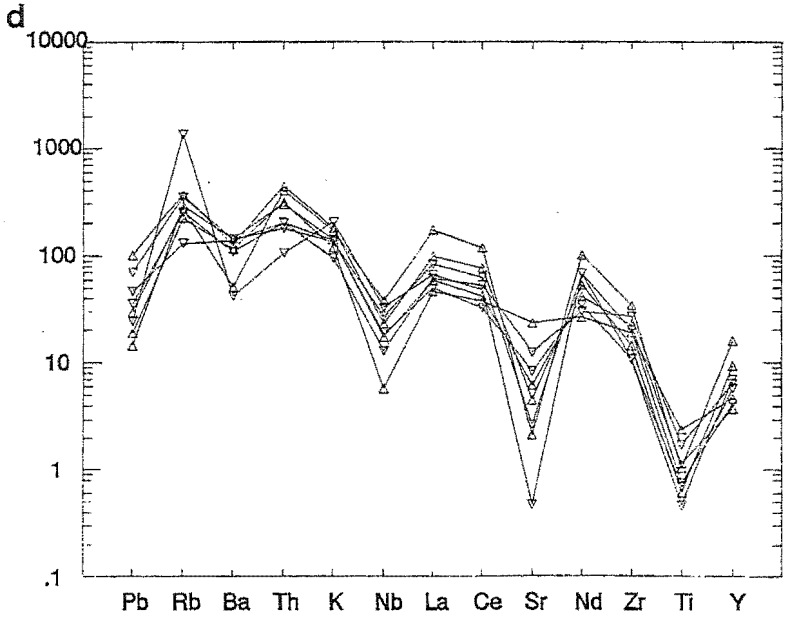
d
10000
1000
100
10
1
.1
Pb Rb Ba Th K Nb La Ce Sr Nd Zr Ti Y

2.3.3 Correlation with Mineralogy

The felsic nature of all samples can be seen distinctly in the geochemistry (high SiO_2, low Fe,Mg) and in thin section by the paucity of mafic minerals. In the majority of samples the only mafic phase recognized was biotite.

The peraluminous granitoids that contain Al-rich minerals were designated S-type. In the more strongly peraluminous samples (ASI > 1.1) there are commonly two Al-rich minerals present (muscovite and garnet). The highly peraluminous syenogranite sample (WB11/23994 - ASI 1.6) is metamorphosed, with secondary muscovite accounting for the majority of 28.2% modal muscovite and, therefore, the extreme peraluminous character. Muscovite is present in metaluminous granitoid samples in minor amounts (< 1%) but is considered secondary and the result of feldspar alteration.

The majority of samples designated I-types contain opaque Fe/Ti oxides that by crystal form were identified as magnetite, plus allanite. Accessory apatite and zircon were not restricted to one mineral composition. Prevalent biotite colour and pleochroism is dark to light brown and could not be used to distinguish I- and S-types (White and Chappell, 1983).

A peraluminous sample (PD16/24021, ASI 1.12) contained significant tourmaline (7.8%) and euhedral garnet (1.0%), and consistently deviated from the general trend in geochemical discrimination diagrams. This sample had a relatively high P_2O_5 content (0.29 wt%, *cf.* average 0.06 wt%), as does PD14/24086, the

sample mentioned previously with regard to unusually high Nb content. In both samples high P_2O_5 abundance is unexpected due to very low calcium content, lack of appreciable apatite and no monazite in thin section. Phosphorous (as PO_4) will replace some of the silica tetrahedral group in spessartine garnet (Deer *et al.*, 1966). The presence of garnet and the elevated MnO content of these samples supports this likelihood, but MnO content can also be accounted for by tourmaline composition (schorl) (Deer *et al.*, 1966). The presence of tourmaline and large muscovite plates may be indicative of late stage metasomatic or fumerolic alteration and it is possible that these samples could originally have formed part of a pegmatite.

The clasts identified as having distinctive geochemical characteristics indicative of A-type granitoids are distinguishable texturally as predominantly undeformed high-level hypersolvus granophyres or subsolvus samples with true granitic texture.

2.3.4 Discrimination of Tectonic Setting

It has been proposed that a fundamental relationship exists between trace element concentrations and tectonic environment (Pearce *et al.*, 1984; Whalen *et al.*, 1987). Pearce *et al.* (1984) suggest that mineralogical and major element based classification systems use discriminants that do not distinguish tectonic setting and they devise diagrams that relate geochemistry to tectonic environment by investigating granites from known tectonic setting. By using total abundances (ppm) and different ratio combinations in such recognized discrimination diagrams a fundamental interpretation of the tectonic setting of granitoid intrusion for the

Chatham Islands conglomerate source area can be made.

The majority of Chatham Island conglomerate clasts plot within the volcanic arc granite (VAG) and syn-collision granite (syn-COLG) fields (Figures 2.18a and b). Nine clasts plot in the within plate granite (WPG) field (PD1/24010, PD4/24013, PD6/24015, PD9/24018, PD14/24086, PD15/24023, PD20/24028, WB19/24001, WB21/24003), and are the same samples that plot apart and to the right of others in the A-type fields developed by Whalen *et al.* (1987) (Figures 2.10 and 2.11). This provides further support of A-type affinities for some of the granitoid and volcanic clasts.

The WPG/A-type samples represent both granitoid and volcanic clasts from Parran Dam, but only volcanic samples from Waihere Bay. Campbell *et al.* (in press) note that the Waihere Bay conglomerate outcrop represents the stratigraphically oldest exposed conglomerate outcrop. This suggests that the exposed source area contained WPG/A-type volcanics at the time of Waihere Bay conglomerate deposition, but that later uplift and/or erosion and the unroofing of subjacent hypabyssal and plutonic equivalents occurred before the Parran Dam conglomerate was deposited.

2.4 Synopsis

Granitoid clasts from the Chatham Islands conglomerate range in modal composition from predominantly leucosyenogranites to leucotonalite. Volcanic clasts are predominantly porphyritic or spherulitic rhyolites with features that suggest a

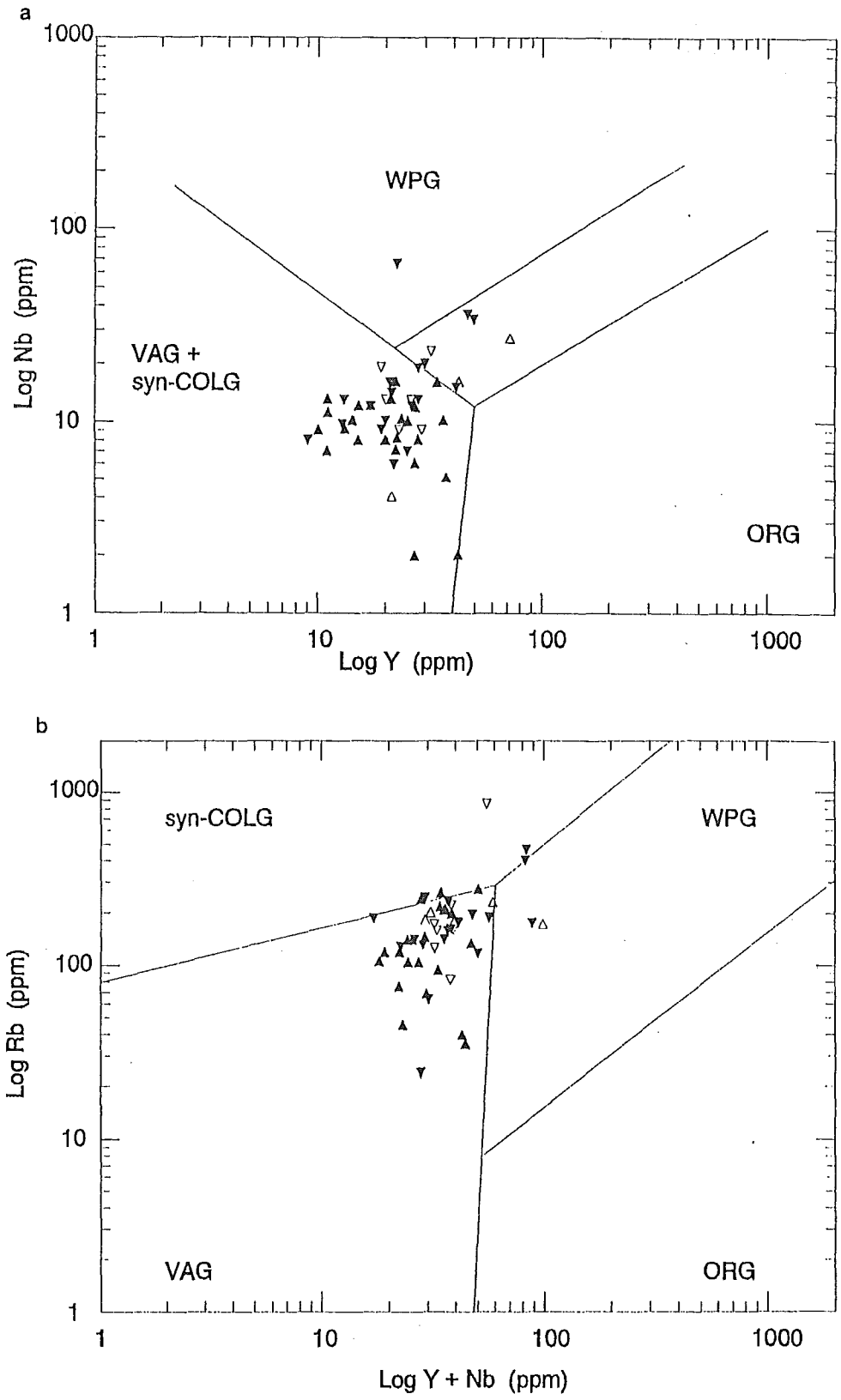

Figure 2.18: Tectonic discrimination diagrams illustrating distribution for Chatham Islands conglomerate igneous clasts within the syn-collision (syn-COLG), volcanic arc granite (VAG), within plate granites (WPG), and ocean ridge granites (ORG) fields:
a Nb-Y
b Rb-Y+Nb.
(after Pearce *et al.*, 1984)

pyroclastic origin or crystallization within a rhyolite dome.

Textural features distinguish high-level hypersolvus granitoids, which could be subvolcanic and related to the rhyolite samples. Undeformed subsolvus granitoids could represent variants of the same magma crystallized under higher water pressure with no vapour exsolution, or central regions in a pluton with foliated margins. Foliated subsolvus granitoid clasts display varying intensities of deformation that indicate either syntectonic crystallisation or post-intrusive tectonism.

Geochemistry distinguishes predominantly I-type and evolved I-type granitoid and volcanic clasts. Clasts with S-type and A-type characteristics are also present.

The majority of Chatham Island conglomerate samples display features indicative of subduction related magmas.

2.5 Discussion

The various geochemical parameters outlined in previous sections indicate that the source terrain for the Chatham Island igneous conglomerate clasts contained igneous rocks, intrusive and extrusive, primarily related to subduction along an active continental margin.

The granitoid clasts examined are primarily I-types, the result of partial melting of an igneous source. Evolved I-types are present, and S-types are represented indicating increased crustal contamination, the involvement of a

supracrustal component, and the temporal and spatial evolution of the volcanic arc.

The A-type characteristics evident in some granitic and volcanic samples suggests that A-type magmatism did occur, perhaps as a consequence of the cessation of subduction and the progression to anorogenic conditions and the alkaline rocks characteristic of such conditions. A-type granitoids are recognized from such environments as representing either melting of I-type granitoids or partial melting of a depleted crustal source as a result of thermal relaxation and a lowering of the geothermal gradient.

The parallelism of granitoid and volcanic clast characteristics and the hypersolvus/hypabyssal textural features exhibited by some plutonic samples indicate a subvolcanic nature and possible cogenesis. The lack of in situ evidence or age control make cogenetic interpretation conjectural.

The absence of mafic clasts (plutonic or volcanic) with a tholeiitic geochemical signature indicates the initial stages of magma intrusion related to subduction are not recorded within the conglomerate. The presence of highly deformed gneissic and mylonitic granitoids indicate intrusive levels below volcanic/subvolcanic were exposed at the time of conglomerate deposition.

Felsic rocks only may have been present in the source area. However, the geochemical signature of most Chatham Island samples indicates that highly evolved samples are present and this implies evolution from a more mafic, primitive source. The trace element abundances of some samples indicate that they could represent

minimum melts.

The conglomerate was not considered to have been selectively sampled. Collection of clasts was undertaken by several individuals who endeavoured to collect anything remotely crystalline. Thousands of clasts were cut and the hand specimens examined prior to final clast selection.

Selective preservation of differing lithologies by the conglomerate may have occurred. Considering clast morphology this could be likely. The interlocking structure of granophyric samples lends itself to preferential preservation. However, the presence of preserved, albeit generally highly weathered, rhyolitic samples within the conglomerate would seem to negate this argument.

It is concluded that preservation of the Chatham Island conglomerate igneous components records the complex evolution of an active continental margin. Subduction with consequential intrusion and related volcanic activity took place at some stage prior to the deposition of the conglomerate in the Early Cretaceous.

At the time of conglomerate deposition (~100Ma), the source area exposed subvolcanic intrusions and related volcanics, presumed to be remnants of rhyolitic domes, plus pyroclastic/ignimbritic deposits.

A spectrum of intrusive levels are indicated by the exposure of hyper- and subsolvus granitoids. The deformed granitoids with mylonitic and gneissic textures indicate synchronous and/or subsequent deformation at subsolvus levels (i.e. $\geq$5kb).

CHAPTER 3

ETHELTON CONGLOMERATE

3.1 Introduction

3.1.1 Locality

The old Kaiwara suspension bridge that spans the Hurunui River about 3.5kms west-northwest of Ethelton, North Canterbury, marks the location of a substantial (~150m thick), moderately indurated, massive to well bedded, clast to matrix supported, pebble to boulder sized conglomerate outcrop (NZMS 260, 1:50,000, N33 Culverden, grid ref. 127/149) (Figures 1.2 and 3.1).

The conglomerate is exposed both sides of the Hurunui River for approximately 300m to the northeast and southwest of the bridge where it fills scour channels in, and is interbedded with, massive and graded sandstones and mudstones that strike northeast and dip vertically (Figure 3.2) (Maxwell, 1964; Smale, 1978).

Detrital plant fragments and the presence of dinoflagellates in the conglomerate matrix suggest a near-shore marine depositional setting (Maxwell, 1964; Smale, 1978). A source area to the southwest is postulated based on flute casts in the underlying sediments, and the angle between the layering within the conglomerate and bedding in enclosing sediments when the latter is rotated back to horizontal (this can vary up to 35°) (Smale, 1978).

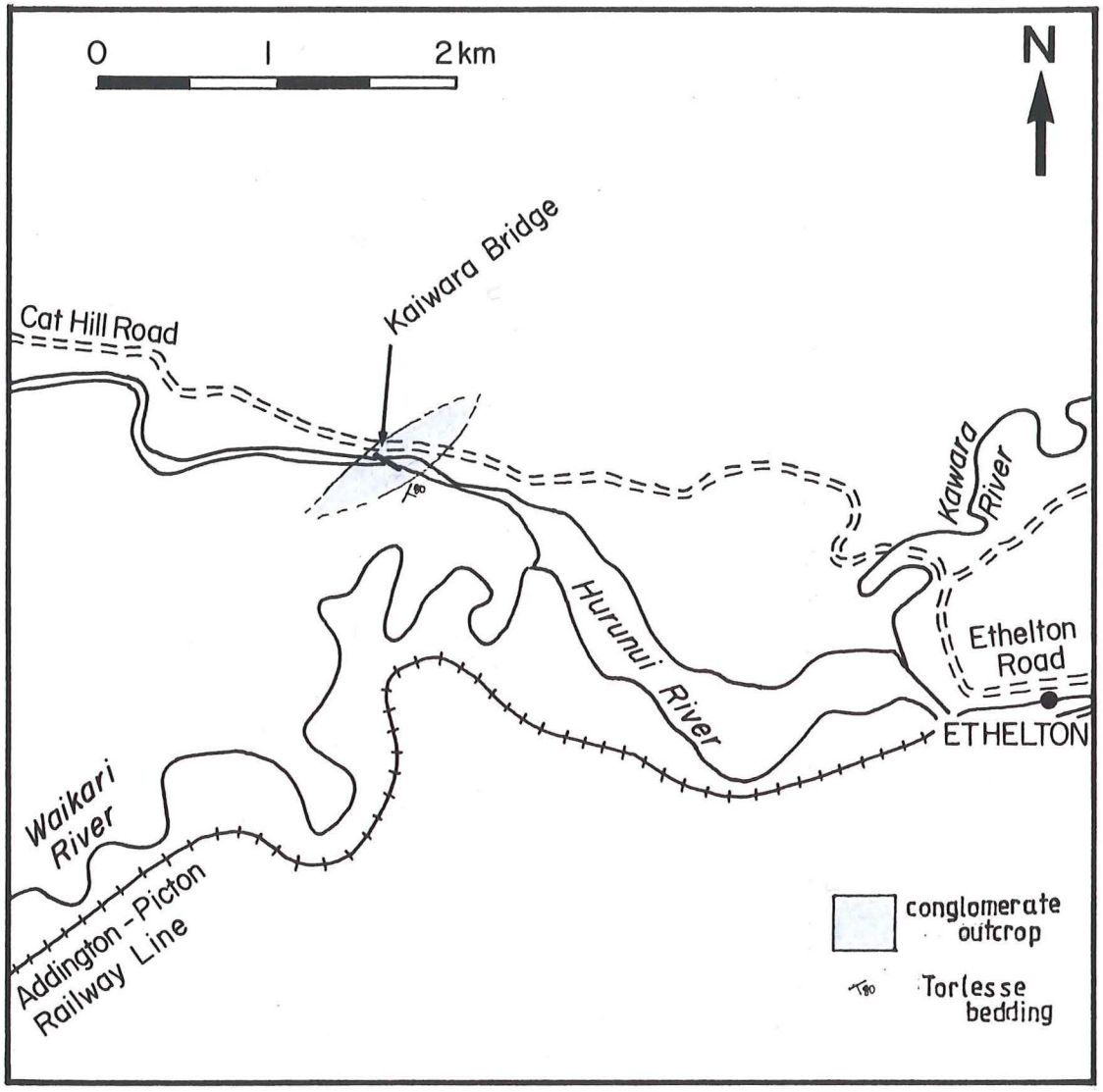

Figure 3.1: Ethelton conglomerate locality map (after Maxwell, 1964).

3.1.2 Previous work

Speight (1914) mentions a conglomerate outcrop along the Hurunui River when discussing the occurrence and provenance of Mesozoic granitoid clasts in several conglomerates. Speight (1928) briefly discusses the similarity and probable association between several North Canterbury conglomerates, including the Hurunui River outcrop.

The conglomerate was described and included in the Kaiwara Bridge Formation by Hamilton (1950). Coombs *et al.*(1959) briefly discusses the presence of schistose pebbles in a conglomerate exposed along the south bank of the Hurunui River, and McKellar *et al.*(1962) make reference to a Late Jurassic belemnite found within the conglomerate. In a general account of the geology of the Kaiwara area the conglomerate was described by Maxwell (1964) and named the Ethelton Conglomerate.

The Torlesse sediments, of which the Ethelton conglomerate is a part, were originally assigned an Upper Jurassic age on the 1:250,000 Hurunui Sheet (Gregg,1964), and on the 1:1,000,000 Geologic Map of New Zealand (1972) at this location. Based on palynological evidence the Ethelton conglomerate is now believed to be Early Cretaceous in age and considered part of the Pahau subterrane (Smale, 1978).

Smale (1978) provides a general petrographic and sedimentological account of the Ethelton conglomerate and its component lithologies and gives a brief discussion

Figure 3.2: Ethelton conglomerate:
a interbedded with massive and bedded sandstones, dipping to the NE
b conglomerate outcrop looking NNE
c bedded conglomerate
d bedded conglomerate showing assortment of clast sizes and compositions.
(Case for scale = 18cms)

a

b

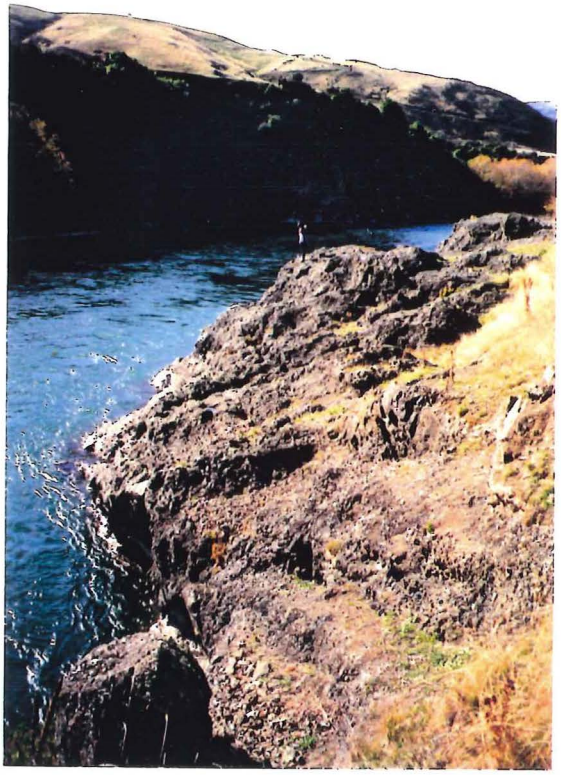

c

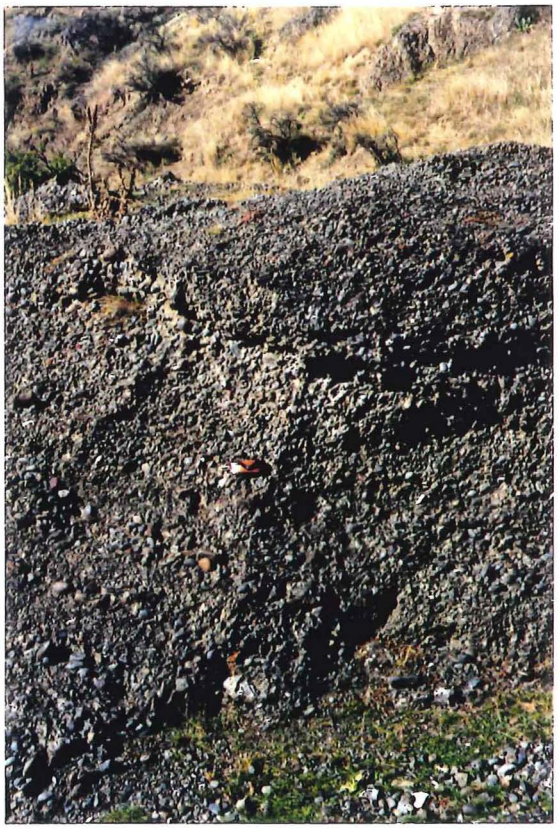

d

on probable provenance.

Limestone and radiolarian chert clasts from the Ethelton conglomerate were sampled by Silberling *et al.* (1988) and used, along with clasts from other Pahau sub-terrane conglomerates, to compare with similar blocks found in the Esk Head mélange.

3.2 Petrography

The recalculated point count data for the Ethelton granitoid clasts (Appendix 3) were plotted on the QAP ternary diagram (Figure 3.3). Samples concentrate within the granodiorite, monzogranite and syenogranite fields.

Further subdivisions are made according to mineralogical and textural analyses following the procedure outlined in Chapter 1, 1.3.4a, and defined in Chapter 2, 2.3.

3.2.1 Granitoid Clast Descriptions

Ethelton granitoid conglomerate clasts are divisible into eight distinctive groups (Figure 3.4):

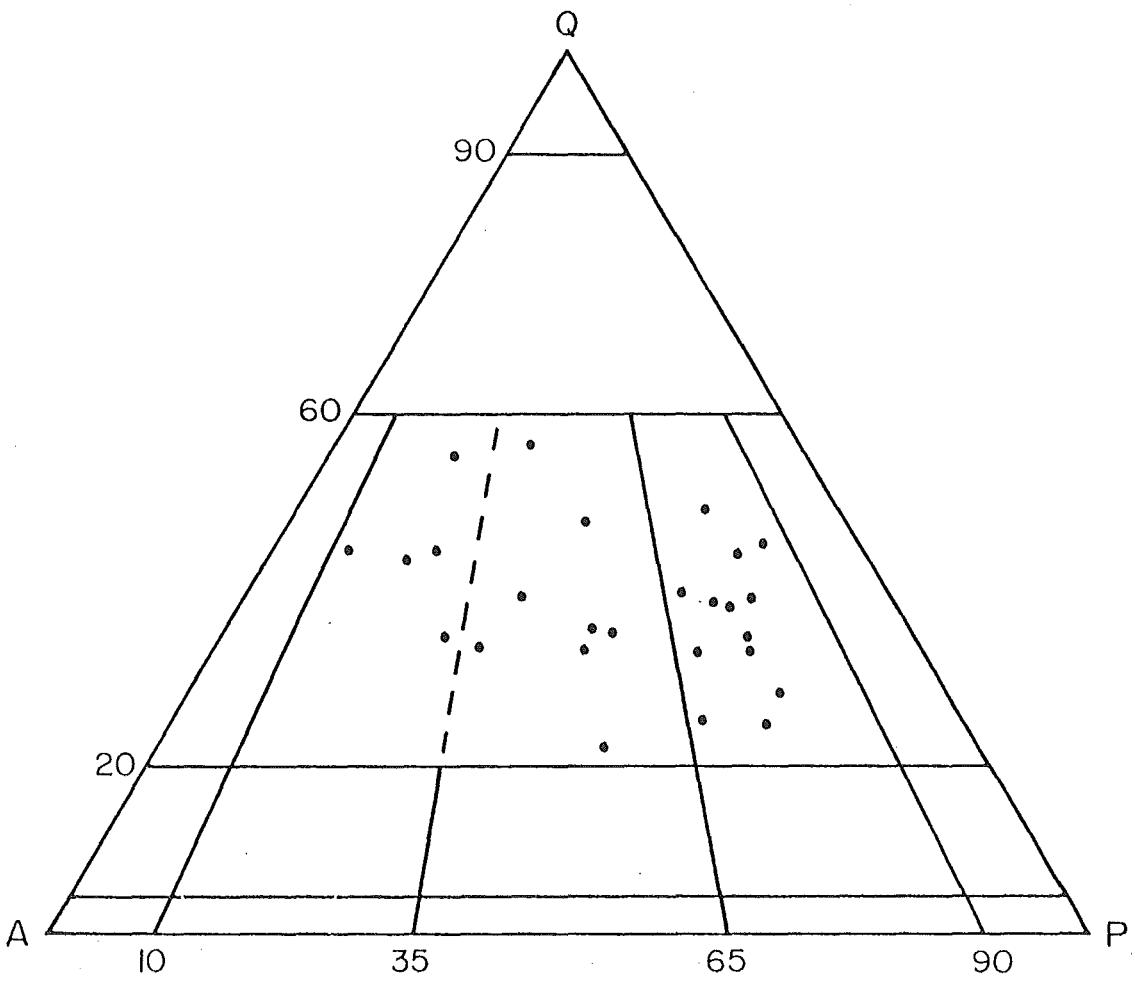

Figure 3.3: Quartz - Alkali Feldspar - Plagioclase ternary diagram illustrating modal distribution for Ethelton conglomerate granitoid clasts (see Chapter 1, 1.3.4a for definition of fields).
(after Le Maitre, 1989)

Group ETHG-1:

Subsolvus, holocrystalline, medium grained, equigranular, muscovite biotite leucosyenogranite:

The subhedral plagioclase is sodic oligoclase (An10-15%) with incipient albite and Carlsbad twinning. The anhedral alkali feldspar was indeterminable due to incipient kaolinization but appeared perthitic.

Chloritized brown biotite and muscovite are both minor phases, in approximately equal proportions, usually associated with anhedral opaque Fe/Ti oxides.

Granitic and poikilitic texture (quartz and feldspar) predominate and deformation is limited to undulose extinction in quartz.

Secondary muscovite is also present, associated with the sericitization of the plagioclase feldspar.

Group ETHG-2:

Subsolvus, holocrystalline, medium to fine grained, equigranular, biotite leucosyenogranite:

The anhedral feldspar is predominantly perthitic alkali feldspar or mesoperthite which exhibits mortar texture around grain boundaries (Figure 3.5a). The subhedral and myrmekite component plagioclase is sodic oligoclase (An10-20%), displays secondary albite twinning, and has been partially saussuritized to epidote.

The anhedral quartz has undulatory extinction and appears as an extensively recrystallized mosaic that displays no distinctive SPO or LPO in the sections examined.

Figure 3.4: Representative photographs of modal, textural, and mineralogical granitoid groups (field of view ~5cms):
a Subsolvus, muscovite, biotite leucosyenogranite (ETHG-1)
b Hypersolvus, biotite leucosyenogranite (ETHG-3)
c Subsolvus, biotite leucomonzogranite (ETHG-4)
d Subsolvus, biotite granodiorite (ETHG-7)

a

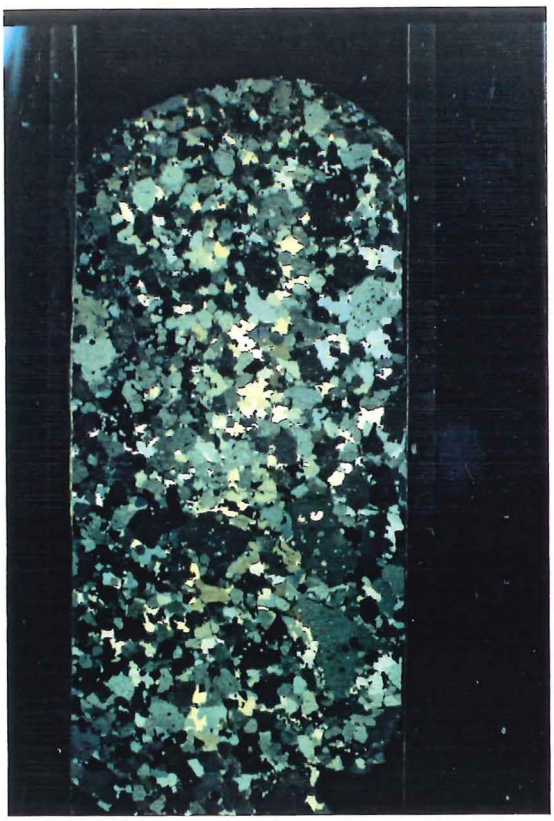

b

c

d

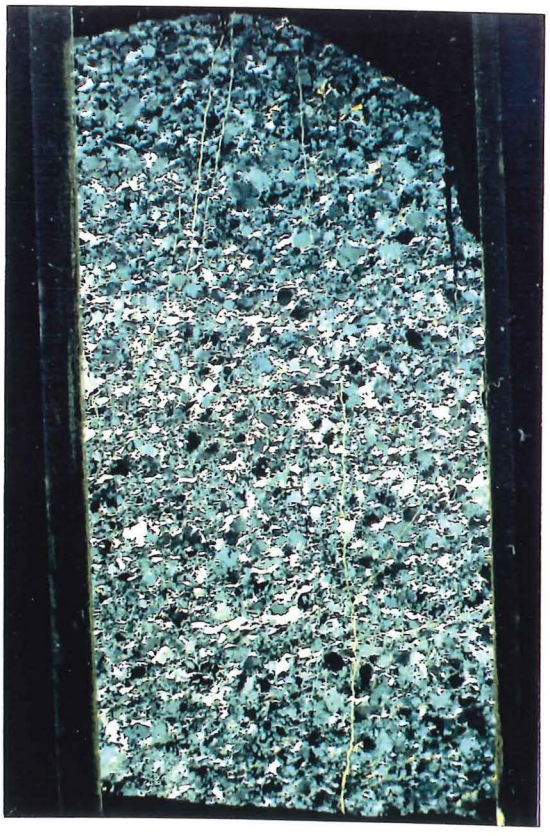

The green/brown pleochroic biotite has been partially altered to chlorite.

Accessory minerals include subhedral titanite, apatite, euhedral zircon, red/brown pleochroic allanite, and anhedral opaque Fe/Ti oxides.

Some secondary muscovite plates are associated with opaque Fe/Ti oxides and the chloritized biotite. Calcite forms anhedral pseudomorphs, and is commonly found infilling veins.

Group ETHG-3:

Hypersolvus, holocrystalline, coarse grained, equigranular, granophyric leucosyenogranite:

Samples in this group are typified by granophyric intergrowths of quartz and alkali feldspar visible in hand specimen.

Plagioclase is only present as exsolution lamellae in discrete perthitic alkali feldspar. Microcline transformation twinning is obvious.

Occasional ($<1\%$) brown biotite grains are almost totally replaced by chlorite.

Apart from the biotite relics, the original mineral(s) replaced by calcite and chlorite pseudomorphs cannot be determined with any certainty because of the lack of distinctive shapes. The pseudomorphs are frequently rimmed by opaque Fe/Ti oxides.

Group ETHG-4:

Subsolvus, holocrystalline, coarse to medium grained, porphyritic, biotite leucomonzogranite:

The subhedral plagioclase is sodic oligoclase (An11-25%) with zoned sericitized cores. The anhedral alkali feldspar is perthitic orthoclase. The anhedral interstitial quartz displays slight undulose extinction.

Euhedral to subhedral dark brown biotite crystals are generally associated with opaque material and have been partially altered to chlorite and epidote. The radioactive elements in included zircons have undergone decay and created dark pleochroic haloes in biotite reducing the pleochroism.

Accessory minerals include euhedral apatite and zircon, red/brown pleochroic allanite and opaque Fe/Ti oxides.

Samples are typically undeformed with granitic texture. Myrmekite was noted only as a minor feature.

Calcite/opaque Fe/Ti oxide pseudomorphs display a distinctive prismatic orthopyroxene shape.

Group ETHG-5:

Hypersolvus, holocrystalline, medium to fine grained, equigranular to porphyritic, granophyric, biotite leucomonzogranite:

Granophyric intergrowth is predominant and surrounds discrete crystals of plagioclase, alkali feldspar, mesoperthite and quartz.

The alkali feldspar is slightly kaolinized and perthitic. The plagioclase is euhedral to subhedral sodic oligoclase (An10-20%) that has been replaced by albite, epidote, clinozoisite, calcite and sericite. Albite has also crystallized as the result of

perthite exsolution. The quartz is relatively undeformed with slight undulatory extinction.

Pleochroic green/brown biotite, the only minor phase, is usually partially altered to chlorite.

Accessory minerals include subhedral red/brown pleochroic allanite, apatite and anhedral opaque Fe/Ti oxides.

Chlorite replacement of interstitial mafic minerals has occurred and pseudomorphs frequently contain apatite inclusions. Relic cleavages intersecting at ~90° suggest some pseudomorphs were originally pyroxene. Some were amphibole, as indicated by relic material within one pseudomorph.

Group ETHG-6:

Subsolvus, foliated, holocrystalline, medium to fine grained, equigranular to porphyritic, muscovite biotite granodiorite:

The plagioclase is subhedral to anhedral albite to sodic oligoclase (An5-15%) with normal zoning that is emphasized by sericitization. The anhedral alkali feldspar is orthoclase. Myrmekite is commonly associated with alkali feldspar/plagioclase grain boundaries.

The large (~2mm) anhedral quartz displays undulatory extinction and in some samples has a well developed SPO.

Dark brown pleochroic biotite and subordinate muscovite are frequently in association and form randomly oriented plates.

Accessory minerals include primary euhedral isotropic garnet, subhedral apatite and anhedral opaque Fe/Ti oxides.

The finer grained hypabyssal forms in this group are relatively undeformed as

indicated by the slight undulose extinction of quartz. Coarser porphyritic samples, however, display a pervasive foliation that is distinctly defined by well developed quartz ribbons and the alignment of sheet silicates. The quartz c-axes are strongly aligned parallel to the elongation direction indicating an LPO accompanies the SPO (Figure 3.5b).

Epidote and chlorite replacement of mafic minerals, notably biotite, is apparent.

Group ETHG-7:

Subsolvus, holocrystalline, medium to fine grained, porphyritic, biotite granodiorite:

The plagioclase is strongly zoned with albite to sodic oligoclase rims (An5-15%). The perthitic alkali feldspar occurs predominantly as interstitial anhedral orthoclase crystals. Myrmekite is common along alkali feldspar/ plagioclase grain boundaries.

In some sections the anhedral quartz exhibits intercumulate poikilitic texture, enclosing other minerals, particularly plagioclase.

Minor green/brown pleochroic biotite is common to all samples and is generally partially chloritized.

Accessory minerals include euhedral zircon, apatite, dark brown allanite (metamict), anhedral opaque Fe/Ti oxides and epidote.

In deformed samples the quartz has undergone a grain size reduction as a result of dynamic recrystallization and plastic deformation of quartz around resistant feldspar crystals.

Hypabyssal samples are relatively undeformed with plagioclase and corroded quartz phenocryst phases in a finer grained, but determinable granitic textured

matrix.

Calcite, chlorite and opaque minerals form pseudomorphs replacing previous mafic minerals that include biotite.

Group ETHG-8:

Hypersolvus, holocrystalline, medium to fine grained, porphyritic, granophyric, biotite granodiorite:

Samples in this group are typified by granophyric intergrowth that varies in coarseness and proportion. Within the matrix of some samples intergrowths are a minor component, very fine-grained, and indicating only the last residual liquid crystallized under hypersolvus conditions, whereas in others they are coarse and extensive.

A subsolvus history is evident in that plagioclase and alkali feldspar are present as independent crystals. The alkali feldspar is microcline ($2V_x$70-90°) which frequently forms a rim around the subhedral plagioclase which is albite (An5-10%).

The anhedral quartz is undeformed with straight extinction, and often skeletal.

The dark brown pleochroic biotite is randomly oriented and often contains inclusions of accessory apatite, zircon and zoned red/brown pleochroic allanite.

Calcite, chlorite and opaque Fe/Ti oxides replace the mafic minerals that were present.

Figure 3.5: Photomicrographs of thin section features (field of view = ~7mm):
- **a** Mesoperthite and quartz
- **b** LPO of quartz with c-axes aligned parallel to foliation
- **c** Bipyrimidal and skeletal quartz
- **d** Chlorite pseudomorph after hornblende with relic cleavages that intersect at 120°
- **e** Skeletal quartz phenocryst in rhyolite
- **f** Chlorite pseudomorph after hornblende surrounded by spherulites

(key to symbols Appendix 4)

a

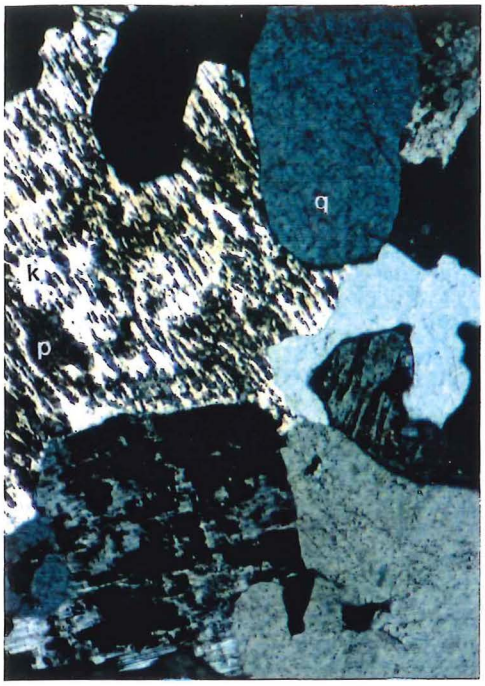

b

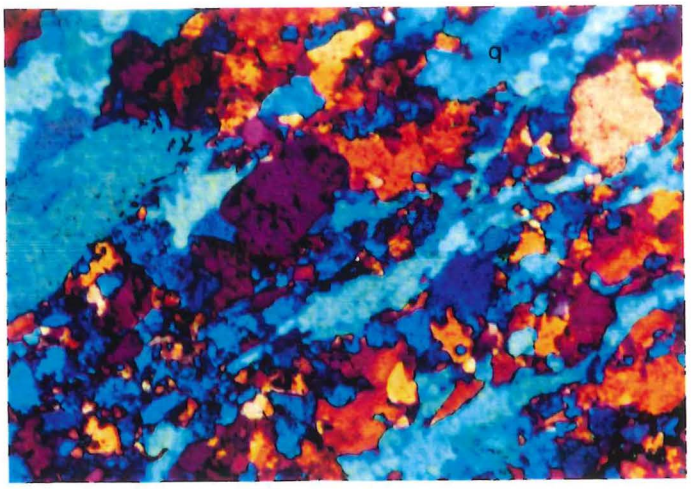

c

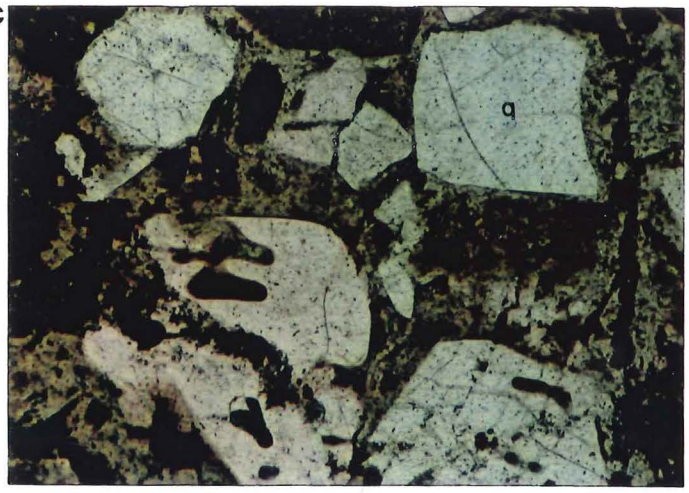

d

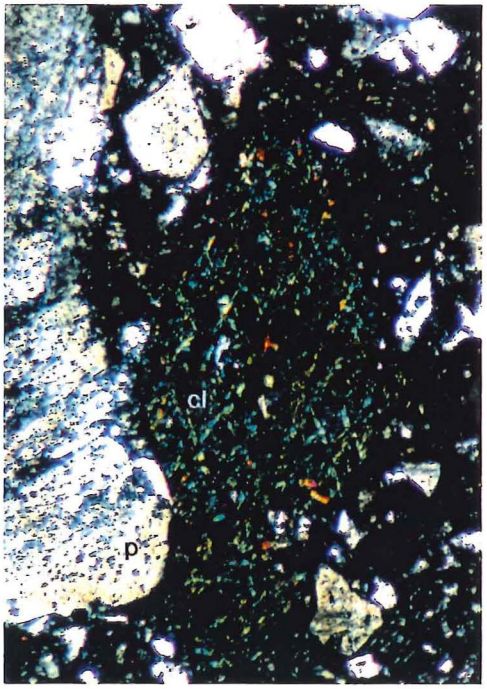

e

f

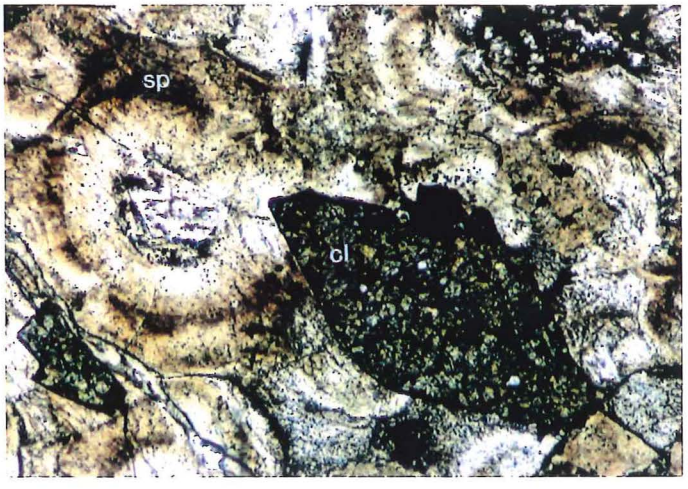

3.2.2 Volcanic Clast Descriptions

Ethelton volcanic clasts are geochemically divisible into two categories but form a continuum from one type to the other as illustrated in Figure 3.6. Mineralogical and textural descriptions are made subsequent to the initial geochemical grouping (Figure 3.7):

Group ETHV-1:

Hypocrystalline porphyritic rhyolite:

Phenocrysts comprise 6 - 70% of the rhyolite samples.

Phenocryst phases include extensively embayed and/or euhedral bipyrimidal undeformed quartz crystals (often >1cm) with symmetrical extinction (Figure 3.5c). Euhedral to subhedral, generally complexly zoned plagioclase that is albite ($An<10\%$) and/or calcic oligoclase ($An\sim25\%$), is often fractured and angular with sericitized or saussuritized cores. The anhedral perthitic alkali feldspar is generally optically indeterminable due to kaolinization, but some sanidine was identified ($2V_x 10\text{-}20^\circ$).

Dark brown biotite is often associated with opaque Fe/Ti oxides and euhedral primary epidote.

Pseudomorphs comprising calcite, chlorite, epidote and opaques with inclusions of apatite, epidote and secondary muscovite are present. One euhedral prismatic chlorite and epidote pseudomorph displayed two cleavages intersecting at $120^\circ/60^\circ$ and lined with sericite indicative of hornblende (Figure 3.5d).

Accessory minerals include euhedral zircon, subhedral apatite, red/brown pleochroic allanite and subhedral titanite.

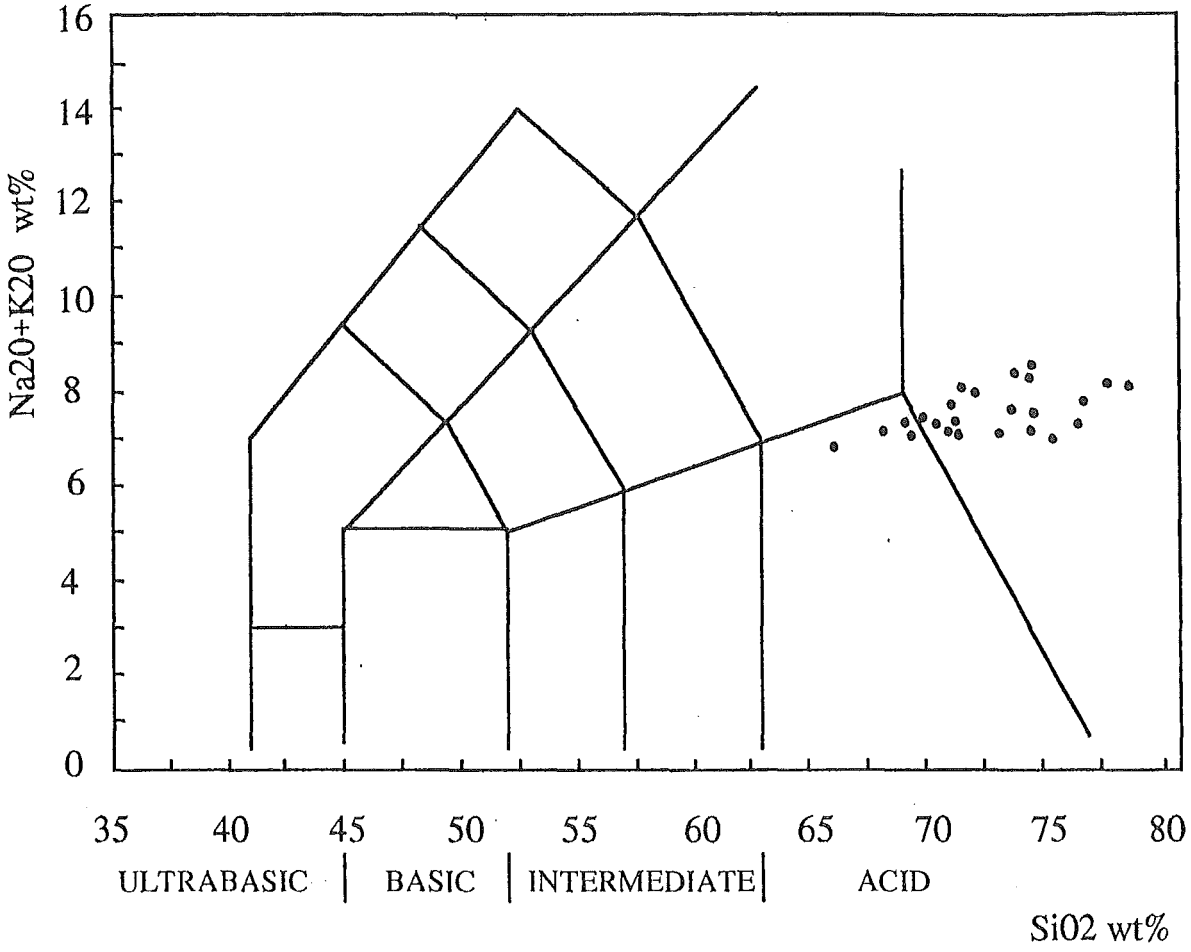

Figure 3.6: TAS classification illustrating distribution for Ethelton conglomerate volcanic clasts.
(after Le Maitre, 1989)

Phenocrysts often cluster producing mono- or polymineralic glomeroporphyritic texture. In some samples quartz phenocrysts are rare or absent.

The matrix comprises a finely crystalline felsitic mixture of quartz, alkali feldspar with disseminated opaque Fe/Ti oxides, chlorite and epidote that have replaced mafic minerals. In some samples the matrix exhibits trachytic texture with feldspar lath alignment due to magmatic flow. Flow texture was frequently observed around phenocrysts. Poikilomosaic texture has developed with the progressive devitrification of quartz and feldspar (Shelley, 1992). Spherulites, often coarsening outwards into fine granophyric intergrowths are a common feature.

Large vesicles (lithophysae) often contain rhombohedral quartz terminations and are filled with calcite or quartz.

Group ETHV2:

Hypocrystalline porphyritic dacite:

Xenoliths contribute between 40 to 80% of these rocks and include a variety of lithic fragments, both volcanic and plutonic, that display a diversity of textures. Textures noted in the volcanic lithic fragments include pumiceous, trachytic, spherulitic, eutaxitic and porphyritic with felsitic matrix.

Phenocrysts are subordinate to xenoliths and include quartz that is anhedral and extensively embayed (Figure 3.5e). The plagioclase phenocrysts are albite ($An < 10\%$) with vague albite twinning.

Accessory minerals include euhedral and fragmental zircon, red/brown allanite, brown biotite and opaque Fe/Ti oxides.

Calcite, chlorite, epidote pseudomorphs have replaced mafic minerals. A relic, identified as amphibole, was noted at the centre of one calcite pseudomorph

Figure 3.7: Representative photographs of Ethelton volcanic groups (field of view ~5cms):
a and b Porphyritic rhyolites with skeletal quartz and fragmental phenocrysts (ETHV-1)
c and d Porphyritic dacites with volcanic lithic fragments and skeletal quartz phenocrysts (ETHV-2)

a

b

c

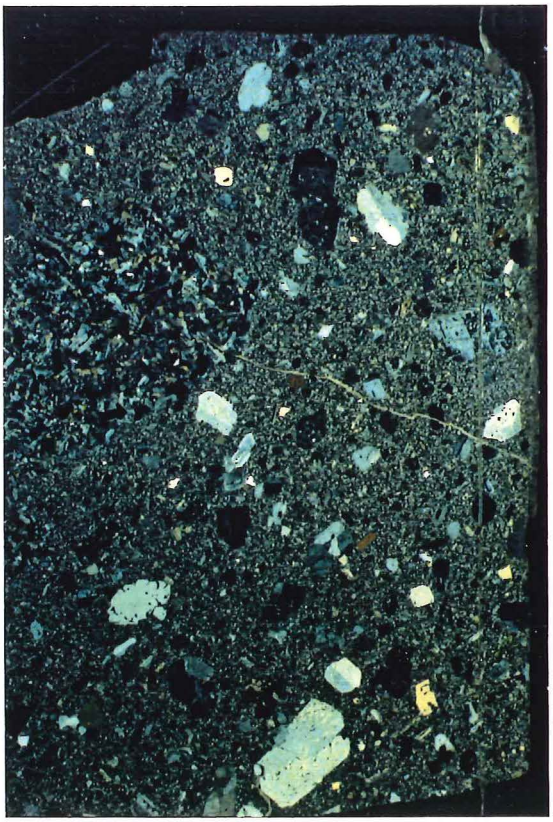

d

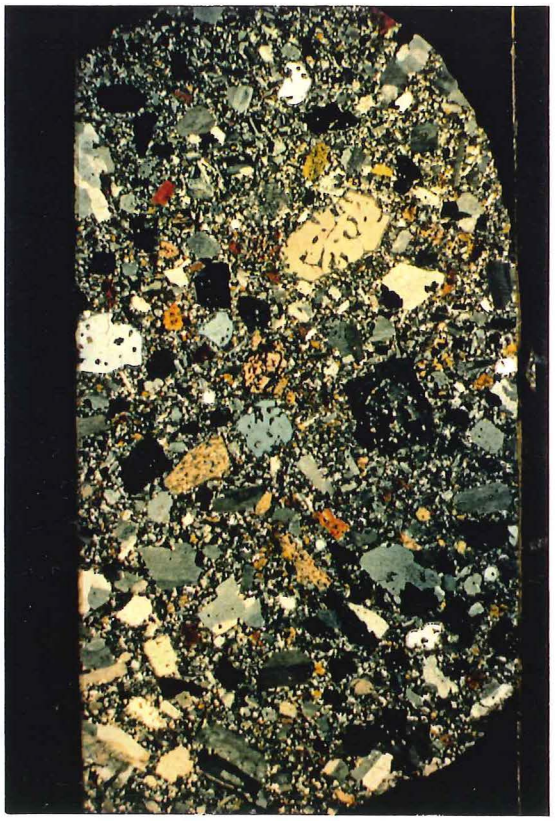

(Figure 3.5f).

The matrix exhibits predominantly felsitic and/or eutaxitic texture with squashed glass shards commonly forked in shape. Shards have occasionally been replaced by calcite. Spherulitic texture is also a feature in the matrix of some samples.

3.2.3 Petrological Interpretation

Ethelton granitoid clasts were compared and contrasted within the two distinctive textural categories defined in Chapter 2, 2.2.

The majority of hypersolvus clasts (ETHG-3,5,8) display typically undeformed euhedral to subhedral crystals with granitic texture, indicating a subsolvus history, surrounded by granophyric intergrowth signifying shallow level subvolcanic crystallization under hypersolvus conditions. There is a gradation in grain size to hypabyssal hypersolvus samples in which mesoperthite and quartz have crystallized together on the granite minimum and the eutectic crystallization of granophyric intergrowths has followed. Hypersolvus samples contain amphibole, or evidence suggestive of amphibole, but no aluminium rich minerals, i.e. muscovite.

Subsolvus biotite and biotite/muscovite groups (ETHG-1,2,4,6,7) predominate among the Ethelton granitoid clasts, displaying undeformed granitic texture or a pervasive foliation defined by quartz ribbon development, alignment of sheet silicates or grain boundary comminution indicating a dynamic metamorphism with plastic

deformation. That c-axes were aligned predominantly parallel to the extension direction is characteristic of high temperature ($>650^{\circ}C$) deformation which suggests synchronicity with emplacement (Mainprice *et al.*1986).

Undeformed subsolvus clasts are generally relatively finer grained representing pressure-quenching of water saturated melts. Porphyritic subsolvus clasts are considered hypabyssal. No miarolitic cavities were noted in hypersolvus or subsolvus samples.

The geochemically classified volcanic clasts are distinguishable petrographically. In dacitic samples lithic fragments of volcanic origin predominate, whereas in rhyolite samples fragmented crystals are abundant. The eutaxitic texture and fragmental, lithic rich nature of dacites indicates a pyroclastic/ignimbritic flow origin. The eutaxitic texture evident in volcanic lithic fragments indicates pyroclastic/ignimbritic activity was ongoing. Smale (1978) identified andesitic volcanic clasts from the Ethelton conglomerate. It is suggested that rhyolitic clasts with quartz and alkali feldspar only present in the matrix could, without geochemical classification, be misidentified as andesites. In hand specimen these rhyolite samples are predominantly dark grey to black with large plagioclase phenocrysts.

The rhyolitic matrix, in detail completely recrystallized, is coherent and homogenous in the majority of samples illustrating a magmatic rather than pyroclastic origin. The viscous nature of rhyolite generally precludes flow as lava, and the coherent clasts are considered, therefore, to have crystallized within a rhyolite dome. Some rhyolites are hypabyssal in appearance, and it is difficult to

draw firm lines within the gradation from volcanic to plutonic; the distinctions are purely arbitrary. Samples such as these are considered to have formed at the core of rhyolite domes, to have been subject to slower cooling, and therefore to be coarser in grain size than the more distal examples with finer grained matrices. The rhyolite samples with phenocryst contents $>50\%$ can be classified as feldspar quartz porphyries.

Both rhyolite and dacite samples contain allanite, titanite and strong evidence of amphibole which strengthens the possibility of a close relationship to the allanite, titanite, amphibole bearing hypersolvus and undeformed subsolvus granitoid samples.

The euhedral bipyrimidal form of quartz noted in many rhyolite samples indicates crystallization at high temperature as beta quartz and subsequent change to low temperature alpha quartz during cooling, with retention of the beta quartz polymorph form.

The majority of clasts, both plutonic and volcanic, were moderately weathered with feldspars, particularly plagioclase, undergoing sericitization or saussuritization indicating low temperature hydrothermal alteration with fluid infiltration and oxidation subsequent to crystallization. Two phases of fluid infiltration in many volcanic samples is evident. Cavities are lined with fine euhedral quartz and filled with a coarser quartz mosaic. Transection by calcite veins is common and is consistent with pore water expulsion processes that are characteristic of subduction zones. Calcite pseudomorphs are also common indicating metasomatism involving a CO_2 rich vapour phase.

3.3 Geochemistry

3.3.1 Categorization of Granitoids

To classify Ethelton igneous clasts according to source characteristics the Aluminium Saturation Indices were calculated and are tabulated in Appendix 5. The distribution for Ethelton samples is illustrated in Figure 3.8. Twenty of the clasts plot in the metaluminous field and of these the highly metaluminous clasts (A/NK >1.2) plot with some scatter from the remainder. The highly metaluminous clasts comprise granodiorites, monzogranites and dacites. Two samples have an ASI >1.1, a syenogranite (ETH9/24042) and granodiorite (ETH22/24055). The remainder plot with an ASI between 1.0 - 1.1. Metaluminous samples are considered I-type granitoids and peraluminous samples with an ASI >1.1 are considered S-type granitoids (White and Chappell, 1983). The remaining peraluminous samples with an ASI between 1.0 and 1.1 could not be assigned a type under this classification as previously stated (Chapter 2, 2.3.1).

In the diagrams which plot Zr + Nb + Ce + Y against various major element ratios (Figure 3.9a and b) the fields for fractionated felsic (FG) and unfractionated (OGT) I- and S-type granites are defined (Whalen *et al.*, 1987). The Ethelton conglomerate samples plot predominantly within these fields displaying fractionated and unfractionated granitoid character. The single granitoid sample that plots outside the defined fields (ETH13/24046) contains a high abundance of Zirconium (326ppm *cf.* 117ppm av. for Ethelton granitoid clasts) but no significant

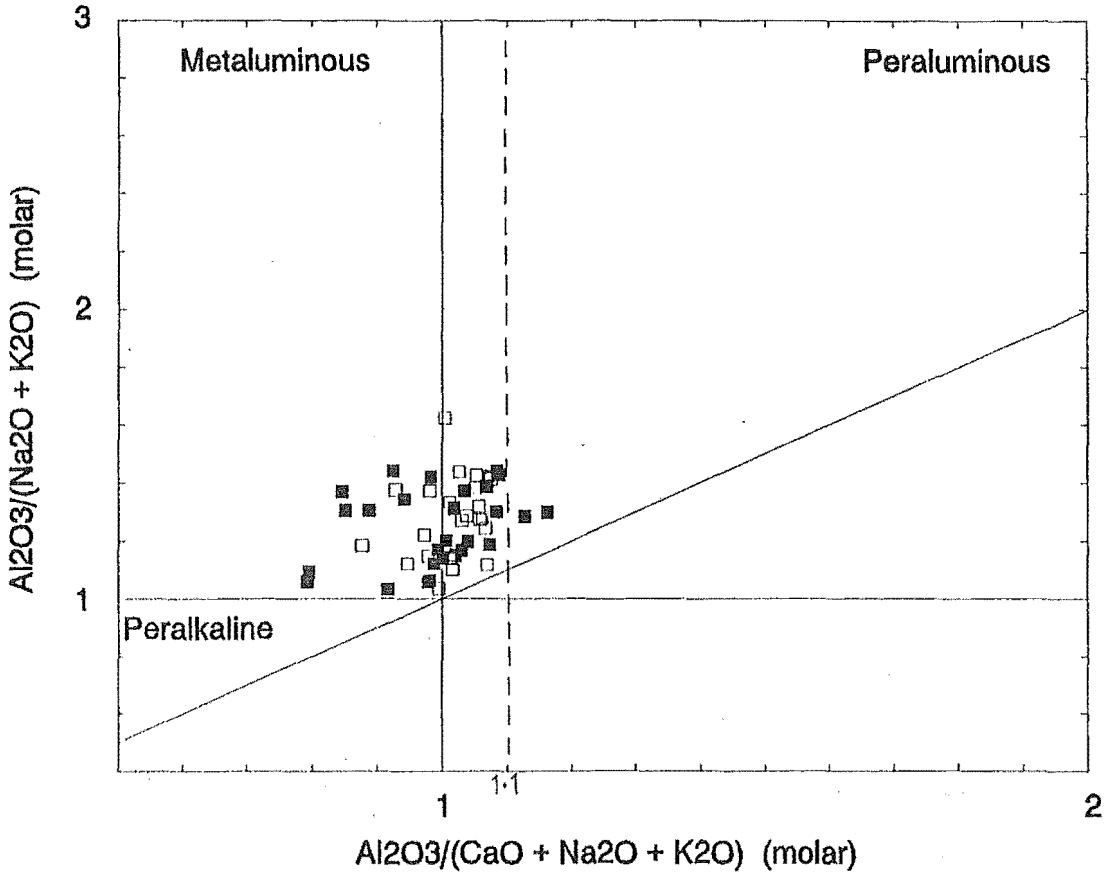

Figure 3.8: Aluminium Saturation Indices plotted for Ethelton conglomerate clasts. A/CNK = 1.1 indicates the boundary between highly fractionated I-type and S-type granitoid/volcanic clasts.
(after Maniar and Piccoli, 1989)

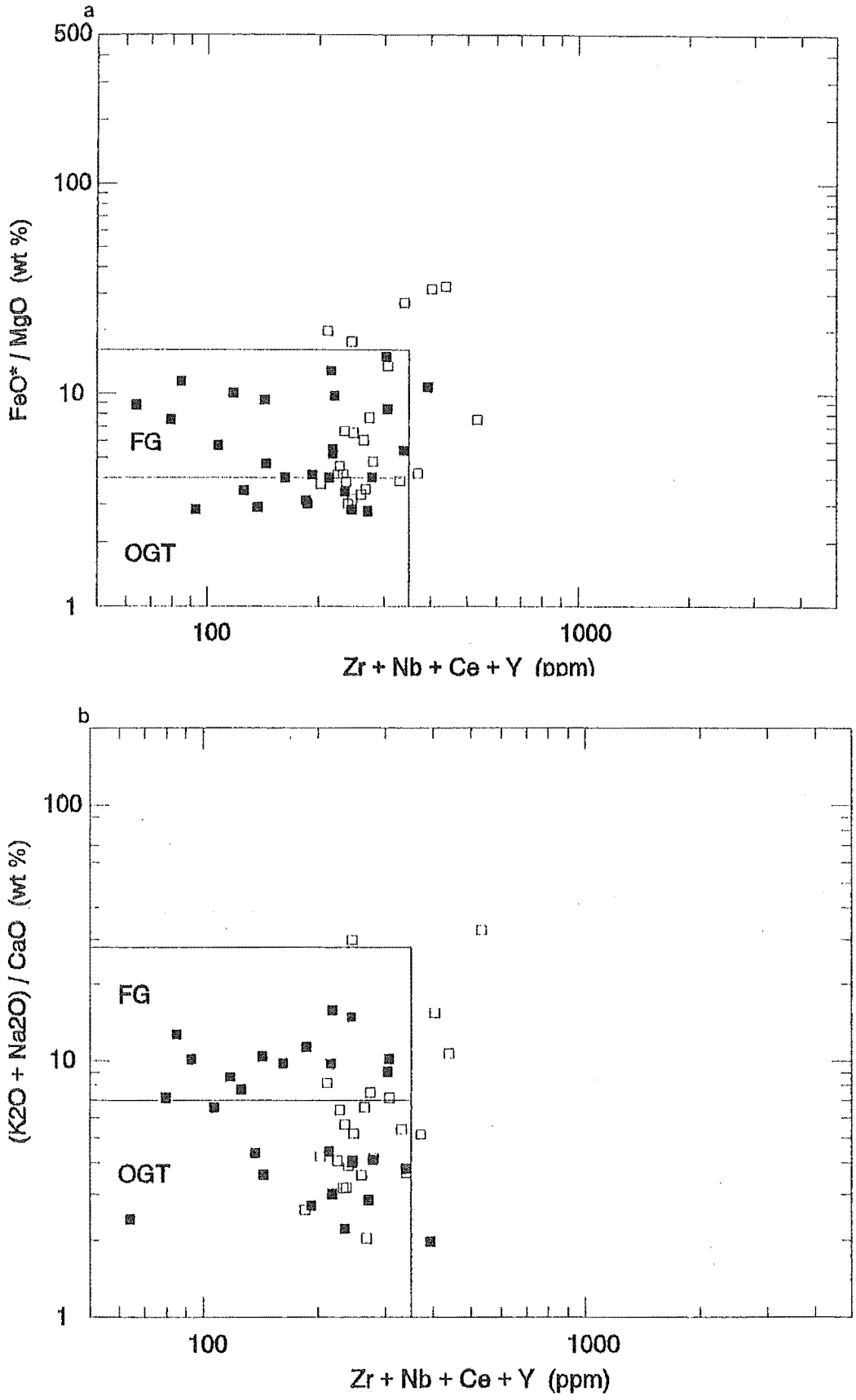

Figure 3.9: High Field Strength trace elements versus major element ratios for Ethelton conglomerate clasts, with fields for fractionated felsic granites (FG), and ordinary granite types (OGT) delineated.
a Zr+Nb+Ce+Y versus FeO*/MgO
b Zr+Nb+Ce+Y versus $(K_2O+Na_2O)/CaO$
(after Whalen *et al.*, 1987)

quantities of other HFS elements that would indicate an A-type character. The volcanics that plot outside the delineated fields will be discussed in the following section.

The predominantly calc-alkaline character (~58 - 60% SiO_2) of the Ethelton samples is indicated by the calculated alkali-lime index (defined in Appendix 4) plotted in Figure 3.10. The presence of relatively mafic granodiorite and dacite clasts explains the extrapolated spread of values toward the calcic field which defines more primitive rock series (Brown, 1982). The AFM diagram (Figure 3.11) and alkalis-silica plot (Figure 3.12) support the calc-alkaline classification.

3.3.2 Plutonic/Volcanic Relationship

The geochemical analyses for volcanic clasts are combined with granitoid clast data in all discrimination diagrams.

The ASI of the Ethelton conglomerate volcanic samples coincides with that obtained for the granitoid clasts (Figure 3.8). Of the seven volcanic samples that are metaluminous, three are highly metaluminous dacites which corresponds to the predominantly granodioritic character of the highly metaluminous granitoid samples.

Volcanic samples plot primarily as a concentration within the OGT field in Figure 3.9a and b. Five rhyolitic samples disperse into the highly fractionated/A-type domain. The granitoids generally have lower HFS values than the volcanics.

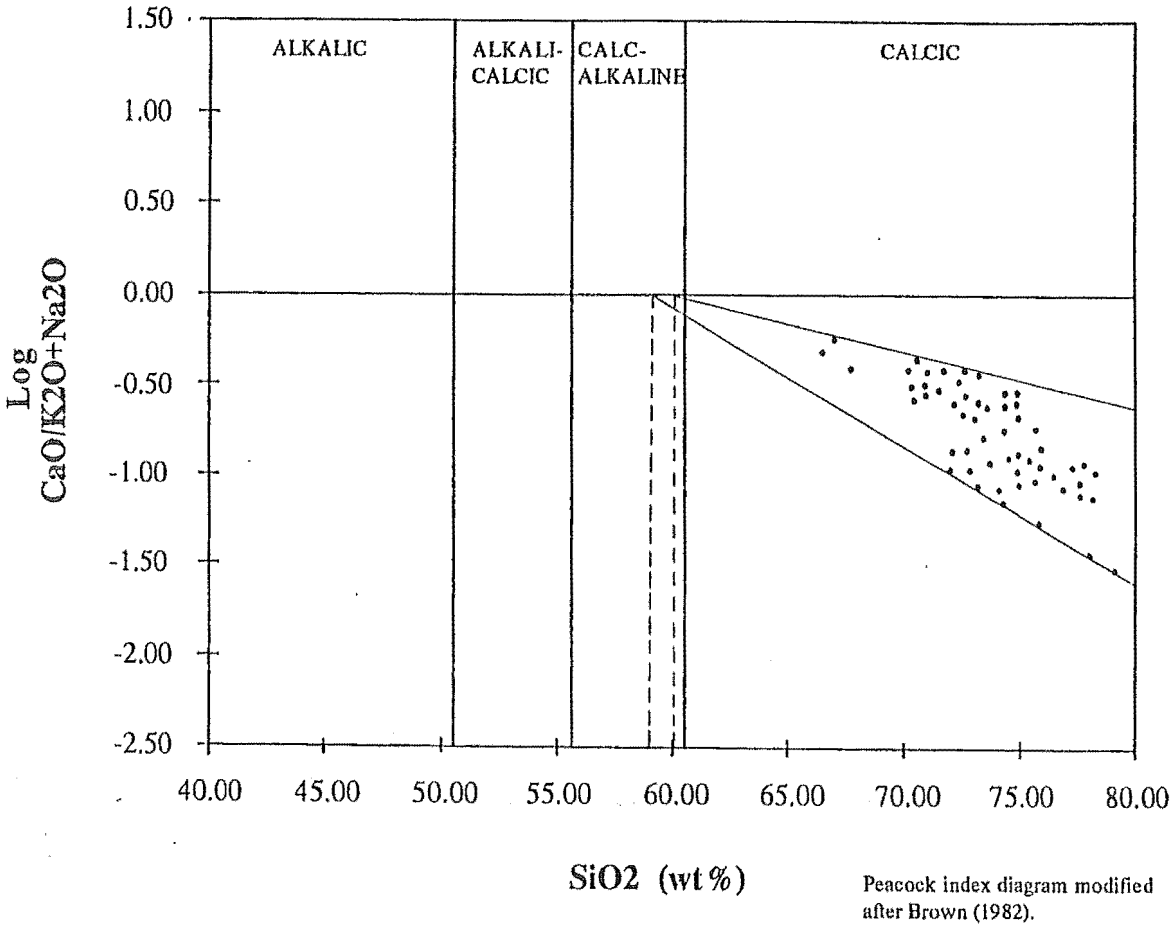

Figure 3.10: Alkali-lime Index (definition Appendix 4) illustrating extrapolated values for Ethelton conglomerate clasts.

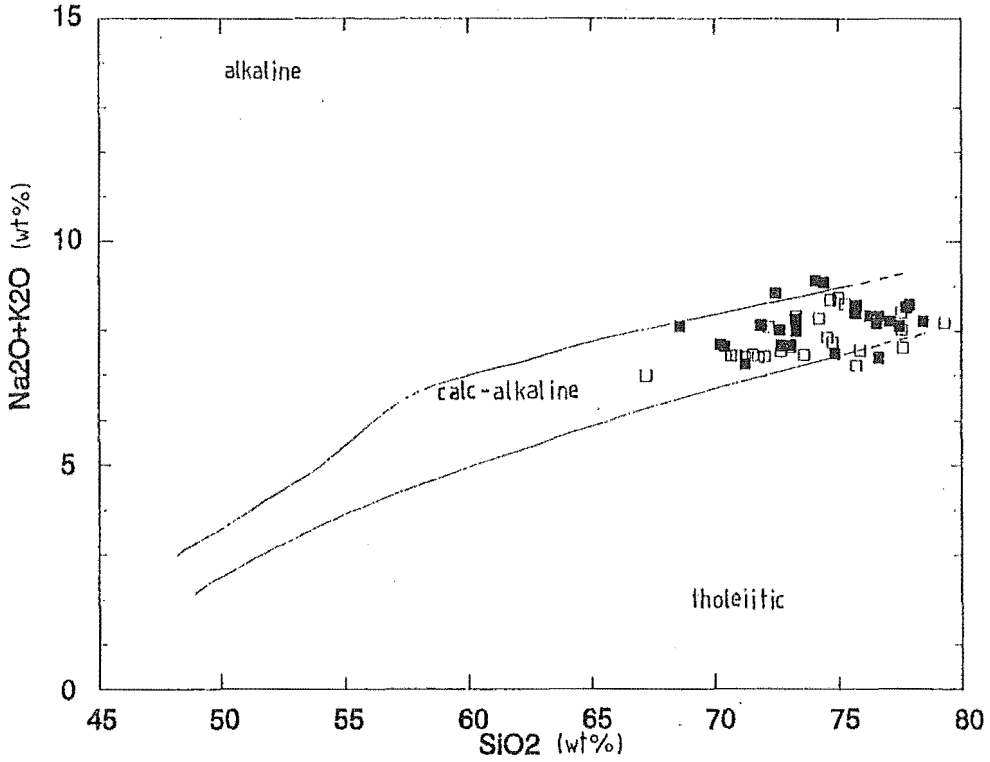

Figure 3.11: Alkali-silica diagram illustrating distribution of Ethelton conglomerate clasts between alkaline, calc-alkaline, and tholeiitic fields. (after Kuno, 1968)

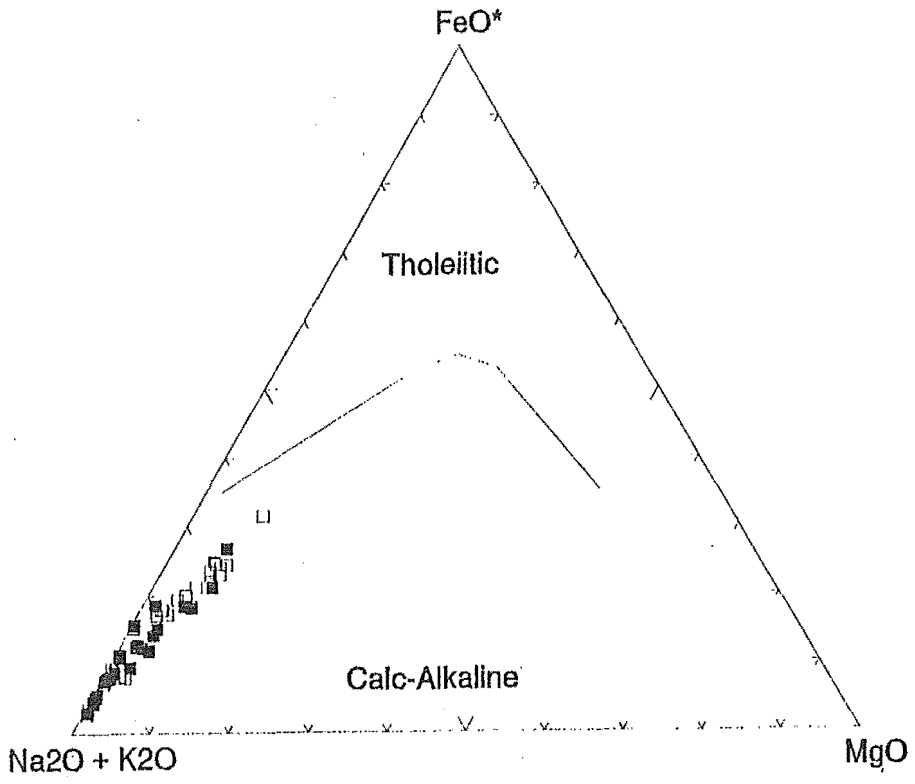

Figure 3.12: AFM (Na_2O+K_2O; Total iron as FeO; MgO) ternary diagram illustrating distribution of Ethelton conglomerate clasts. The dashed line separates tholeiitic and calc-alkaline composition. (after Irvine and Baragar, 1971)

The plots of 10000*Ga/Al versus major and trace elements (Figure 3.13a and b) suggest that Ethelton samples are predominantly felsic I- or S-types with a fractionated character. Many samples plot outside the defined I-,S-type field, within the fractionated field with some separation from the calculated average A-type.

Assuming a cogenetic relationship, crystal fractionation or partial melting of the same source, is indicated by the decreasing concentration of Sr coupled with the increasing concentration of Rb in some samples as illustrated by the Harker diagrams which compare silica against major element abundances (Figure 3.14a and b). The Rb-Ba-Sr ternary diagram (Figure 3.15) supports this and also emphasizes the relatively constant Ba content in Ethelton samples for the total range of silica values illustrated by the Si_2O versus Ba Harker diagram (Figure 3.14c). The Rb-Ba-Sr ternary plot (Figure 3.15) isolates four samples outside the determined fields (ETH44/24077, ETH46/24079, ETH47/24080) all of which display a pervasive foliation and contain secondary calcite in veins and as a replacement product indicating their metamorphosed/metasomatized character. Sr will replace Ca and concentrate in calcite. The presence of muscovite and euhedral garnet in two of the samples (ETH44/24077, ETH47/24080) suggests they were part of a late stage pegmatite crystallized from a volatile rich magma. The failure of the Rb-Ba-Sr ternary diagram to emphasize the evolved character of the volcanic samples already defined by Figures 3.9 and 3.13 is attributed to that fact that each granitoid group occupies a wide range in this diagram (El Bouseily and El Sokkary, 1975).

The K_2O-Na_2O-CaO ternary plot (Figure 3.16) indicates a trend within both granitoid and volcanic samples from higher CaO and Na_2O values to an intermediate Na_2O-K_2O composition (~1:1) with low CaO.

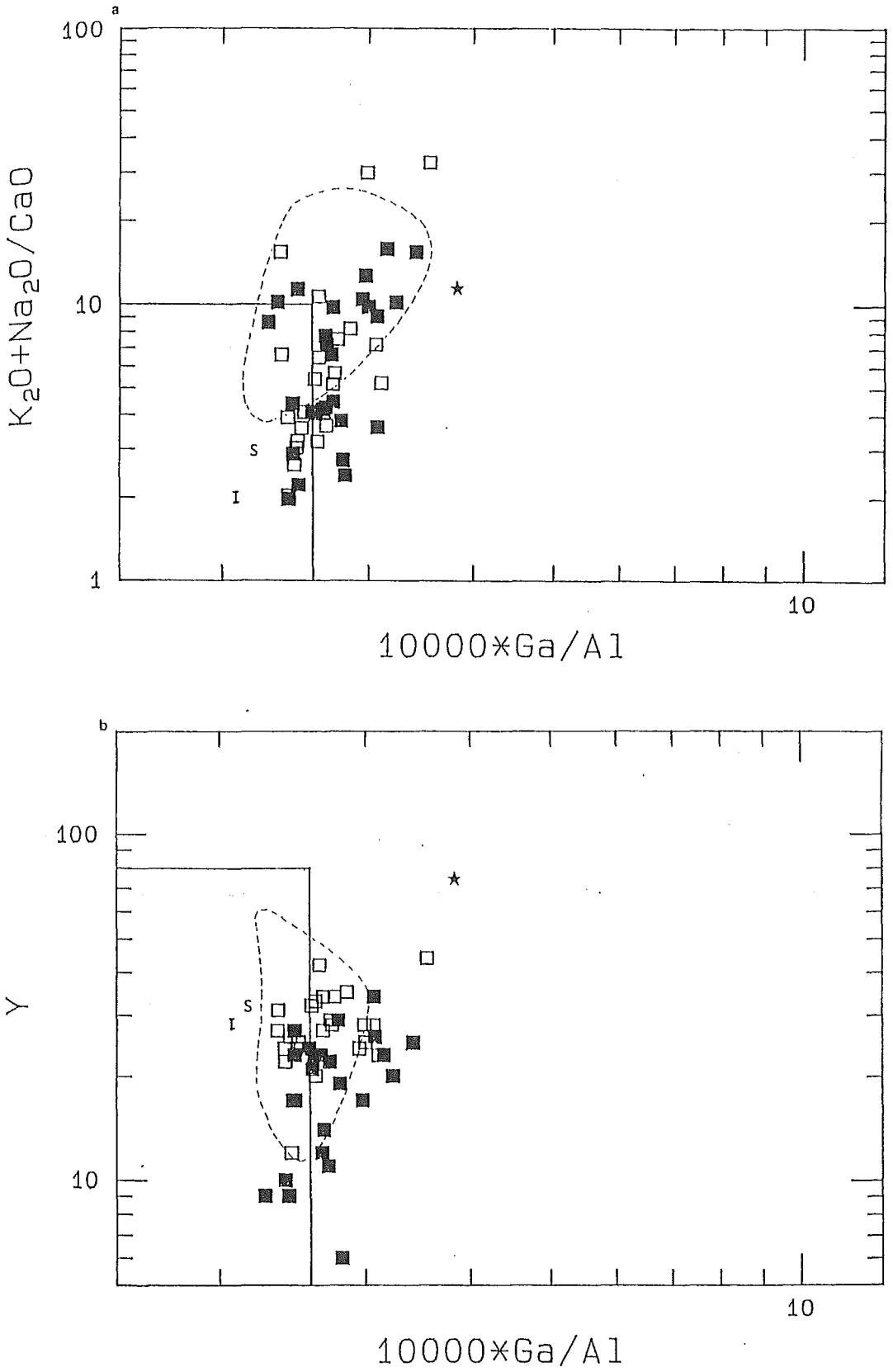

Figure 3.13: Plots of 10000*Ga/Al versus **a** K_2O+Na_2O/CaO, and **b** Y illustrating Ethelton conglomerate clast distribution. I- and S-type granite field delineated, dashed line represents fractionated granite field, *= calculated average A-type, I = calculated average I-type, S = calculated average S-type.
(after Whalen *et al.*, 1987)

Figure 3.14: Harker variation diagrams for Ethelton conglomerate clasts
a SiO_2 versus Sr
b SiO_2 versus Rb
c SiO_2 versus Ba
d SiO_2 versus Al_2O_3

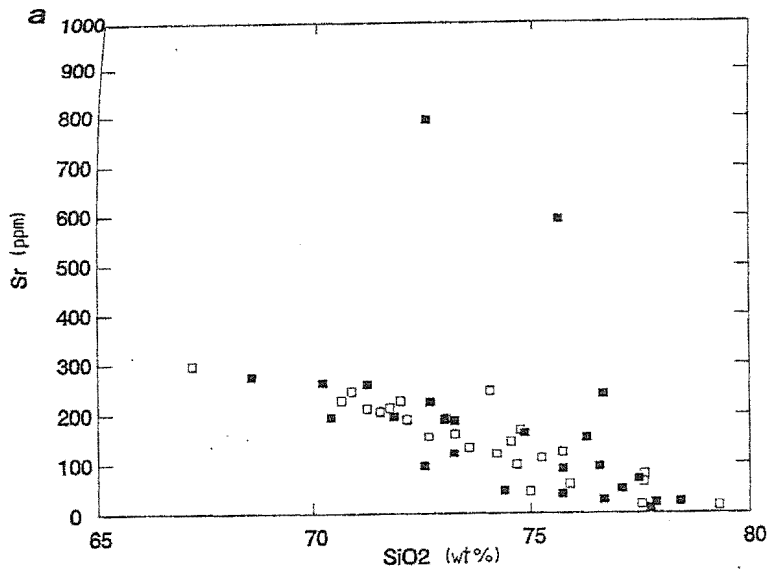
a
Sr (ppm)
SiO2 (wt%)
1000
900
800
700
600
500
400
300
200
100
0
65
70
75
80

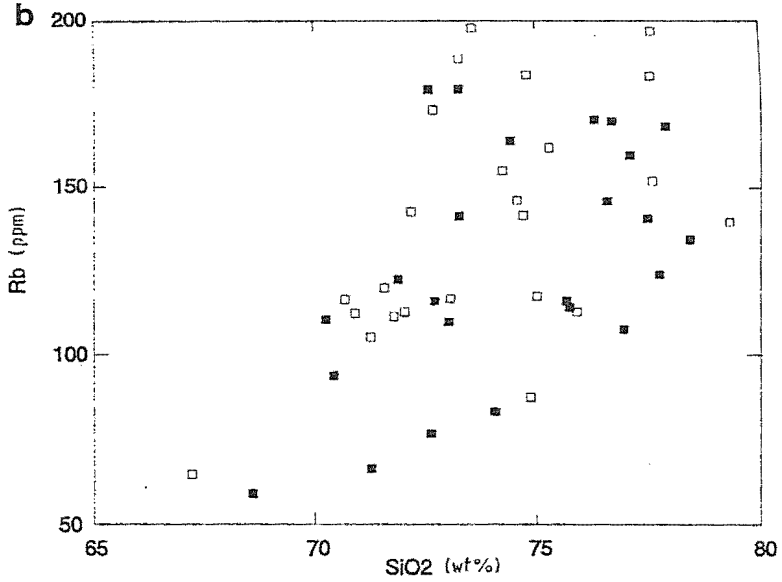
b
Rb (ppm)
SiO2 (wt%)
200
150
100
50
65
70
75
80

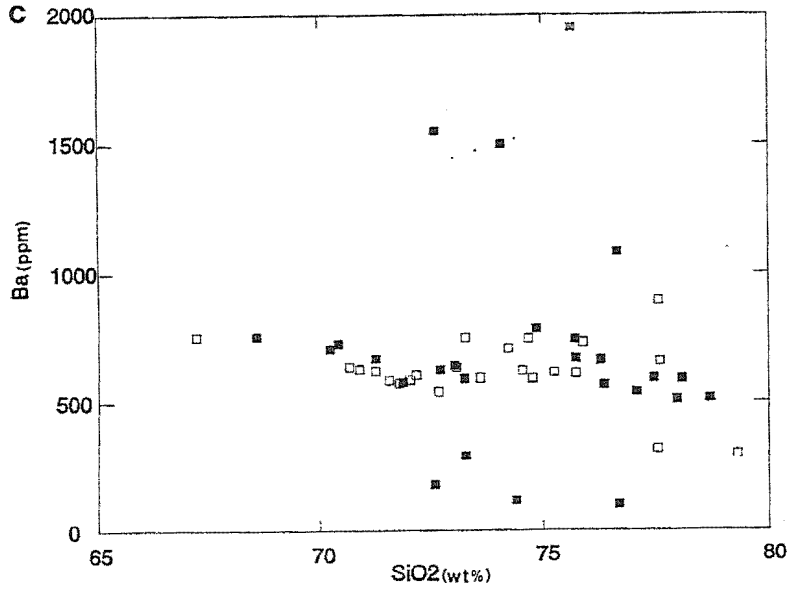
c
Ba(ppm)
SiO2(wt%)
2000
1500
1000
500
0
65
70
75
80

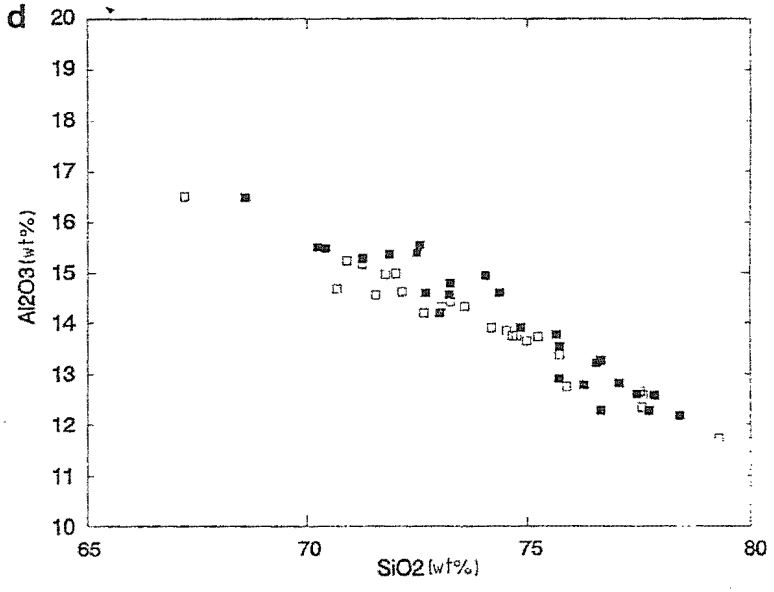
d
Al2O3(wt%)
SiO2(wt%)
20
19
18
17
16
15
14
13
12
11
10
65
70
75
80

3.3.3 Correlation with Mineralogy

The Ethelton samples can be divided geochemically according to silica content (< or >70% silica). This is reflected in the mineralogy by the modal concentration in the granodiorite field with scatter into the monzogranite and syenogranite fields that corresponds to an increase in alkali feldspar (Figure 3.3).

The highly felsic nature of samples is evident in the low abundance of mafic minerals. Evolved granitoid samples generally contain both minor biotite and muscovite. Amphibole and pyroxene, as preserved cores and identified by euhedral pseudomorph shape, were present in the relatively more mafic samples.

Highly metaluminous granodiorite, monzogranite and dacite clasts typically contain green/brown biotite, titanite and amphibole remnants which supports the I-type classification and suggest an oxidized igneous source (White and Chappell, 1983). Highly peraluminous samples contain red/brown biotite, muscovite with or without primary euhedral garnet indicating their S-type classification and reduced sedimentary source. Those samples with an ASI between 1.0 and 1.1 generally contain dark brown biotite and the minerals diagnostic of type, as prescribed by White and Chappell (1983), are absent.

The geochemical division of volcanic clasts is supported by distinctive mineralogical features noted, only the dacites have a high percentage of lithic fragments and were identified as being predominantly pyroclastic in nature. The matrix of rhyolite samples was noticeably more coherent in nature than dacitic

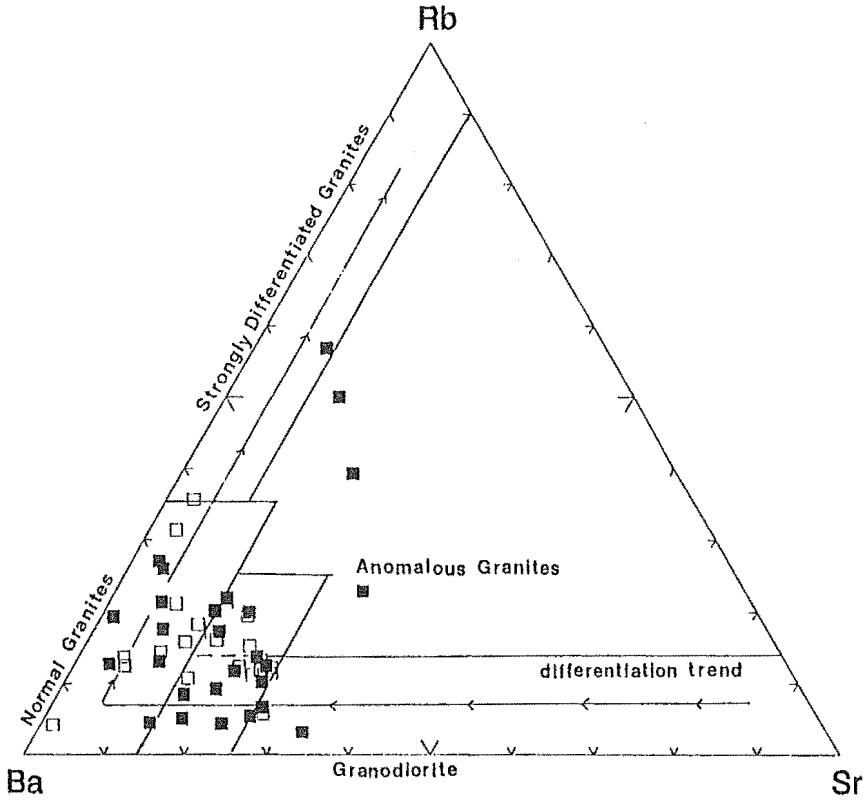

Figure 3.15: Rb-Sr-Ba ternary diagram illustrating relationship between Ethelton conglomerate clasts.
(after El Bouseily and El Sokkary, 1975)

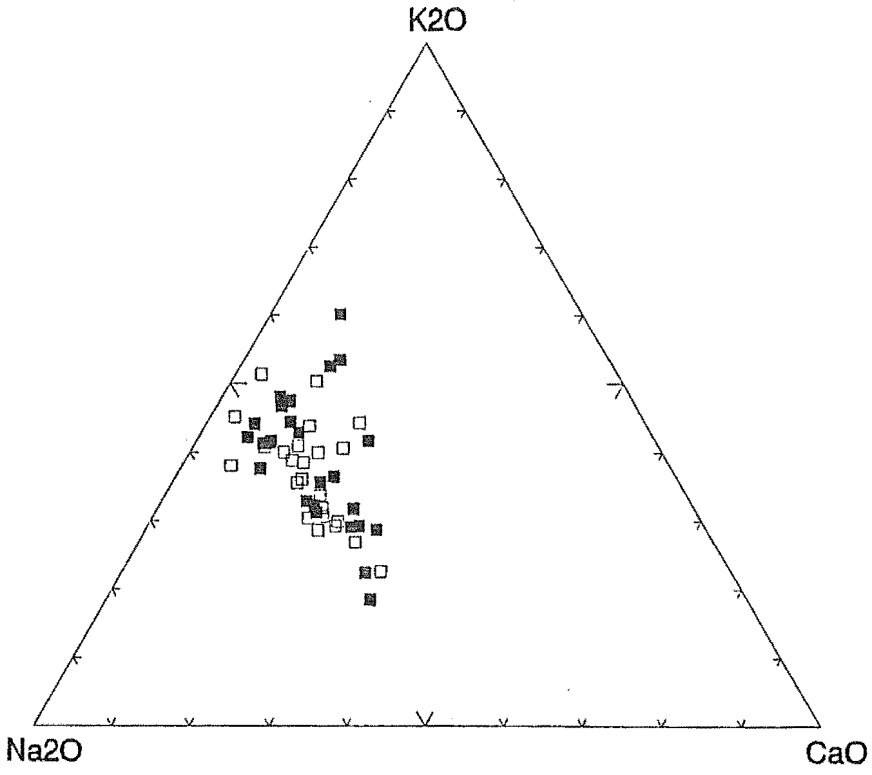

Figure 3.16: K_2O-Na_2O-CaO ternary diagram which illustrates the K_2O/Na_2O ratio and considers CaO for Ethelton conglomerate clasts.

samples despite the recrystallization of previously glassy material. The rhyolites also displayed a gradual increase in matrix grain size which could indicate a progressive unroofing of increasingly more plutonic material, i.e. the hypabyssal part of the igneous complex.

The Rb-Ba-Sr ternary diagram (Figure 3.15) emphasizes the metasomatic character of Ethelton conglomerate samples which is reflected in the high abundance of secondary calcite recognized in the majority of samples as veins and pseudomorphs.

The primitive-mantle-normalized (Sun and McDonough, 1989) multi-element abundance diagrams used to distinguish overall trace element characteristics within the Ethelton conglomerate clasts display the distinctive spiked pattern and LIL enrichment indicative of subduction related magmas (Figure 3.17) (Wilson, 1989; Saunders *et al.*, 1991). Patterns show a general concordance that suggests a similar petrogenesis, between the biotite bearing granitoids and the volcanics in particular (Figure 3.17a, b and d). The deviations from these patterns noted in the biotite/ muscovite bearing granitoids are attributed to varying degrees of crustal contamination, differences in the character of sedimentary source composition or to the effects of metasomatism (Figure 3.17c). The dacite clasts parallel the pattern displayed by the rhyolite clasts but are distinctly less evolved. Two samples (ETH9/24042, ETH48/24081) were noted to have a positive Sr anomaly which is attributed to the presence of secondary calcite.

Figure 3.17: Multi-element primitive-mantle-normalized (Sun and McDonough, 1989) abundance diagrams for Chatham Islands conglomerate clasts:
a biotite granitoids (I-types)
b evolved biotite granitoids (evolved I- or S-types)
c muscovite biotite granitoids (S-types)
d volcanic clasts.

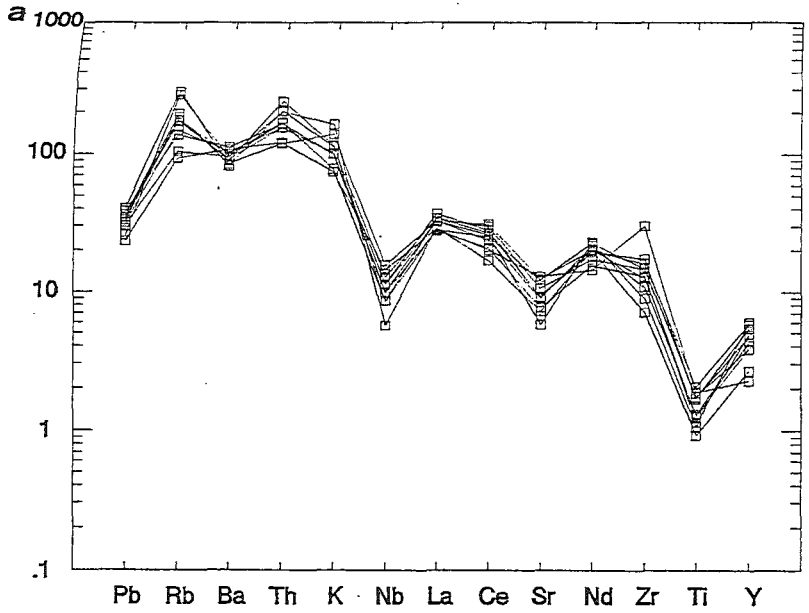
a
1000
100
10
1
.1
Pb Rb Ba Th K Nb La Ce Sr Nd Zr Ti Y

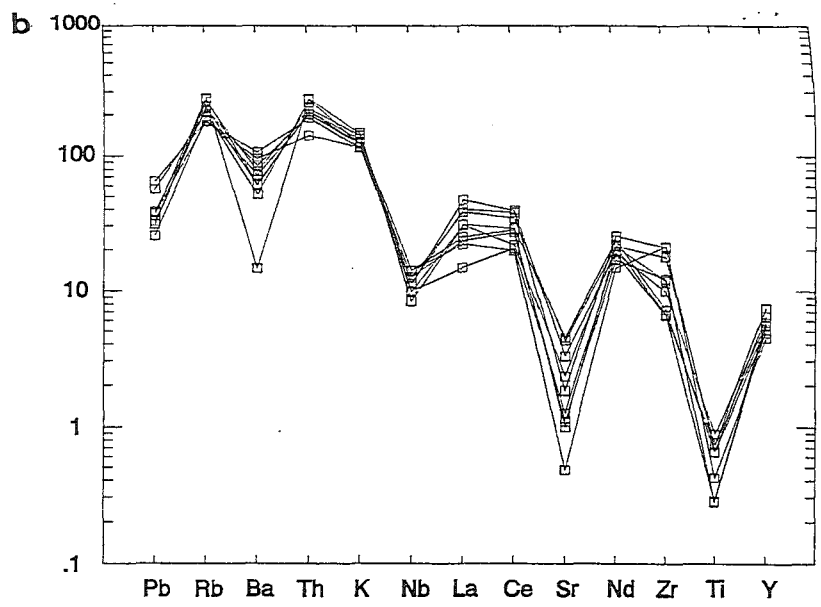
b
1000
100
10
1
.1
Pb Rb Ba Th K Nb La Ce Sr Nd Zr Ti Y

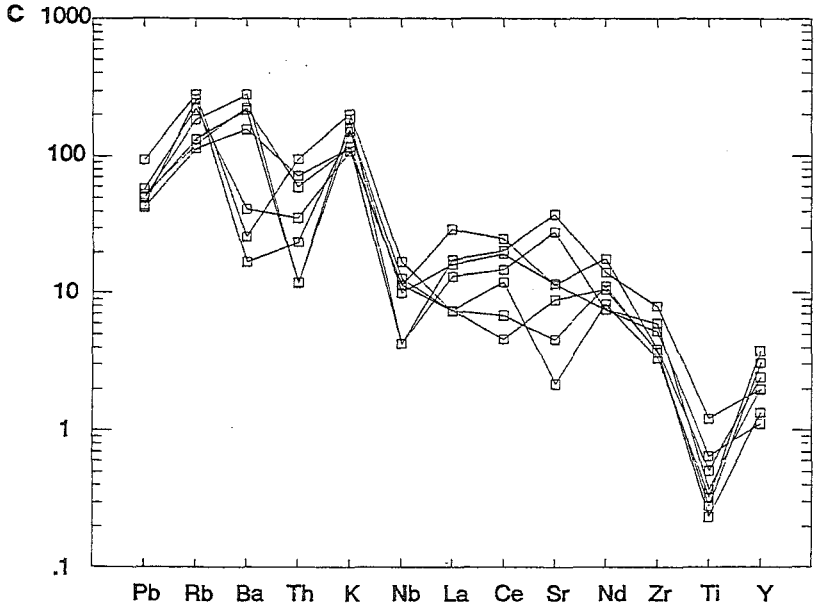
c
1000
100
10
1
.1
Pb Rb Ba Th K Nb La Ce Sr Nd Zr Ti Y

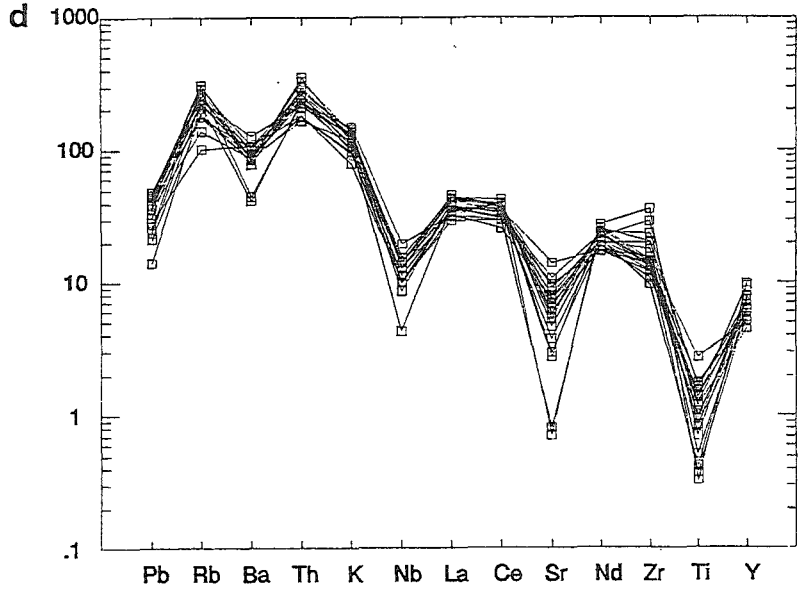
d
1000
100
10
1
.1
Pb Rb Ba Th K Nb La Ce Sr Nd Zr Ti Y

3.3.4 Discrimination of Tectonic Setting

Diagrams used to discriminate tectonic setting unequivocally place Ethelton conglomerate clasts, plutonic and volcanic, within the volcanic arc granite field (VAG) (Figure 3.18a and b). There is a trend from granodiorite/dacite to leucosyenogranite toward the within plate granite (WPG) field which could indicate crystal fractionation, or the progressive maturity of the volcanic arc.

3.4 Synopsis

Mineralogy and modal compositions indicate that Ethelton conglomerate granitoid clasts are predominantly biotite $\pm$ muscovite granodiorites, and leucomonzogranites and leucosyenogranites. Volcanic clasts are predominantly porphyritic or spherulitic rhyolites, once part of rhyolitic domes and porphyritic dacites that are predominantly ignimbrites.

Subsolvus and hypersolvus granitoid type are distinguishable texturally. Hypersolvus samples are undeformed and predominantly hypabyssal. Subsolvus granitoids can be undeformed or foliated.

Geochemically classified I-type granitoids predominate. Present also are weakly peraluminous evolved I-type and two distinctly S-type granitoids. The volcanics relate mineralogically and geochemically to the I-type granitoids which are generally the subvolcanic, hypersolvus, hypabyssal clasts.

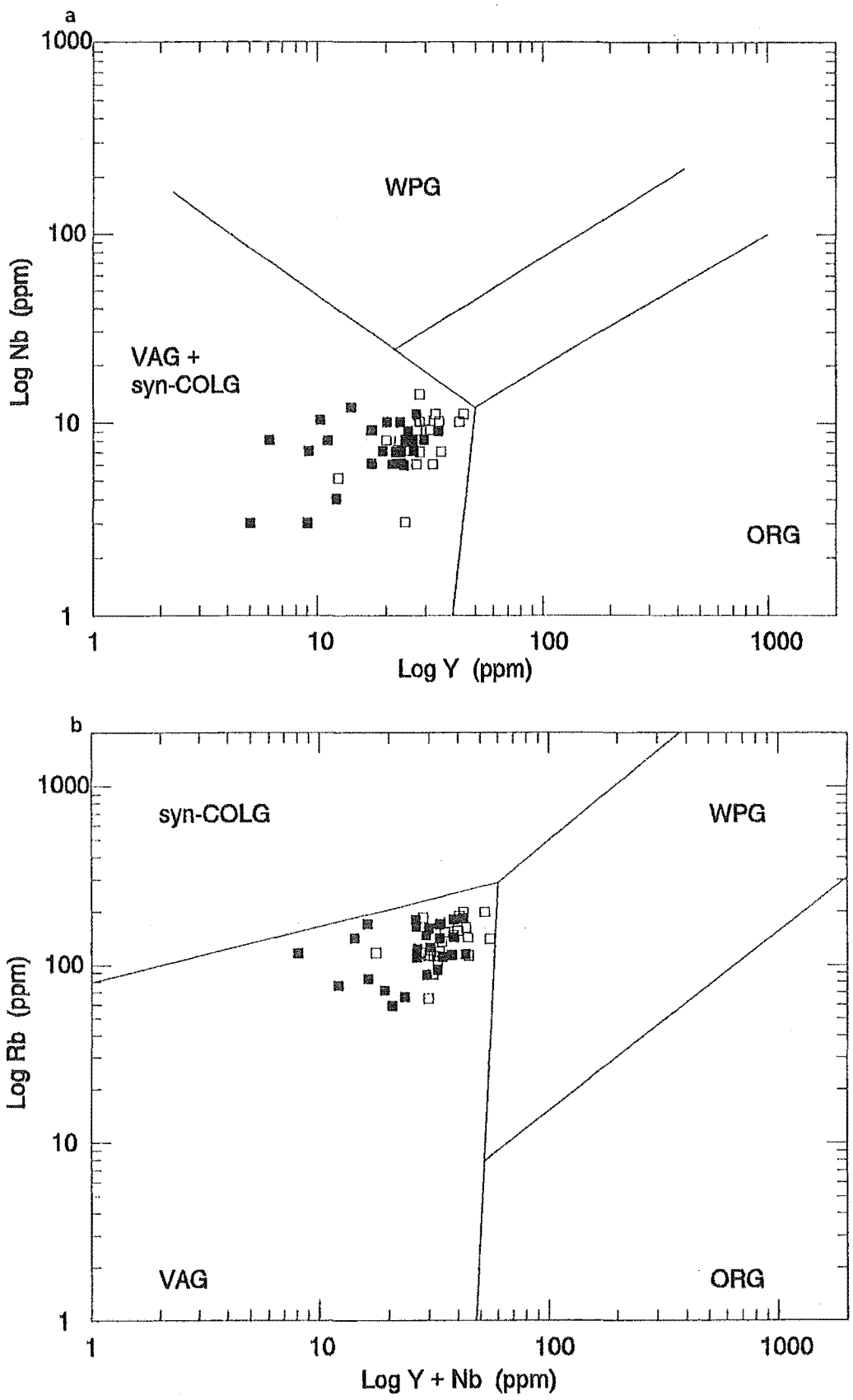

Figure 3.18: Tectonic discrimination diagrams illustrating distribution for Ethelton conglomerate igneous clasts within the syn-collision (syn-COLG), volcanic arc granite (VAG), within plate granites (WPG), and ocean ridge granites (ORG) fields:
a Nb-Y
b Rb-Y+Nb
(after Pearce *et al.*, 1984)

The Ethelton conglomerate igneous clasts are calc-alkaline and display elemental features indicative of magmas related to subduction.

3.5 Discussion

The Ethelton conglomerate igneous clasts generally display linear trends on Harker diagrams (Figure 3.14). This, combined with the close association of analyses (plutonic and volcanic) in discrimination diagrams implies a chemical coherency and probable genetic relationship. The Ethelton conglomerate igneous clasts may represent the primitive biotite (± amphibole) granitoids and evolved biotite (± muscovite granitoids) of one suite (ASI=1.0-1.1, Zen, 1986). Volcanic clasts represent an extrusive phase primarily associated with the early, relatively more mafic stages of intrusion. Features that support this include a gradual increase in elemental ratios (e.g. K/Na) and increasing concentrations of incompatible (with regard to source) trace elements. The mineralogical and textural differences displayed by Ethelton conglomerate clasts are those that could be expected in granitoids formed from separate partial melting events of a specific source.

Provenance for the Ethelton conglomerate igneous clasts is determined as a dissected and well developed active continental margin where the subduction of oceanic crust beneath continental crust has initiated partial melting of the subcontinental lithosphere and the production of I-type magmas. The high geothermal gradient associated with partial melting permitted intrusion to shallow levels with associated extrusive volcanic activity. Granodiorite intrusion was accompanied by episodic dacite ignimbritic eruptions. Subsequent evolution of

magma occurred at depth and highly evolved magmas were intruded, accompanied by diminishing volcanic activity in the form of rhyolitic domes as the magmatic arc thickened. This hypothesis is supported by the increase in K_2O/Na_2O ratio and the presence of at least two S-type granitoids. The subsolvus foliated clasts indicate that intrusives display a variety of cooling histories. The deformation that has affected some granitoid samples is determined as having accompanied intrusion rather than being an imposed post kinematic episode (as indicated by the LPO of c-axes parallel to the elongation direction). The well annealed mosaic quartz and mortar texture around feldspar crystals present in some samples indicates a dynamic recrystallization with fine grain sizes indicating a substantial differential stress subsequent to crystallization.

Conglomerate deposition in the Early Cretaceous occurred following the dissection of a volcanic province which unroofed associated subvolcanic and plutonic intrusives. That the volcanic arc was mature is indicated by the felsic character of the clasts. Calc-alkaline granodiorites are the most mafic rock present, therefore the early tholeiitic stage of arc development is not recorded in the clasts analyzed.

Collection procedures were the same as those previously stated (Chapter 2, 2.5) and it is assumed that a representative sample of the igneous clasts from the Ethelton conglomerate were collected. It is concluded that the high abundance of calcite in all clasts (including sedimentary) is the result of fluid infiltration after conglomerate deposition.

CHAPTER 4

MOUNT SAUL CONGLOMERATE

4.1 Introduction

4.1.1 Locality

Extensive conglomerate outcrops occur along the southeast side of the Waiau Basin in the catchment of the Pahau River (N32 Hanmer,grid ref.910/474, M32 Boyle, grid ref.865/446). This locality is representative of the Pahau subterrane. Two facies dominate the area, alternating flysch type and sandstone and conglomerate rich sequences. Bradshaw and Andrews (1980) suggested the latter could be marginal marine, but further research shows that the conglomerates are channelized mass flow deposits, and that both facies are parts of a submarine fan complex (Bradshaw, pers.comm.).

Mount Saul, a prominent peak in the area (1020m), represents the centre of an ~600m thick lens shaped body that comprises faulted slivers of predominantly matrix supported, poorly to well bedded and cross bedded, pebble to boulder conglomerate with clasts of well rounded and angular volcanics and plutonics, sandstones, jasperlite, crinoidal limestone and large (~1m) masses of ripped up bedded mudstone (Figures 4.1 and 4.2). The structure at this location has been identified as the western limb of a simple, upright, southwest plunging syncline with strata dipping 45-80°SSE (Bradshaw and Andrews, 1980) (Figures 4.1 and 4.2).

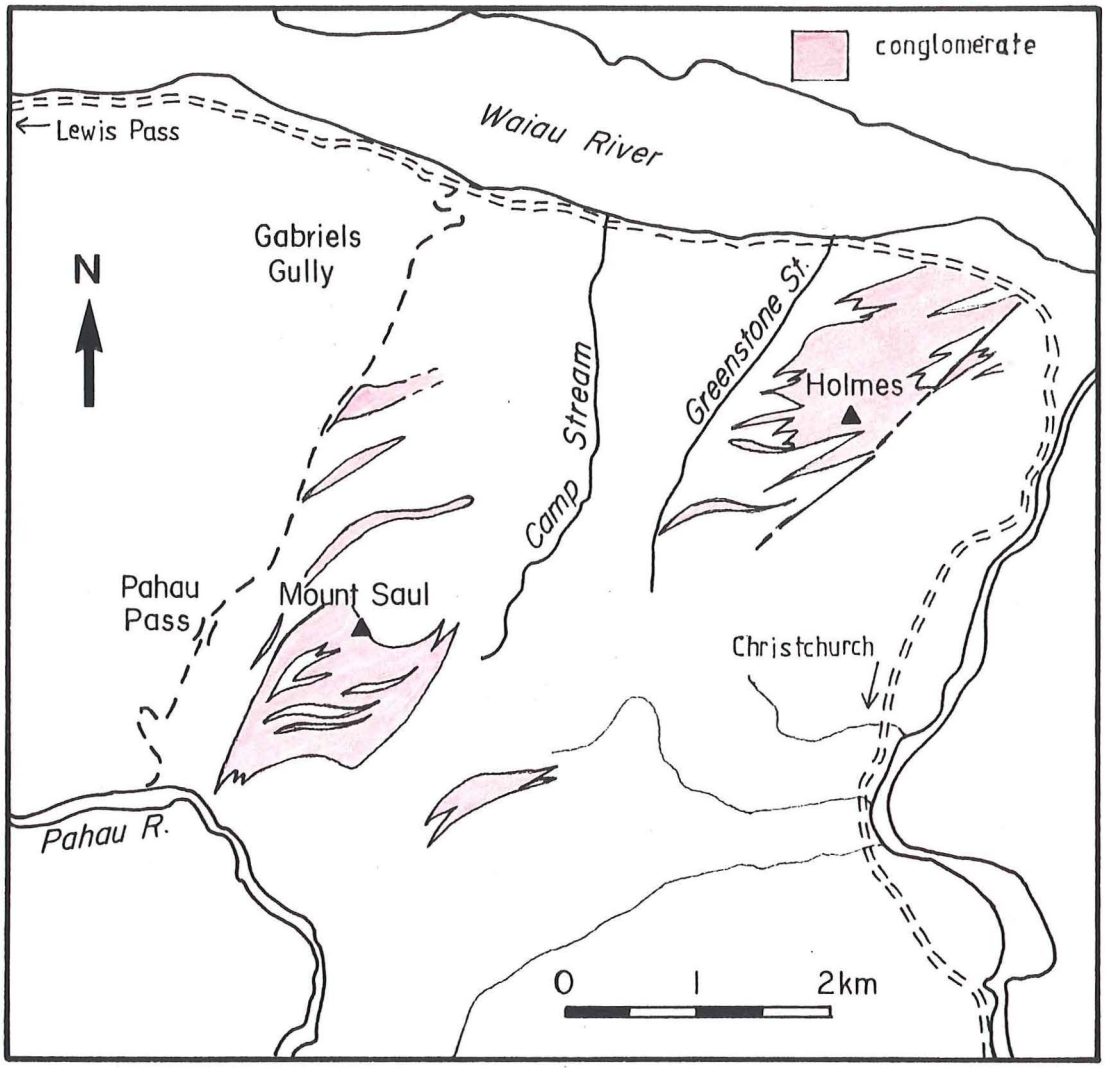

Figure 4.1: Mount Saul conglomerate locality map. (after Bradshaw and Andrews, 1980)

The conglomerate is underlain by carbonaceous sandstone and overlain by flysch sequences. Paleocurrent data obtained from cross bedding and imbrication suggest derivation from the
northwest (Bradshaw and Andrews, 1980).

4.1.2 Previous work

Several general references concerned with the occurrence of conglomerates in this area were made by early reconnaissance geologists in various exploration reports published last century and early this century (Haast, 1871; McKay, 1885; Fyfe, 1931, 1935).

The age of the Torlesse Pahau subterrane in this area was considered Upper Jurassic on the 1:250,000 Hurunui sheet (Gregg,1964), and the 1:1,000,000 Geological Map of New Zealand (1977). Spores, pollen and rare dinoflagelletes now indicate deposition was upper Lower Cretaceous (late Neocomian to early Aptian) (Bradshaw and Andrews, 1980).

R. Freund (1971) attributed the morphology of the high country in this area to a lithological change within the Torlesse greywacke. He noted conglomerate beds along the south side of the Hope Fault that extend toward the Pahau River to the south/southeast, and that on the northern side of the Hope Fault the conglomerates appear ~32kms to the east from Hossack Station to Lottery River. Freund (1971) used this as evidence for dextral strike slip movement along the Hope Fault.

Figure 4.2: Mount Saul conglomerate:
a Panoramic view of Mount Saul conglomerate outcrop
b Conglomerate outcrop showing variable clast composition and size
c Bedded conglomerate dipping to the east offset by minor faulting
d Steeply dipping conglomerate interbedded with sandstone. (Hammer = 33cms)

a

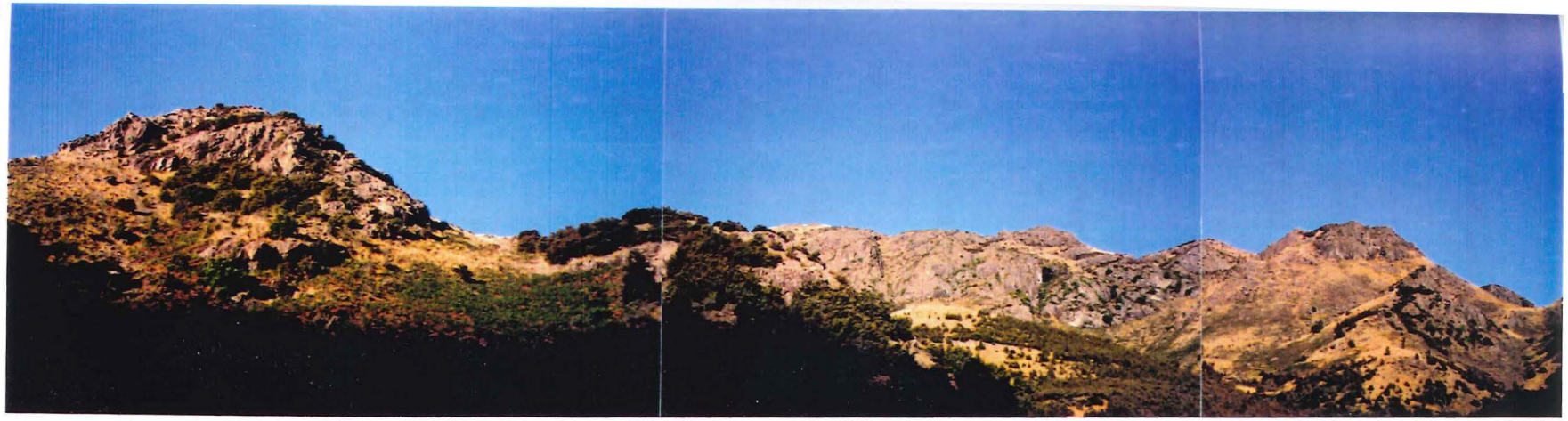

b

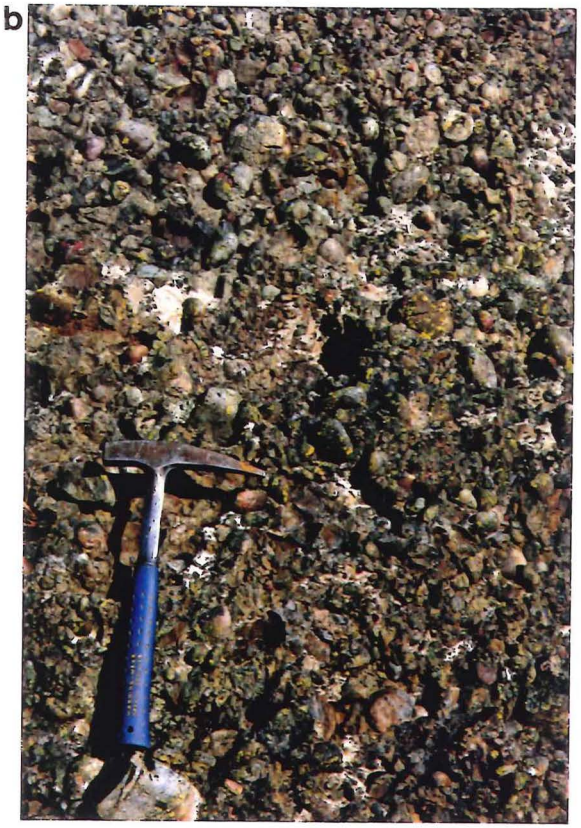

c

d

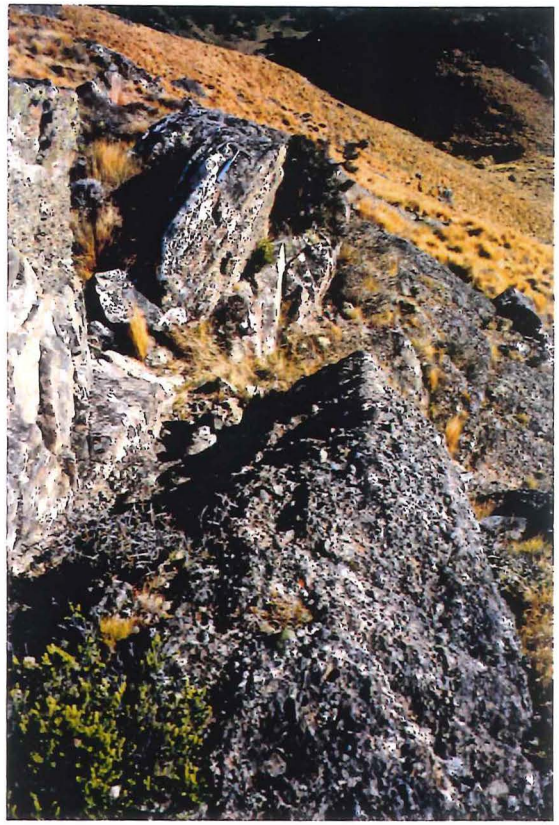

The Mount Saul/Pahau River area was briefly reviewed in the 1980 Geological Society conference field trip guide book (Bradshaw and Andrews, 1980).

Silberling *et al.* (1988) collected fossiliferous limestone boulders from the Mount Saul conglomerate which were interpreted as Late Triassic to Early Jurassic in age.

4.2 Petrography

4.2.1 Granitoid Clast Descriptions

The recalculated point count data for Mount Saul conglomerate granitoid clasts were calculated and are tabulated in Appendix 3. Data are plotted on the QAP ternary diagram (Figure 4.3). Clasts plot predominantly within the monzogranite field with some scatter into the syenogranite and granodiorite fields.

From a sample of over 500 clasts collected from the conglomerate on Mount Saul seven distinctive granitoid groups are recognized based on modal, mineralogical and textural differences as outlined in Chapter 1, 1.3.4a and defined in Chapter 2, 2.2 (Figure 4.4):

Group MSG-1:

Subsolvus, coarse grained, equigranular, biotite leucosyenogranite:

The anhedral alkali feldspar crystals exhibit poikilitic texture, enclosing both plagioclase and quartz. The plagioclase is subhedral sodic oligoclase (An 10-20%)

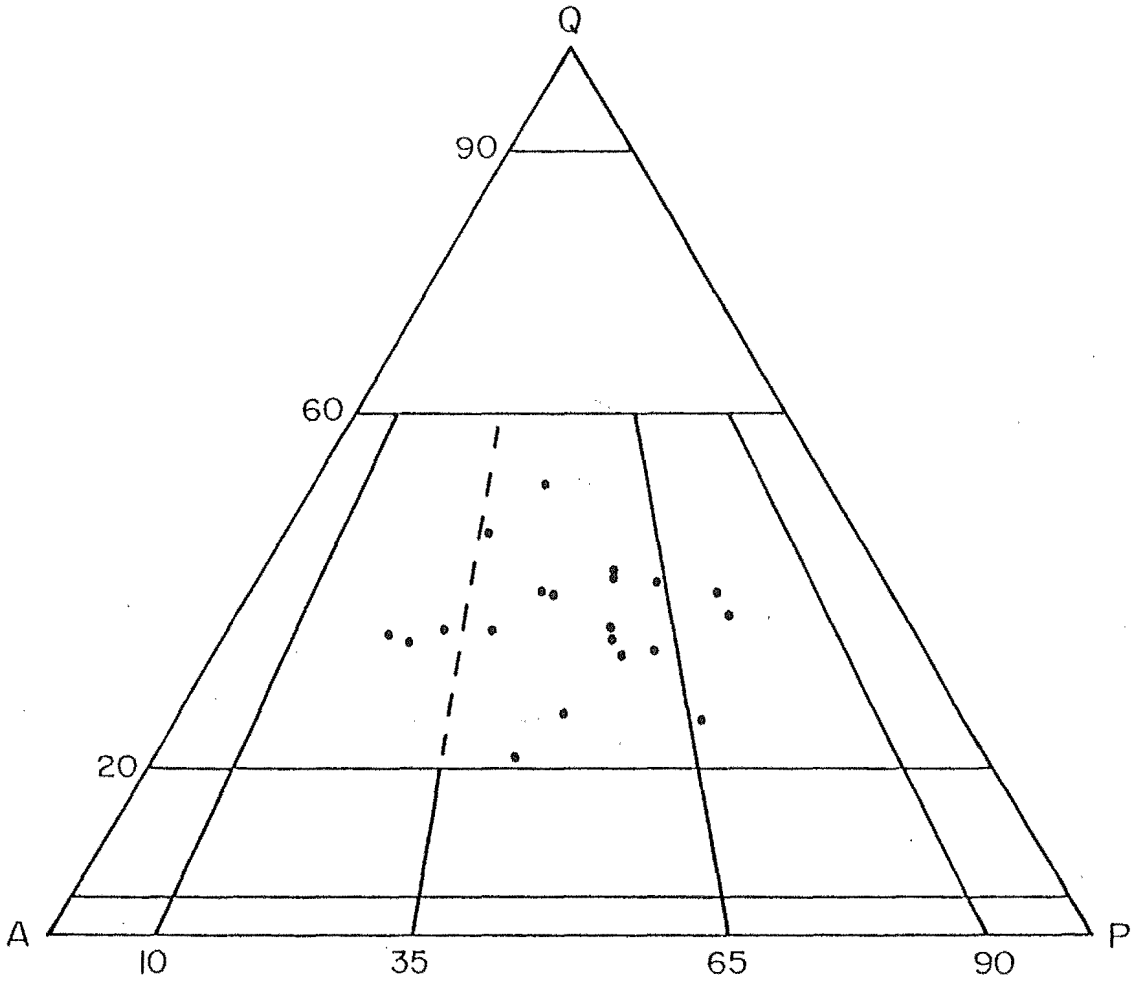

Figure 4.3: Quartz - Alkali Feldspar - Plagioclase ternary diagram illustrating modal distribution for Mount Saul conglomerate granitoid clasts (see Chapter 1, 1.3.4a for definition of fields).
(after Le Maitre, 1989)

with sericitized cores.

The anhedral quartz has sutured subgrain margins and a slight SPO.

The brown pleochroic biotite is an interstitial minor phase and is partially chloritized (Figure 4.5a)

Euhedral zircon included in biotite crystals was the only accessory phase recognized (Figure 4.5a).

Thin calcite veins (< 1mm) are present.

Group MSG-2:

Hypersolvus, medium grained, granophyric, biotite leucosyenogranite:

Granophyric intergrowths predominate and surround anhedral relatively undeformed quartz with straight to slightly undulose extinction, mesoperthitic feldspar, independent subhedral zoned sodic oligoclase (rim An10-15%) with sericitized cores, and subhedral perthitic alkali feldspar.

Partially chloritized brown pleochroic biotite is the only minor phase identified, but complete chlorite replacement of other mafic phases may also have occurred.

Accessory minerals include subhedral apatite, euhedral zircon and anhedral opaque Fe/Ti oxides.

Group MSG-3:

Subsolvus, holocrystalline, foliated, medium to fine grained, muscovite biotite leucomonzogranite:

The subhedral plagioclase is sericitized albite (An < 10%) generally laced with secondary muscovite laths. The anhedral alkali feldspar is microcline with

Figure 4.4: Representative photographs of modal, mineralogical and textural granitoid groups
(field of view ~5cms):
a Hypersolvus, biotite leucosyenogranite (MSG-2)
b Subsolvus, biotite leucomonzogranite (MSG-4)
c Hypersolvus, biotite monzogranite (MSG-5)
d Subsolvus, biotite granodiorite (MSG-6)

a

b

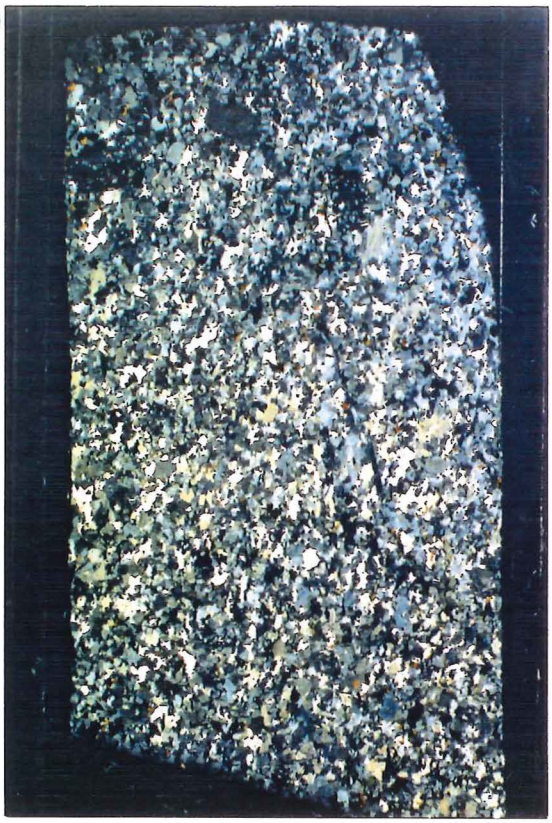

c

d

distinctive transformation twinning (Figure 4.5b)

The dark brown pleochroic biotite has been partially altered to chlorite and the high abundance of chlorite indicates additional mafic minerals may have been replaced. Minor primary muscovite is usually associated with biotite.

Accessory minerals include opaque Fe/Ti oxides and euhedral primary garnets that are fractured and slightly altered to chlorite (Figure 4.5c).

The foliation present is defined primarily by smeared out biotite and muscovite and incipient development of elongate quartz ribbons; the strain involved is insufficient to cause significant bending of quartz around feldspar crystals.

Myrmekite is common along alkali feldspar/plagioclase grain boundaries. Occasional thin (~1mm) calcite veins transect the sections.

Group MSG4:

Subsolvus, holocrystalline, medium to fine grained, equigranular to porphyritic, biotite leucomonzogranite:

The subhedral plagioclase is sericitized albite ($2V_z \sim 90^\circ$, $An < 10\%$) with albite twinning and is associated with secondary muscovite laths. The anhedral alkali feldspar is orthoclase and/or perthitic microcline with transformation twinning.

The green/brown pleochroic biotite is usually associated with euhedral opaque magnetite. Dark pleochroic haloes in basal biotite sections have formed due to lattice damage induced by the decay of radioactive elements within included minerals (Figure 4.5d)

Myrmekite is associated with alkali feldspar/plagioclase grain boundaries.

Accessory minerals include euhedral zircon, titanite, red/brown zoned pleochroic allanite (Figure 4.5e) and subhedral apatite. The titanite is present as

discrete crystals or clustered with opaque Fe/Ti oxides.

The anhedral quartz displays undulose extinction and sutured grain margins indicating some grain boundary migration and subgrain development. The alignment of sheet silicates defines the incipient foliation.

Chlorite is a common secondary mineral in most samples and has replaced mafic minerals. A remnant at the core of a chlorite pseudomorph has a distinctive pyroxene cleavage (~90°). Haematite surrounds and is associated with the alteration of opaque Fe/Ti oxides.

Group MSG-5:

Hypersolvus, coarse to medium grained granophyric, biotite leucomonzogranite:

This group is typified by generally coarse granophyric intergrowths that surround discrete plagioclase, alkali feldspar and quartz.

The plagioclase is euhedral to subhedral zoned and sericitized albite ($An < 10\%$) with albite twinning visible around rims. The alkali feldspar exhibits patch perthite as a result of exsolution and has completely overgrown the plagioclase.

The quartz is subhedral and undeformed, and in some samples shows sign of corrosion.

The subhedral green/brown pleochroic biotite is chloritized and generally associated with euhedral opaque magnetite. Biotite also forms small inclusions within plagioclase.

Accessory minerals include euhedral zircon, subhedral titanite and apatite. Titanite forms a rim around anhedral opaque Fe/Ti oxide cores. Subhedral interstitial epidote appears primary.

Chlorite, epidote, calcite and opaque Fe/Ti oxides have replaced mafic

minerals. One calcite pseudomorph has a pyroxene shape and is rimmed by opaque minerals. Thin (~1mm) calcite veins transect some sections.

Group MSG-6:

Subsolvus, holocrystalline, medium to fine grained, porphyritic, biotite leucogranodiorite:

Clasts in this group comprise a fine grained, but determinable, matrix that surrounds medium grain size phenocrysts of plagioclase and alkali feldspar. The subhedral plagioclase is zoned sodic oligoclase (An 18-20%) with sericitized cores. The anhedral alkali feldspar is orthoclase.

The quartz is anhedral, sometimes with slight undulose extinction.

The green/brown pleochroic biotite is partially chloritized and associated with opaque Fe/Ti oxides.

Titanite and opaque Fe/Ti oxides are the only accessory minerals present.

Group MSG-7:

Hypersolvus, holocrystalline, fine grained, granophyric, biotite granodiorite:

In this group fine granophyric intergrowths surround discrete plagioclase and quartz crystals.

The subhedral plagioclase is zoned with albite composition rims ($An < 10\%$) and sericitized cores. The anhedral quartz is relatively undeformed with slight undulose extinction.

Partially chloritized green/brown pleochroic biotite is the only minor phase.

Accessory minerals include apatite, euhedral zircon and titanite, and anhedral opaque Fe/Ti oxides. The zircon is frequently associated with chlorite and epidote

Figure 4.5: Photomicrographs of thin section features (field of view = ~7mm):

a Partially chloritized biotite with included euhedral zircon.

b Transformation twinning in microcline.

c Fractured and partially altered igneous garnet (PPL).

d Basal biotite section with inclusions (PPL).

e Red/brown pleochroic allanite.

f Poikilomosaic texture in a volcanic xenolith.

g Blue amphibole (riebeckite or arfvedsonite) in the matrix of a rhyolite.

h Glass shards and chlorite infilling vesicles in a rhyolite (PPL).

a

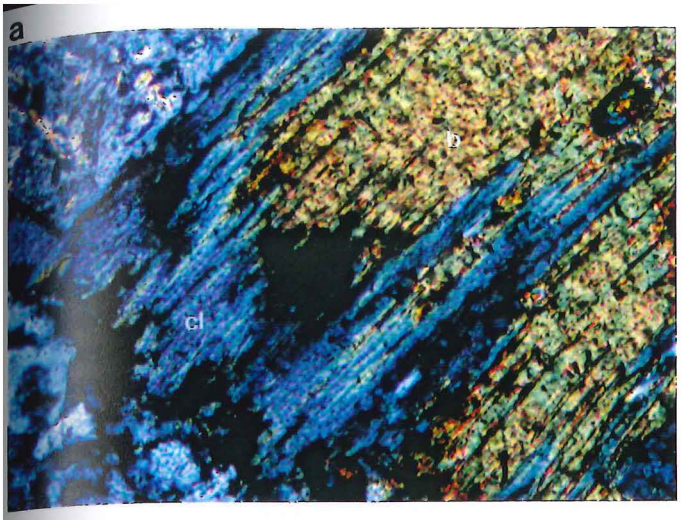

b

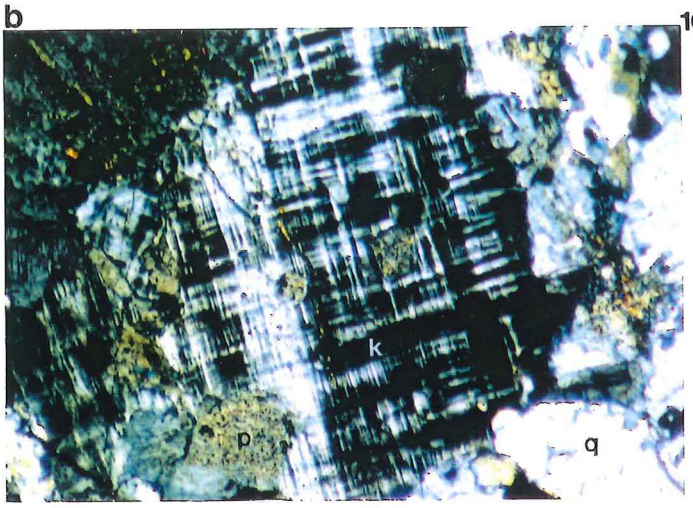

c

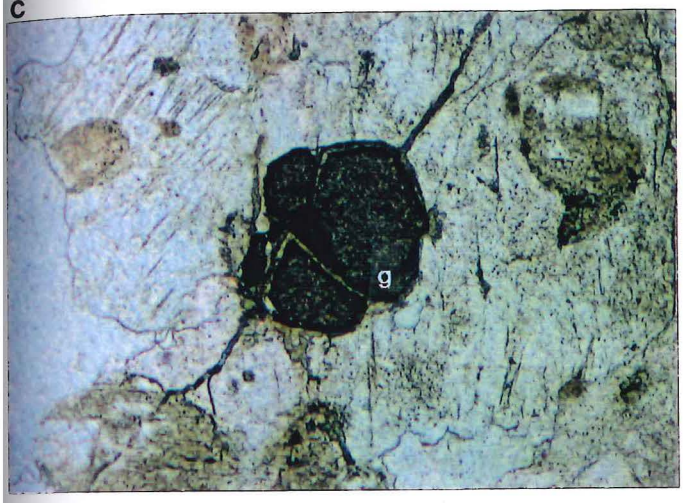

d

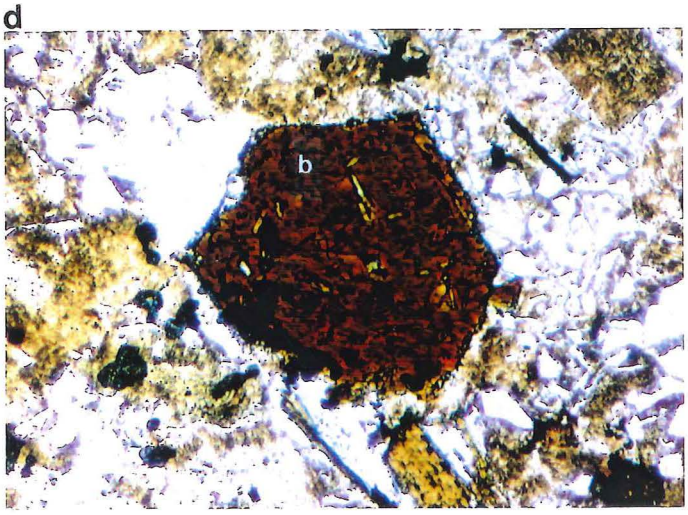

e

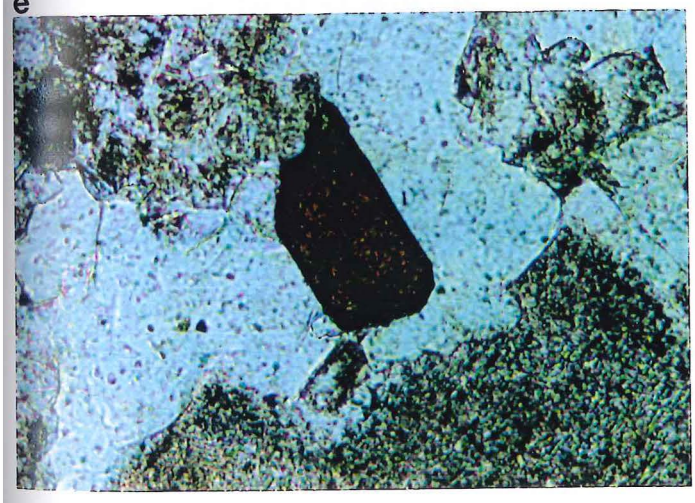

f

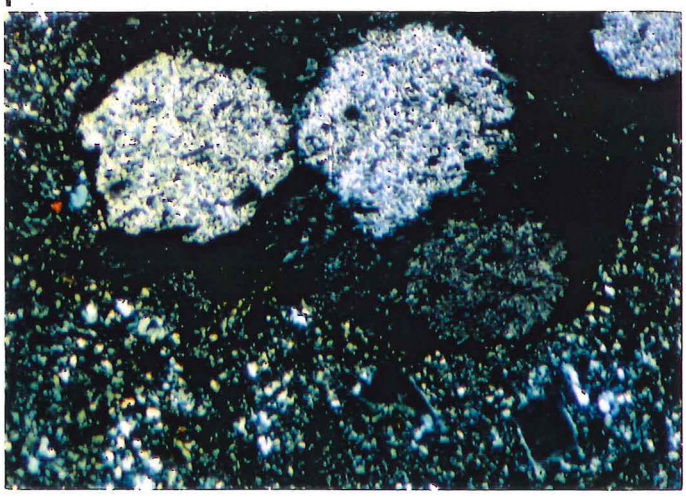

g

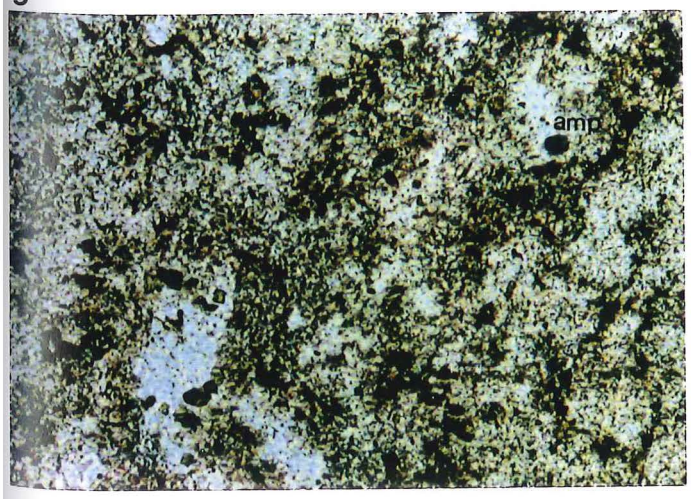

h

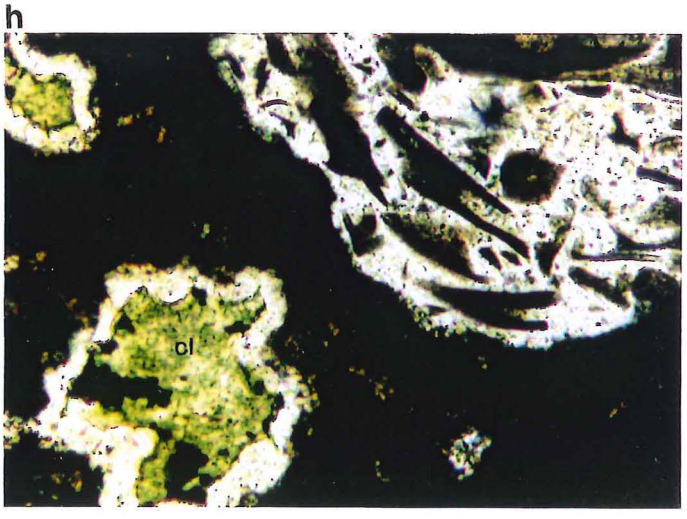

which have replaced mafic minerals.

4.2.2 Volcanic Clast Characteristics

Volcanic clasts are the predominant rock variety in the Mount Saul conglomerate. Clasts concentrate primarily in two areas, that occupy three fields within the TAS classification (Figures 4.6 and 4.7):

Group MSV1:

Hypocrystalline, porphyritic rhyolite:

Phenocrysts comprise 10-40% of these clasts and include euhedral bipyrimidal or deeply embayed quartz with symmetrical and slightly undulatory extinction. The euhedral to subhedral plagioclase is zoned with albite to sodic oligoclase rims (An5-15%) and has been replaced by large epidote crystals during saussuritization. The subhedral alkali feldspar phenocrysts are perthitic orthoclase. Volcanic lithic fragments display porphyritic texture with predominant plagioclase phenocrysts, poikilomosaic, spherulitic, and trachytic texture (Figure 4.5f).

Accessory minerals include euhedral zircon, apatite, titanite and large (>2mm) subhedral opaque Fe/Ti oxides determined as magnetite and ilmenite that can be embayed. One rhyolite contains numerous small crystals of a pleochroic blue amphibole, presumably riebeckite or arfvedsonite but difficult to determine optically (MS23,24417) (Figure 4.5g).

Pyroxene shaped chlorite pseudomorphs, peppered with opaque Fe/Ti oxides were recognized. Phenocrysts, specifically plagioclase, are often clustered, exhibiting glomeroporphyritic texture. In some samples, quartz and/or alkali

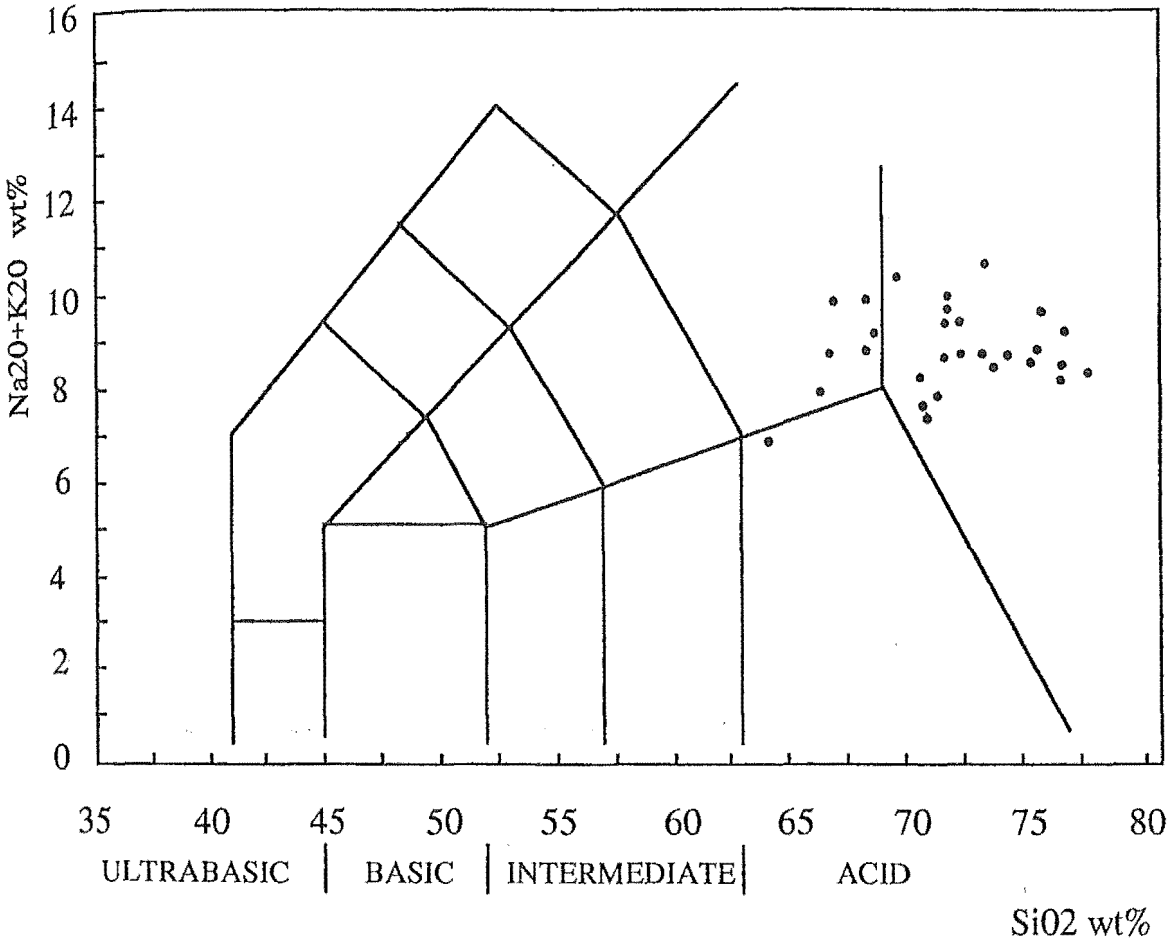

Figure 4.6: TAS classification illustrating distribution for Mount Saul conglomerate volcanic clasts.
(after Le Maitre, 1989)

feldspar phenocrysts are absent.

The matrix generally exhibits a finely crystalline felsitic texture. Becke line movement indicates a quartz/alkali feldspar mixture with minor epidote and chlorite and disseminated opaques. Poikilomosaic (snowflake) texture, with a quartz mosaic enclosing small feldspar crystals (Shelley, 1992) is common and spherulites frequently centred on phenocrysts or glass shards were noted. Flow texture around phenocrysts is present in some samples.

Pumiceous rhyolites exhibit large (>5mm) round vesicles, lined with euhedral quartz and infilled with mosaic quartz.

The matrix of one rhyolite has a coarse felsitic texture and contains tourmaline and muscovite (MS29/24423).

Two rhyolites with eutaxitic texture, incoherent matrix and fragmented phenocrysts were identified as ignimbrites (MS16/24410,MS24/24418)(Figure 4.7).

Group MSV2:

Hypocrystalline, porphyritic dacite:

Xenoliths comprise 60% of this clast and are predominantly fragmental volcanic lithics that display felsitic and trachytic texture. Phenocrysts are predominantly fragmental plagioclase that is albite (An>10%) with albite twinning. The angular anhedral quartz displays straight extinction.

The matrix is felsitic with flow texture in parts, but is generally dark brown glassy and indeterminable. Glass shards and eutaxitic texture suggest an ignimbritic origin (Figure 4.5h)

No accessory phases were noted.

Epidote and chlorite have replaced the mafic minerals originally present.

Figure 4.7: Representative photographs of volcanic groups (field of view ~5cms):
a and b Porphyritic rhyolites (MSV-1)
c and d Ignimbrite displaying eutaxitic texture (PPL and CPL).

a

b

c

d

Group MSV3:

Hypocrystalline, porphyritic trachyte/trachydacite:

Clasts are considered trachyte if the normative quartz value in Q + an + ab + or is <20% (Appendix 1).

Xenoliths comprise 20 - 70% of the clasts. Volcanic lithic fragments can contribute up to 92% of this total. Plagioclase phenocrysts are zoned with albite rims (An<10%). Minor anhedral quartz is present as phenocrysts with slight undulatory extinction and also forms mosaics infilling lithophysae. Epidote/chlorite/Fe/Ti oxide pseudomorphs indicate mafic minerals have been replaced.

Accessory minerals include apatite associated with large euhedral diamond shaped magnetite, anhedral titanite and zircon.

The matrix comprises a fine dark hypocrystalline mixture of quartz, alkali feldspar, epidote, chlorite, calcite and opaque Fe/Ti oxides, some patches of which display an alignment of microlites which wrap around phenocrysts.

Three samples are considered to be quartz/feldspar porphyries because of abundant phenocrysts (>50%) (MS20/24414, MS30/24424, MS49/24443). The xenoliths can exceed 1cm in diameter.

4.2.3 Petrographic Interpretation

The conglomerate clasts examined from Mount Saul are interpreted within the confines of the textural categories outlined in Chapter 1, 1.3.4a and defined in Chapter 2, 2.2.

The Mount Saul conglomerate granitoid clasts, according to modal analysis, are predominantly monzogranites with approximately equal proportions of alkali feldspar and plagioclase. Granodiorites and syenogranites are also present. Granitoid clasts display hypersolvus and subsolvus textures indicating crystallization/cooling histories affected by differing water pressures (Chapter 2, 2.2).

Hypersolvus granitoids (groups MSG-2,5,7) comprise biotite leucomonzogranites, leucosyenogranites and a biotite granodiorite. Hypersolvus clasts are undeformed and frequently porphyritic, with granophyric intergrowths, indicating rapid crystallization of the magma, and suggesting hypabyssal/subvolcanic emplacement. A change from subsolvus to hypersolvus conditions is indicated by the presence of discrete plagioclase and alkali feldspar surrounded by granophyric intergrowths of perthitic alkali feldspar to mesoperthite and quartz. This change reflects a relative change in magma position to shallower levels with a resultant change in pressure.

Subsolvus granitoids (groups MSG-1,3,4,6) comprise predominantly biotite ($\pm$ muscovite) leucomonzogranites, with granodiorites and leucosyenogranites.

Texture, and the presence of euhedral primary garnet in some samples, suggests magma genesis and emplacement was at lower crustal levels. Secondary foliations are only found in clasts of subsolvus granitoids, and these relate to post-intrusive incipient strain, probably within a shear zone.

Biotite is the prevalent minor phase in all granitoid clasts, accompanied by subordinate muscovite in some samples perhaps indicating a more evolved character. The low percentage of biotite in leucocratic samples (i.e. $<5\%$) suggests magmas were relatively H_2O poor with low Fe and Mg.

Concentric zoning in plagioclase crystals in plutonic and volcanic clasts is emphasized by sericitization which preferentially affects the more calcic zones.

The volcanic clasts from the Mount Saul conglomerate are distinguished geochemically as predominantly rhyolite, with some trachyte, trachydacite and dacite. In rhyolites the phenocryst content is generally under 30%, whereas in trachydacites/trachytes and dacites it can be over 50%. The mineralogy observed in most granitoid clasts is also found in the volcanic clasts. Accessory biotite, titanite and apatite were observed and support a possible relationship to granitoid clasts that also contain these minerals. The zircons observed in the majority of samples are euhedral and prismatic indicating a primary igneous origin. The presence of blue amphibole in the matrix of one rhyolite clast distinguished this from any of the plutonic clasts examined.

Volcanic lithic fragments are present in the majority of volcanic clasts

irrespective of geochemical type. The volcanic nature of the enclaves suggests they are cognate, representing earlier stages of volcanic eruption, or fragmentation within the volcanic conduit during an explosive pyroclastic/ignimbritic eruption. The spherulitic and felsitic texture predominant in volcanic samples indicates devitrification and a high degree of undercooling of a previously glassy matrix. Becke line movement observed in some spherulites indicates, that at the eutectic, quartz was dominant over alkali feldspar. The presence of plagioclase but lack of quartz and alkali feldspar phenocrysts in some rhyolites indicates crystallization of these minerals only occurred during the last stages of magma development. Eutaxitic texture indicates that several of the volcanic clasts are ignimbrites. However, the coherent and continuous flow layers in the majority of volcanic clasts suggests they were emplaced within a rhyolite dome and/or as a flow.

The presence of tourmaline with muscovite, and the coarse recrystallized matrix in one rhyolite (MS29/24423), indicates pneumatolysis or hydrothermal activity. The varying degrees of sericitization and saussuritization displayed by feldspar in plutonic and volcanic clasts indicates low temperature hydrothermal alteration subsequent to crystallization.

4.3 Geochemistry

4.3.1 Categorization of Granitoids

To determine granitoid classification according to implied source characteristics for the Mount Saul conglomerate igneous clasts, the Aluminium Saturation Indices for each sample were calculated (Appendix 5) and are displayed in Figure 4.8. Of the 17 metaluminous samples, 5 are granitoids (4 monzogranites and a syenogranite) and considered I-types (Chapter 2, 2.3.1) (White and Chappell, 1983). Eight samples are highly metaluminous (A/NK >1.2), 3 granitoid and 5 volcanic clasts (Appendix 5). Three volcanic clasts plot with an ASI >1.1 and will be discussed in the following section. The majority of samples plots in a tight cluster with ASI values close to 1.0 so that classification of type according to source using the ASI is not possible (Chapter 2, 2.3.1). The peralkaline clast (MS16/24417), a rhyolite, has an ASI of 0.99 and A/NK = 0.94.

Using trace element abundances to support type character, the Mount Saul clasts were plotted against various major element ratios (Figure 4.9a and b). Granitoid clasts plot predominantly within the fractionated felsic (FG) I- and S- type granite field (Whalen *et al.*, 1987). Some volcanic clasts also plot within this field exhibiting, in general, higher abundances of the discriminatory HFS elements used. The majority of volcanic samples, however, plot within the field considered indicative of highly fractionated/A-type character and will be discussed further in the following sections.

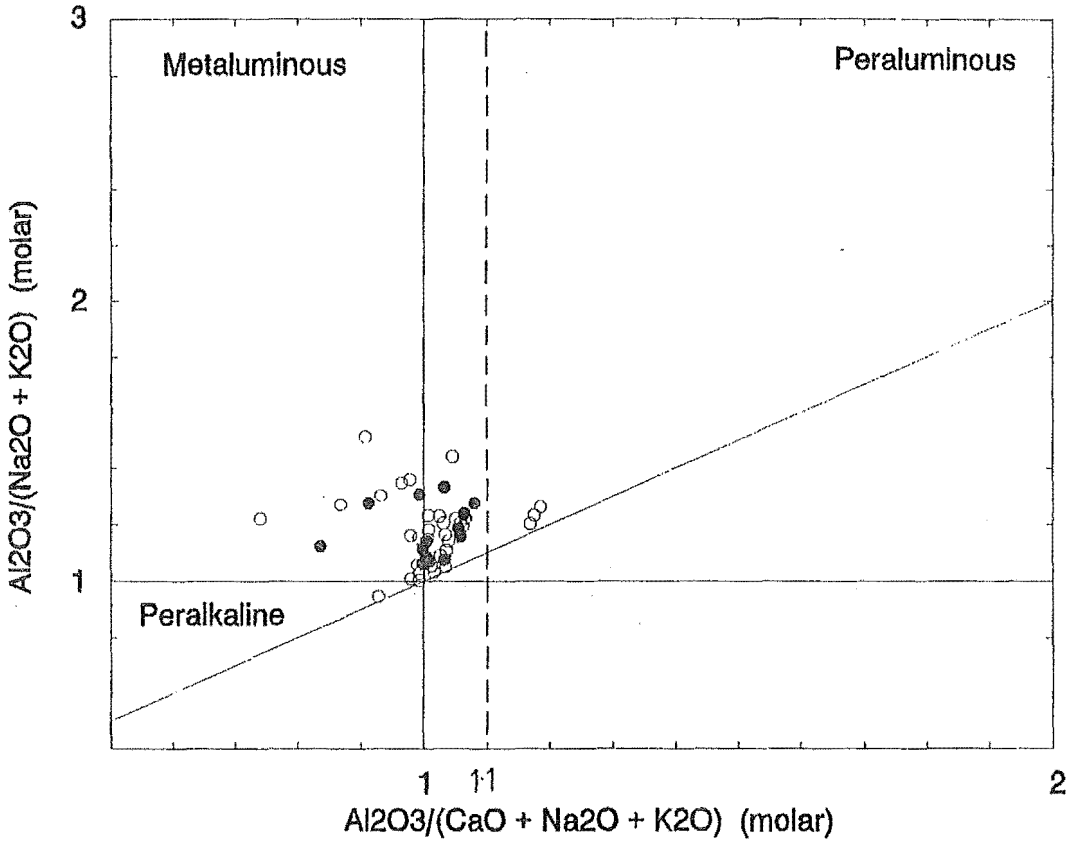

Figure 4.8: Aluminium Saturation Indices for Mount Saul conglomerate clasts. A/CNK = 1.1 indicates the boundary between highly fractionated I-type and S-type granitoid/volcanic clasts.
(after Maniar and Piccoli, 1989)

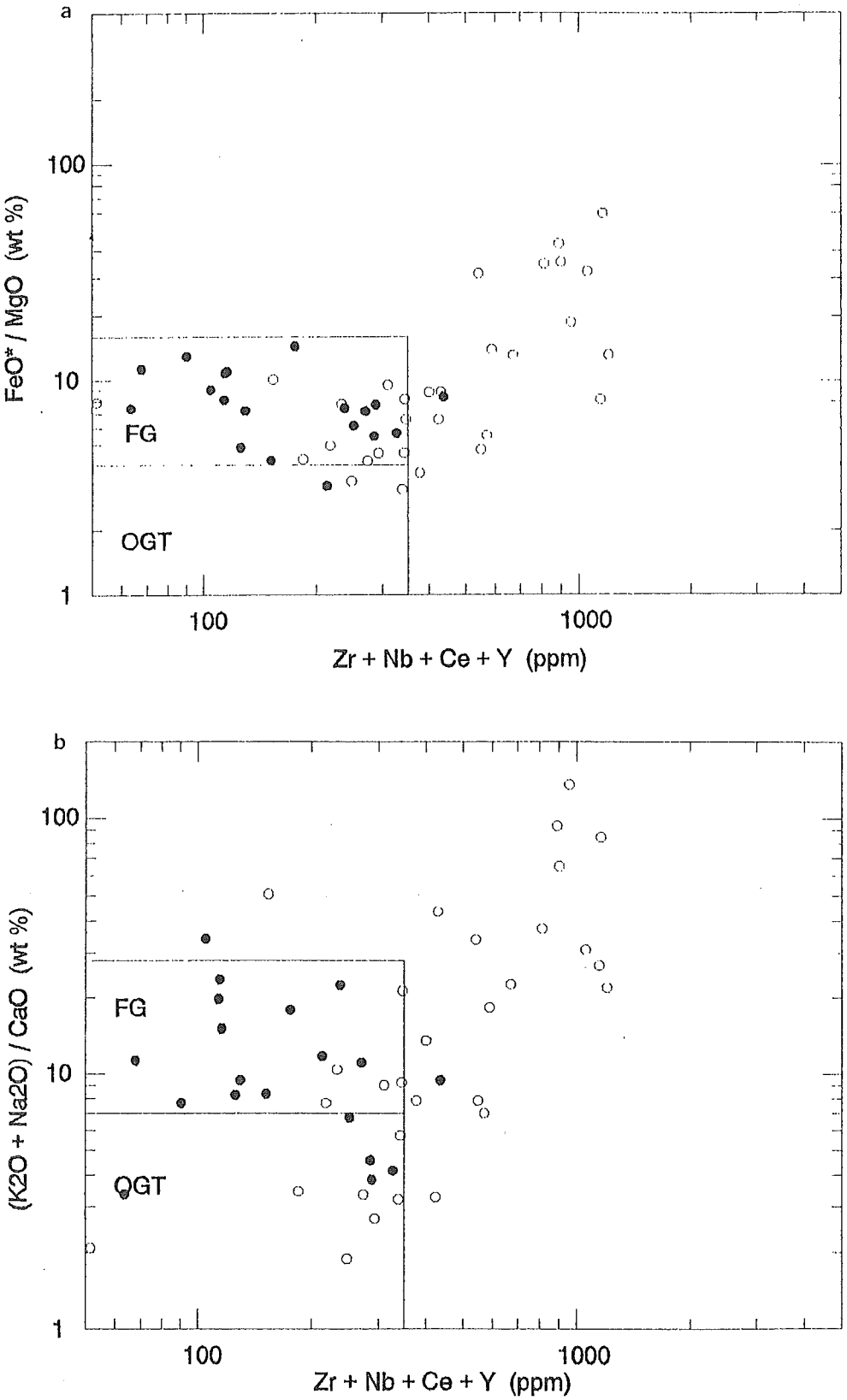

Figure 4.9: High Field Strength trace elements versus major element ratios with fields for fractionated felsic granites (FG), and ordinary granite types (OGT) delineated.
a Zr+Nb+Ce+Y versus FeO*/MgO
b Zr+Nb+Ce+Y versus $(K_2O+Na_2O)/CaO$
(after Whalen *et al.*, 1987)

The alkali lime index for Mount Saul samples was calculated (Appendix 4) and plotted (SiO_2~48-59%)(Figure 4.10). Data indicate clasts are alkalic to calc-alkaline. Although generally the Mount Saul clasts are silica-rich, slight heterogeneities allow an extrapolation to be made. This classification is supported by the silica-alkalis plot (Figure 4.11) which indicates a predominance of alkaline samples, and by the AFM ternary diagram (Figure 4.12).

4.3.2 Plutonic/Volcanic Relationship

The geochemical analyses for Mount Saul volcanic clasts have been combined with granitoid clast data in all discrimination diagrams.

Twelve of the metaluminous samples identified by ASI are volcanic, and of these, five are highly metaluminous (A/NK >1.2). Two of the three volcanic clasts with an ASI~1.2 were considered S-types (MS29/24423, MS33/24427). MS36/24430 also exhibits an ASI >1.1, but was considered to have undergone pnematolytic alteration, as indicated by the presence of interstitial euhedral tourmaline and muscovite. In the absence of granitoids with similar ASI values, the two S-type volcanic clasts were considered separate and unrelated to the plutonic samples examined. Only one volcanic sample displays a peralkaline character. However, this does not preclude a relationship with some of the weakly peraluminous samples (primarily volcanics) which appear to trend toward the peralkaline field (Figure 4.8).

The ASI plot (Figure 4.8) does not differentiate the volcanic clasts that display A-type characteristics in Figure 4.9. The volcanic clasts that plot in the

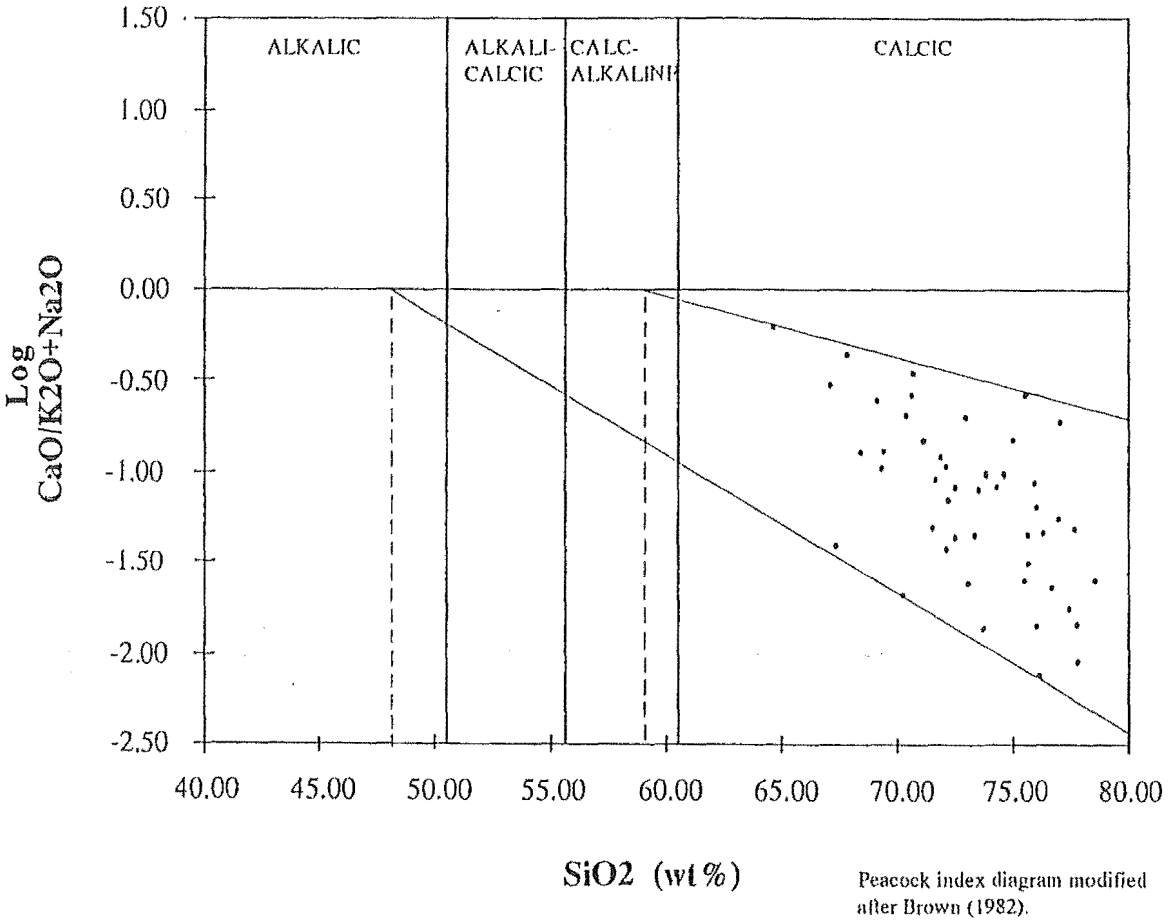

Figure 4.10: Alkali-lime Index (definition Appendix 4) illustrating extrapolated values for Mount Saul conglomerate clasts.

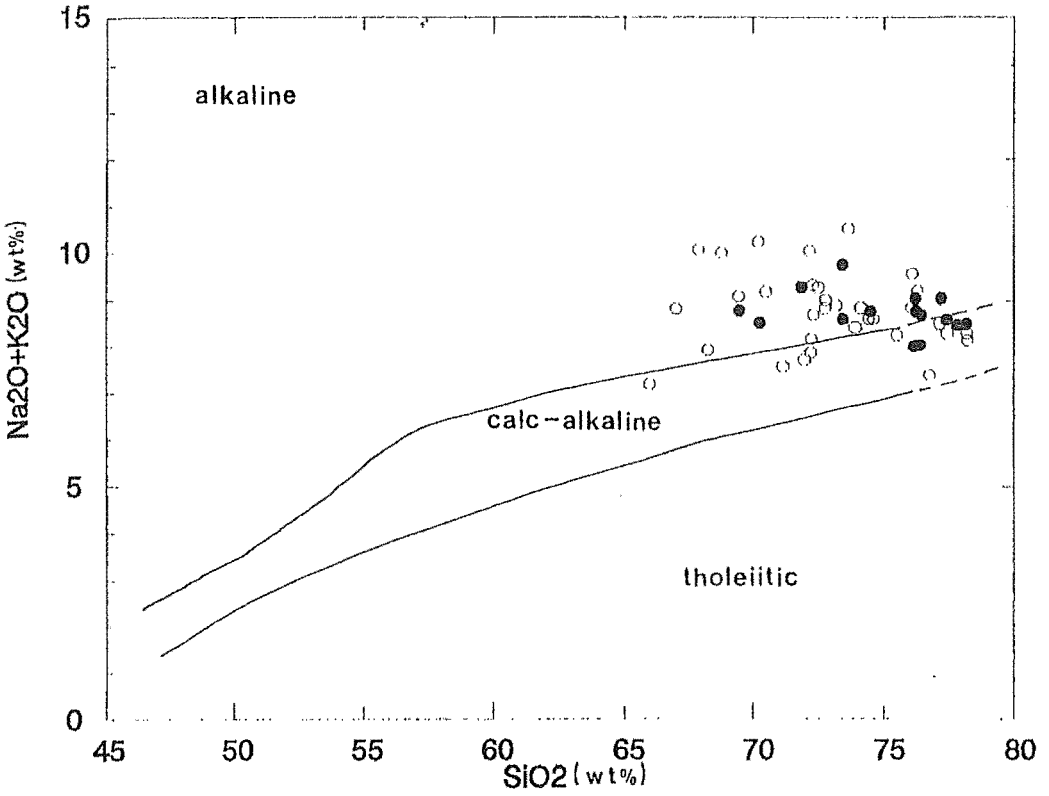

Figure 4.11: Alkali-silica diagram illustrating distribution of Mount Saul conglomerate samples between alkaline, calc-alkaline, and tholeiitic fields.
(after Kuno, 1968)

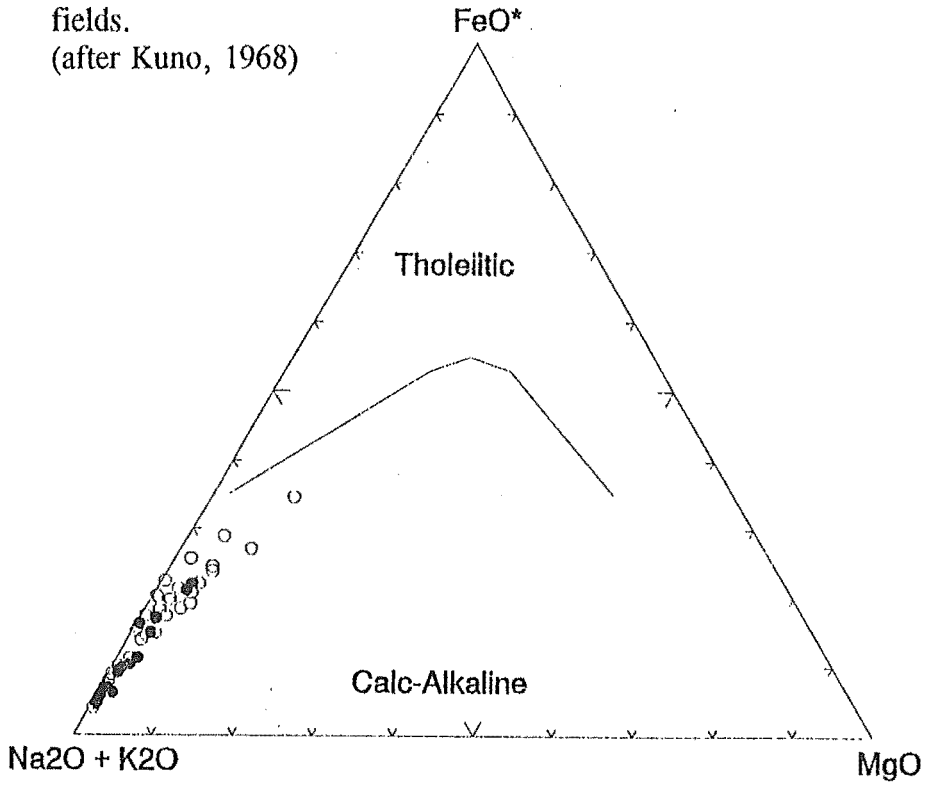

Figure 4.12: AFM (Na_2O+K_2O; Total iron as FeO; MgO) ternary diagram illustrating distribution of Mount Saul conglomerate clasts. The dashed line separates tholeiitic and calc-alkaline compositions.
(after Irvine and Baragar, 1971)

highly fractionated/A-type field of Figure 4.9 have relatively high abundances of the HFS elements (Zr, Nb, Ce, Y and Ga) and display a range of silica values from 66% - 76%.

In plots of Ga/Al-K_2O+Na_2O/CaO (Figure 4.13a), also used to discriminate I-, S-, and A-type granitoids (Whalen *et al.*, 1987), samples plot predominantly in the fields defined for fractionated granitoids, at some distance from the calculated average A-type. A plot of Ga/Al-Y (Figure 4.13b), however, separates distinctly a group of eight volcanic clasts with high HFS characteristics (MS22/24416, MS23/24417, MS25/24419, MS27/24421, MS32/24426, MS37/24431, MS47/24441, MS48/24442). The eight samples have comparable ASI values between 0.92 and 1.03, and include the peralkaline clast (MS23/24417).

Harker diagrams, using major elements as discriminants, indicate a possible cogenetic relationship between the Mount Saul igneous clasts (Figure 4.14a and b). Plots with silica versus various trace elements, however, display no discernable correlation (Figure 4.14c and d). The Rb-Ba-Sr ternary diagram (Figure 4.15) indicates a fractionation trend from granodiorite to granite (*sensu stricto*) and associated volcanics. There is a marked separation between these samples and those that plot within the strongly differentiated field. Samples that display the strongest A-type characteristics plot in the strongly differentiated field, as do three highly felsic and fractionated granitoids (SiO_2 ~76%) (MS7/24401, MS12/24406, MS41/24435).

The K_2O-Na_2O-CaO ternary plot (Figure 4.16) indicates a concentration of

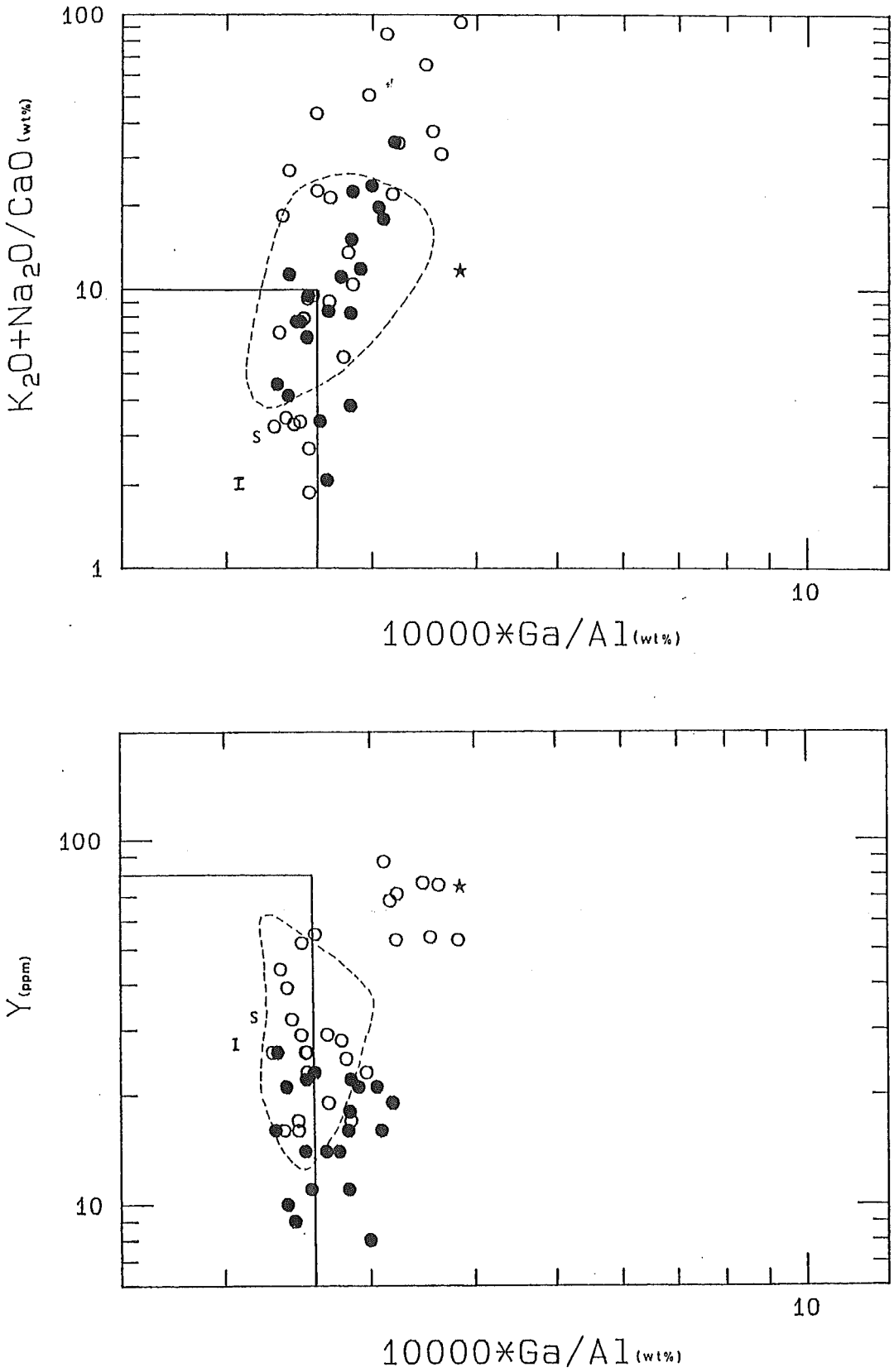

Figure 4.13: Plots of 10000*Ga/Al versus a)K_2O+Na_2O/CaO and b) Y illustrating Mount Saul conglomerate clast distribution. I- and S-type granite field delineated, dashed line represents fractionated granite field, ⋆ = calculated average A-type, I = calculated average I-type, S = calculated average S type.
(after Whalen *et al.*, 1987)

Figure 4.14: Harker variation diagrams for major and trace elements illustrating distribution of Mount Saul conglomerate clasts:
a SiO_2 versus Al_2O_3
b SiO_2 versus TiO_2
c SiO_2 versus Zr
d SiO_2 versus Rb.

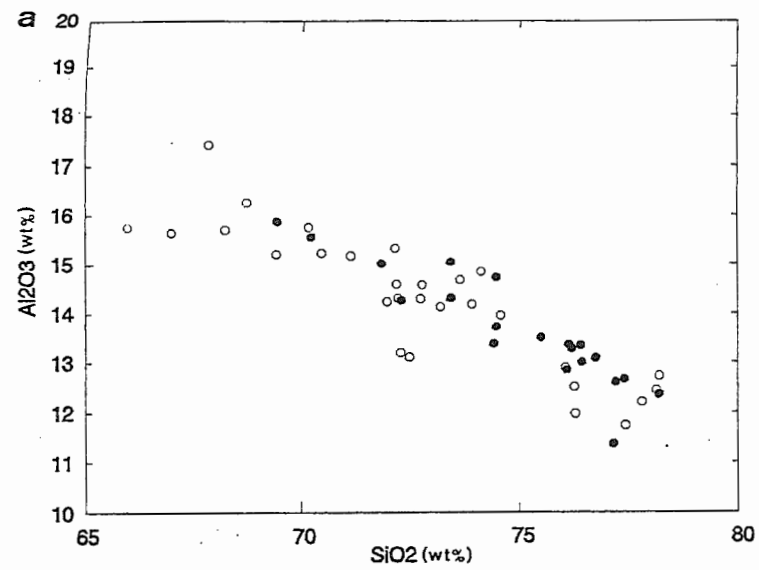
a
Al2O3 (wt%)
SiO2 (wt%)
20
19
18
17
16
15
14
13
12
11
10
65
70
75
80

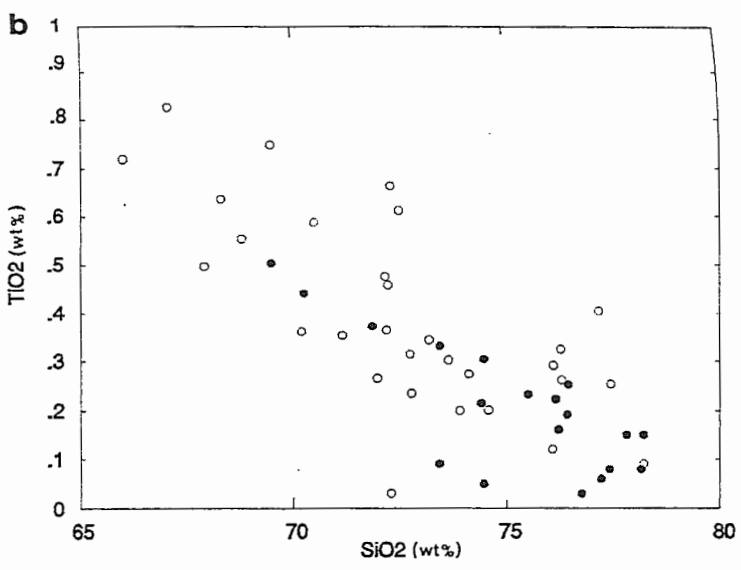
b
TiO2 (wt%)
SiO2 (wt%)
1
.9
.8
.7
.6
.5
.4
.3
.2
.1
0
65
70
75
80

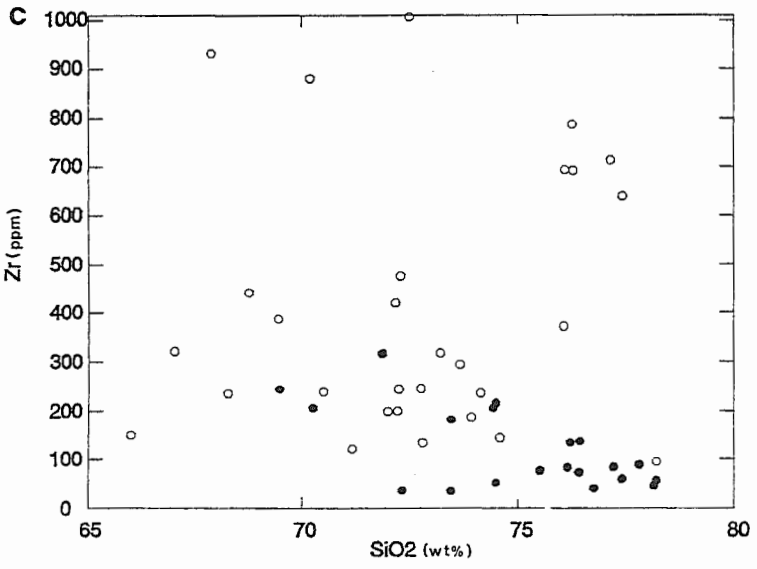
c
Zr (ppm)
SiO2 (wt%)
1000
900
800
700
600
500
400
300
200
100
0
65
70
75
80

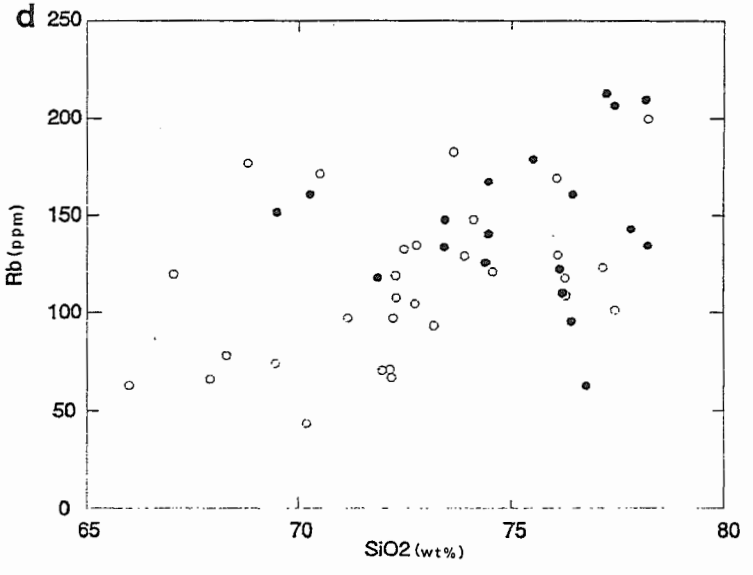
d
Rb (ppm)
SiO2 (wt%)
250
200
150
100
50
0
65
70
75
80

volcanic clasts with lower CaO values than the granitoid clasts, and volcanic clasts with relatively lower K_2O values and higher CaO values than the granitoid clasts.

Primitive mantle normalized (Sun and McDonough, 1989) multi-element abundance diagrams were used to distinguish gross trace element features within the Mount Saul conglomerate clasts. The distinctive spiked pattern and overall LIL enrichment indicates magmas contain a distinctive crustal signature and were related to subduction (Figure 4.17) (Wilson, 1989; Saunders *et al.*, 1991). The majority of volcanic clasts mirror the trace element characteristics exhibited by granitoids and display a typically fractionated character, but with higher Ba and variable Th values (Figure 4.17a and c). Four granitoid samples display erratic trace element characteristics which could relate to a heterogeneous source, varying degrees of crustal contamination or subsequent hydrothermal or metasomatic alteration (Figure 4.17b). Figure 4.17d displays the samples designated A-type, and emphasizes the extreme fractionation of Strontium with high HFS element abundances.

4.3.3 Correlation with Mineralogy

The Mount Saul samples display a range of silica values (64% - 78%) which corresponds to the modal distribution across the granodiorite, monzogranite, syenogranite fields at moderate (40-50%) quartz values (Figure 4.3).

Clasts determined as I-type according to ASI values contain green/brown biotite and titanite (White and Chappell, 1983). Samples with an ASI between 1.0 and 1.1 frequently contain brown pleochroic biotite ($\pm$ muscovite), and may contain

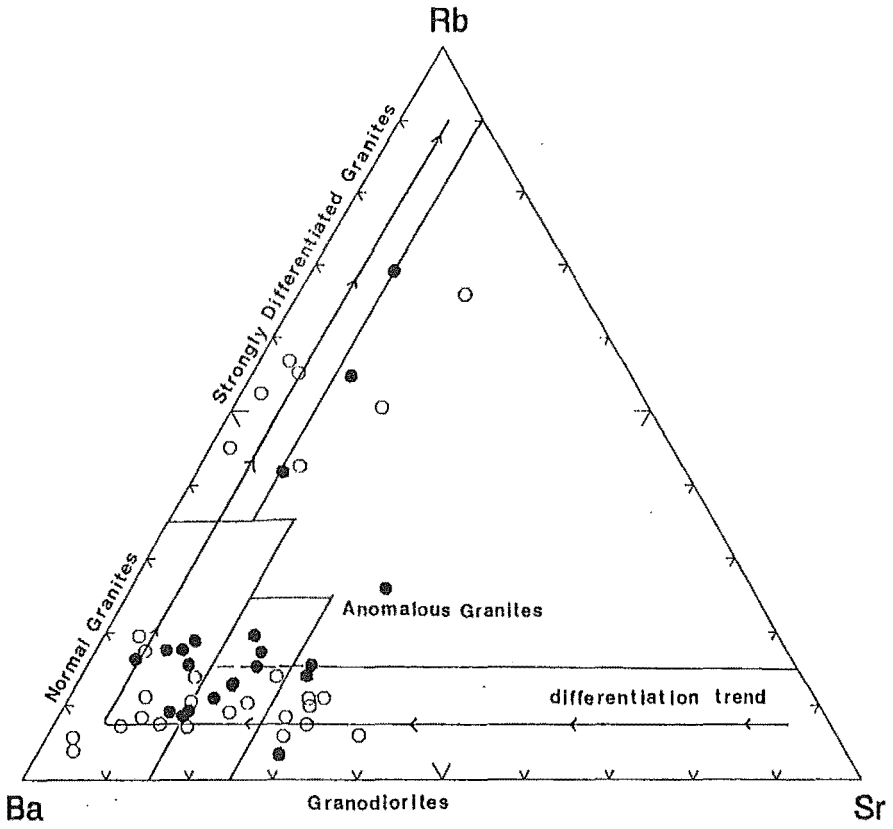

Figure 4.15: Rb-Sr-Ba ternary diagram illustrating relationship between Mount Saul conglomerate clasts.
(after El Bouseily and El Sokkary, 1975)

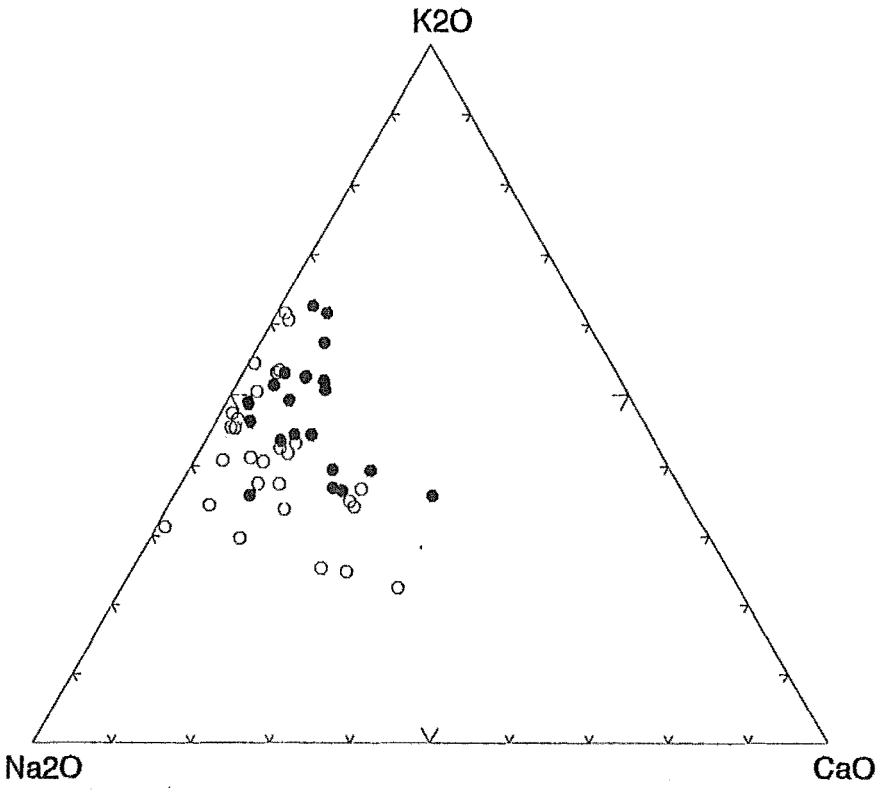

Figure 4.16: K_2O-Na_2O-CaO ternary diagram which illustrates the K_2O/Na_2O ratio, and considers CaO for Mount Saul conglomerate clasts.

titanite. The two samples with an S-type classification contain biotite and muscovite, but not garnet. The samples that contain euhedral igneous garnets have a weakly peraluminous (MS42/24436 - ASI=1.07) and unusual metaluminous (MS44/24438 - ASI=0.74) character. Igneous garnets can be associated with the late stage Mn-rich fluid crystallization of pegmatites. However, the low Mn content and high abundance of secondary calcite in this clast indicates the ASI may be unreliable.

The zircon, generally present in granitoid and volcanic clasts as an accessory phase included in biotite, is less conspicuous in thin section than might be expected for samples with up to 1002ppm Zirconium (MS47/24441) (Figure 4.14c).

Some xenoliths observed in volcanic clasts exhibit trachytic texture with an alignment of feldspar laths. This feature is common to trachytes and supports the alkaline character displayed geochemically by these samples.

The peralkaline rhyolite (MS23/24417) contains numerous small (<0.1mm) euhedral to subhedral crystals of a blue sodic amphibole, probably riebeckite or arfvedsonite, has a high silica content (~75%), and high HFS values, all typical A-type characteristics (Whalen *et al.*, 1987; Eby, 1990, 1992).

Pyroxene pseudomorphs were recognized in the relatively more mafic samples. Generally, however, the felsic nature of samples was supported by the lack of mafic material, and biotite was the only mafic phase present.

The presence of secondary calcite in veins and as pseudomorphs is reflected

Figure 4.17: Multi-element primitive-mantle-normalized (Sun and McDonough, 1989) abundance diagrams for Mount Saul conglomerate clasts:
a granitoids (I-types)
b granitoids (evolved I-types and S-types)
c volcanics (related to I-type granitoids)
d volcanics (peralkaline/A-type characteristics).

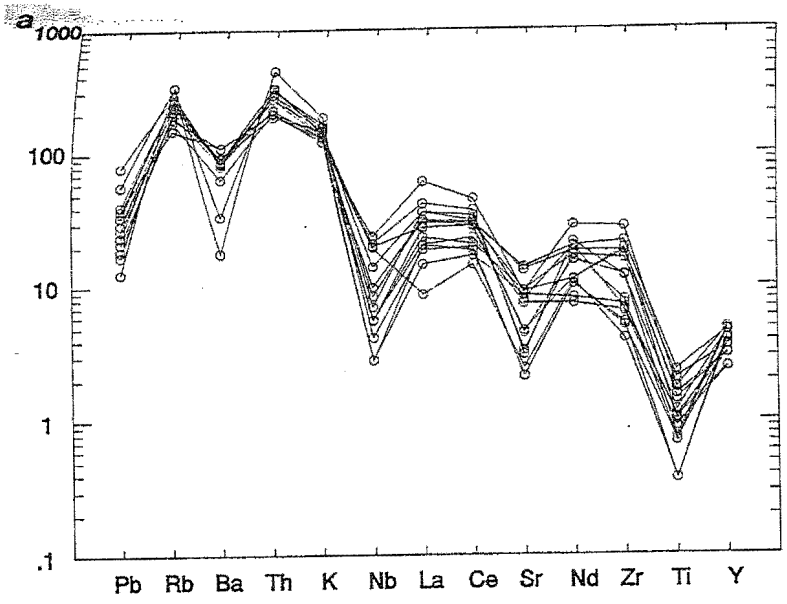
a
1000
100
10
1
.1
Pb Rb Ba Th K Nb La Ce Sr Nd Zr Ti Y

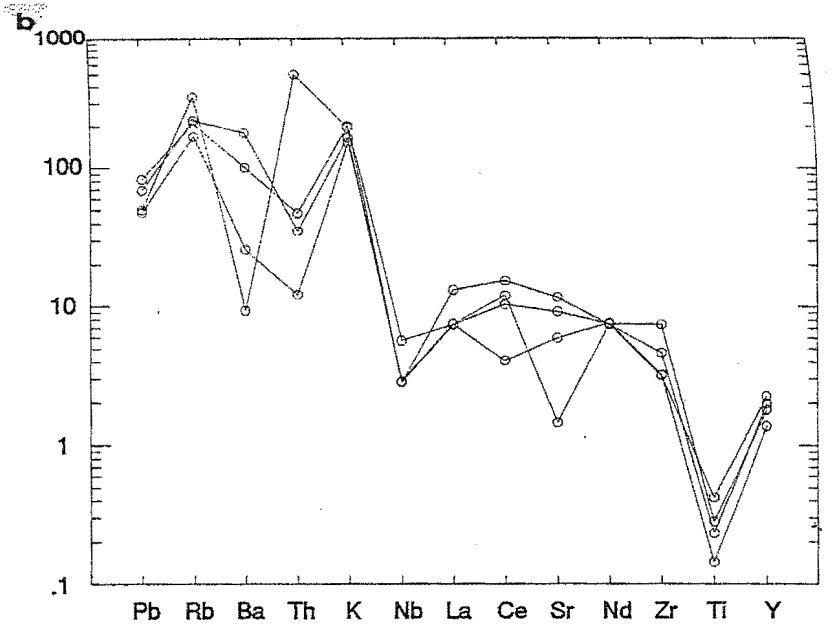
b
1000
100
10
1
.1
Pb Rb Ba Th K Nb La Ce Sr Nd Zr Ti Y

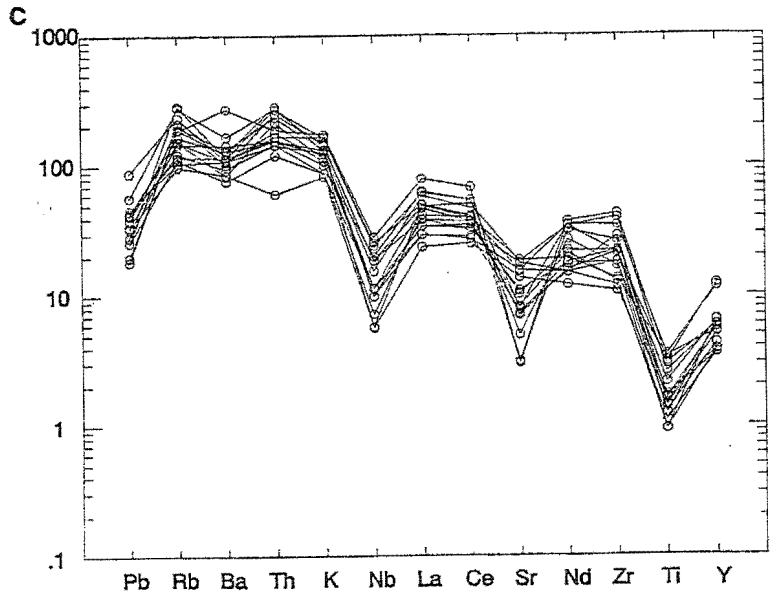
c
1000
100
10
1
.1
Pb Rb Ba Th K Nb La Ce Sr Nd Zr Ti Y

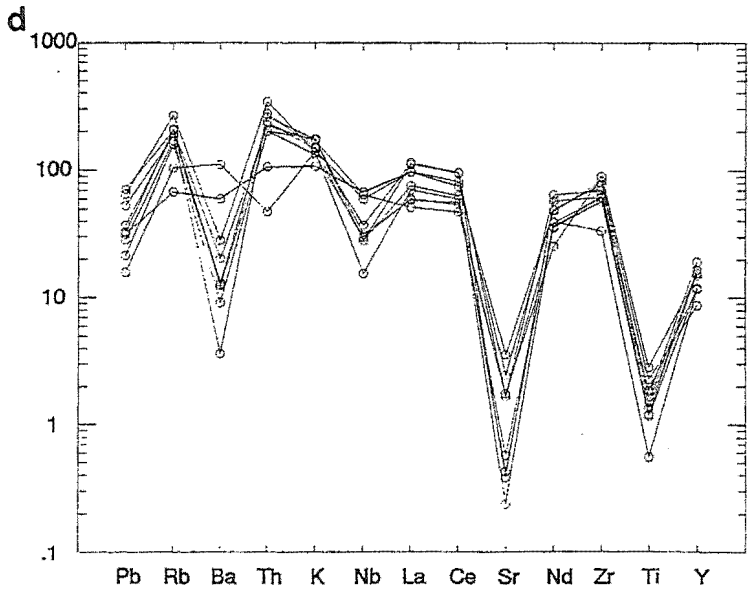
d
1000
100
10
1
.1
Pb Rb Ba Th K Nb La Ce Sr Nd Zr Ti Y

in the Rb-Ba-Sr ternary diagram (Figure 4.15) by the clasts that plot outside the delineated fields. The sample that plots with extreme separation from the others is MS44/24438, the metaluminous clast containing garnet, again indicating metasomatism.

4.3.4 Discrimination of Tectonic Setting

The majority of Mount Saul clasts plot within the volcanic arc (VAG) field of Pearce et al.(1984) (Figure 4.18 a and b). The previously identified A-type volcanic samples plot in the within plate granite (WPG) field along with five other volcanic samples that display some A-type character (i.e. higher HFS trace element abundances).

4.4 Synopsis

Mount Saul conglomerate granitoid clasts range in mineralogy and modal composition from biotite ($\pm$ muscovite) granodiorite/leucogranodiorite to predominantly leucomonzogranites, with some leucosyenogranites.
Subsolvus and hypersolvus granitoid clasts are distinguishable texturally. The geochemical analyses support the petrographic features noted and indicate that all granitoid clasts are subduction related and have a predominantly calc-alkaline character. Granitoid clasts include I-types and evolved I-types, and two S-types.

The TAS classification places volcanic samples in the dacite, rhyolite, trachyte and trachydacite fields. Some volcanic clasts are identified as ignimbrites

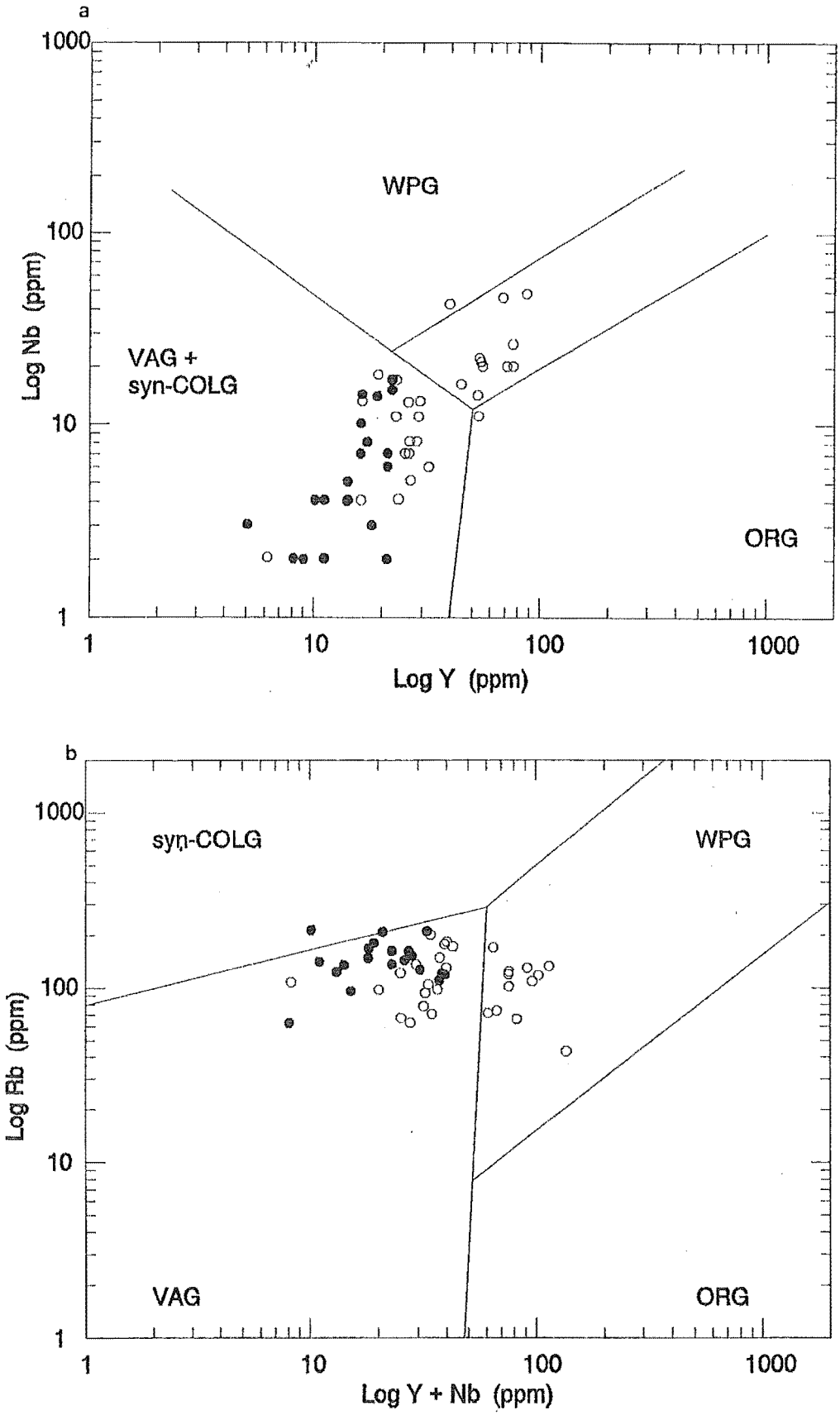

Figure 4.18: Tectonic discrimination diagrams illustrating distribution for Mount Saul conglomerate igneous clasts within the syn-collision (syn-COLG), volcanic arc granite (VAG), within plate granites (WPG), and ocean ridge granites (ORG) fields; **a** Nb-Y, **b** Rb-Y+Nb. (after Pearce *et al.*, 1984)

and pyroclastic. Regardless of type, volcanic clasts are porphyritic and divisible geochemically into two broad groups based on trace element abundances. The two groups separate volcanic clasts that relate to the granitoid clasts present in the Mount Saul conglomerate and those that do not relate to any intrusive phase present. Volcanic clasts that do not relate to granitoids exhibit an alkaline character and A-type granitoid characteristics.

4.4 Discussion

The source for the Mount Saul conglomerate igneous clasts was dominated by calc-alkaline to alkaline volcanics. This volcanic province incorporated rhyolitic domes and/or lavas with ignimbrites and pyroclastic deposits and was the response to subduction along an active continental margin. Extrusive activity was probably accompanied by intrusion at subvolcanic, hypersolvus and subsolvus crustal levels.

The scatter displayed by Mount Saul igneous clasts in Harker diagrams using major and trace elements as discriminators (Figure 4.14) indicate that, although trends can be seen, it is unlikely that they represent a single cogenetic suite.

Intrusives present include mineralogically and geochemically distinguished I-type granitoids related to the partial melting of a crustal igneous source. Present also are weakly peraluminous evolved I-type granitoids and volcanics (ASI between 1.0-1.1, Zen, 1986), relatively depleted in Ba and Sr, and enriched in Rb, which can be attributed to varying degrees of feldspar fractionation. Volcanics that relate to intrusives generally have higher K_2O values and represent a more evolved magma.

The presence of geochemically distinct S-types indicates a sedimentary source which could relate to a thickening of the continental margin.

The continuum displayed by trachyte to rhyolite composition volcanic clasts in the TAS diagram (Figure 4.6) is reflected in the progression toward distinctly peralkaline/A-type magma characteristics and suggests a gradual change from calc-alkaline to alkaline composition magma. It has been noted that A-type magmas have been emplaced in a variety of tectonic settings that as yet cannot be distinguished chemically with confidence (Collins et al., 1982; White and Chappell, 1983; Whalen *et al.*, 1987; Eby, 1990, 1992; Chappell and White, 1992). The Mount Saul volcanic clasts that display A-type character are relatively more mafic, but exhibit extremely low Nd, Sr and Ba, and have higher HFS elemental abundances than the granitoid and other volcanic clasts examined. White and Chappell (1992) suggest A-type magmas from the Lachlan Fold Belt represent the partial melt of a residue depleted in water by the earlier extraction of minimum melt I-type magmas. The data from Mount Saul suggest that the peralkaline and weakly peralkaline/A-type volcanic clasts present are sourced from crust that has a subduction related signature. The volcanic clasts could be the result of partial melting of a crustal igneous source of tonalitic to granodioritic composition (Creaser *et al.*, 1991). This A-type volcanicity could relate to late anorogenic magmatism, after subduction along the continental margin had ceased. It has been noted that magmas often reflect the tectonic setting of their source rather than the environment into which they are emplaced (Weaver *et al.* 1992). The Mount Saul volcanic clasts, therefore, could also indicate rifting and extensional tectonism prior to or during the Early Cretaceous.

The Mount Saul conglomerate igneous clasts preserve a record of at least three different magmatic phases that have a distinctive chemical and mineralogical character that reflects different source rock features.

Conglomerate deposition took place at some stage during the Early Cretaceous (~120Ma) when the volcanic province source had been partially dissected to expose hypabyssal/hypersolvus, foliated and unfoliated, subsolvus granitoid bodies. Present also at the time of conglomerate formation were volcanics relating to a phase of activity representative of the closing stages of subduction and possibly a change in tectonic regime.

CHAPTER 5

LAKE HILL CONGLOMERATE

5.1 Introduction

5.1.1 Locality

Lake Hill (709m) is located to the east of Lake Coleridge, adjacent to the Rakaia River in mid Canterbury (NZMS 260, 1:50,000, K35 Coleridge, grid ref.940/606) (Figures 1.1b and 5.1). The conglomerate, which in outcrop extends laterally to the northwest and southeast along the northeasterly face of Lake Hill, comprises granitoid, volcanic and greywacke clasts of pebble to boulder size, generally cemented by a quartz-rich, coarse sandstone matrix (Figure 5.2). The conglomerate is primarily massive to well bedded and clast supported, but can grade to matrix supported where fine silt is the predominant matrix material (Figure 5.2). The conglomerate is interformational, and is interbedded with massive to well bedded coarse to fine sandstones and fine laminated siltstones that dip to the east (~15 - 20°) (Figure 5.2). The conglomerate and basement greywacke are unconformably overlain by Upper Cretaceous coal measures, Pleistocene lake sediments and till, and recent gravels (Lauder, 1962).

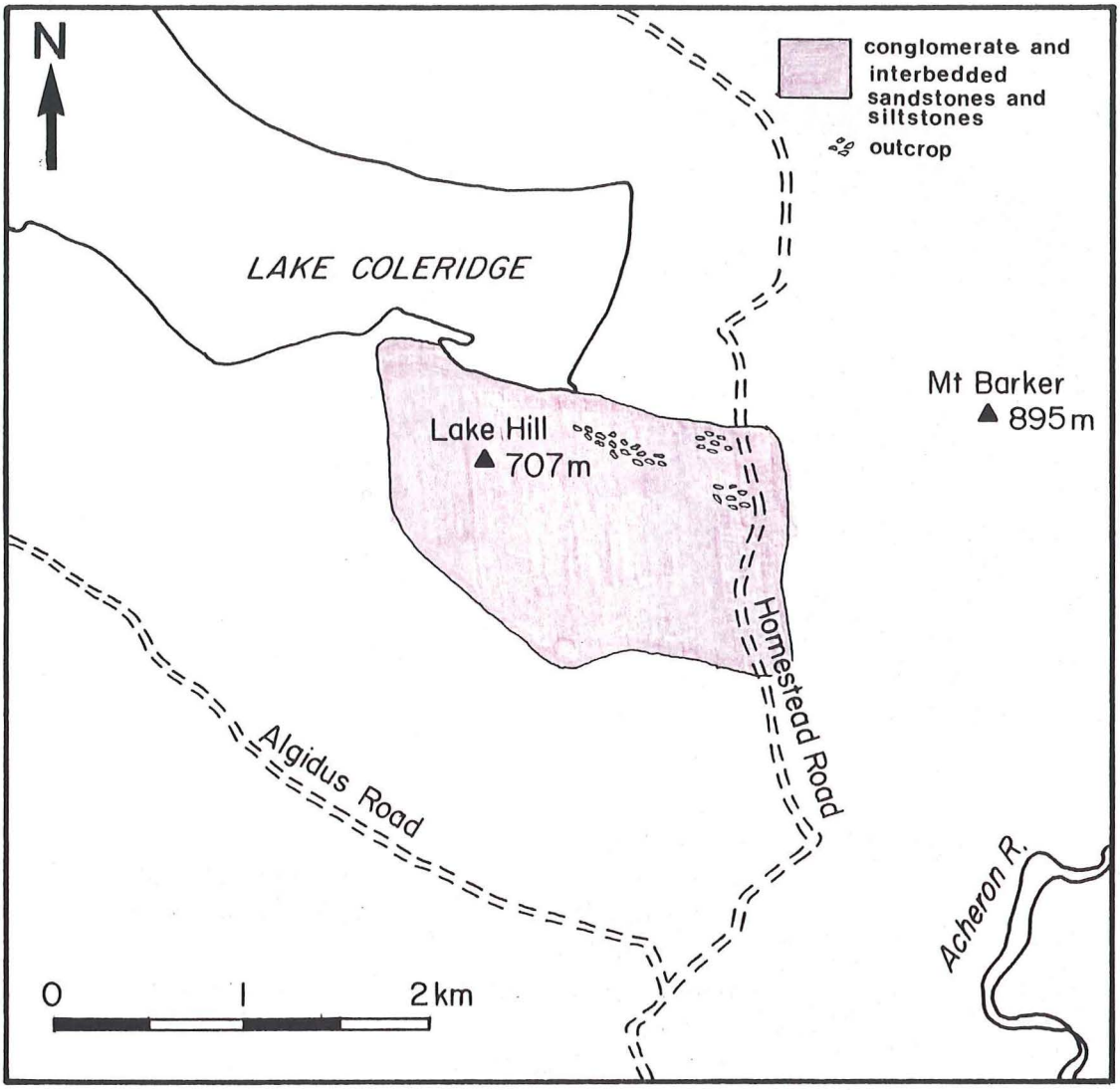

Figure 5.1: Lake Hill conglomerate locality map.

Figure 5.2: Lake Hill conglomerate:
a Panoramic view of Lake Hill conglomerate outcrop
b Joint plane illustrating clast size and composition (Case = 18cms)
c Conglomerate interbedded with sandstone dipping to the northeast (Hammer = 33cms)

a

b

c

5.1.2 Previous Work

Mention is made of the basement greywacke, of which the conglomerate is part, in many of the geological reports written in the late stages of last century (Hector, 1871; Haast, 1872, 1879). Speight (1928) associated the Lake Hill conglomerate with plant beds and suggested a fluviatile derivation.

Lauder (1962) recorded the components of the Lake Hill conglomerate, and makes brief petrographical descriptions of the granodiorite clasts, in a paper concerning teschenites from the Acheron River. He indicated the conglomerate was derived from the granitic rocks to the west of the Alpine Fault.

5.2 Petrography

The recalculated point count data for the Lake Hill granitoid clasts (Appendix 3) were plotted on the QAP ternary diagram (Figure 5.3). Samples concentrate primarily within the granodiorite field with some scatter into the monzogranite and tonalite fields.

5.2.1 Granitoid Clast Descriptions

The Lake Hill granitoid clasts are divisible into eight groups according to modal, mineralogical and textural data, following the procedure outlined and defined in Chapter 1, 1.3.4a and Chapter 2, 2.2 (Figure 5.4):

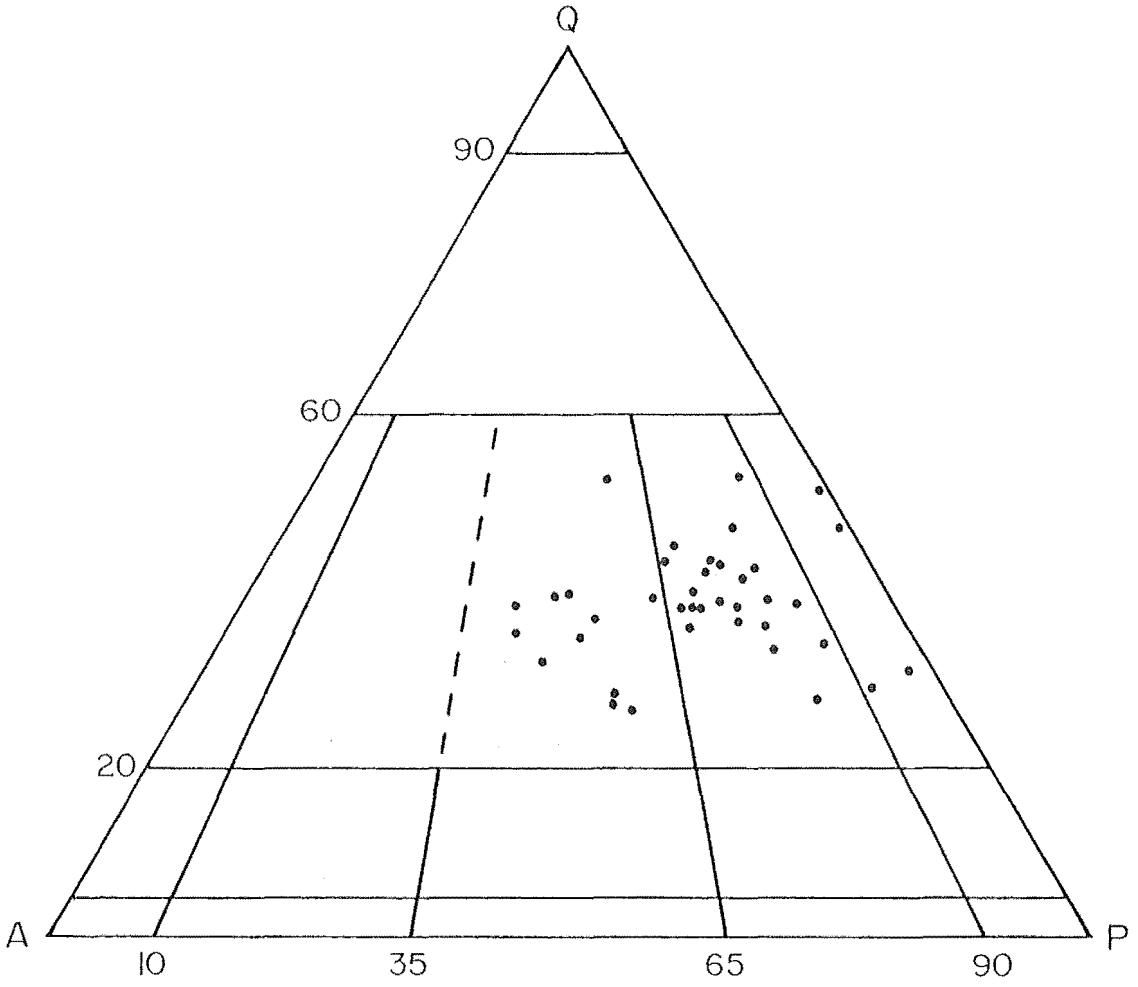

Figure 5.3: Quartz - Alkali Feldspar - Plagioclase ternary diagram illustrating modal distribution for Lake Hill conglomerate granitoid clasts (see Chapter 1, 1.3.4a for definition of fields) (after Le Maitre, 1989)

Group LHG-1

Subsolvus, coarse grained, equigranular, muscovite leucomonzogranite:

The subhedral quartz is slightly deformed with undulatory extinction and dominates the section.

The relatively small (*cf.* to quartz) euhedral to subhedral plagioclase is sodic oligoclase (An 10-20%) and has albite twinning. The alkali feldspar is anhedral interstitial orthoclase.

Accessory minerals include euhedral isotropic garnet and anhedral opaque Fe/Ti oxides (Figure 5.5a)

Coarse euhedral randomly oriented undeformed primary muscovite plates are the only minor phase (Figure 5.5b).

Group LHG-2

Subsolvus, medium grained, equigranular, muscovite biotite leucomonzogranite to monzogranite:

The plagioclase is albite to sodic oligoclase (An8-16%) with normal zoning and core regions emphasized by sericitization and the development of secondary muscovite laths. Plagioclase is also present as small recrystallized crystal due to the exsolution of perthite. The alkali feldspar is euhedral perthitic microcline with distinctive transformation twinning.

The anhedral quartz is interstitial and exhibits variable deformation from undulatory extinction to sutured subgrain boundaries and incipient ribbon development with SPO (Figure 5.5c).

Chloritized, often kinked, red/brown to brown weakly pleochroic biotite is present as large (>2mm) euhedral plates commonly displaying included phases

Figure 5.4: Representative photographs of modal, mineralogical and textural granitoid groups (field of view ~5cms):
a Subsolvus, muscovite biotite monzogranite (LHG-2)
b Subsolvus, muscovite biotite granodiorite (LHG-4)
c Subsolvus, foliated, biotite granodiorite (LHG-5)
d Subsolvus, muscovite biotite leucotonalite (LHG-6)

a

b

c

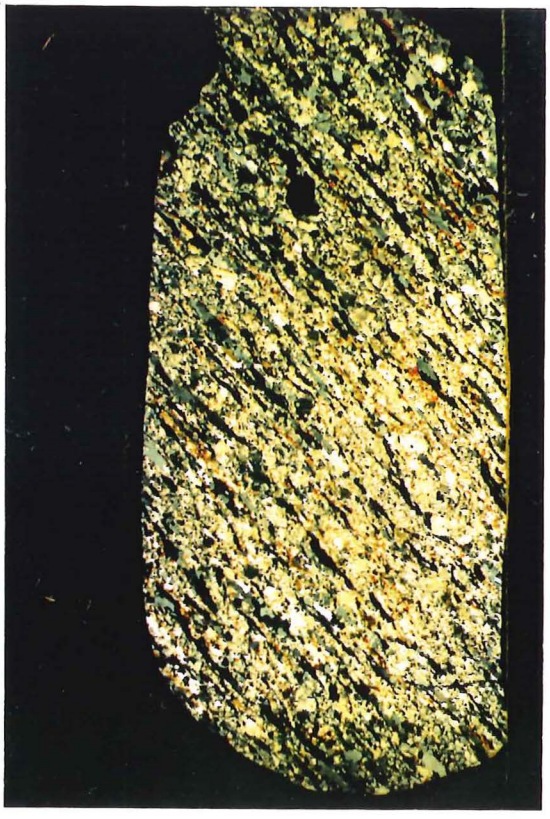

d

surrounded by pleochroic haloes due to radioactive decay of constituent elements. Primary subhedral muscovite is subordinate and usually associated with biotite.

Accessory minerals include euhedral garnet, zircon, subhedral apatite and opaque Fe/Ti oxides.

Myrmekitic intergrowths of quartz and plagioclase form embayments in the alkali feldspar.

Deformation is frequently partitioned between various zones in the clasts indicating that strain was heterogeneous.

Veining is common in some clasts with quartz, calcite and laumontite observed.

Group LHG-3

Hypersolvus, holocrystalline, medium to fine grained, granophyric, leucomonzogranite:

Granophyric intergrowths dominate and surround large (>2.5mm) euhedral plagioclase, anhedral alkali feldspar and quartz. The plagioclase is albite (An <10%). The alkali feldspar is perthitic orthoclase.

Partially chloritized brown biotite and muscovite are present in minor quantities (<1%). Muscovite is secondary and related to the sericitization of the feldspar, particularly plagioclase.

Accessory minerals include euhedral zircon and opaque Fe/Ti oxides.

Chlorite pseudomorphs replace biotite and chlorite infills miarolitic cavities.

Group LHG-4

Subsolvus, medium grained, muscovite biotite granodiorite:

Euhedral to anhedral sodic oligoclase plagioclase (An 10-20%) is the dominant feldspar. Normal zoning of the plagioclase is emphasized by the sericitization of crystal cores. The anhedral alkali feldspar is orthoclase and sometimes comprises patch perthite.

The anhedral quartz has sutured subgrain boundaries indicating a dynamic metamorphism.

In some clasts biotite and muscovite are equally proportioned, but generally the ratio is 5:1. Biotite is partially chloritized, brown and pleochroic. Muscovite is relatively finer grained, subhedral and of primary magmatic origin.

Accessory minerals include large (>2mm) euhedral isotropic garnet, zircon, subhedral apatite and anhedral opaque Fe/Ti oxides.

Myrmekite occurs along alkali feldspar/plagioclase grain boundaries (Figure 5.5d).

The well developed mylonitic fabric of some clasts is defined by the development of elongate quartz ribbons and the alignment of sheet silicates. Quartz ribbons display SPO and LPO. The feldspar in some clasts exhibits mortar texture that has resulted in the rounding of crystal form and albite twins have been bent with deformation.

Epidote and chlorite replacement of previous mafic minerals has occurred.

Group LHG-5

Subsolvus, holocrystalline, medium to fine grained, biotite granodiorite:

The subhedral to anhedral plagioclase is albite to oligoclase (An5-25%) and is sericitized or saussuritized with associated secondary muscovite and epidote (Figure 5.5e). The alkali feldspar is subhedral, perthitic microcline with transformation twinning. In one sample a single twin predominates and forms patches (Figure 5.5f). The quartz forms unusually large, regular elongate ribbons that do not bend around feldspar which have been extensively recrystallized to form a regular mosaic with undulose extinction.

Biotite dominates over alkali feldspar in some clasts with modal proportions >20%. The biotite is green/brown pleochroic and partially chloritized.

Accessory minerals include titanite, apatite, red/brown zoned allanite, euhedral zircon and opaque Fe/Ti oxides. Titanite in some clasts is a minor phase (<1%) and also forms rims around opaque Fe/Ti oxides. The euhedral epidote present in some clasts could be primary.

Some clasts are undeformed and porphyritic with phenocrysts exhibiting glomeroporphyritic texture. The coarse granitic textured matrix is interpreted to have been glass that has undergone devitrification.

Mafic minerals have been replaced by chlorite, epidote and opaque Fe/Ti oxides and calcite veins transect some clasts.

Group LHG-6

Hypersolvus, holocrystalline, fine grained, biotite leucogranodiorite:

Granophyric intergrowths surround discrete plagioclase, alkali feldspar and biotite.

The euhedral to subhedral plagioclase is zoned with cores exhibiting sericitization and is albite ($2V \sim 90^{\circ}$, $An < 10\%$). The alkali feldspar is perthitic orthoclase.

The anhedral quartz is only present associated with granophyric intergrowths.

The subhedral brown pleochroic biotite forms large (>2mm) plates and is partially chloritized. Secondary muscovite is the result of feldspar sericitization.

Accessory minerals include subhedral allanite, zircon and opaque Fe/Ti oxides.

Chlorite, apatite and opaque Fe/Ti oxide replacement of mafic minerals has occurred. A relic pyroxene was identified by cleavage ($\sim 90^{\circ}$) within the core of one chlorite pseudomorph that has an orthopyroxene shape and is peppered with disseminated opaques.

Group LHG-7

Subsolvus, coarse to medium grained, equigranular, muscovite biotite leucotonalite:

The plagioclase is sodic oligoclase ($An \sim 15\%$) with sericitized cores indicating normal zoning. The alkali feldspar is a minor constituent ($\sim 5\%$) and is usually interstitial anhedral microcline.

Quartz extinction is undulose and sutured boundaries indicates grain boundary migration.

Chloritized brown pleochroic biotite and subordinate muscovite are both

minor phases. Large primary muscovite plates and a lack of alkali feldspar were noted in some clasts.

Accessory minerals include euhedral zircon, apatite and opaque Fe/Ti oxides.

Secondary muscovite is associated with the sericitization of feldspar.

Myrmekite is associated with the small amount of alkali feldspar present. Clasts are relatively undeformed with granitic texture.

Group LHG-8

Hypersolvus, medium grained, granophyric, leucotonalite:

A single clast comprises large (>2.5mm) euhedral to subhedral plagioclase that is sodic oligoclase (An 10-20%) and euhedral quartz surrounded by granophyric-like intergrowths of plagioclase and quartz (Figure 5.5g). No alkali feldspar was found. Secondary muscovite laths have replaced plagioclase cores.

Accessory minerals include euhedral zircon and opaque Fe/Ti oxides.

The euhedral subsolvus minerals form an adcumulate texture.

Chlorite, epidote and opaque Fe/Ti oxides have replaced mafic minerals and calcite veins cut some clasts.

Figure 5.5: Photomicrographs of thin section features
(field of view = ~7mm):

a Euhedral garnet with muscovite and biotite (PPL).

b Large muscovite plate enclosing plagioclase and euhedral garnet.

c Undulose extinction in quartz with subgrain development, microcline, and plagioclase exhibiting sericitization.

d Foliation development with alignment of muscovite and quartz ribbon development. Myrmekite is embayed into alkali feldspar.

e Sericitization of plagioclase with secondary muscovite laths.

f Microcline with one twin forming patches.

g Granophyric-like intergrowths of plagioclase and quartz.

h Flow texture around a plagioclase phenocryst in a rhyolite.

a

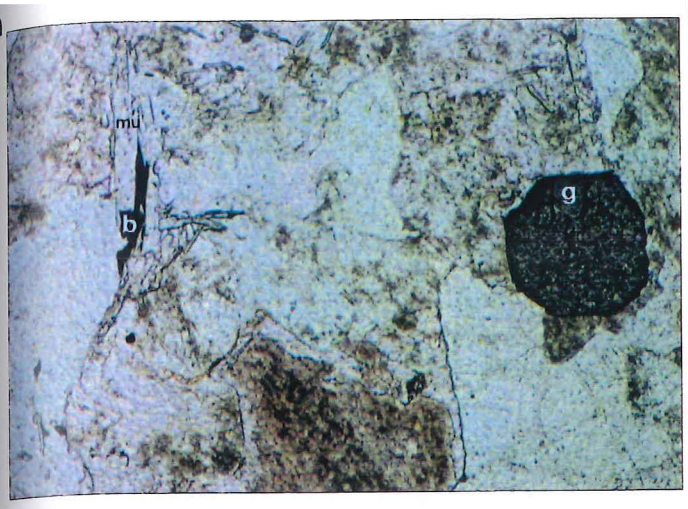

b

c

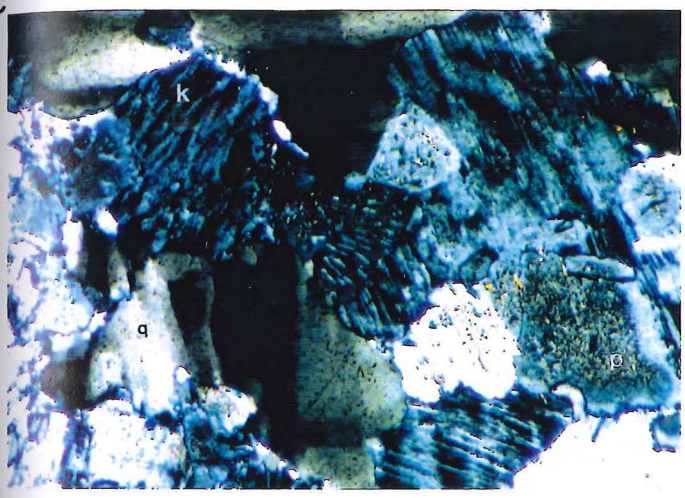

d

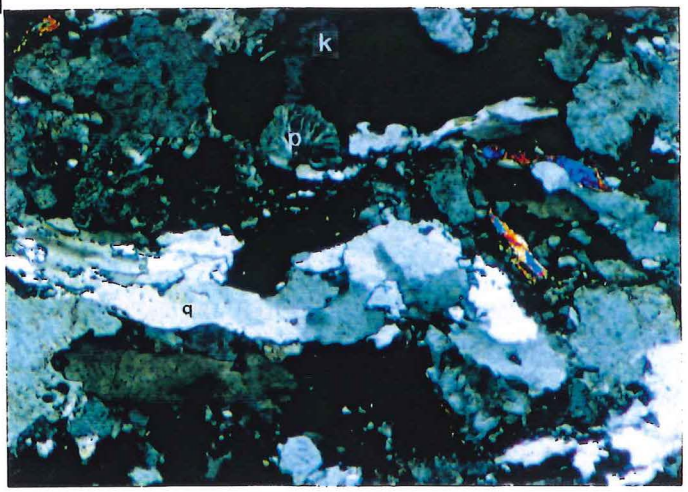

e

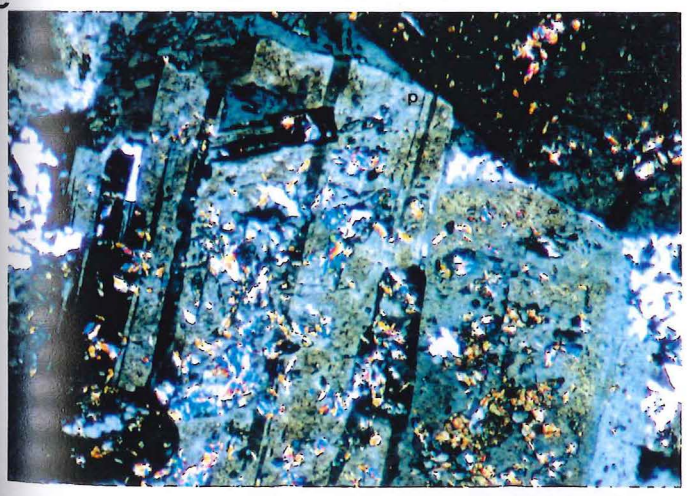

f

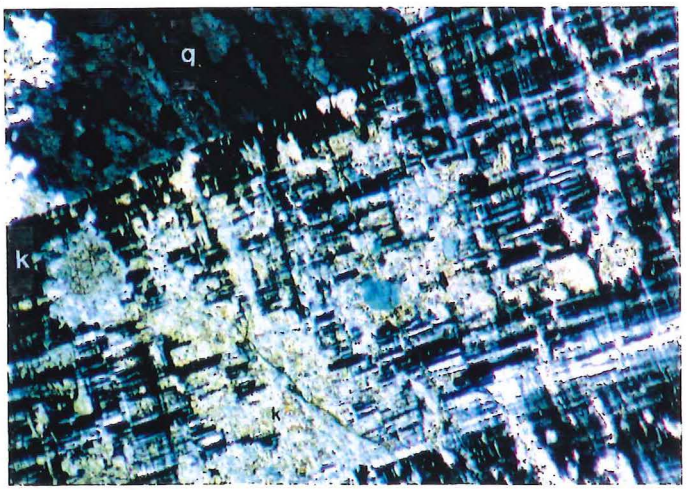

g

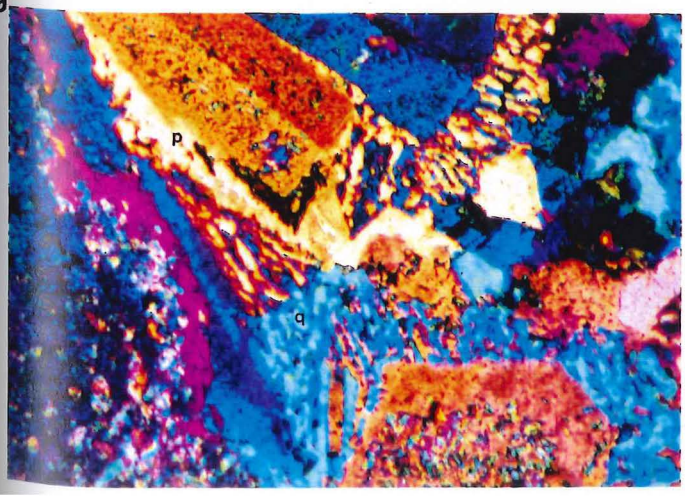

h

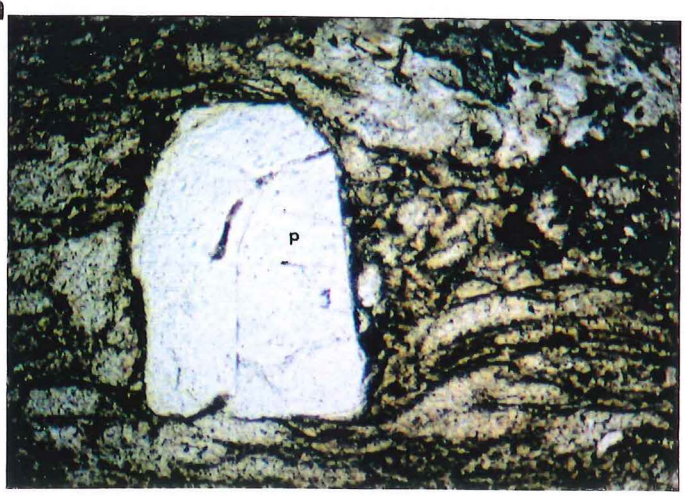

5.2.2 Volcanic Clast Characteristics

The seven volcanic clasts examined from the Lake Hill conglomerate fall into two fields of the TAS diagram (Figure 5.6), and specimens from each field are described below (Figure 5.7):

Group LHV-1

Hypocrystalline, porphyritic rhyolites:

Phenocrysts comprise 20 - 50% of the rhyolite clasts.

Plagioclase phenocrysts are fragmental and angular, and have the composition of albite ($2V \sim 90^\circ$, $An < 10\%$). Albite twinning gives a checkerboard effect. Alkali feldspar phenocrysts are anhedral ($2V_x \sim 60^\circ$) orthoclase that is perthitic or microperthitic. The quartz is severely corroded and exhibits pitted rims with slight undulose extinction.

Accessory minerals include subhedral apatite, zircon, and anhedral opaque Fe/Ti oxides.

Epidote, chlorite and opaque Fe/Ti oxides have replaced mafic minerals which include biotite with apatite inclusions. Large (>2.5mm) opaque mineral grains are associated with chlorite pseudomorphs.

The matrix usually has a fine crystalline felsitic texture that comprises a mixture of feldspar and quartz, with minor epidote, chlorite and opaques. In some clasts the matrix exhibits trachytic texture with an alignment of feldspar laths (Figure 5.5h). Secondary quartz infills lithophysae which are aligned as a result of flow of magma.

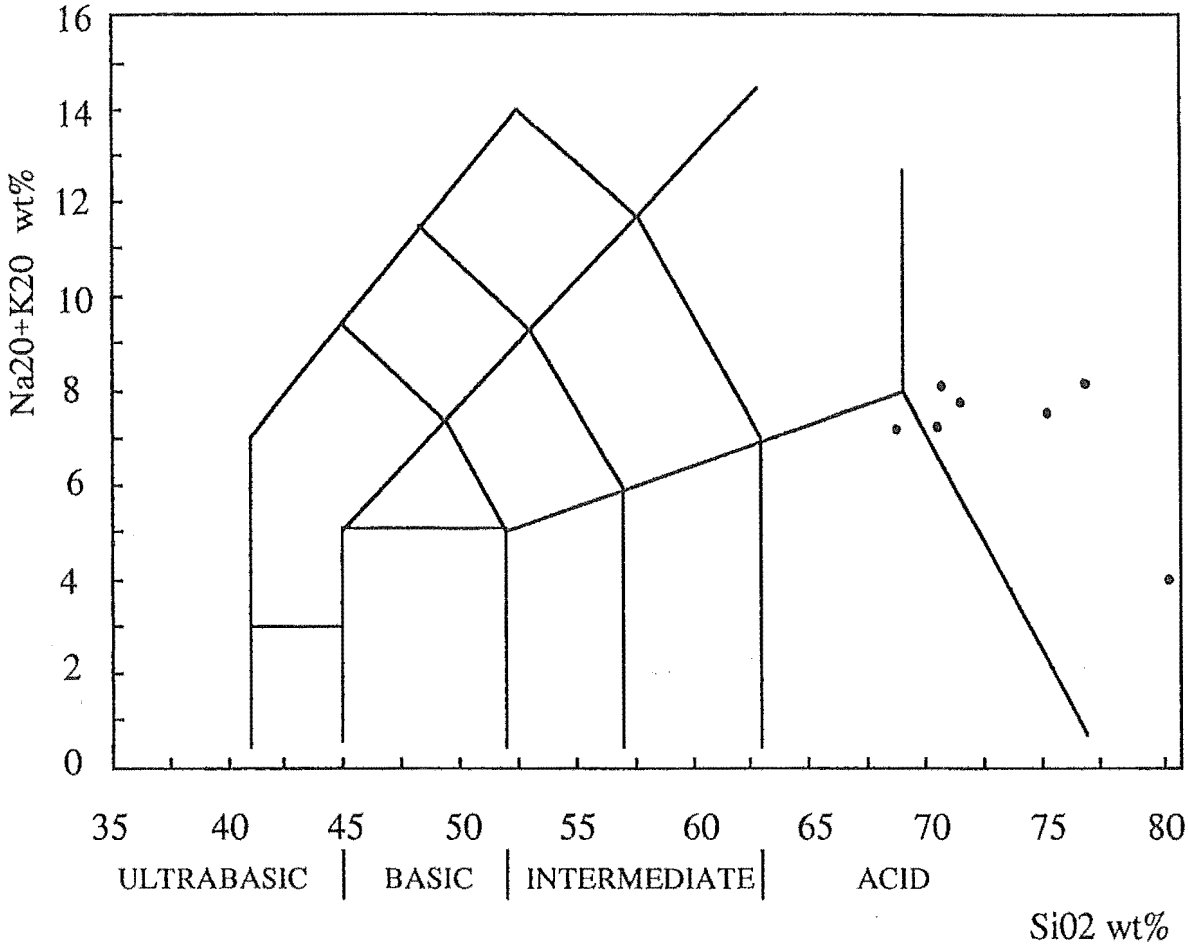

Figure 5.6: TAS classification illustrating distribution for Lake Hill conglomerate volcanic clasts.
(after Le Maitre, 1989)

Group LHV-2

Hypocrystalline porphyritic dacite:

Phenocrysts comprise 29% of this clast. The quartz is anhedral, rounded (due to solution), and undeformed. The plagioclase is albite (An<5%) with albite twinning. Epidote frequently replaces plagioclase cores and is also present as large (>3mm) anhedral crystals rimmed with a shadow effect indicating growth was secondary. Quartz and plagioclase phenocrysts display glomerophorphyritic texture. Distinctive calcite and chlorite pseudomorphs after hornblende are present. Green/brown biotite phenocrysts are abundant, but smaller relative to quartz and feldspar and are partially chloritized.

Accessory minerals include abundant euhedral titanite, primary euhedral epidote, yellow brown euhedral amphibole and opaque Fe/Ti oxides.

The matrix is a felsitic combination of quartz, feldspar, titanite, epidote, chlorite and opaque Fe/Ti oxides and contains spherulites in some areas.

5.2.3 Petrological Interpretation

Lake Hill granitoid clasts were compared and contrasted within the hypersolvus/subsolvus textural categories defined in Chapter 2, 2.2.

The hypersolvus granitoid clasts (groups LHG-3,6,8) range in modal composition from leucomonzogranite to leucogranodiorite and leucotonalite. All are typified by granophyric intergrowths that surround subsolvus discrete minerals, indicating a change in crystallisation pressure prior to final consolidation. The hypersolvus leucotonalite (LH10/24454) contains no alkali feldspar, therefore

Figure 5.7: Representative photographs of volcanic group clasts (field of view ~5cms):
a b and **c** Porphyritic rhyolites (LHV-1)
d Phorphyritic dacite (LHV-2)

a

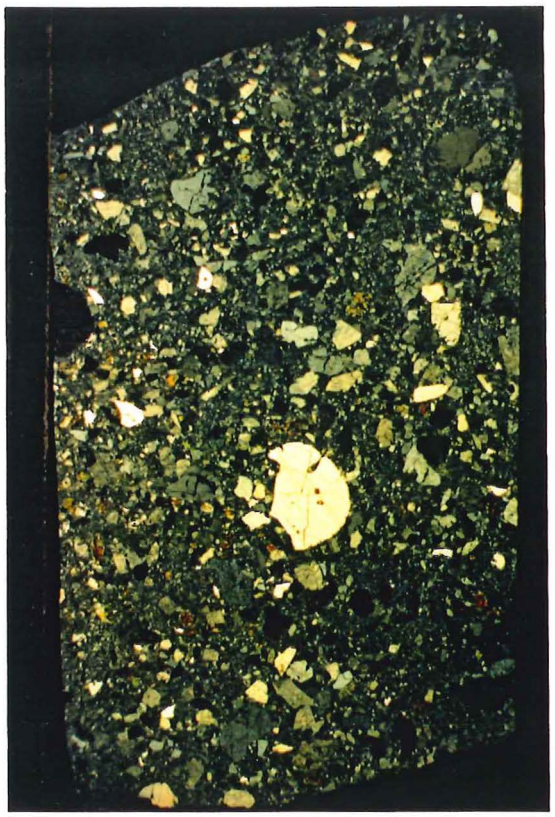

b

c

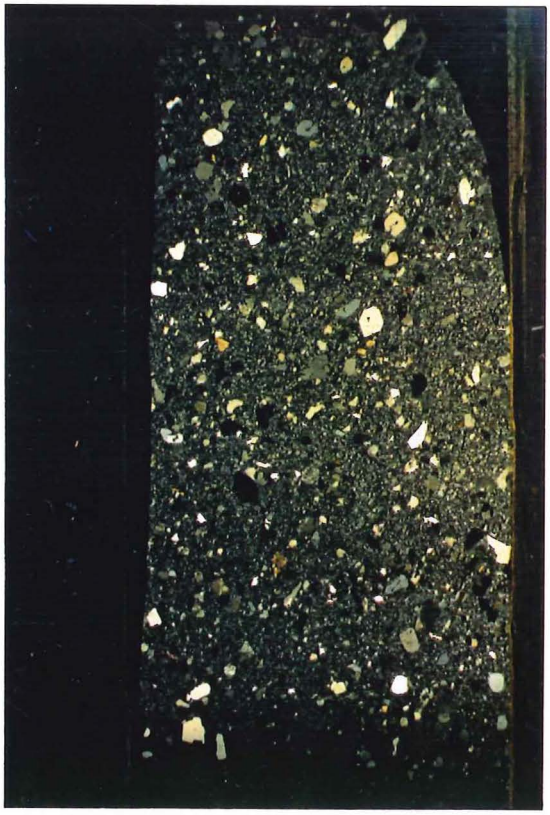

d

intergrowths, which are plagioclase and quartz, must be considered granophyric-like. The hypersolvus clasts contain little mafic material (<1%), and most of it is replaced by epidote or chlorite. One clast (LH35/24479) contains miarolitic cavities infilled with epidote which indicate hypabyssal emplacement, the exsolution of a vapour phase, and a possible subvolcanic relationship to the volcanic clasts examined.

Subsolvus granitoid clasts (LHG-1,2,4,5,7) display a full range of deformation features from undeformed to mylonitic and gneissic granitoids. The SPO, LPO and recrystallization of elongate quartz ribbons indicates post-intrusive deformation, probably within a sheer zone. In undeformed granitoids original igneous texture is preserved. With increasing deformation, feldspars become rounded and twin lamellae contorted. The grain size of recrystallized quartz decreases with metamorphism (recrystallization grain size is inversely proportional to differential stress), and undulatory extinction is universal. The biotite in subsolvus clasts is usually associated with minor muscovite.

An undeformed subsolvus clast (LH31/24475) displays porphyritic texture and a coarse felsitic matrix and is interpreted to have undergone devitrification within a high level pluton. The clast probably originated at the centre of a large dome where the magma was chilled, but cooling relatively slow.

A coarse grained, subsolvus, garnet, muscovite monzogranite (LH24/24468) that contains large primary muscovite crystals is interpreted to be a pegmatite related to late stage volatile rich fluid crystallization.

The Lake Hill volcanic clasts are primarily classified on the basis of geochemistry (see section 5.2.2). Clasts generally contain biotite, or pseudomorphs after biotite, and minor titanite. This compares favourably with the hypersolvus and some subsolvus clasts that contain these minerals and is consistent with a cogenetic relationship.

The matrix of volcanic clasts has crystallized to a felsitic or spherulitic texture indicating a high degree of undercooling. No evidence of a pyroclastic origin is present, and clasts are assumed to have been derived from rhyolitic domes and/or flows.

The dacite clast (LH28/24472) is distinguished petrographically from the rhyolite clasts by the presence of hornblende pseudomorphs and abundant biotite phenocrysts. The dacite also contains rounded quartz as opposed to the more usual embayed quartz common to the rhyolitic clasts. Embayed quartz is generally interpreted to result from dissolution due to changes in pressure as a magma rises, but could be the result of rapid skeletal growth and/or solution aided by gas bubble boring effects (Shelley, 1992). The rounded form exhibited by the dacite clast is in keeping with experimental results in which smooth rounded forms are produced by the dissolution of silicates (Donaldson and Henderson, 1988).

The majority of clasts, particularly the volcanics, contains secondary calcite, chlorite and epidote indicating low pressure hydrothermal alteration. The laumontite present in one vein indicates the low pressures and temperatures of the zeolite facies. Calcite and quartz veins also transect some sections.

5.3 Geochemistry

5.3.1 Categorization of Granitoids

To ascertain source characteristics for the Lake Hill conglomerate igneous clasts, the Aluminium Saturation Indices were calculated (Appendix 5) and are plotted in Figure 5.8. All granitoid and volcanic clasts examined are peraluminous with an ASI > 1.0. Four granitoid samples plot with an ASI > 1.1 and are considered S-types, and include two leucotonalites (LH8/24452, LH10/24454) and two granodiorites (LH9/24453, LH14/24458). The leucomonzogranite (LH24/24468) is considered to have originated within a pegmatite. The majority of clasts are weakly peraluminous with an ASI between 1.0 - 1.1 and cannot be assigned a type under this classification as previously stated (Chapter 2, 2.3.1)

Clasts plot predominantly in the fractionated granite field (FG) with some scatter into the ordinary granite field (OGT) of Figures 5.9a and b, which use HFS elements and major element ratios to discriminate characteristics. The fields also define determined I- and S-type granitoid limits (Whalen *et al.*, 1987). In both plots, samples concentrate in two broad areas that correspond to lower and higher HFS element values.

The alkali-lime index (Appendix 4) for Lake Hill clasts was calculated and plotted (Figure 5.10). An extrapolation of results indicates an overall calc-alkaline association that scatters into the tholeiitic and alkali-calcic fields (~53 - 64% SiO_2). The alkalis-silica diagram (Figure 5.11) and the AFM ternary diagram (Figure 5.12)

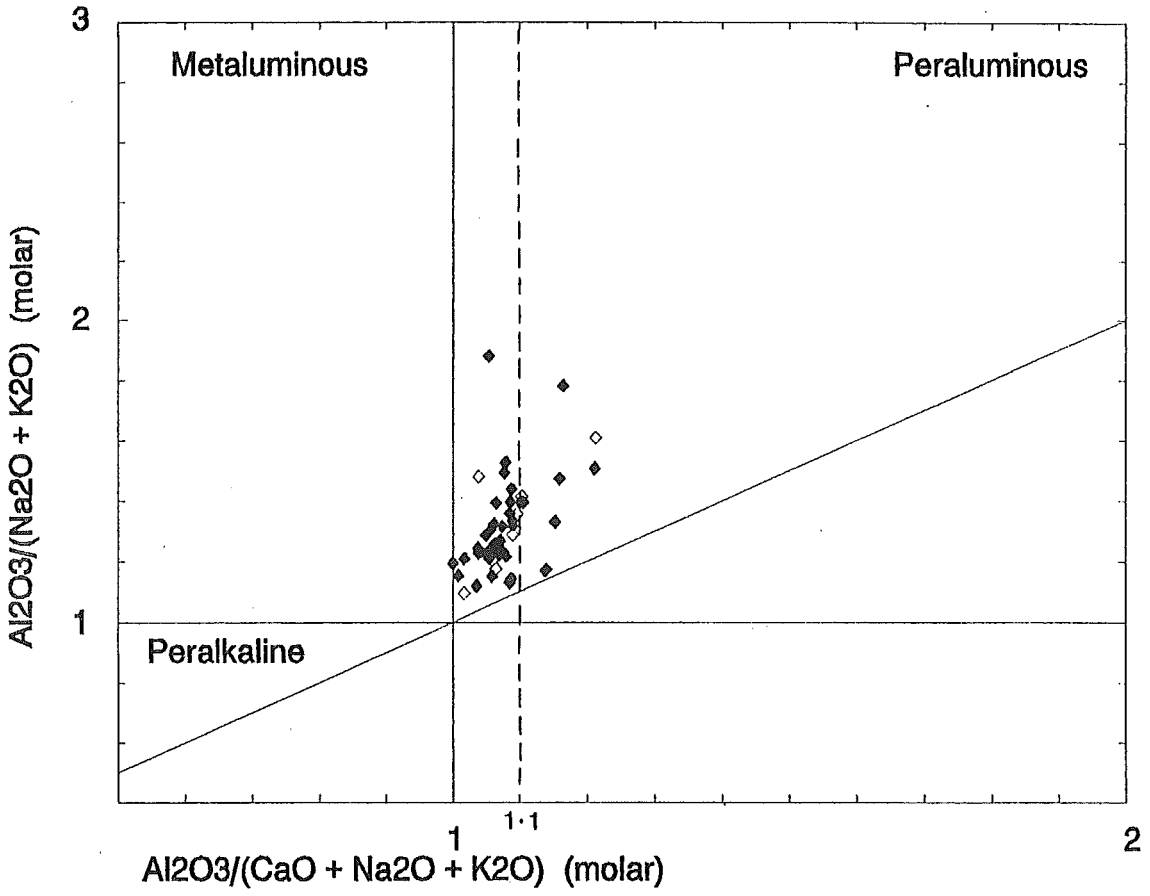

Figure 5.8: Aluminium Saturation Indices plotted for Lake Hill conglomerate clasts. A/CNK = 1.1 indicates the boundary between highly fractionated I-type/S-types and S-type granitoid/volcanic clasts. (after Maniar and Piccoli, 1989)

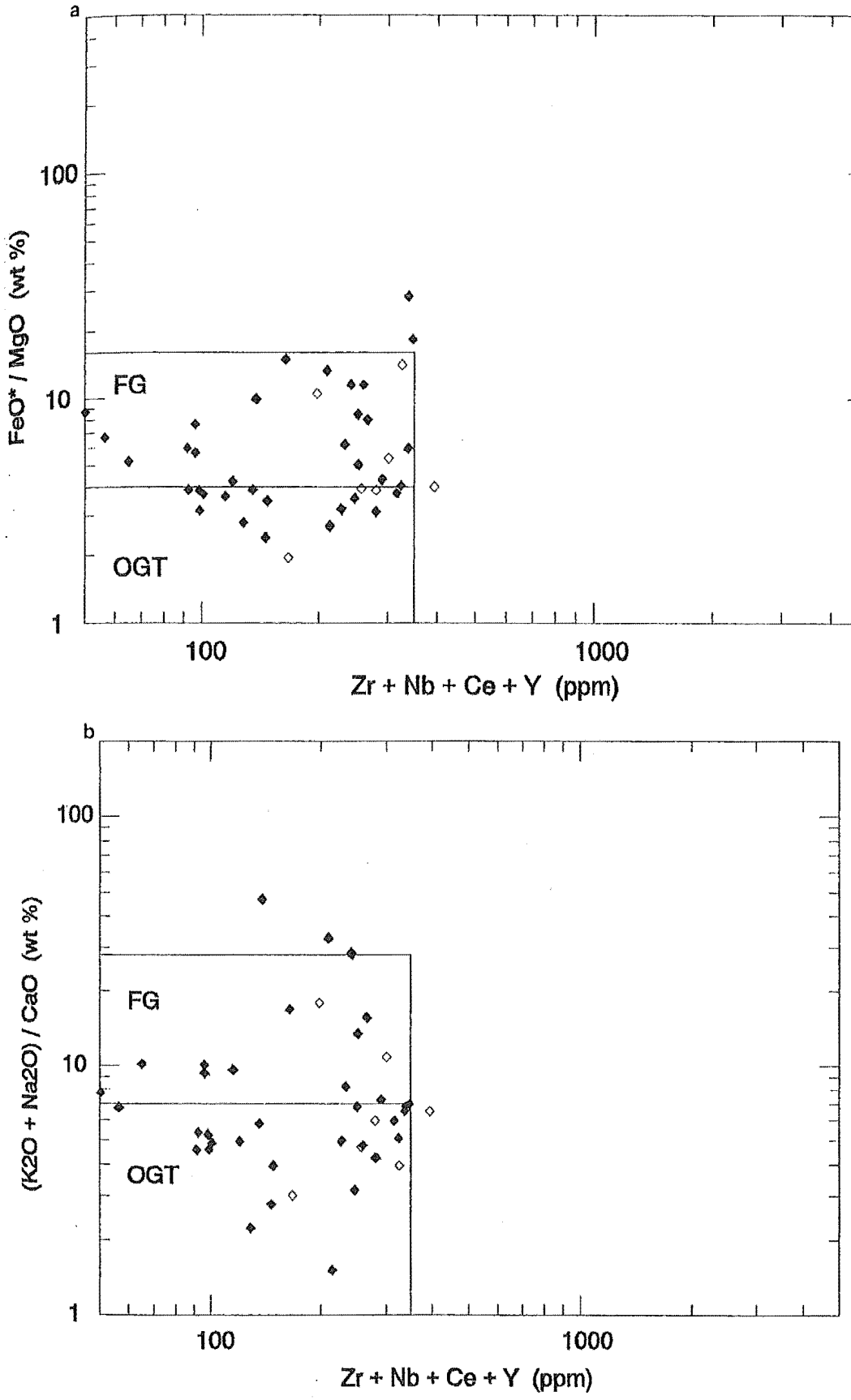

Figure 5.9: High Field Strength trace elements versus major element ratios with fields for fractionated felsic granites (FG), and ordinary granite types (OGT) delineated:
a Zr+Nb+Ce+Y versus FeO^*/MgO
b Zr+Nb+Ce+Y versus $(K_2O+Na_2O)/CaO$
(after Whalen *et al.*, 1987)

support this classification, indicating tholeiitic affinities.

The QAP diagram of modal analyses can be used to give an idea of magmatic lineage (Lameyre and Bowden, 1982). The modal analysis of Lake Hill clasts (Figure 5.3) displays two concentrations, medium to low K clasts that concentrate in the granodiorite field, and medium to high K clasts that concentrate in the monzogranite field. The two S-type leucotonalites (LH8/24452, LH10/24454) plot in the overlapping field for granitoids formed by crustal melting. Geochemical analyses indicate that these samples have very little K (between 1.06 and 0.65 wt%) with a high silica contents (~73 - 75%).

5.3.2 Plutonic/Volcanic Relationship

Volcanic clasts are in the minority in this conglomerate and only seven were analyzed. The data obtained are included with granitoid clasts in all discriminatory diagrams.

The volcanic clasts concentrate predominantly with an ASI between 1.0 and 1.1 (Figure 5.8). One rhyolite (LH34/24478) has an ASI = 1.21 and, with a silica content of 80% and extremely low alkali content (Figure 5.6), is considered to have lost alkalis in solution, therefore the ASI is unreliable.

In Figure 5.9 the rhyolites plot with the group of granitoids that have higher HFS trace element abundances. The dacite (LH28/24472) has a lower HFS elemental abundance, and plots closer to the granitoid group with similar HFS

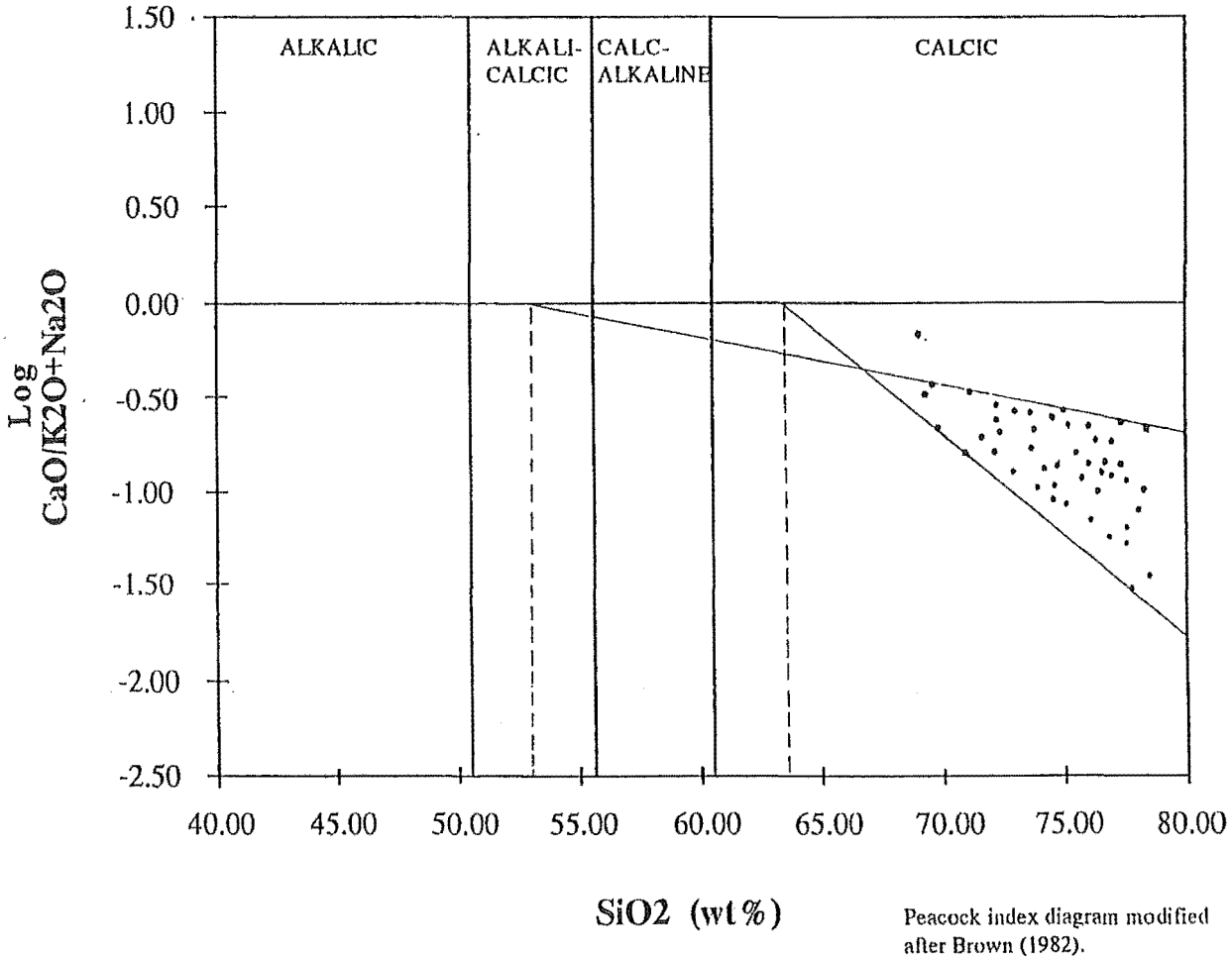

Figure 5.10: Alkali-lime Index (definition Appendix 4) illustrating extrapolated values for Lake Hill conglomerate clasts.

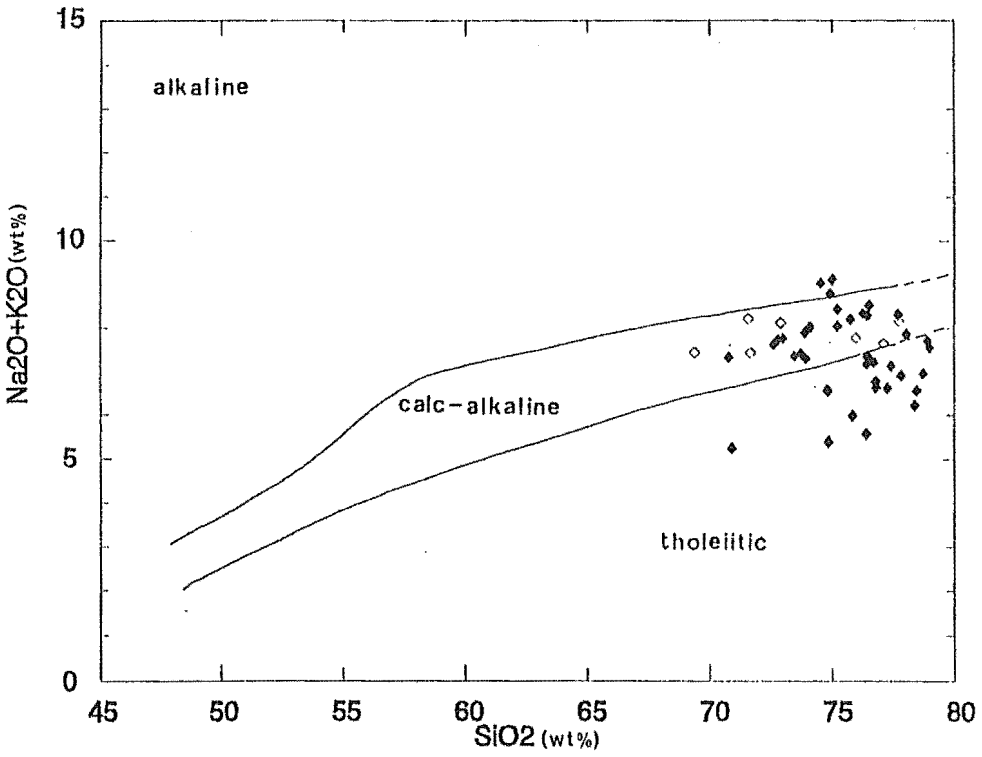

Figure 5.11: Alkali - silica diagram illustrating distribution of Lake Hill conglomerate clasts between alkaline, calc-alkaline, and tholeiitic fields.
(after Kuno, 1968)

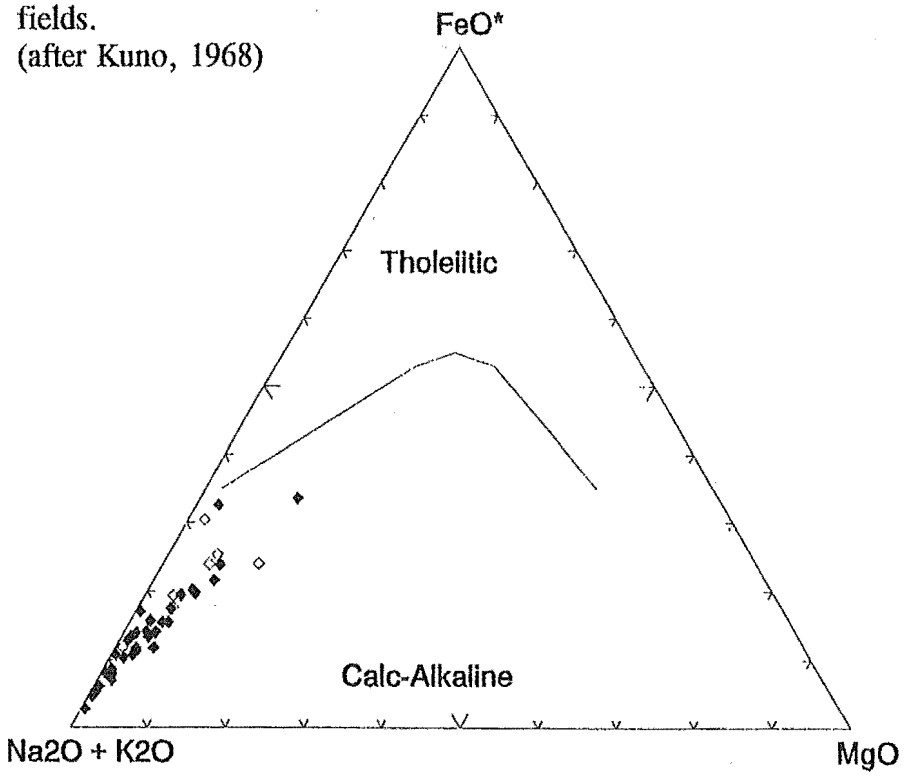

Figure 5.12: AFM (Na_2O+K_2O; Total iron as FeO; MgO) ternary diagram illustrating distribution of Lake Hill conglomerate clasts.
The dashed line separates tholeiitic and calc-alkaline compositions.
(after Irvine and Baragar, 1974)

element content. Plots to distinguish fractionated and A-type granitoids, using 10000*Ga/Al versus K_2O+Na_2O/CaO and Y (Figures 5.13a and b) indicate Lake Hill clasts plot primarily within the I-, S-, and fractionated I- and S-type granitoid fields. The dacite clast plots outside these fields, as does a granodiorite (LH17/24461), which plots close to the calculated A-type in Figure 5.13b. This clast has relatively high Y (75ppm), but average abundances for the other HFS elements.

The variable K_2O/Na_2O ratio of Lake Hill conglomerate clasts is emphasized by the K_2O-Na_2O-CaO plot (Figure 5.14). Clasts group in two concentrations, which cannot be distinguished mineralogically (i.e. each group contains biotite or biotite + muscovite granitoids). Volcanic clasts plot predominantly with the high K_2O/Na_2O ratio clasts. A Harker diagram comparing SiO_2 with K_2O also illustrates this separation (Figure 5.15a).

The SiO_2 versus Rb Harker diagram (Figure 5.15b) indicates the generally low values for this element. The Rb-Ba-Sr ternary diagram (Figure 5.16) also reflects a low Rb content, and illustrates the predominantly granodioritic character of the Lake Hill conglomerate clasts. Granitoid clasts without related volcanics have high Sr values and a primitive character. Three clasts plot in the strongly differentiated field, a granodiorite (LH17/24461), and two monzogranites (LH19/24463, LH24/24468) with silica contents between 75 and 78%.

The multi-element, primitive-mantle-normalized (Sun and McDonough, 1989) abundance diagrams, which display overall trace element characteristics, indicate the

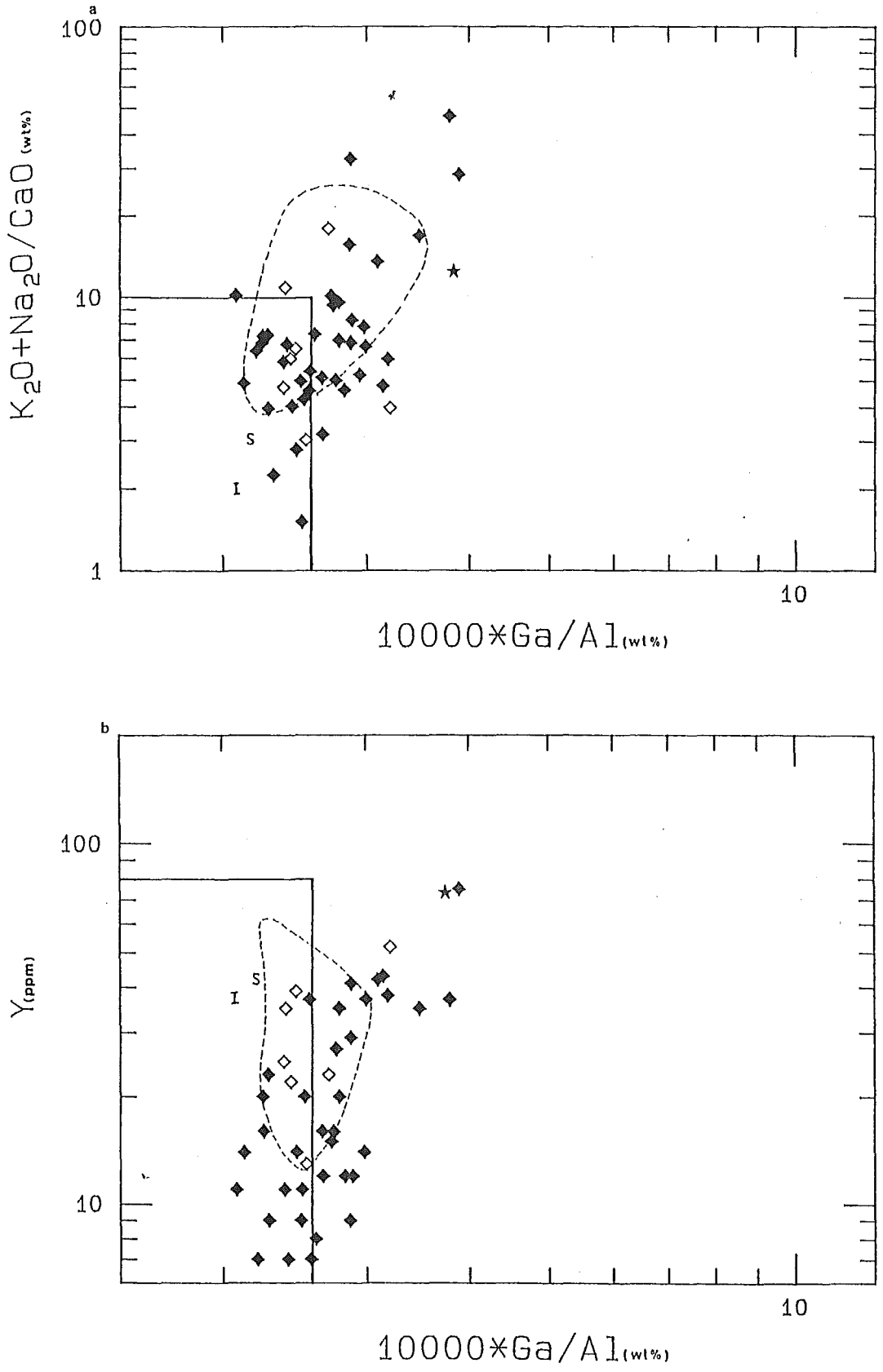

Figure 5.13: Plots of 10000*Ga/Al versus **a** K_2O+Na_2O/CaO and **b** Y illustrating Lake Hill conglomerate clast distribution. I- and S-type granite field delineated, dashed line represents fractionated granite field, * = calculated A-type, I = calculated average I-type, S = calculated average S-type.
(after Whalen *et al.*, 1987)

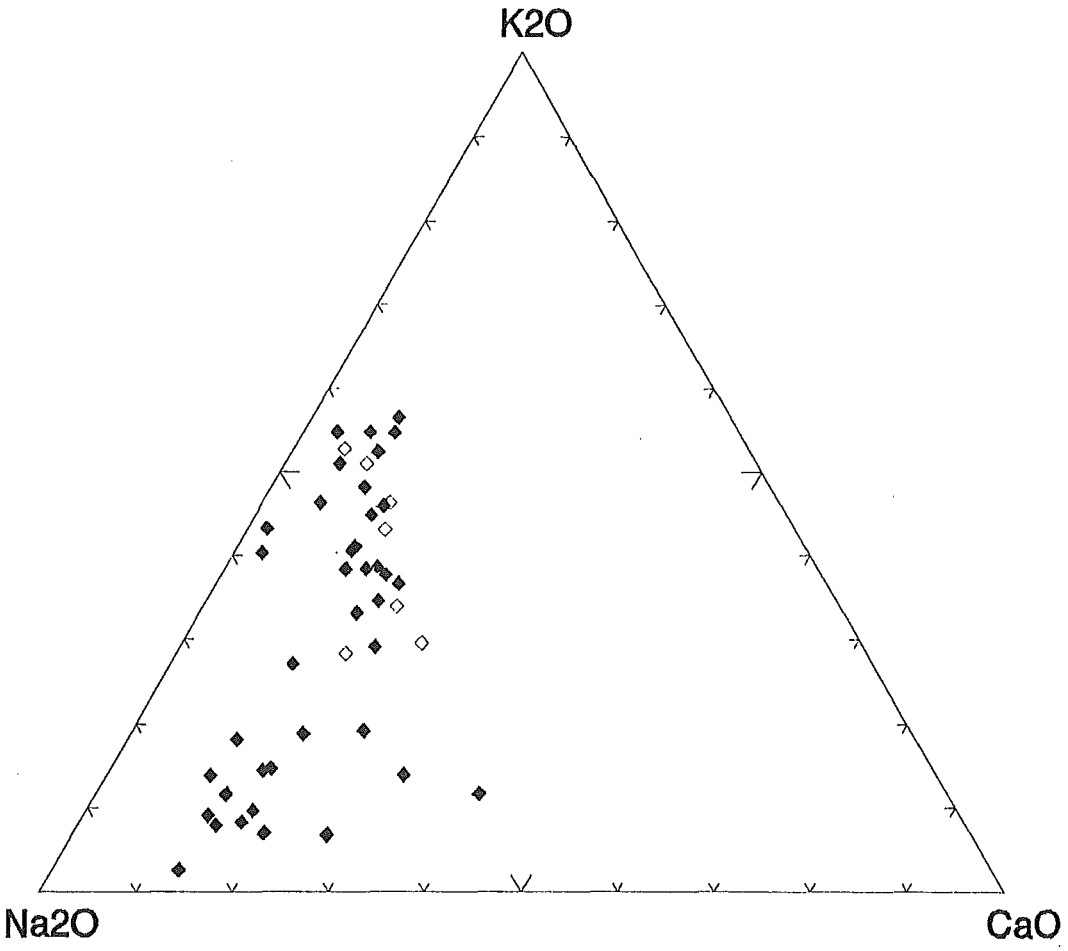

Figure 5.14: K_2O-Na_2O-CaO diagram which illustrates the K_2O/Na_2O ratio, and considers CaO for Lake Hill conglomerate clasts.

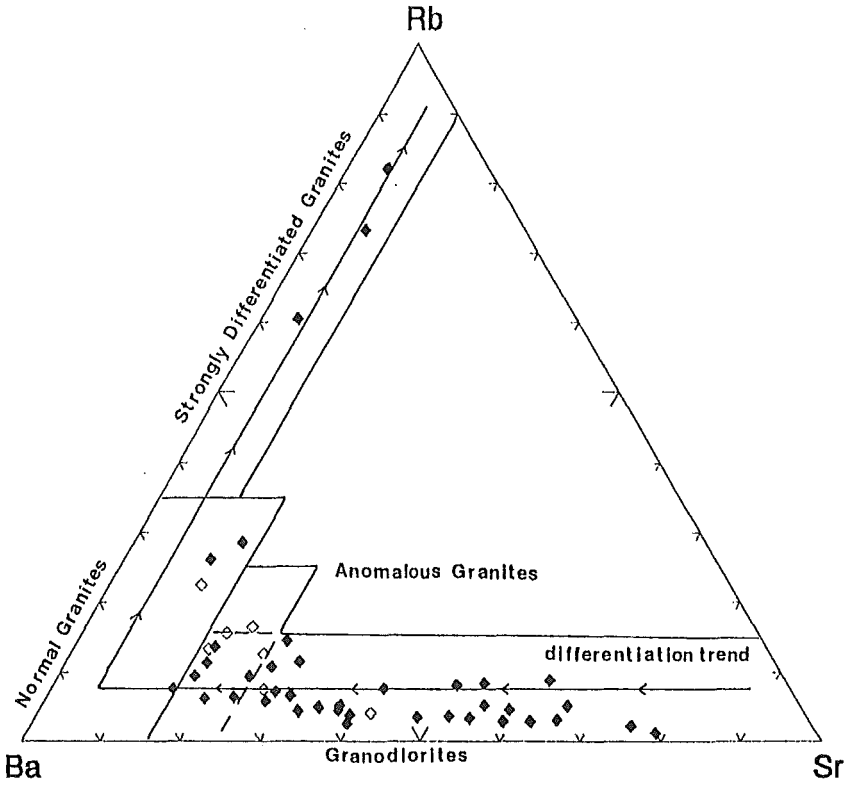

Figure 5.16: Rb-Sr-Ba ternary diagram illustrating the relationship between Lake Hill conglomerate clasts.
(after El Bouseily and El Sokkary, 1975)

Lake Hill conglomerate granitoid and volcanic clasts are enriched in LIL elements and exhibit a strong negative Nb anomaly characteristic of subduction-related magmasn (Figure 5.17). The granitoid clasts can be divided into the relatively more primitive S-types (Figure 5.17a) which display variable trace element features that can be related to source heterogeneities and, generally, a positive Sr anomaly. The remainder of granitoid clasts plot with strong negative Sr and Ba anomalies, and a positive Rb anomaly indicating an evolved character (Figure 5.17b). The rhyolites reflect the pattern displayed by the evolved granitoids (Figure 5.17c). The dacite clast, however, plots with a positive Sr anomaly consistent with its higher CaO content and more mafic character.

5.3.3 Correlation with Mineralogy

Lake Hill conglomerate clasts display silica values that range from 68-80%. Clasts contain modal quartz values between 30 and 50%, and plot from tonalite to monzogranite with a corresponding increase in alkali feldspar (Figure 5.3). Leucocratic clasts have low modal abundances of mafic minerals (<5%).

The granitoid clasts considered S-types have muscovite and sometimes garnet, supportive of this classification. The S-type granitoids are subsolvus and include the clasts that display a pervasive foliation development.

Granitoids with green/brown biotite and accessory titanite (± muscovite) are found to have an I-type character. That these clasts generally contain minor secondary muscovite supports their geochemical classification as weakly

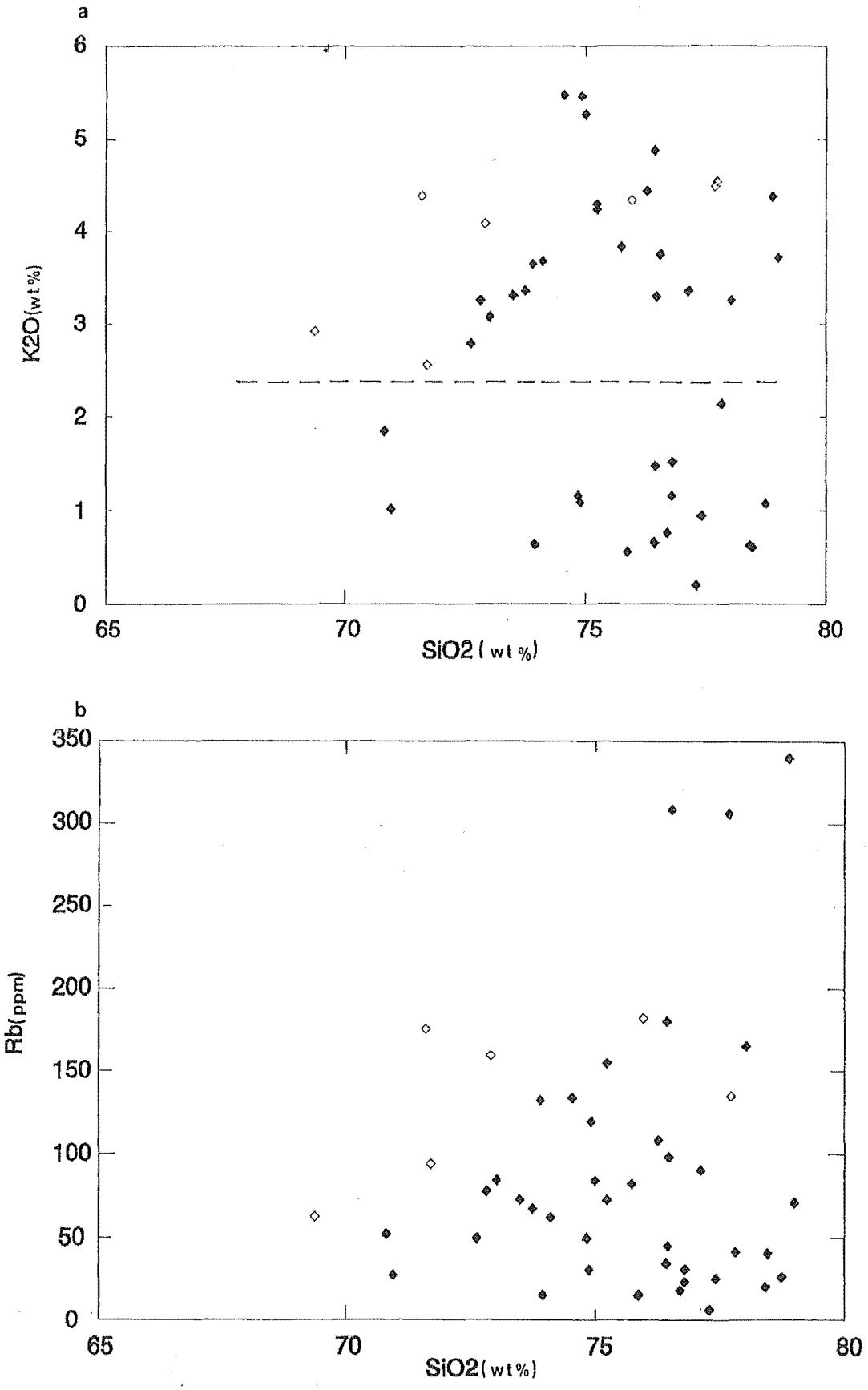

Figure 5.15: Harker variation diagrams for major and trace elements illustrating distribution of Lake Hill clasts:
a SiO_2 versus K_2O
b SiO_2 versus Rb

Figure 5.17: Multi-element primitive-mantle-normalized (Sun and McDonough, 1989) abundance diagrams for Mount Saul conglomerate clasts:
a S-type granitoids with positive Sr anomaly
b Evolved I-type granitoids
c Volcanic clasts - dacite plots with positive Sr anomaly.

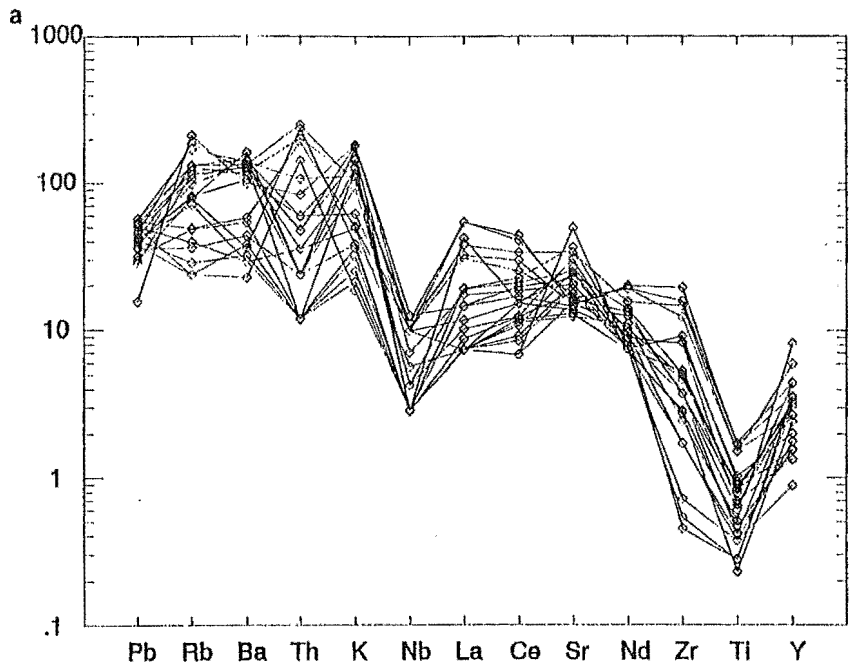
a
1000
100
10
1
.1
Pb Rb Ba Th K Nb La Ce Sr Nd Zr Ti Y

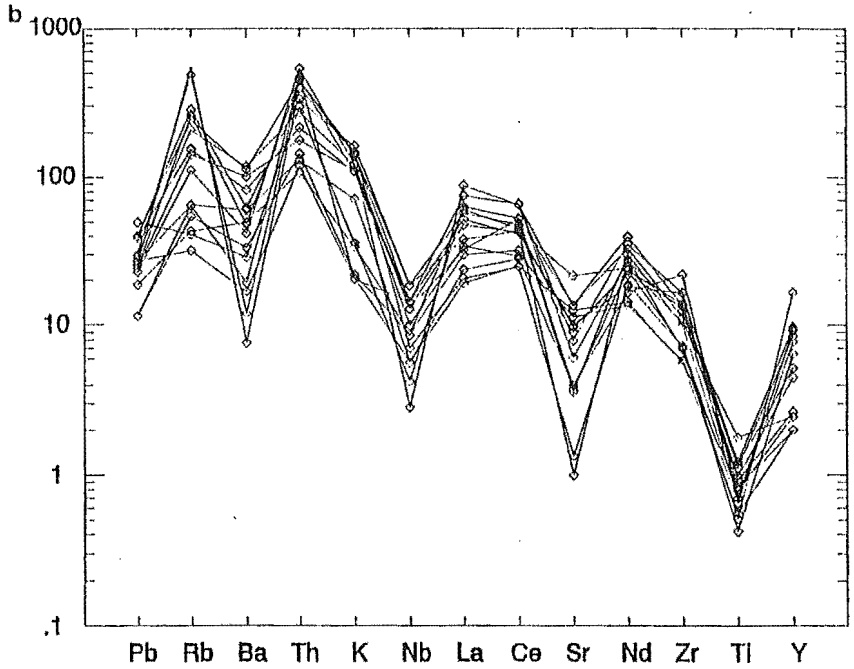
b
1000
100
10
1
.1
Pb Rb Ba Th K Nb La Ce Sr Nd Zr Ti Y

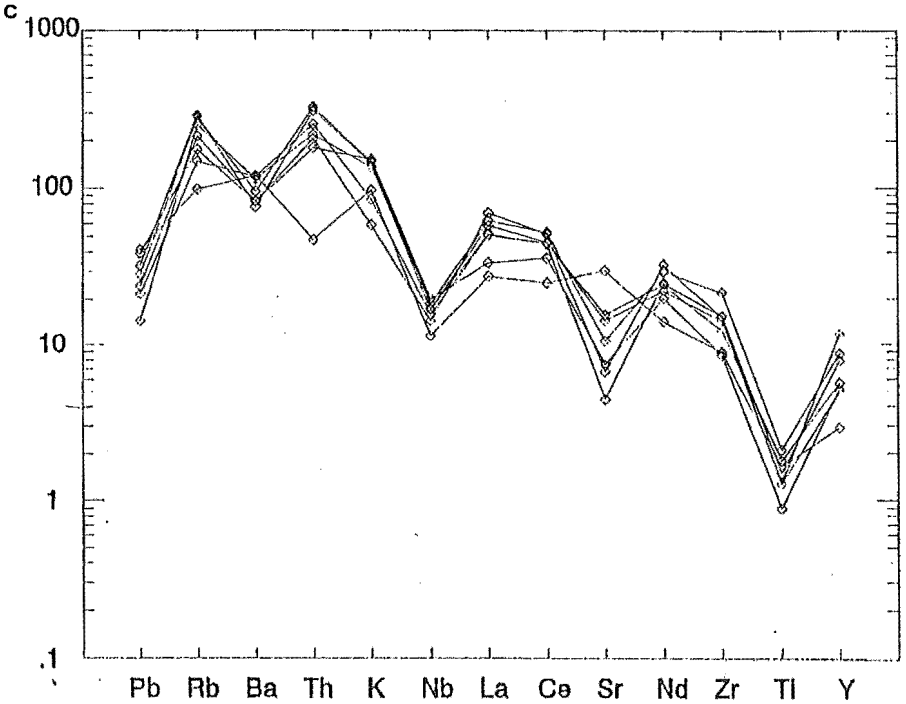
c
1000
100
10
1
.1
Pb Rb Ba Th K Nb La Ce Sr Nd Zr Ti Y

peraluminous and evolved. The evolved I-type granitoid clasts include those identified as hypersolvus. The rhyolites which generally contain accessory titanite are also considered evolved I-types.

The distinctive mineralogical features displayed by the dacite (i.e. abundant green/brown biotite, titanite and pseudomorphs after hornblende) indicate it must be considered a weakly peraluminous (ASI = 1.03) I-type despite the frequent association in discriminatory diagrams with the more primitive S-types.

Granodiorites and leucotonalite clasts contain relatively higher CaO contents due to higher plagioclase contents. In general, however, CaO content is low due to the predominantly albite to sodic oligoclase (i.e. Na-rich) composition of the plagioclase identified.

5.3.4 Discrimination of Tectonic Setting

The majority of Lake Hill conglomerate clasts plot within the volcanic arc granite (VAG) field of Figures 5.18a and b, which use trace elements to discriminate tectonic setting (Pearce *et al.*, 1984). In Figure 5.18a a granodiorite (LH17/24461), and a rhyolite (LH34/24478), plot in the ocean ridge granite (ORG) field, and a monzogranite (LH24/24468) plots in the within plate granite (WPG) field. In Figure 5.18b the low Rb and primitive nature of the low K clasts is emphasized, and the granodiorite (LH15/24459) has extremely low Rb (6ppm). The clasts that plotted in the ORG field of Figure 5.18a both plot with LH24/24468 in the WPG field.

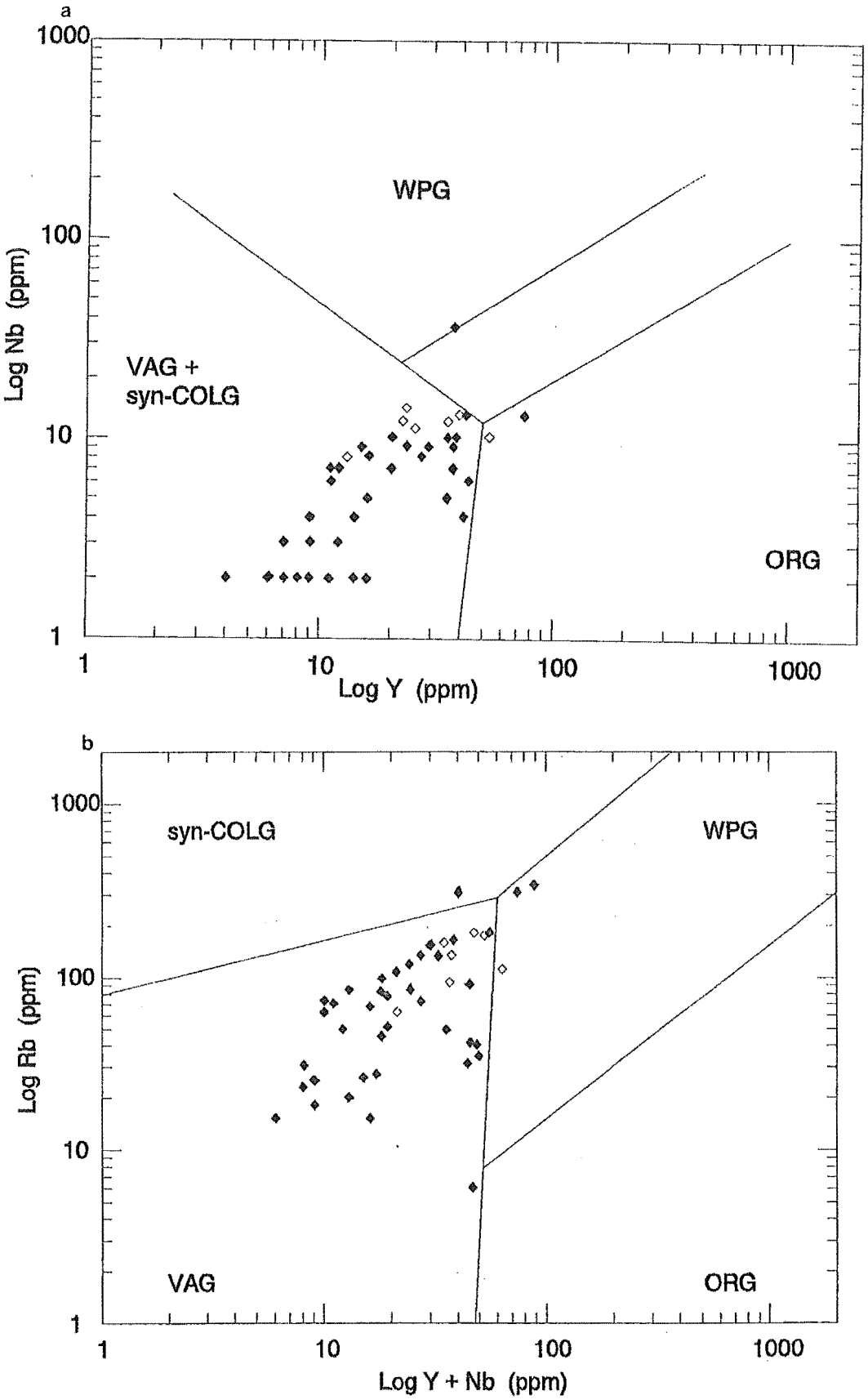

Figure 5.18: Tectonic discrimination diagrams illustrating distribution for Lake Hill conglomerate igneous clasts within the syn-collision (syn-COLG), volcanic arc granite (VAG), within plate granite (WPG), and ocean ridge granites (ORG) fields:
a Nb-Y
b Rb-Y+Nb
(after Pearce *et al.*, 1984)

5.4 Synopsis

The Lake Hill conglomerate granitoid clasts range in mineralogical and modal character from biotite (± muscovite) leucotonalite to leucogranodiorite/granodiorite to leucomonzogranite. Volcanic clasts are porphyritic/spherulitic rhyolites and a porphyritic dacite that were extruded as lava domes and/or flows.

Geochemically, the texturally distinguished subsolvus foliated granitoids are distinguished as S-types that display a relatively primitive character. The hypersolvus and undeformed subsolvus granitoid types are considered evolved I-types that chemically and mineralogically relate to the rhyolite and dacite volcanic clasts. Hypersolvus granitoids are hypabyssal and relate to the volcanic clasts cogenetically.

The Lake Hill conglomerate clasts are predominantly tholeiitic to calc-alkaline and display trace element features that indicate magmas were related to subduction.

5.5 Discussion

During the Triassic (~235-190Ma), deposition of the Lake Hill conglomerate occurred in response to the erosion and dissection of a dominantly plutonic arc that had developed previously in response to subduction along an active continental margin.

Igneous clasts comprise peraluminous primitive S-type granitoids that exhibit major and trace element features indicating heterogeneous source compositions. The

pervasive foliation noted in subsolvus S-type clasts records a post-intrusive deformation. The weakly peraluminous I-type granitoids indicate crystal fractionation from a mafic igneous source. The dacite volcanic clast, although primitive in character, displays mineralogical features that relate it to the evolved I-type rhyolite clasts, with which it forms a continuum in the TAS diagram (Figure 5.6). The intrusive evolved I-types are deemed to be the subvolcanic representation of the volcanic clasts examined.

The accepted model for S-type intrusion involves a mature continental margin with the full thickness of continental crust. S-types are intruded, usually inland of earlier, or coeval I-types as a result of partial melting of a meta-sedimentary source in response to a high geothermal gradient that probably relates to the entrapment, or underplating of I-types at the base of the crust (Chappell and White, 1992). The low K_2O content of the Lake Hill conglomerate S-type clasts suggests this is not the case.

The tholeiitic character of the S-type granitoid clasts suggests a more mafic source for these magmas. It has been hypothesized that some S-type magmas are intruded oceanwards of the continental margin in response to thickening of the accretionary wedge sediments during the waning stages of subduction (Shaw and Flood, 1981).

Collection procedures followed those already stated (Chapter 2, 2.5) and it is assumed that samples examined are representative of the clasts in the Lake Hill conglomerate.

CHAPTER 6

INTEGRATION AND COMPARISON OF GEOCHEMICAL DATA

6.1 Introduction

This chapter amalgamates the information obtained from the data presented in previous chapters and makes comparisons internally, between the conglomerate localities, and externally, with potential source regions. Extrapolations to potential protoliths, or known provinces are constrained by geochronological information from recent literature.

6.2 Comparison between Conglomerate Localities

6.2.1 Gross Geochemical Features

The igneous clasts from all four conglomerates studied have gross chemical features by which they may be compared. Normative calculations (Appendix 5) emphasize the chemical features discussed separately in each chapter and provide a useful measure of bulk chemical character.

The igneous clasts from all four conglomerates are quartz normative, a feature expected in rocks that display such high silica contents. Mount Saul volcanic clasts display the lowest silica values relative to clasts from the other conglomerates.

The percentage of clasts generating normative corundum (which indicates peraluminous character and S-type character, specifically if $>1.0\%$), as opposed to diopside (which indicates metaluminous/peralkaline character, and I- or A-type character), is variable. Of the 50 Ethelton conglomerate clasts, 27 exhibit normative corundum, with only 9 $>1.0\%$, indicating a predominance of I-types or fractionated I-types. In the Lake Hill conglomerate all 46 clasts have normative corundum and of these 28 have values $>1.0\%$. Some fractionated I-types are present, including the volcanic clasts, but the majority are S-type granitoids. Of the 49 Mount Saul clasts, 37 have normative corundum, 6 of which have values $>1.0\%$. Of the 55 Chatham Islands conglomerate clasts 51 exhibit normative corundum, and 16 are $>1.0\%$. Mount Saul and Chatham Island clasts comprise a mixture of I-type, S-types fractionated I- and S-type, and/or A-types.

The Mount Saul conglomerate contained one clast that generated NMS (sodium metasilicate) and acmite (a sodic pyroxene) in the normative calculation indicating a peralkaline character. The Ethelton conglomerate clasts record wollastonite in the norm, which supports the conclusion (Chapter 3, 3.5) that clasts from this conglomerate have undergone metasomatic alteration involving the addition of calcium.

The wide degree of scatter displayed in Harker diagrams by most clasts from all four localities emphasizes the mixture of granitoid and volcanic types each conglomerate contains. The coherent linear trends, displayed by the majority of Ethelton conglomerate clasts (Figure 3.14), however, indicates a cogenetic relationship and derivation from a common, or similar source. In the Ethelton

conglomerate mineralogical differences can be attributed to heterogeneities within a cogenetic suite. The high Zr content of Mount Saul volcanic clasts relative to other areas, and the low Rb, and separable low and high K content of Lake Hill conglomerate clasts are distinctive (Figures 4.14c and 5.15b). The geochemical differences noted indicate that distinct granitoid and volcanic suites have been preserved as clasts within each conglomerate.

Multi-element abundance diagrams, compiled for groups of clasts from each conglomerate, display significant similarities and differences. The distinctive negative Nb anomaly and enrichment in incompatible (with respect to source) large ion lithophile (LIL) elements, clearly indicate that the source for all clasts has been through at least one subduction cycle (Figures 2.17, 3.17, 4.17, 5.17). The predominantly high K (excepting Lake Hill S-type granodiorites) and low Ni in all samples preclude a mantle source.

The presence of granitoid and volcanic clasts within each conglomerate indicates the source province for all clasts was a volcano-plutonic arc(s). Petrographic evidence indicates that many of the plutonic clasts are subvolcanic and can geochemically, and mineralogically, be related genetically to a proportion of the volcanic clasts present in the same conglomerate.

The igneous clasts from all four conglomerates compare favourably with rocks described from modern active continental margin settings, such as the Taupo Volcanic Zone, North Island, New Zealand (Cole, 1979; S.J.A. Brown, pers.comm.). The absence of associated mafic intrusives and volcanics (gabbros and

basalts) indicate oceanic island arc volcanism and plutonism was not involved.

6.2.2 Correlation between the Torlesse and Chatham Islands Conglomerate

The Chatham Islands conglomerate, deposited during the middle Cretaceous (~100Ma), is relatively undeformed and post-dates the three Torlesse conglomerates sampled, which display variable deformation attributable to either one (Ethelton and Mount Saul), or both (Lake Hill) phases of the Rangitata orogeny. The attenuation of thick continental crust in response to extension, prior to actual separation between New Zealand and Western Antarctica, has resulted in the spatial separation of the Torlesse and Chatham Islands conglomerates, which must have been considerably closer in the middle Cretaceous.

The conglomerate clasts of the Chatham Islands compare in mineralogical content and geochemical data to some of the clasts found in all three Torlesse conglomerates. The Mount Saul conglomerate, with the most variable clast content of the Torlesse conglomerates, contains A-type volcanic clasts that could correspond to the A-type features displayed by some Chatham Island granitoid clasts.

The freshness of Chatham Islands clasts indicate the possibility of this conglomerate containing reworked Torlesse conglomerate derived clasts is unlikely.

The Chatham Islands conglomerate should contain clasts representative of the Western Antarctica margin which, at the time of deposition, was adjacent to the northeast and east (Mayes *et al.*, 1990). This will be discussed further in section

6.4.3.

6.2.3 Correlation within the Pahau Subterrane

The Mount Saul and Ethelton conglomerates both occur within the Pahau subterrane of the Torlesse, and, by their close proximity both spatially and temporally, could be expected to display similar features with regard to clast content.

The geochemical data indicate that Ethelton clasts represent a spectrum of intrusive depths within an evolved cogenetic suite. Mount Saul clasts, however, display a range of characteristics that indicate multiple sources. The presence of both I-types and S-types of similar mineralogy in both conglomerates suggests some affinity and a common source may have contributed to both.

That both conglomerates contain igneous clasts representative of subduction along an active continental margin, and are present in such close proximity (~30km) within the same subterrane, indicates clasts are likely to be derived from the same province, but that distribution of rock types within this province is not uniform.

The presence of peralkaline volcanic clasts within the Mount Saul conglomerate emphasizes the different catchments accessible to each of the Pahau conglomerates. The occurrence of peralkaline volcanism and intrusion in New Zealand is limited to a granite dyke in northwest Nelson (Tulloch, 1992), an exposure of gneissic granite in Fiordland (Wood B.L., 1969), the French Creek Granite in the Hohonu Range, West Coast and numerous related alkaline rhyolite

dykes ((Tulloch *et al.*, in press; T.E. Waight, pers. comm.), the Kerikeri volcanics, Northland (Ashcroft, J., 1986) and the Quaternary to Recent Mayor Island volcano (Houghton, *et al.*, 1992). North Island peralkaline volcanism is Late Pliocene to Recent, and the West Coast granite and dykes were intruded during the Late Cretaceous, too young to be related to the Mount Saul conglomerate. The peralkaline granite in northwest Nelson is Late Triassic in age and could feasibly relate to incorporated volcanics in the Mount Saul conglomerate, as could the Fiordland gneissic granite which has a Paleozoic intrusive age. The possibility of a Western Province source for the Torlesse is discussed in Section 6.4.2.

6.2.4 Correlation between the Rakaia and Pahau Subterranes

The Triassic Lake Hill conglomerate occurs in the Rakaia subterrane of the Torlesse. The ~100Ma interval between deposition of this conglomerate, and the Mount Saul and Ethelton conglomerates as part of the Pahau subterrane in the Early Cretaceous, suggests it is unlikely that they preserve clasts that record the same subduction event.

The main feature of the Lake Hill conglomerate that distinguishes it from the Pahau conglomerates is the presence of pervasively deformed S-type granodiorite clasts with distinctively low potassium content. The overall geochemical signature for clasts is subduction related and fractionated I-types are present, as for the Pahau subterrane conglomerates.

The longevity of subduction, indicated by the conglomerates, suggests that

convergent tectonics dominated along an active continental margin prior to the deposition of the Rakaia and Pahau subterrane sediments. Whether the active continental margin was the same for both subterranes is not clear, but evidence suggests basic chemical differences. In granitic provinces exposed at the present time (e.g. the Western Province) a multitude of plutons of differing ages displaying unique mineralogical and geochemical differences can be contained in a relatively small area (Tulloch, 1983; Muir *et al.*, in press).

6.3 Constraints on Potential Protoliths

6.3.1 Geochronology

Recent work (U-Th-Pb SHRIMP isotopic analysis) by Ireland (1992) indicates that inherited zircons in typical Torlesse greywacke from the Rakaia subterrane are dominantly 260 $\pm$8Ma in age (Figure 6.1a), indicating a Permian granitoid province supplied the Torlesse with detritus. Frost and Coombs (1989), on the basis of Nd isotopic analyses on Torlesse sediment, provide a Proterozoic separation age from the mantle for the contributing source. Ireland (1992) suggests that the dominantly Permian granitoids that provided the Torlesse detritus represent remelted older crust which preserves a Proterozoic Nd isotopic signature. Zircons analysed by SHRIMP from the Chatham Island Schist/Matarakau Greywacke are also predominantly Permian in age (i.e. ~260Ma, Figure 6.1b) (T. Ireland, J.D. Bradshaw, and S.D. Weaver, unpublished data). This allows correlation between the Chatham Islands Schist/Matarakau Greywacke and the Rakaia subterrane, and suggests a dominantly Permian granitoid province for the Torlesse detritus may be a regional feature, at l

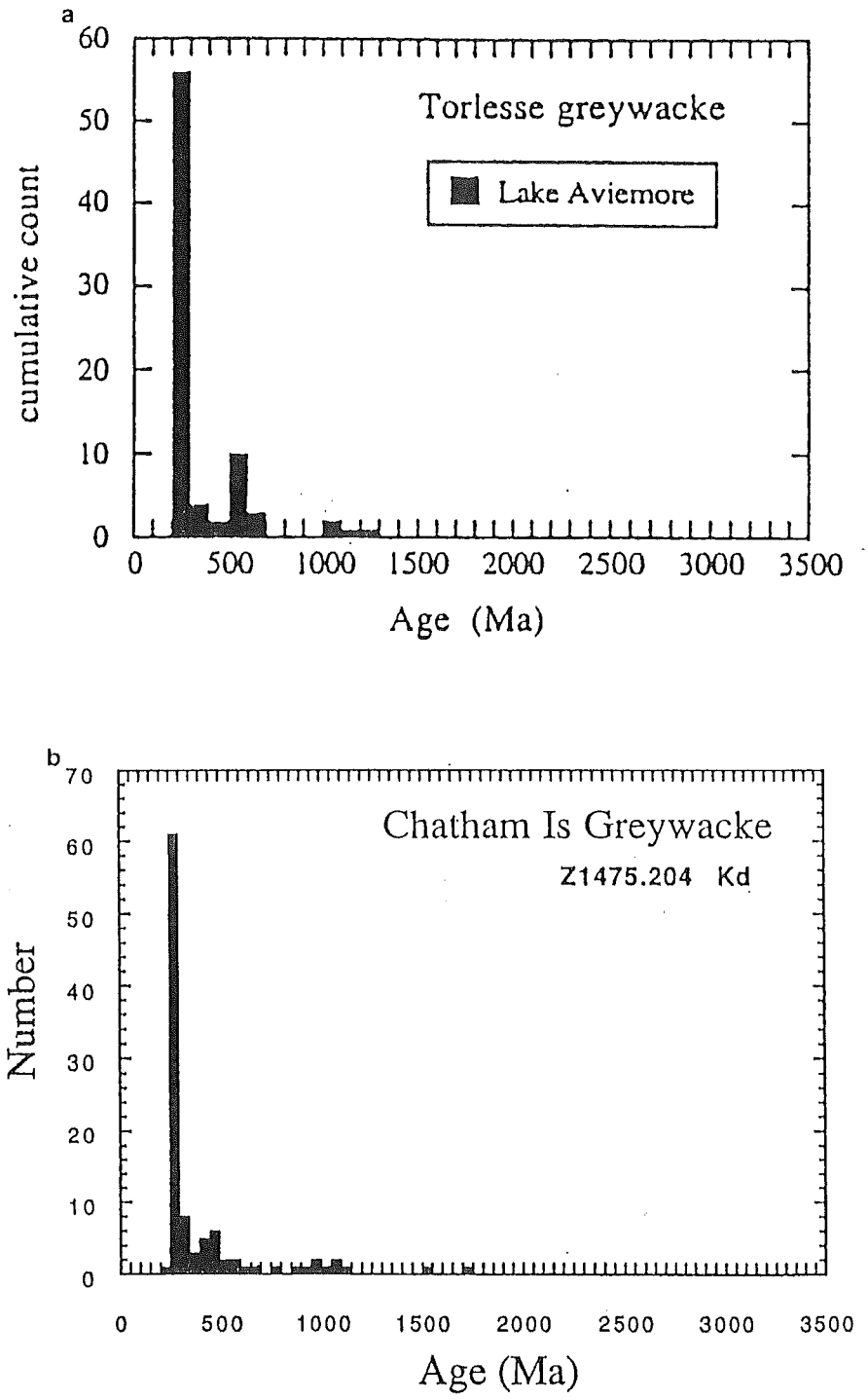

Figure 6.1: Age distributions of zircons from:
a Torlesse greywacke
b Matarakau greywacke
both dominated by a Permian zircon population.
(after Ireland, 1992; T. Ireland, J.D. Bradshaw, S.D. Weaver, unpublished data)

least at subterrane level.

6.3.2 Paleocurrent Data

The bulk of the Torlesse is of submarine fan/turbidite origin. The conglomerates examined (apart from the Chatham Islands conglomerate) are considered to be mass flow/channel deposits. All contain clasts of variable size and composition that indicate wide catchments. Paleocurrent data from within the Torlesse are available, but provide inconsistent information, particularly between the subterranes.

6.4 Correlation with Potential Source Areas

6.4.1 Bounty Islands

The Bounty Islands are a group of nine small islets and isolated rocks that comprise biotite (± muscovite) granite cut by various igneous dykes (Figure 6.2) (Speight and Finlayson, 1909; Tulloch, 1983). Rb-Sr and K-Ar dating of biotite from Bounty Islands samples yields a Late Triassic/Early Jurassic age (~189Ma) for emplacement (Tulloch, 1983; Adams, pers.comm.). The geographical location of the Bounty Islands, and their granitic character, suggest they may have provided the Chatham Islands conglomerate with detritus prior to the opening of the Bounty Trough, which supposedly occurred as a precursor to separation of the New Zealand continent from Antarctica prior to 85Ma (Figure 1.1b) (Mayes *et al.*, 1990; Herzer and Wood, 1992).

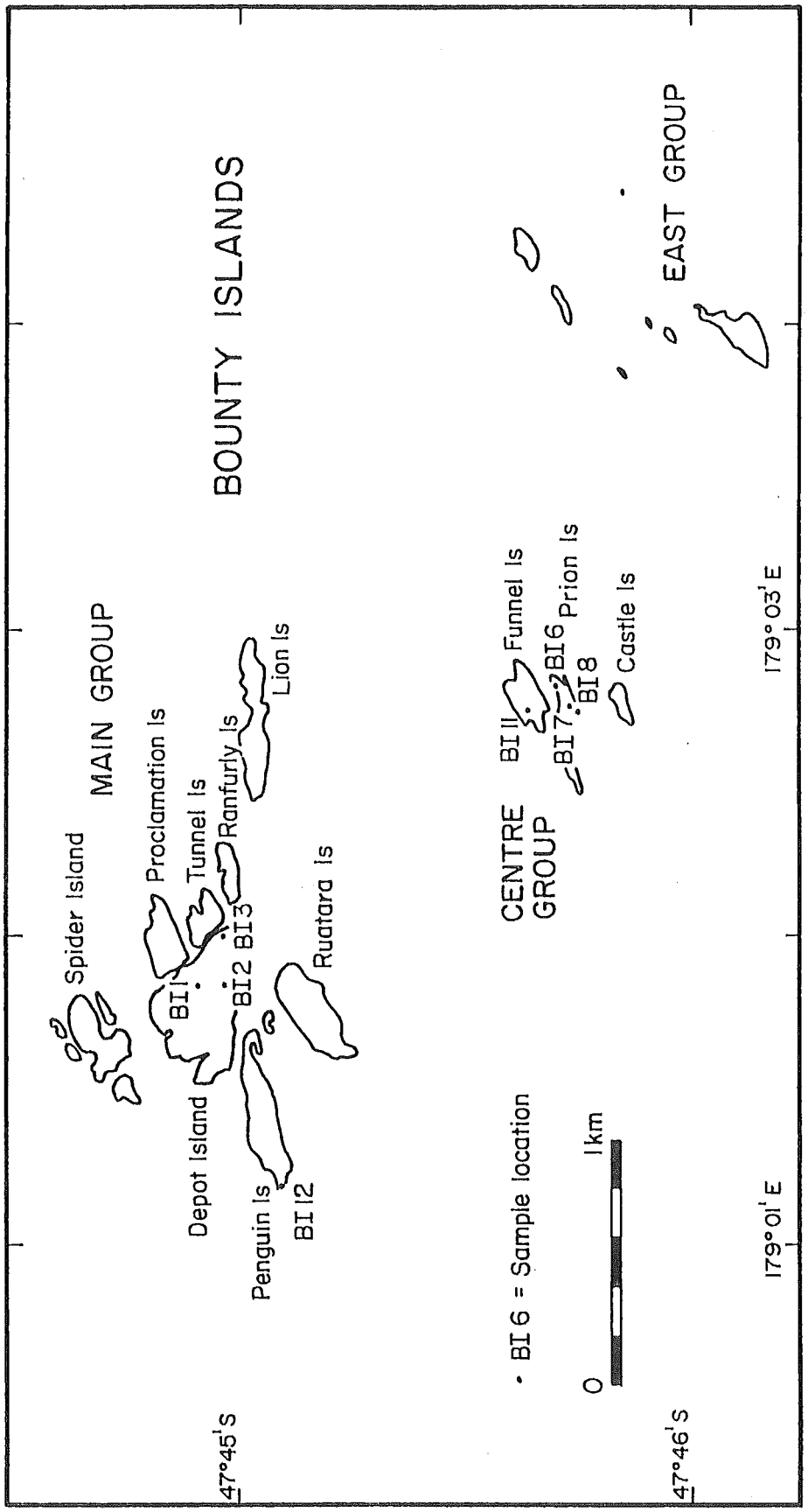

Figure 6.2: Bounty Islands locality map.
(after C.J.D. Adams, unpublished data)

Whole rock powders for twelve Bounty Islands samples were analyzed by XRF and data are included in Appendix 1. The Al-rich character of Bounty Islands samples is displayed in Figure 6.3 which plots the calculated Aluminium Saturation Indices. All samples, apart from the metaluminous lamprophyre dyke (BI3/24101), plot in the peraluminous field (ASI > 1.0). The majority form a continuum with an ASI between 1.05 and 1.15, indicating S-type affinities. Two samples (BI6/24102, BI7/24103), quartz porphyry dykes, plot separately from the other samples. All samples contain normative corundum except the lamprophyre dyke, which contains diopside (Appendix 1). Of the 11 that have normative corundum, 8 have values that > 1.0%, and are considered S-types.

Analyses were plotted on the K_2O-Na_2O-CaO ternary diagram (Figure 6.4) to compare the Bounty Islands samples with plots made for conglomerate clasts. The Bounty Islands samples plot in close association, but do not overlap with any conglomerate clasts analyzed.

In primitive-mantle-normalized multi-element diagrams the Bounty Island samples display the typical spiked pattern and LIL element enriched character of subduction related magmas, as do all the conglomerate clasts examined (Figure 6.5).

Using a Rb versus Y+Nb diagram (Figure 6.6) to discriminate the tectonic setting, the Bounty Islands samples fall well within the volcanic arc granite (VAG) field, supporting the subduction related classification. The lamprophyre dyke, whilst having a more mafic source that is emphasized by higher Ti, lower K and Y, mirrors the features displayed by the granitic samples and is also subduction related.

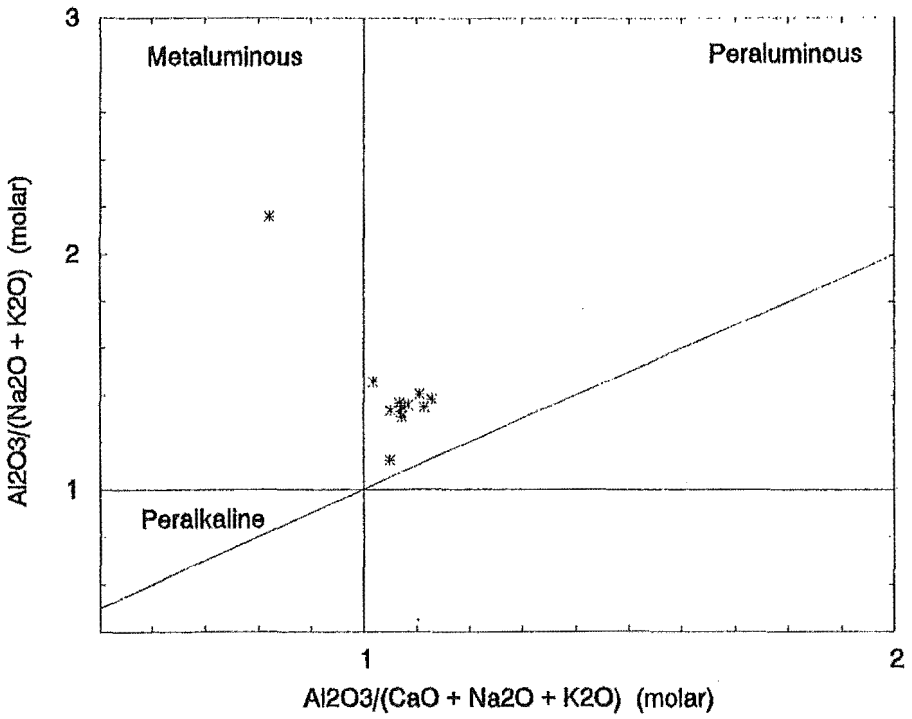

Figure 6.3: Aluminium Saturation Indices plotted for Bounty Island samples. A/CNK = 1.1 indicates the boundary between highly fractionated I-type/S-types and S-type granitoid/volcanic clasts. (after Maniar and Piccoli, 1989)

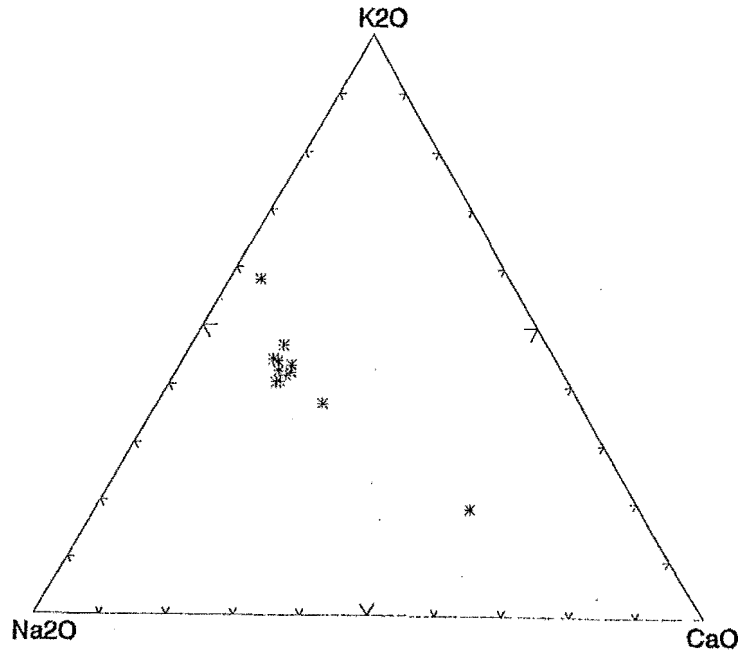

Figure 6.4: K_2O-Na_2O-CaO ternary diagram, which compares the K_2O/Na_2O ratio, and considers CaO for Bounty Island samples.

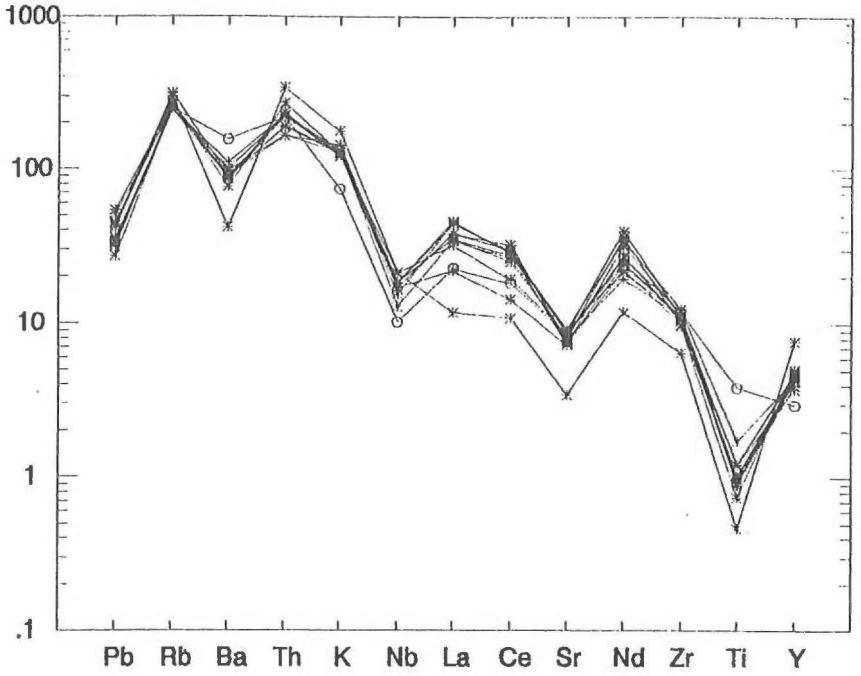

Figure 6.5: Multi-element primitive-mantle-normalized (Sun and McDonough, 1989) abundance diagrams for Bounty Island samples.
o = lamprophyre dyke

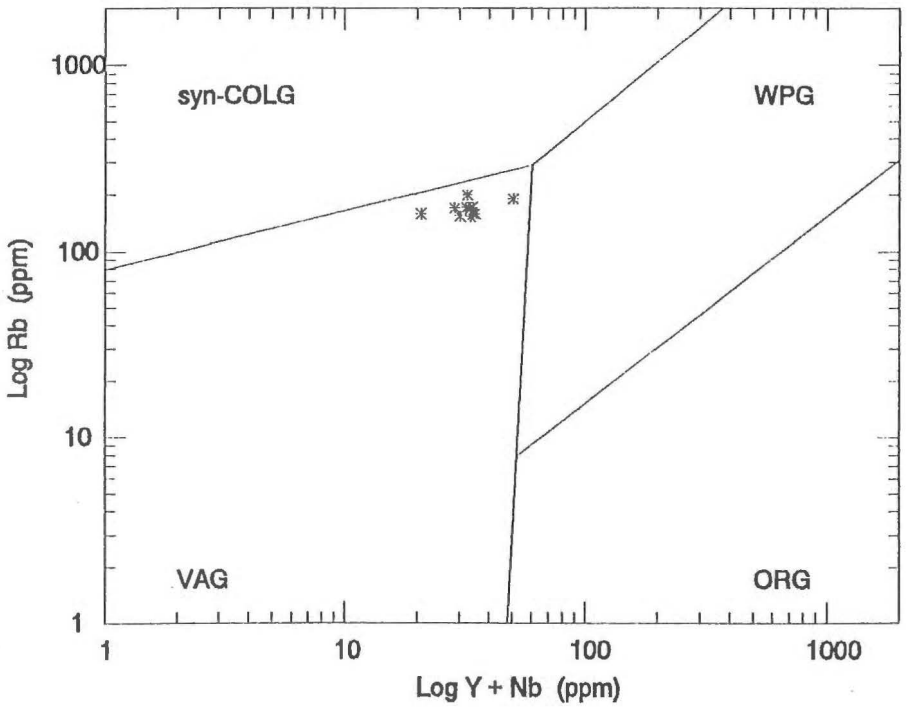

Figure 6.6: Tectonic discrimination diagram illustrating distribution for Bounty Islands samples within the syn-collision (syn-COLG), volcanic arc granite (VAG), within plate granite (WPG), and ocean ridge granite (ORG) field.
(after Pearce *et al.*, 1984)

The absence of basement exposure on the Bounty Islands does not allow the intrusives they contain to be placed in any terrane with confidence and any correlation must be tentative. Intrusion could relate to the Chatham Island schist metamorphism that occurred prior to the ~162Ma uplift age (Adams and Robinson, 1977). However, samples are predominantly undeformed which makes this unlikely (Speight and Finlayson, 1909).

The present day exposure could represent the deeply dissected remnants of a batholith which, during the middle Cretaceous, exposed highly evolved granitoids that were subsequently included within the Chatham Islands conglomerate. The uniformity of the samples analyzed suggests that the Bounty Islands granite may have contributed to the clasts examined from the Chatham Islands, but the predominantly S-type character makes it unlikely as a primary source.

6.4.2 Western Province

The close proximity and comparable composition of granitoids in the Western Province (Figure 1.2) lead to the consideration of these as possible sources for the Torlesse terrane (Landis and Bishop, 1972; Suggate *et al.*, 1978; MacKinnon, 1983). Three granitoid suites that contain plutons with similar chemical and mineralogical characteristics, and ages are defined within the Western Province, the Paleozoic Karamea Suite, and the Mesozoic Rahu and Separation Point Suites (Tulloch, 1988).

The Karamea Suite granitoids are confined to the western Buller terrane, and comprise predominantly Devonian/Carboniferous S-type intrusives that are typified

geochemically by relatively high K and enrichments in Fe, Mg, Ti and Rb (Tulloch, 1983; Cooper and Tulloch, 1991). By comparing data on K_2O-Na_2O-CaO ternary diagrams (Figures 2.16, 3.16, 4.16, 5.14, 6.7) it can be seen that Karamea Suite granitoids generally plot with a much higher K_2O value than the majority of clasts examined. The Triassic Lake Hill igneous clasts are predominantly S-type granitoids, however, unlike the Karamea Suite rocks they exhibit characteristic low K_2O values (Figure 5.14). Typical trace element patterns from the Cape Foulwind Granite (327Ma R.Muir, pers.comm.) and the O'Sullivans Granite (380Ma R.Muir, pers.comm.), components of the Karamea Suite, are displayed in Figure 6.8a and b (analyses Appendix 1, R.Muir, pers.comm.). Trace element patterns conform to those obtained for the evolved granitoid and volcanic clasts examined from the conglomerates with no significant differences.

A Rb/Sr isotope age of 285 $\pm$5Ma has been obtained from biotite within the Red-Jacket Granite north of Meybelle Bay (C.J. Adams, unpublished data). Providing the age obtained represents emplacement, this confined coastal outcrop is the only Permian granitoid recognized thus far from the New Zealand continent. Unless it is representative of previously more substantial Permian granitic province, it is unlikely to have provided the detritus for the Torlesse. Granitic rock has been dredged from the Challenger Plateau/Lord Howe Rise, but this provided a Carboniferous age (Cooper and Tulloch, 1991).

Graham and Korsch (1990) show evidence that the intrusive age of conglomerate granitoid clasts can fall within the range of sedimentary ages for a

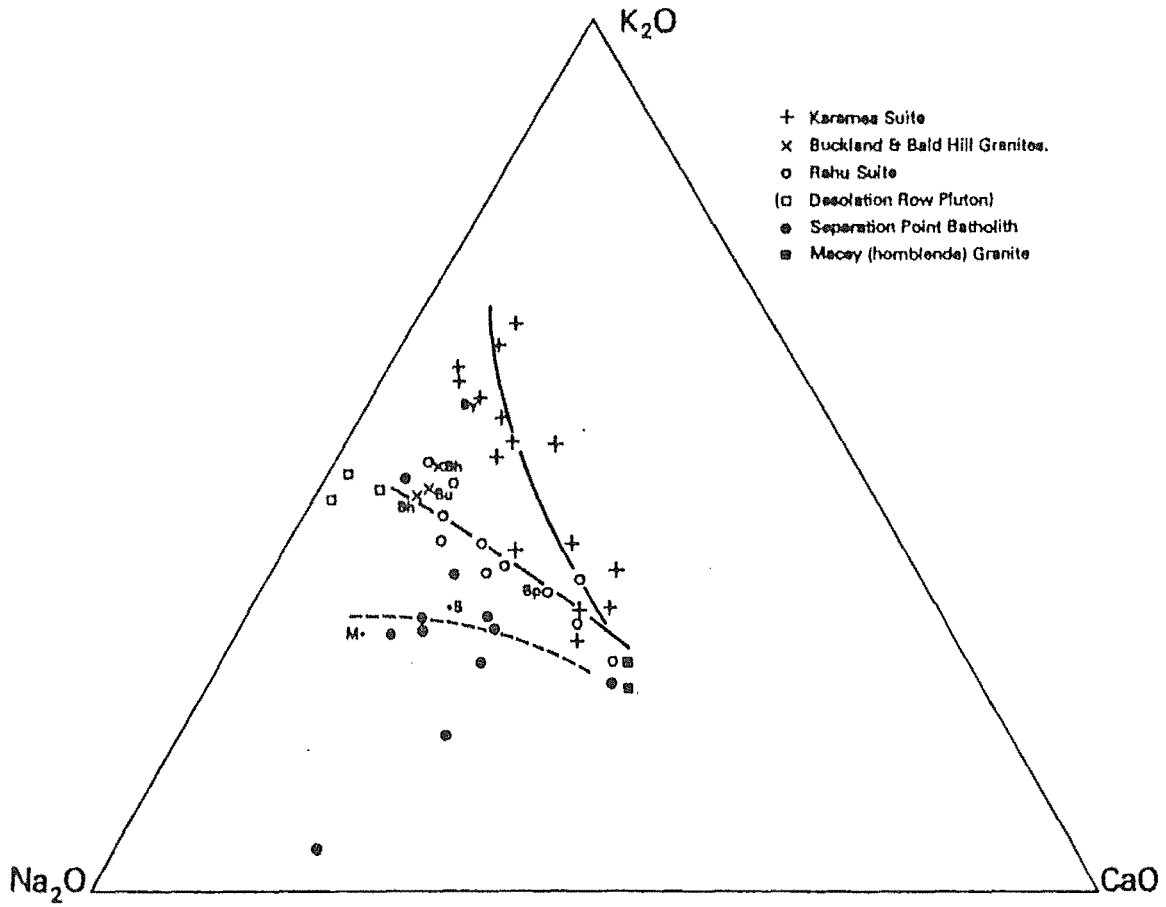

Figure 6.7: K_2O-Na_2O-CaO ternary diagram for Western Province granitoids. (after Tulloch, 1983)

Figure 6.8: Multi-element primitive-mantle-normalized (Sun and McDonough, 1989) abundance diagrams for Western Province granitoids:
a Cape Foulwind Granite (Karamea Suite)
b O'Sullivans Granite (Karamea Suite)
c Separation Point Granite (Separation Point Suite)
d Bucklands Granite (Rahu Suite)

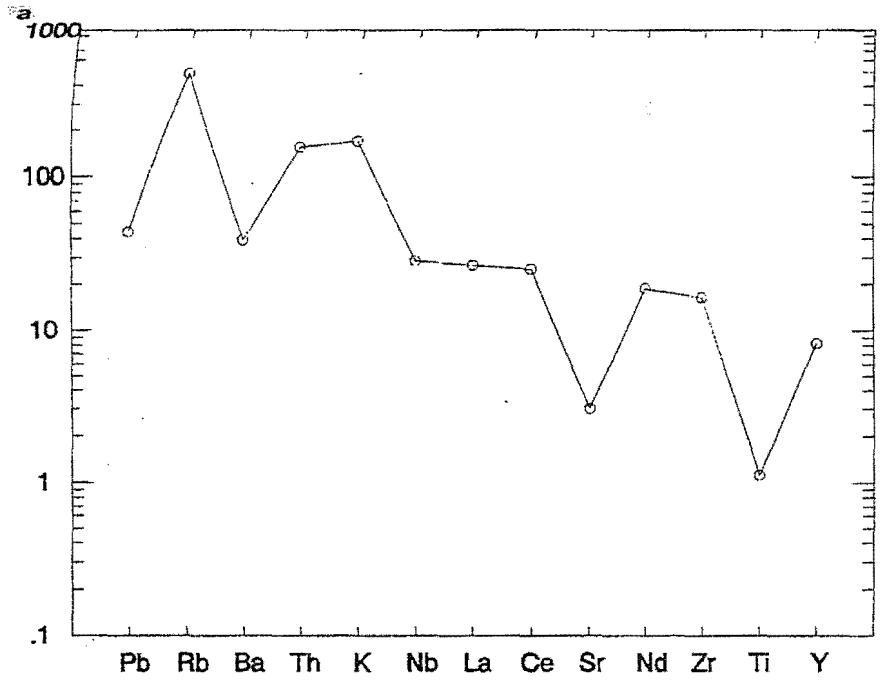
a
1000
100
10
1
.1
Pb Rb Ba Th K Nb La Ce Sr Nd Zr Ti Y

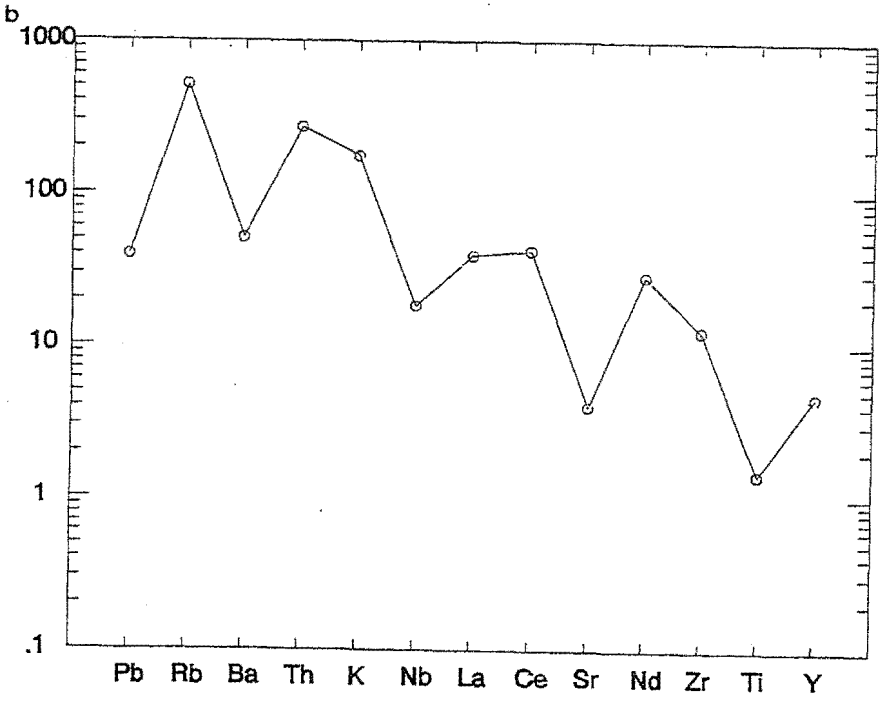
b
1000
100
10
1
.1
Pb Rb Ba Th K Nb La Ce Sr Nd Zr Ti Y

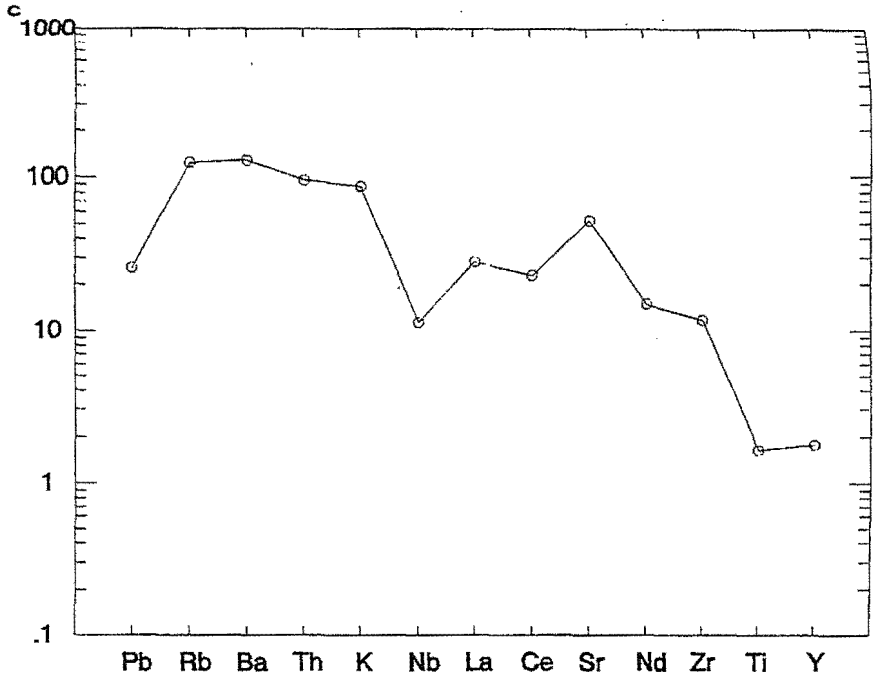
c
1000
100
10
1
.1
Pb Rb Ba Th K Nb La Ce Sr Nd Zr Ti Y

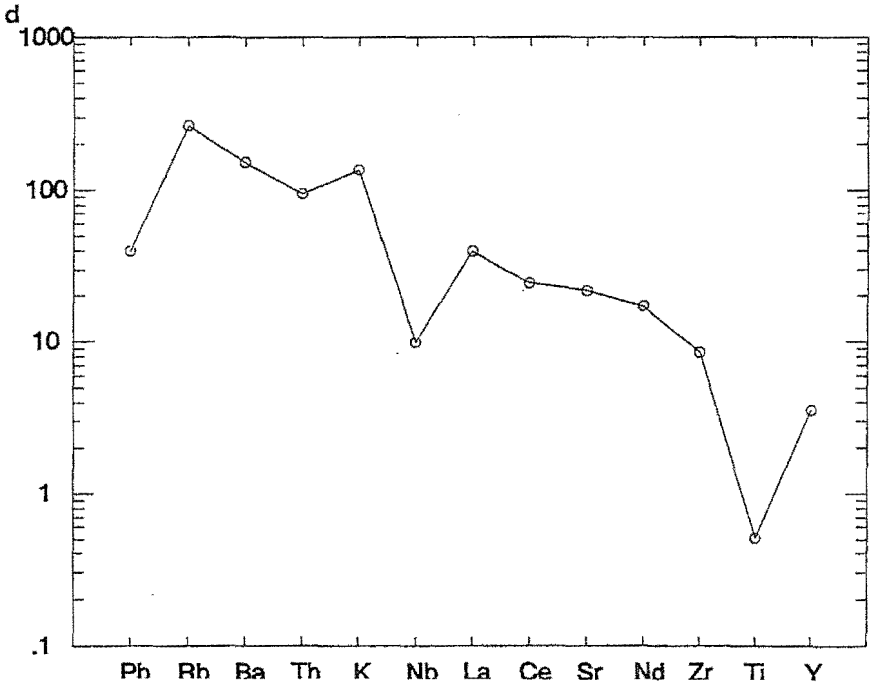
d
1000
100
10
1
.1
Pb Rb Ba Th K Nb La Ce Sr Nd Zr Ti Y

conglomerate with rapid uplift and erosion of the protolith. The Rahu Suite and Separation Point Suite, intruded during the middle Cretaceous, are considered as possible sources for the younger Pahau subterrane, and Chatham Islands, conglomerates. The Separation Point Suite displays a distinctively high Sr and low Y content (Figure 6.8c) indicating the melting of a subducted oceanic crustal source following ridge subduction (Muir *et al.*, in press). Two Ethelton clasts display positive Sr anomalies, the result in this case of metasomatism and the introduction of Ca and Sr. Lake Hill clasts also show positive Sr anomalies, but lack the low Y values of the Separation Point Suite, and are too old to be considered comparable. The Rahu Suite contains granitoids of mixed I-, A- and S-type charactersitics which display a K_2O/Na_2O ratio of approximately 1:1. Some clasts from all the conglomerates examined plot with similar ratios. The multi-element abundance diagram for the Buckland Granite (~110Ma), part of the Rahu Suite, also indicates comparable abundances (Figure 6.8d).

Volcanic rocks that can be related to granitoid intrusion are not common in the Western province. The ubiquitous presence of predominantly rhyolitic volcanic clasts in the conglomerates examined was distinctive. However, it is possible that extrusive equivalents to the granitoids present in the Western Province have been subsequently removed by erosion.

The presence of several intervening terranes, dominated by basic and intermediate detritus, between the Torlesse and the Western Province terranes is a major problem in sediment derivation from the west. The strong petrological contrast between the Torlesse terrane and the rocks of the western Eastern Province

terranes (Brook Street, Murihiku, Maitai and Caples) precludes any cogenetic relationship. The Murihiku, a major sedimentary basin during the Triassic/Jurassic records no evidence of similar sediment derivation. Recent research by Frost and Coombs (1989) indicates little Sm/Nd isotopic similarity between the Eastern Province terranes, and discounts the intra-oceanic volcanic-arc dominated Brook Street terrane as a possible source for the other volcanogenic-rich terranes. This information, combined with oxygen isotope, paleomagnetic and paleotectonic data, suggests the probability that all Eastern Province terranes are allochthonous with respect to each other, and to the Western Province/Gondwana margin (Bradshaw, 1993).

The Caples terrane and the Rakaia subterrane were amalgamated by the Middle Jurassic as both were affected by the metamorphism that resulted in the Haast schist. The Pahau subterrane was still receiving sediment until the late Early Cretaceous which supports provenance from another direction. It is possible, given the suggested mobility of terranes (Bradshaw, 1993), that Torlesse sedimentation from a western continental source was unimpeded by intervening terranes. Derivation of Torlesse detritus from a source to the east, possibly West Antarctica, has been suggested by several studies (Bradshaw, 1973; Blake *et al.*, 1974; Coombs *et al.*, 1976; Spörli, 1978; Kamp, 1980; Bradshaw *et al.*, 1981; MacKinnon, 1983; Korsch and Wellman, 1988; Weaver *et al.*, 1991).

6.4.3 West Antarctica

The West Antarctica region contains predominantly Paleozoic and Mesozoic intrusives cutting Paleozoic metasediments that resemble the Western Province of New Zealand, particularly the Buller terrane. They may have been amalgamated with the East Antarctica/Gondwana margin as early as the Carboniferous (Figure 6.9) (Borg *et al.*, 1987; Weaver *et al.*, 1991).

The igneous rocks of Marie Byrd Land (Figure 6.9) comprise predominantly middle Paleozoic and late Mesozoic calc-alkaline intrusives. Devonian (350-380Ma) granitoids are best known from the Ford Ranges and comprise a granodiorite-monzogranite suite that is characteristically calc-alkaline I-type/evolved I-type emplaced in a continental margin subduction-related environment (Weaver et al., 1991). The Late Jurassic/Early Cretaceous granitoids (140-110Ma) are typically calc-alkaline biotite leucogranites that are anorogenic A-types. Compositionally and geochemically the rocks described resemble some of the clasts examined from each conglomerate. Volcanic rocks are found in Marie Byrd Land, and are predominantly Tertiary olivine basalts and interbedded pyroclastics. A Cretaceous trachyte/rhyolite suite occurs in the Ruppert Coast area (Figure 6.9) (Grindley, 1981; S.D.Weaver and J.D.Bradshaw, pers.comm.)

The Antarctic Peninsula comprises eroded Paleozoic to Tertiary volcano-plutonic arc rocks formed during the eastern subduction of the proto-Pacific oceanic crust beneath the margin of Gondwana (Cooper *et al.*, 1982; Storey and Garrett, 1985). Calc-alkaline plutonism and volcanicity were more or less continuous from

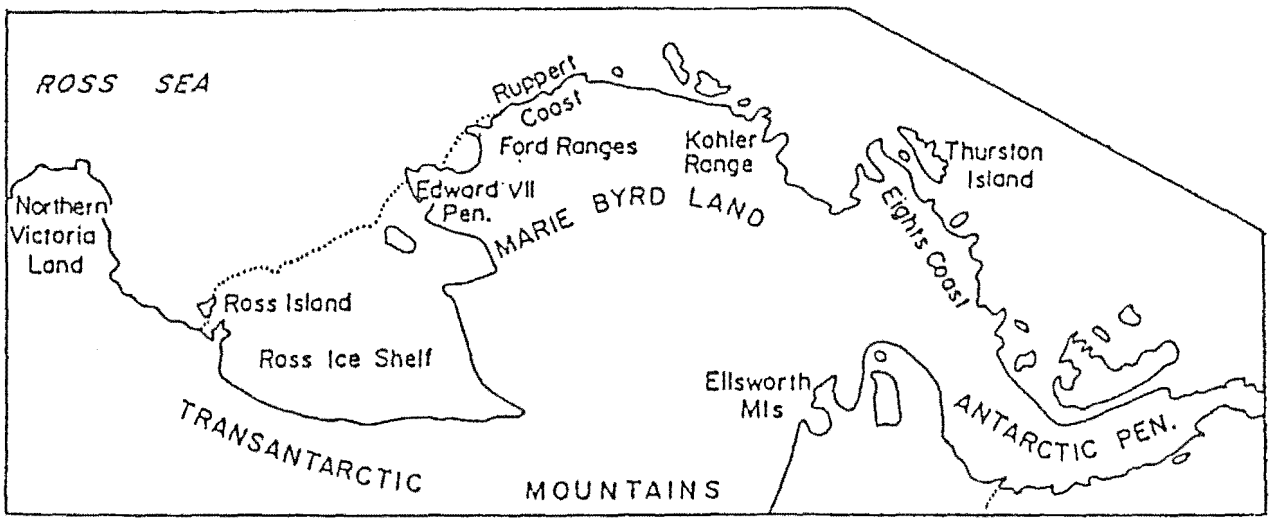

Figure 6.9: Sketch map of West Antarctica and Northern Victoria Land. (after Weaver *et al.*, 1992)

the Triassic to the Late Tertiary. The older plutons have a geochemical signature that indicates interaction with continental crust, whereas younger plutons emplaced within the accretionary prism are more mafic (Storey and Garrett, 1985). The incorporation within the conglomerates of continentally derived granitoid and volcanic material from the Antarctic Peninsula is possible, particularly for the Chatham Islands conglomerate. However, the later mafic intrusives are not represented.

In East Marie Byrd Land K/Ar and Rb/Sr isotopic ages that range from 230 - 295Ma have been obtained from minerals within, and whole rock analyses of syenogranites, granodiorites, diorites and volcanic porphyries (Halpern, 1972). This suggests a period of Permian magmatism that may be masked by later intrusive phases. Lopatin and Orlenko (1972) note the possibility of Cretaceous intrusives resetting the isotopic ages of older rocks.

Northern Victoria Land (Figure 6.9), part of East Antarctic contains intrusives comparable with the conglomerate clasts examined. Northern Victoria Land can be divided into three terranes, all allochthonous with respect to each other (Borg *et al.*, 1987). The Wilson terrane which contains intrusives that relate to Cambrian/Ordovician plutonism (500-480Ma), and Carboniferous volcanic activity which records rhyolitic composition magmas and compostionally related hypabyssal intrusives, the Bowers terrane and Robertson Bay terrane into which the Admiralty intrusives of Devonian age intrude (390-360Ma). The Admiralty intrusives comprise a calc-alkaline, granodiorite dominated I-type suite of similar chemistry to the Devonian intrusives described from the Ford Ranges, Marie Byrd Land (Borg *et al.*,

1987; Weaver *et al.*, 1991). Frost and Coombs (1989) obtained from Nd isotope data on Northern Victoria Land granitoid crustal residence ages that were deemed too old to have provided the sole source for the Torlesse sediment.

Convincing data have been produced that place the eastern margin of the Chatham Rise/Campbell Plateau against the Western Antarctica margin prior to continental separation (Mayes *et al.*, 1990). Granites described from the Edward VII Peninsula (95-100Ma) bear a striking resemblance to the clast assemblage examined from the Chatham Islands conglomerate. No mafic igneous rocks are present and granites from this area are highly fractionated metaluminous to weakly peraluminous I- to A-types, with $K_2O > Na_2O$, high Rb and low Ba and Sr (Weaver *et al.*, 1992). The A-types retain a weak subduction-related geochemical signature characteristic of their source, similar to that displayed by the A-type clasts noted from the Mount Saul and Chatham Islands conglomerate. The subvolcanic nature of the A-type granites, indicated by features such as miarolitic cavities (also seen in Chatham Islands clasts), suggest there may have been volcanic rocks associated with them. Rift margin uplift, associated with the separation of New Zealand from West Antarctica, has resulted in their subsequent removal.

6.4.4 Eastern Australia

The granitoid rocks of the southeast Australian Lachlan Fold Belt (Figure 6.10) are comparable with the Western Province of New Zealand and West Antarctica, and range in age from Cambrian to Devonian/Carboniferous. Subparallel suites of I- and S-type, with late stage anorogenic A-type granitoids have been

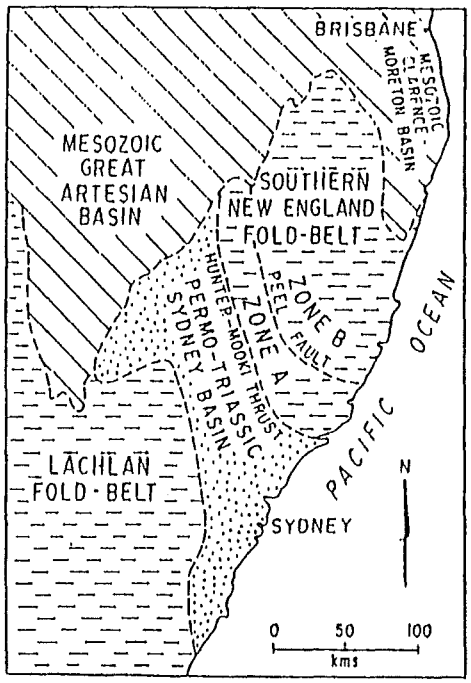

Figure 6.10: Sketch map of eastern Australia indicating the Lachlan Fold Belt, the Sydney Basin and the New England Fold Belt.
(after Shaw and Flood, 1981)

identified (White and Chappell, 1983; Chappell and White, 1992). The granitoid suites of the Lachlan Fold Belt represent a sequence of magmas that have developed along an active continental margin in response to subduction (Chappell and White, 1992). The geochemistry of various plutons within suites is comparable with the conglomerate clasts examined from all conglomerates. However, at the time of Torlesse accumulation parts of the Lachlan Fold Belt were either buried by Permian/Triassic sedimentary basins, or were contributing primarily quartz-rich sediment into such basins. If a dominantly Permian granitoid province provided detritus for the Torlesse as isotopic data suggest (Ireland, 1992), then the granitoids contained within the Lachlan Fold Belt cannot have been the sole contributors.

The New England Fold Belt, separated from the Lachlan Fold Belt by the Sydney Basin, contains an extensive Late Paleozoic to Early Mesozoic granitic province (Figure 6.10). The New England Fold Belt was for much of the Late Paleozoic a convergent plate margin at the edge of the Australian continent (Cawood, 1982; Murray *et al.*, 1987). The southern province of the fold belt contains the New England Batholith, with an outcrop area of ~15,000km^2 (Shaw and Flood, 1981). Two major phases of magmatism are recognized, the first during the Late Carboniferous and the second during the Late Permian and Early Triassic (Shaw and Flood, 1981). The suites that comprise the batholith display both I- and S-type characteristics (Hensel *et al.*, 1985). Extensive volcanism, ranging in composition from basaltic to rhyolitic, accompanied plutonic emplacement and culminated during the Early Permian (Shaw and Flood, 1981; Hensel *et al.*, 1985).

The New England granitoid province contains many plutons comparable in

mineralogy and geochemistry with the clasts examined. The mafic S-types contained within the province are believed to have been intruded into the ocean side of coeval I-type volcanism (Shaw and Flood, 1981). The geochemistry of the Lake Hill clasts (Chapter 5) suggests a similar environment of emplacement. The Sydney Basin, to the south of the New England Fold Belt, began subsidence in the Early Permian and during the Triassic was accepting continental detritus from the uplifted New England Fold Belt (Roberts and Engel, 1987; Collins, 1991). Contribution from the west, during the Triassic, to the Lake Hill conglomerate, and during the Early Cretaceous to the Mount Saul or Ethelton conglomerates is possible. Sm/Nd isotopic data from the New England granitoids are not available for comparison with Torlesse rocks, but could provide valuable information as to the likelihood of this occurrence. The main consideration in derivation of the Torlesse detritus from eastern Australia is the possible presence of intervening sedimentary basins, represented now by terranes, which should record evidence of similar sediment accumulation.

CHAPTER 7

SUMMARY AND CONCLUSIONS

7.1 Summary

The information recorded in the previous chapters can be summarized as follows:

- Igneous clasts examined from the Chatham Island conglomerate comprise predominantly calc-alkaline leucosyenogranites and leucomonzogranites. From geochemistry and mineralogy the granitoid types are identified as metaluminous I-types and weakly peraluminous evolved I-types, with a subduction-related signature. Some peraluminous S-types are present suggesting increased crustal contamination. A-type magmatism is recorded by some clasts, probably intruded and/or erupted at the concluding stages of subduction, in response to a change in tectonic regime. The clasts preserved indicate a spectrum of intrusive levels were exposed at the time of conglomerate deposition. Volcanic clasts present may be cogenetically related to the hypersolvus clasts, which generally display features that indicate subvolcanic emplacement.

The Ethelton conglomerate granitoid clasts are predominantly calc-alkaline granodiorites, leucomonzogranites and leucosyenogranites. The volcanic clasts are rhyolites and dacites. Geochemistry and petrography indicate granitoids are primarily metaluminous I-types and weakly peraluminous evolved I-types.

Volcanics relate to the I-types identified as hypabyssal. Trace element abundances indicate all clasts display features indicative of subduction-related magmas. The Ethelton conglomerate clasts represent partial melting events of a specific source and are considered a cogenetic suite. Granodiorite intrusion was probably accompanied by dacitic ignimbrite eruptions. Following the evolution of magma, leucosyenogranites and leucomonzogranite were intruded and rhyolite domes and/or flows were extruded. Hydrothermal alteration has resulted in Ca enrichment of the majority of clasts.

- Mount Saul conglomerate clasts indicate alkaline to calc-alkaline composition granitoids and volcanics. Granitoid rock types are predominantly leucomonzogranites, with some granodiorites and leucosyenogranites that were intruded at subvolcanic, hypersolvus and subsolvus levels. Granitoid clasts are predominantly I-types, evolved I-types, with some S-types. The volcanic clasts include dacites, trachydacites, trachytes and rhyolites that were extruded as ignimbrites and pyroclastic deposits, and as rhyolite domes and/or flows. The volcanic clasts examined can be subdivided into two groups. One group correlates with the intrusive clasts examined. The other group displays features indicative of A-type magmatism and an alkaline chemistry. The lack of coherent trends indicates that Mount Saul clasts do not represent a single cogenetic suite. The A-type volcanic clasts retain a subduction related signature, probably inherited from their source, and could indicate a progression toward anorogenic intrusion during the waning stages of subduction, or a change to an extensional regime at some stage prior to conglomerate deposition during the Early Cretaceous.

- The Lake Hill igneous clasts display calc-alkaline to tholeiitic characteristics. The granitoid clasts are silica-rich leucotonalites, granodiorites to and leucomonzogranites. Granitoids can be subdivided into a low K group of S-type intrusives that are subsolvus granodiorites generally displaying a pervasive post-intrusive deformation, and a high K group that are weakly peraluminous I-type hypersolvus granodiorites and leucomonzogranites, and correlate with the volcanic rhyolite and dacite clasts also present. Volcanic clasts are not prevalent within the Lake Hill conglomerate and exhibit no evidence of pyroclastic or ignimbritic activity. The peraluminous primitive S-types indicate a heterogeneous source and are thought to have intruded into oceanic sediments of a thickened accretionary prism during the final stages of subduction along an active continental margin.

- The Chatham Islands conglomerate clasts compare mineralogically and geochemically with clasts from the three Torlesse conglomerates. Chatham Islands clasts have generally higher K_2O values with a corresponding higher proportion of syenogranites.

- The two Pahau subterrane conglomerates display features that indicate predominantly I-type volcano-plutonic provinces. However, lithologies of similar appearance need not necessarily be derived from a single pluton. The Ethelton clasts do not record the A-type magmatism displayed by some of the Mount Saul volcanic clasts.

- The Rakaia subterrane Lake Hill conglomerate preserves record of an

extensive S-type granitic province not represented in the clasts examined from the two Pahau subterrane conglomerates. Chemical differences suggest Torlesse detrital sediment, although continentally derived, was from different sources for each subterrane.

- The clasts from all four conglomerates display a trace element chemistry indicative of subduction related magmatism. The absence of associated mafic intrusives and the silica rich character of the majority of clasts indicates oceanic island arc magmatism was not involved near the site for conglomerate(s) deposition.

- The granitoid clasts from each conglomerate contained examples representative of subvolcanic emplacement which probably accompanied cogenetic volcanic activity.

- The overall predominant lithologies are geochemically identified I-type and evolved I-type granitoids.

- The intrusive and extrusive lithologies examined exhibit geochemistries that reflect the different source rocks from which they were derived.

- The predominance of pyroclastics and ignimbrites as opposed to rhyolitic magmas and/or domes varies between conglomerates.

7.2 Conclusions

The main conclusions derived from this research are:

- Clasts from the three Torlesse conglomerates indicate subduction related magmas were intruded into an active continental margin, and that the Torlesse sediments were deposited as a submarine fan complex oceanward of this. The exact location of this margin is unknown, but could be a part of the Mesozoic Gondwana margin prior to crustal separation.

- The continental margin at the time of intrusion and conglomerate preservation was of full crustal thickness as indicated by the presence of S-type intrusives in all three areas.

- The catchment area(s) in the vicinity of the conglomerates examined at the time of deposition comprised volcano-plutonic provinces of predominantly calc-alkaline igneous rocks that exposed a range of intrusive levels.

- The presence of A-type volcanic and intrusive clasts in the Mount Saul and Chatham Islands conglomerate indicates the final stages of subduction are preserved in these two conglomerates and that an extensional regime may have been initiated prior to conglomerate deposition (~120-100Ma).

- The predominance of S-type intrusives of primitive character within the Lake Hill conglomerate indicates a thickening of the accretionary wedge and the

waning stages of subduction.

- The differences discerned provide evidence that the Torlesse detritus has undergone homogenization, but can be considered as having been derived from continental crust of a diverse and varied nature.

- Many provinces exist with mineralogical and geochemical similarities to the clasts examined. Isotope analysis and rare earth element data would further add to the knowledge gained and allow more realistic correlations to be made.

- The conglomerates sampled must be the subject of detailed study in their entirety before a composite picture of provenance can be discerned.

- The source for the Chatham Islands may in part be derived from the Bounty Islands granitoids, but contains clasts that exhibit features too diverse to have come exclusively from this plutonic body.

- There is a possibility that the source for the Torlesse detritus has been erroded completely and the only evidence remaining is the clasts preserved within the conglomerates.

REFERENCES

Adams, C.J.D., Bishop, D.G., and Gabites, J.E., 1985, Potassium-argon age studies of a low-grade progressively metamorphosed greywacke sequence, Dansey Pass, South Island, New Zealand. **Journal of the Geological Society of London, Vol.142, pp.339-349.**

Adams, C.J.D., and Robinson, P., 1977, Potassium-Argon Ages of Schists from Chatham Island, New Zealand Plateau, Southwest Pacific. **New Zealand Journal of Geology and Geophysics, Vol.20, No.2, pp.287-301.**

Andrews, P.B., 1974, Deltaic Sediments, Upper Triassic Torlesse Supergroup, Broken River, North Canterbury. **New Zealand Journal of Geology and Geophysics, Vol.17, No.4, pp.881-905.**

Andrews. P.B., Campbell, H.J., and Watters W.A., 1978, The Forty Fours: the most easterly outcrop of Mesozoic basement in the New Zealand region. **N.Z. Journal of Geology and Geophysics, Vol.21, No.5, pp.649-652.**

Andrews, P.B., Speden, I.G., and Bradshaw, J.D., 1976, Lithological and paleontological content of the Carboniferous - Jurassic Canterbury Suite, South Island, New Zealand. **N.Z. Journal of Geology and Geophysics, Vol.19, No.6, pp.791-819.**

Ashcroft, J., 1986, The Kerikeri Volcanics: A Basalt-Pantellerite Association in Northland. **The Royal Society of New Zealand, Bulletin 23, pp.48-63.**

Barley, M.E., 1987, Origin and evolution of mid Cretaceous garnet bearing intermediate and silicic volcanics from Canterbury, New Zealand. **Journal of Volcanology and Geothermal Research, Vol.32, pp.247-268.**

Bhatia, M.R. and Taylor, S.R., 1981, Trace-Element Geochemistry and Sedimentary Provinces: A study from the Tasman Geosyncline, Australia. **Chemical Geology, Vol.33, pp.115-125.**

Bishop, D.G., Bradshaw,J.D., and Landis,C.A., 1985, Provisional Terrane Map of South Island, New Zealand. In Howell, D.G., ed, **Tectonostratigraphic Terranes of the Circum-Pacific Region.** Circum-Pacific Council for Energy and Mineral Resources Earth Science Series 1. Houston, USA.

Blake, Jr, M.C., Jones, D.L., and Landis, C.A., 1974, Active Continental Margins: Contrasts Between California and New Zealand. In Burk, C.A., and Drake, C.L., eds, **The Geology of Continental Margins.** Springer-Verlag, New York, USA, pp.853-872.

Borg, S.G., Stump, E., Chappell, B.W., McCulloch, M.T., Wyborn, D., Armstrong, R.L., and Holloway, J.R., 1987, Granitoids of Northern Victoria Land, Antarctica: Implications of Chemical and Isotopic Variations to Regional Crustal Structure and Tectonics. **American Journal of Science, Vol.287, pp.127-169.**

Bradshaw, J.D., 1971, Stratigraphy and structure of the Torlesse Supergroup (Triassic - Jurassic) in the foothills of the Southern Alps near Hawarden (S60-61), Canterbury. **N.Z. Journal of Geology and Geophysics, Vol.15, No.1, pp.71-87.**

Bradshaw, J.D., 1973, Allochthonous Mesozoic Fossil Localities in Mélange Within the Torlesse Rocks of North Canterbury. **Journal of the Royal Society of New Zealand, Vol.3, No.2, pp.161-167.**

Bradshaw, J.D., 1989, Cretaceous Geotectonic Patterns in the New Zealand Region. **Tectonics, Vol.8, No.4, pp.803-820.**

Bradshaw, J.D., 1993, A review of the Median Tectonic Zone: terrane boundaries and terrane amalgamation near the Median Tectonic Line. **New Zealand Journal of Geology and Geophysics, Vol.36, No.1, pp.117-125.**

Bradshaw, J.D., submitted, Brook Street and Murihiku Terranes of New Zealand in the context of a mobile South Pacific Gondwana Margin. **Journal of South American Earth Sciences.**

Bradshaw, J.D., Adams, C.J., and Andrews, P.B., 1981, Carboniferous to Cretaceous on the Pacific margin of Gondwana: The Rangitata Phase of New Zealand. **In** Cresswell, M.M. and Vella, P., eds, 1981, **Gondwana Five, Proceedings of the Fifth International Gondwana Symposium, Wellington, New Zealand.** A.A. Balkema, The Netherlands, pp.217-221.

Bradshaw, J.D., and Andrews, P.B., 1980, Torlesse Terrane excursion. **In** Weaver,S.D. and Lewis,D.W., eds, **N.Z. Geological Society Conference, Christchurch 1980, Field Excursions Guide Book, pp.C1-C12.**

Brown, G.C., 1982, Calc-alkaline intrusive rocks: their diversity, evolution, and relation to volcanic arcs. **In** Thorpe, R.S., ed, 1982, **Andesites.** John Wiley and Sons, Great Britain.

Campbell, H.J., Andrews, P.B., Beu, A.G., Edwards, A.R., Hornibrook, N.deB., Laird, M.G., Maxwell, P.A., Mildenhall, D.C., and Walters, W.A., in press, Cretaceous - Cenozoic geology of the Chatham Islands. **New Zealand Geological Survey bulletin.**

Campbell, H.J., Andrews, P.B., Beu, A.G., Edwards, A.R., Hornibrook, N.deB., Laird, M.G., Maxwell, P.A., and Walters, W.A., 1988, Cretaceous - Cenozoic lithostratigraphy of the Chatham Islands. **Journal of the Royal Society of New Zealand, Vol.18, No.3, pp.285-308.**

Carter, R,M., Hicks, M.D., Norris, R.J., and Turnbull, I.M., 1978, Sedimentation patterns in an ancient arc-trench-ocean basin complex: Carboniferous to Jurassic Rangitata Orogen, New Zealand. **In** Stanley, D.J., and Kelling, G., eds, **Sedimentation in submarine canyons, fans and trenches.** Stroudsburg, Pennsylvania, Dowden, Hutchinson, and Ross, pp.340-361.

Cawood, P.A., 1982, Structural Relations in the Subduction Complex of the Paleozoic New England Fold Belt, Eastern Australia. **Journal of Geology, Vol.90, pp.381-392.**

Chappell, B.W. and White, A.J.R., 1992, I- and S-type granites in the Lachlan Fold Belt. **Transactions of the Royal Society of Edinburgh: Earth Sciences, Vol.83, Parts 1 and 2, pp.1-26.**

Cole, J.W., 1979, Structure, petrology, and genesis of Cenozoic volcanism, Taupo Volcanic Zone, New Zealand - a review. **New Zealand Journal of Geology and Geophysics, Vol.22, No.6, pp.631-657.**

Collins, W.J., Beams, S.D., White, A.J.R., and Chappell, B.W., 1982, Nature and Origin of A-type Granites with Particular Reference to Southeastern Australia. **Contributions to Mineralogy and Petrology, Vol.80, pp.189-200.**

Collins, W.J., 1991, A reassessment of the 'Hunter-Bowen Orogeny': Tectonic implications for the southern New England Fold Belt. **Australian Journal of Earth Sciences, Vol.38, pp.409-423.**

Coombs, D.S., Ellis, A.J., Fyfe, W.S., and Taylor, A.M., 1959, The Zeolite Facies, with comments on the interpretation of hydrothermal syntheses. **Geochimica et Cosmochimica Acta, Vol.17, pp.53-107.**

Coombs, D.S., Landis, C.A., Norris, R.J., Sinton, J.M., Borns, D.J. and Craw, D., 1976, The Dun Mountain Ophiolite Belt, New Zealand, Its Tectonic Setting, Constitution, and Origin, with Special Reference to the Southern Portion. **American Journal of Science, Vol.276, pp.561-603.**

Cooper, R.A., 1989, Early Paleozoic terranes of New Zealand. **Journal of the Royal Society of New Zealand, Vol.19, pp.73-112.**

Cooper, R.A., Landis, C.A., LeMasurier, W.E. and Speden, I.G., 1982, Geologic History and Regional Patterns in New Zealand and West Antarctica - their Paleotectonic and Paleogeographic Significance. **In** Craddock, C., ed, 1982, **Antarctic Geoscience.** International Union of Geological Sciences, Series B, No.4, pp.43-53.

Cooper, R.A., and Tulloch, A.J., 1992, Early Palaeozoic terranes in New Zealand and their relationship to the Lachlan Fold Belt. **Tectonophysics, Vol.214, pp.129-144.**

Cox, K.G., Bell, J.D., and Pankhurst, R.J., 1979, **The Interpretation of Igneous Rocks.** Allen and Unwin Ltd, London, England.

Cox, S., 1991, Caples/Aspiring terrane boundary - the translation surface of an early nappe structure in the Otago Schist. **New Zealand Journal of Geology and Geophysics, Vol.34, pp.73-82.**

Creaser, R.A., Price, R.C., and Wormald, R.J., 1991, A-type granites revisited: Assessment of a residual-source model. **Geology, Vol.19, pp.163-166.**

Deer, W.A., Howie, R.A., and Zussman, J., 1966, **An Introduction to the Rock Forming Minerals.** Longman Scientific and Technical, Longman Group U.K.Ltd., England.

Dickinson, W.R., 1974, Plate Tectonics and Sedimentation. **In** Dickinson, W.R., ed, 1974, **Tectonics and Sedimentation. Society of Economic Paleontologists and Mineralogists, Special Publication, No.22, pp.1-27.**

Dickinson, W.R., 1982, Compositions of Sandstones in Circum-Pacific Subduction Complexes and Fore-Arc Basins. **The American Association of Petroleum Geologists Bulletin, Vol.66, No.2, pp.121-137.**

Donaldson, C.H., and Henderson, C.M.B., 1988, A new interpretation of round embayments in quartz crystals. **Mineralogical Magazine, Vol.52, pp.27-33.**

Eby, G.N., 1990, The A-type granitoids: A review of their occurrence and chemical characteristics and speculations on their petrogenesis. **Lithos, Vol.26, pp.115-134.**

Eby, G.N., 1992, Chemical subdivision of the A-type granitoids: Petrogenetic and tectonic implications. **Geology, Vol.20, pp.641-644.**

El Bouseily, A.M., and El Sokkary, A.A., 1975, The relation between Rb, Ba, and Sr in granitic rocks. **Chemical Geology, Vol.16, pp.207-219.**

Fleming, C.A., 1970, The Mesozoic of New Zealand: Chapters in the history of the Circum-Pacific Mobile Belt. **Quarterly Journal of the Geological Society London, Vol.125, pp.125-170.**

Freund, R., 1971, The Hope Fault. **New Zealand Geological Survey, Bulletin No.86.**

Frost, C.D., and Coombs, D.S., 1989, Nd isotope character of New Zealand sediment: implications for terrane concepts and crustal development. **American Journal of Science, Vol.289, pp.744-770.**

Fyfe H.E., 1931, Amuri Subdivision. **New Zealand Geological Survey, No.29, pp.5-6.**

Fyfe, H.E., and Healy, J., 1935, Amuri Subdivision. **New Zealand Geological Survey Annual Report, No.25, pp.4-5.**

Graham, I.J., and Korsch, R.J., 1990, Age and provenance of granitoid clasts in Moeatoa Conglomerate, Kawhia Syncline, New Zealand. **Journal of the Royal Society of New Zealand, Vol.20, No1, pp.25-39.**

Gregg, D.R., 1964, Sheet 18, Hurunui (1st edition), "Geological Map of New Zealand", 1:250,000. **Department of Scientific and Industrial Research, Wellington, N.Z..**

Grindley, G.W., Adams, C.J.D., Lumb, J.T., and Watters, 1977, Paleomagnetism, K-Ar dating and Tectonic Interpretation of Upper Cretaceous and Cenozoic Volcanic Rocks of the Chatham Islands, New Zealand. **N.Z. Journal of Geology and Geophysics, Vol.20, No.3, pp.425-467.**

Grindley, G.W., Oliver, P.J., and Sukroo, J.C., 1981, Lower Mesozoic position of southern New Zealand determined from paleomagnetism of the Glenham Porphyry, Murihiku terrane, eastern Southland. **In** Creswell, M.M. and Vella, P., eds, **Gondwana Five, pp.319-326.** Balkema, Rotterdam.

Haast, J. von, 1871, On the Geology of the Amuri District, in the Provinces of Nelson and Marlborough. **Reports of Geological Exploration for 1870-71, pp.25-46.**

Haast, J. von, 1872, Report on the Geology of the Malvern Hills, Canterbury. **Reports of Geological Exploration for 1871-1872, pp.1-88.**

Haast, J. von, 1879, **Geology of Canterbury and Westland.** Christchurch.

Halpern, M., 1972, Rb-Sr total-rock and mineral ages from Marguerite Bay area Kohler Range and Fosdick Mountains. In Adie, R.J., ed, **Antarctic Geology and Geophysics.** Universitetsforlaget, Oslo, pp.197-204.

Hamilton, D., 1950, The Geology of the Waikari Valley and its Northern Ridges, North Canterbury, New Zealand. Unpublished MSc thesis held at the University of Canterbury Library, Christchurch.

Harris, N.B.W., Pearce, J.A., and Tindle, A.G., 1986, Geochemical characteristics of collision-zone magmatism. In Coward, M.P. and Ries, A.C., eds, 1986, **Collision Tectonics, Geological Society Special Publication No.19, pp.67-81.**

Harvey, P.K., Taylor, D.M., Hendry, R.D. and Bancroft, F., 1973, An accurate fusion method for the analysis of rocks and chemically related materials by X-ray Fluoresence spectrometry. **X-Ray Spectrometry, Vol.2, pp.33-44.**

Haston, R.B., Luyendyk, B.P., Landis, C.A., and Coombs, D.S., 1989, Paleomagnetism and the question of the original location of the Permian Brook Street terrane, New Zealand. **Tectonics, Vol.8, pp.791-801.**

Hay, R.F., Mutch, A.R., and Watters, W.A., 1970, Geology of the Chatham Islands. **N.Z. Geological Survey Bulletin 83.**

Hector, J., 1871, On the Geological Structure of the Malvern Hills District, Canterbury. **Reports of Geological Exploration for 1870-1871, pp.46-55.**

Hensel, H.D., McCulloch, M.T., and Chappell, B.W., 1985, The New England Batholith: constraints on its derivation from Nd and Sr isotopic studies of granitoids and country rocks. **Geochimica et Cosmochimica Acta, Vol.49, pp.369-384.**

Herzer, R.H., and Wood, R.A., 1988, The Geology and Structure of Mernoo Bank and Surrounding Area, Western Chatham Rise. **N.Z. Geological Survey Record 29, D.S.I.R., New Zealand.**

Herzer, R.H., and Wood, R.A., 1992, Tectonic History, Sedimentation, and Changes in Relative Sea Level, Chatham Rise, New Zealand. **In** Watkins, J.S., Zhiqiang, F., and McMillen,K.J., 1992, **Geology and Geophysics of Continental Margins.** The American Association of Petroleum Geologists Memoir 53, pp.55-73.

Houghton, B.F., Weaver, S.D., Wilson, C.J.N., and Lanphere, 1992, Evolution of a Quaternary peralkaline volcano: Mayor Island, New Zealand. **Journal of Volcanology and Geothermal Research, Vol.51, pp.217-236.**

Howell, D.G., 1980, Mesozoic accretion of exotic terranes along the New Zealand segment of Gondwanaland. **Geology, Vol.8, pp.487-491.**

Howell, D.G., 1981, Submarine fan facies in the Torlesse terrane, New Zealand. **Journal of the Royal Society of New Zealand, Vol.11, No.2, pp.113-122.**

Ireland, T.R., 1992, Crustal evolution of New Zealand: Evidence from age distributions of detrital zircons in Western Province paragneisses and Torlesse greywacke. **Geochimica et Cosmochimica Acta, Vol.56, pp.911-920.**

Irvine, T.N., and Baragar, W.R.A., 1971, A guide to the chemical classification of the common volcanic rocks. **Canadian Journal of Earth Sciences, Vol.8, pp.523-548.**

Kamp, P.J.J., 1980, Pacifica and New Zealand: proposed eastern elements in Gondwanaland's history. **Nature, Vol.288, pp.659-664.**

Korsch, R.J., and Wellman, H.W., 1988, The Geological Evolution of New Zealand and the New Zealand Region. **In** Nairn, A.E.M., Stehli, F.G., and Uyeda, S., eds, **The Ocean Basins and Margins, Vol.7B: The Pacific Ocean.** Plenum Press, New York, USA.

Kuno, H., 1968, Differentiation of Basalt Magmas. **In** Hess, H.H., and Poldervaart, A., eds, **Basalts, Volume 2.** Interscience Publishers, John Wiley and Sons, New York, USA.

Laird, M.G., 1981, The Late Mesozoic fragmentation of the New Zealand segment of Gondwana. **In** Cresswell, M.M. and Vella, P., eds, 1981, **Gondwana Five, Proceedings of the Fifth International Gondwana Symposium, Wellington, New Zealand.** A.A. Balkema, Rotterdam, pp.311-318.

Laird, M.G., in press, Geological aspects of the opening of the Tasman Sea. **In** van der Lingen, Swanson, K.M., and Muir, R.J., eds, **Evolution of the Tasman Sea Basin.** A.A.Balkema, Rotterdam.

Landis, C.A. and Bishop, D.G., 1972, Plate Tectonics and Regional Stratigraphic-Metamorphic Relations in the Southern Part of the New Zealand Geosyncline. **Geological Society of America Bulletin, Vol.83, pp.2267-2284.**

Lameyre, J., and Bowden, P., 1982, Plutonic rock types series: discrimination of various granitoid series and related rocks. **Journal of Volcanology and Geothermal Research, Vol.14, pp.169-186.**

Landis, C.A. and Coombs, D.S., 1967, Metamorphic Belts and Orogenesis in Southern New Zealand. **Tectonophysics, Vol.4, pp.501-518.**

Lauder, W.R., 1962, Teschenites from Acheron River, Mid-Canterbury, New Zealand, with Notes on the Geology of the Surrounding Country. **Transactions of the Royal Society of New Zealand (Geology), Vol.1, No7., pp.109-127.**

Le Maitre, R.W., ed, 1989, **A Classification of Igneous Rocks and Glossary of Terms: Recommendations of the International Union of Geological Sciences Subcommision of the Systematics of Igneous Rocks.** Blackwell Scientific Publications, Great Britain.

Lewis, D.W., 1984, **Practical Sedimentology.** Hutchinson Ross Publishing Company, New York, USA.

Lopatin, B.G., and Orlenko, E.M., 1972, Outline of the geology of Marie Byrd Land and the Eights Coast. **In** Adie, R.J., ed, **Antarctic Geology and Geophysics.** Universitetsforlaget, Oslo, pp.245-50.

MacKinnon, T.C., 1983, Origin of the Torlesse terrane and coeval rocks, South Island, New Zealand. **Geological Society of America Bulletin, Vol.94, pp.967-985.**

Mainprice, D., Bouchez, J., Blumenfeld, P., and Tubiá, J.M., 1986, Dominant *c* slip in naturally deformed quartz: Implications for dramatic plastic softening at high temperatures. **Geology, Vol.14, pp.819-822.**

Maniar, P.D., and Piccoli, P.M., 1989, Tectonic discrimination of granitoids. **Geological Society of America Bulletin, Vol.101, pp.635-643.**

Maxwell, P.A., 1964, Structural geology and pre-Quaternary stratigraphy of the Kaiwara District, North Canterbury, New Zealand. Unpublished MSc thesis, University of Canterbury, New Zealand.

Mayes, C.L., Lawyer, L.A., and Sandwell, D.T., 1990, Tectonic History and New Isochron Chart of the South Pacific. **Journal of Geophysical Research, Vol.95, No.B6, pp.8543-8569.**

McKay, A., 1885, On the Geology of the East part of Marlborough Province. **Reports of Geological Exploration, No.17, pp.27-136.**

McKellar, I.C, Mutch, A.R., and Stevens, G.R., 1962, An Upper Jurassic Outlier in the Pyke Valley, Northwest Otago, and a note on Upper Jurassic Belemnites in the South Island. **New Zealand Journal of Geology and Geophysics, Vol.5, No.3, pp.487-492.**

Mildenhall, D.C., 1977, Cretaceous palynomorphs from the Waihere Bay Group and Kahuitara Tuff, Chatham Islands, New Zealand. **New Zealand Journal of Geology and Geophysics, Vol.20, No.4, pp.655-672.**

Mortimer, N., 1993, Jurassic tectonic history of the Otago Schist, New Zealand. **Tectonics, Vol.12, pp.237-244.**

Mortimer, N. and Roser, B.P., 1992, Geochemical evidence for the position of the Caples - Torlesse boundary in the Otago Schist, New Zealand. **Journal of the Geological Society of London, Vol.149, pp.967-977.**

Muir, R.J., Bradshaw, J.D., and Weaver, S.D., in press, Crustal extension prior to the opening of the Tasman Sea Basin: evidence from New Zealand granites. In van der Lingen, G.J., Swanson, K.M., and Muir, R.J., eds, **Evolution of the Tasman Sea Basin**. A.A. Balkema, Rotterdam.

Murray, C.G., Fergusson, C.L., Flood, P.G., Whitaker, W.G., and Korsch, R.J., 1987, Plate tectonic model for the Carboniferous evolution of the New England Fold Belt. **Australian Journal of Earth Sciences, Vol.34, pp.213-236.**

New Zealand Geological Survey, 1972, "Geological Map of New Zealand", South Island (1st edition), 1:1,000,000. **Department of Scientific and Industrial Research, Wellington, New Zealand.**

New Zealand Lands and Survey, 1981, Chatham Islands, Sheet 2, 1:50,000, NZMS260. **Department of Lands and Survey, Wellington, New Zealand.**

Norris, R,N., 1964, Sediments of the Chatham Rise. **N.Z. Oceanographic Memoir, No.26, N.Z.D.S.I.R., Bulletin No.159.**

Norrish, K., and Hutton, J.T., 1969, An accurate X-ray spectrographic method for the analysis of a wide range of geologic samples. **Geochimica et Cosmochimica Acta, Vol.33, pp.431-453.**

Peacock, M.A., 1931, Classification of igneous rock series. **Journal of Geology, Vol.39, pp.54-67.**

Pearce, J.A., Harris, N.B.W., and Tindle, A.G., 1984, Trace Element Discrimination Diagrams for the Tectonic Interpretation of Granitic Rocks. **Journal of Petrology, Vol.25, No.4, pp.956-983.**

Roberts, J., and Engel, B.A., 1987, Depositional and tectonic history of the southern New England Orogen. **Australian Journal of Earth Sciences, Vol.34, pp.1-20.**

Roser, B.P. and Cooper, A.F., 1990, Geochemistry and terrane affiliation of Haast Schist from the western Southern Alps, New Zealand. **New Zealand Journal of Geology and Geophysics, Vol.33, pp.1-10.**

Roser, B.P. and Korsch, R.J., 1986, Determination of Tectonic Setting of Sandstone-Mudstone Suites using SiO_2 Content and K_2O/Na_2O Ratio. **The Journal of Geology, Vol.94, No.5, pp.635-650.**

Roser, B.P. and Korsch, R.J., 1988, Provenance signatures of sandstone-mudstone suites determined using discriminant function analysis of major-element data. **Chemical Geology, Vol.67, pp.119-139.**

Saunders, A.D., Norry, M.J., and Tarney, J., 1991, Fluid influence on the trace element compositions of subduction zone magmas. **Philosophical transactions of the Royal Society of London, Vol.335, pp.377-392.**

Schroeder, B., Thompson, G., Sulanowska, M., and Ludden, J.N., 1980, Analysis of geologic materials using an automated X-ray fluorescence system. **X-ray Spectrometry, Vol.9, pp.198-205.**

Shaw, S.E., and Flood, R.H., 1981, The New England Batholith, Eastern Australia: Geochemical Variations in Time and Space. **Journal of Geophysical Research, Vol.86, No.B11, pp.10530-10544.**

Shelley, D., 1985, **Optical Mineralogy**. Elsevier Science Publishing Co. Inc., New York, USA.

Shelley, D., 1992, **Igneous and Metamorphic Rocks under the Microscope.** Chapman and Hall, London, England.

Silberling, N.J., Nichols, K.M., Bradshaw, J.D., and Blome, C.D., 1988, Limestone and chert in tectonic blocks from the Esk Head subterrane, South Island, New Zealand. **Geological Society of America Bulletin, Vol.100, pp.1213-1223.**

Simpson, C., and Wintsch, R.P., 1989, Evidence for deformation induced K-feldspar replacement by myrmekite. **Journal of Metamorphic Geology, Vol.7, No.2, pp.261-275.**

Smale, D., 1978, The composition of a Torlesse conglomerate - Ethelton, North Canterbury. **N.Z. Journal of Geology and Geophysics, Vol.21, No.6, pp.699-711.**

Speight, R., 1914, The Intermontane Basins of Canterbury. **Transactions and Proceedings of the New Zealand Institute, Vol.47, pp.336-353.**

Speight, R., 1928, The Geology of the Malvern Hills. **New Zealand Department of Scientific and Industrial Reasearch, Geological Memoir No.1.**

Speight, R. and Finlayson, A.M., 1909, Physiography and Geology of the Auckland, Bounty, and Antipodes Islands. **In** Chilton, C., ed, **The Subantarctic Islands of New Zealand.** Philosophical Institute of Canterbury, Vol.2, pp.705-744.

Spörli, K.B., 1978, Mesozoic Tectonics, North Island, New Zealand. **Geological Society of America Bulletin, Vol.89, pp.415-425.**

Spörli, K.B. and Bell, A.B., 1976, Torlesse Mélange and Coherent Sequences, Eastern Ruahine Range, North Island, New Zealand. **New Zealand Journal of Geology and Geophysics, Vol.19, No.4, pp.427-447.**

Storey, B.C. and Garrett, S.W., 1985, Crustal growth of the Antarctica Peninsula by accretion, magmatism and extension. **Geological Magazine, Vol.122, No.1, pp.5-14.**

Suggate, R.P., Stevens, G.R., and Te Punga, M.T., 1978, **The Geology of New Zealand.** Government Printer, Wellington, 2 vols, 820p.

Sun, S., and McDonough, W.F., 1989, Chemical and isotopic systematics of oceanic basalts: implications for mantle composition and processes. **In** Saunders, A.D., and Norry, M.J., eds, 1989, **Magmatism in the Ocean Basins. Geological Society Special Publication, No.42, pp.313-345.**

Tulloch, A.J., 1983, Granitoid Rocks of New Zealand - A brief review. **Geological Society of America, Memoir 159, pp.5-20.**

Tulloch, A.J., 1988, Batholiths, plutons, and suites: nomenclature for granitoid rocks of Westland - Nelson, New Zealand. **Journal of Geology and Geophysics, Vol.31, pp.505-509.**

Tulloch, A.J., 1992, Petrology of the Sams Creek peralkaline granite dike, Takaka, New Zealand. **New Zealand Journal of Geology and Geophysics, Vol.35, pp.193-200.**

Tulloch, A.J. and Kimbrough, D.L., 1989, The Paparoa Metamorphic Core Complex, New Zealand: Cretaceous Extension Associated with Fragmentation of the Pacific Margin of Gondwana. **Tectonics, Vol.8, No.6, pp.1217-1234.**

Tulloch, A.J., Kimbrough, D.L., and Waight, T.E., in press, The French Creek Granite, North Westland, New Zealand - Late Cretaceous A-type plutonism on the Tasman Passive Margin. **In** van der Lingen, G.J., Swanson, K.M., and Muir, R.J., eds, **Evolution of the Tasman Sea Basin.** A.A. Balkema, Rotterdam.

Van Der Plas, L., and Tobi, A.C., 1965, A Chart for Judging the Reliability of Point Counting Results. **American Journal of Science, Vol.263, pp.87-90.**

Wade, F.A., and Wilbanks, J.R., 1972, Geology of Marie Byrd and Ellsworth Lands. **In** Adie, R.J., ed, **Antarctic Geology and Geophysics.** Universitetsforlaget, Oslo, pp.207-214.

Weaver, S.D., Adams, C.J., Pankhurst, R.J., and Gibson, I.L., 1992, Granites of Edward VII Peninsula, Marie Byrd Land: anorogenic magmatism related to Antarctic-New Zealand rifting. **Transactions of the Royal Society of Edinburgh: Earth Sciences, Vol.83, pp.281-290.**

Weaver, S.D., Bradshaw, J.D. and Adams, C.J.,1991, Granitoids of the Ford Ranges, Marie Byrd Land, Antarctica. **In** Thomson, M.R.A., Crame, J.A. and Thomson, J.W., eds, 1991, **Geological Evolution of Antarctica.** Cambridge University Press, England.

Weaver, S.D., Gibson, I.L., Houghton, B.F., and Wilson, C.J.N., 1990, Mobility of rare earth and other elements during crystallization of peralkaline silicic lavas. **Journal of Volcanology and Geothermal Research, Vol.43, pp.57-70.**

Whalen, J.B., Kenneth, L.C., and Chappell, B.W., 1987, A-type granites: geochemical characteristics, discrimination and petrogenesis. **Contributions to Mineralogy and Petrology, Vol.95, pp.407-419.**

White, A.J.R., and Chappell, B.W., 1983, Granitoid Types and their distribution in the Lachlan Fold Belt, southeastern Australia. **Geological Society of America, Memoir 159, pp.21-34.**

Wilson, M., 1989, **Igneous Petrogenesis.** Unwin Hyman Ltd, London, United Kingdom.

Wood, B.L., 1969, Geology of Tuatapere Subdivision, Western Southland. **New Zealand Geological Survey Bulletin, No.79.**

Wood, B.L, 1978, The Otago Schist Megaculmination: Its Possible Origins and Tectonic Significance in the Rangitata Orogen of New Zealand. **Tectonophysics, Vol.47, pp.339-368.**

Wood, R.A., and Anderson, H.J., 1989, Basement structure at the Chatham Islands. **Journal of the Royal Society of New Zealand, Vol.19, No.3, pp.269-282.**

Wood, R.A., Andrews, P.B., and Herzer, R.H., 1989, Cretaceous and Cenozoic Geology of the Chatham Rise Region, South Island, New Zealand. **N.Z. Geological Survey Basin Studies 3, N.Z. Geological Survey, Lower Hutt, New Zealand.**

Zen, E-An, 1986, Aluminium Enrichment in Silicate Melts by Fractional Crystallization: Some Mineralogic and Petrographic Constraints. **Journal of Petrology, Vol.27, pp.1095-1117.**

ACKNOWLEDGEMENTS

First and foremost I would like to extend thanks to my supervisors. To Dr David Shelley, for not frowning even as I entered the room with ten thin sections at a time. To Dr Steve Weaver and Dr John Bradshaw for first suggesting this topic of research, accompanying me to the Chatham Islands, providing stimulating discussion, and encouragement when I most needed it.

I wish to express gratitude for the monetary assistance provided by the Mason Trust, which allowed me to complete this thesis and continue eating.

My thanks to the people of the Chatham Islands, particularly the hotel management and staff at Waitangi, the Lanauze family, for ferrying us to and from Pitt Island safely (I have a lot more respect for the fishermen who go out in those seas every day), and Karen Preace and family for making us welcome at Flowerpot Bay. Thanks to Mr Dunbar, the manager at Lochiel Station, and the Murchisons at the Homestead, Lake Coleridge for allowing access to outcrops. I would also like to thank Chris Adams of IGNS for company on the Chatham Islands and for supplying the Bounty Islands powders and isochron.

Thankyou to the technicians of the Geology Department. To Rob for making so many thin sections, and showing me how. To Stephen and Catherine for instruction in fusion bead and pellet preparation and for helping me with my computer. To Arthur for teaching me to drive a four wheel machine and for company in the field. To Albert and Kerry for photography assistance.

My friends deserve the most thanks, as without them I wouldn't have coped. I especially want to thank my congenial roommate Tod for all his help and support, and for consistently identifying epidote and allanite without even looking down the microscope. To Sacha for disturbing me at the right (and wrong times) (it didn't take much) and for being the best living scale a person could wish for (you've got a friend back at long last!). To Tony for incentive and for lovely diagrams (maybe I'll get my pens back permanently now). To Nigel for making me his best man, and giving me something else to worry about besides writing this. To Barbara for fitting my samples into her busy microprobe schedule. To Stu for all round personal appearance, and his printer and computer

knowhow and of course Richard for just being there.

Thanks Julie and Ray for encouragement right from the start, and for being so understanding in the past few months (I'll make it up to you).

I would like to thank Rob for providing a diversion just when required, even if I didn't think so at the time. A special thanks to Kell for making me realize that I'm not permanently attached to my computer, and that I'm still alive.

A particular thankyou to Tim for astute timing in leaving home, which cut my work load considerably. Special thanks also to my parents for always believing that I could do it, despite the fact that it took years for me to come to my senses.

Finally I wish to thank God that this is finished, I don't believe I ever thought it would be.

APPENDIX 1 WHOLE ROCK MAJOR AND TRACE ELEMENT GEOCHEMISTRY

The analyses for each geographic locality are presented separately in order of initial field and laboratory number. Original analyses with totals between 98.5 to 100.5% (inclusive) were considered acceptable for the purpose of this research.

The data used in this thesis is expressed on an anhydrous basis (i.e. LOI (loss on ignition) free). Anhydrous analyses reduce the variation caused by variable losses due to moisture gains and/or sample preparation, rather than variation due to original rock composition.

Ratios used for discrimination diagrams have also been included.

Total iron content is given as Fe_2O_3.

CHATHAM ISLANDS - GRANITOID CLASTS

Sample	23984	23985	23986	23987	23988	23989	23990	23991
SiO_2	74.57	77.31	74.04	75.93	76.31	76.13	76.77	75.93
TiO_2	0.09	0.13	0.08	0.09	0.16	0.10	0.09	0.13
Al_2O_3	14.50	12.57	12.93	13.91	12.53	12.88	12.10	13.41
Fe_2O_3	0.45	1.23	0.50	0.82	1.06	1.00	0.70	0.66
MnO	0.02	0.02	0.01	0.03	0.01	0.01	0.02	0.01
MgO	0.05	0.24	0.05	0.12	0.05	0.05	0.07	0.05
CaO	0.89	1.34	0.66	1.02	0.47	0.86	0.67	0.58
Na_2O	4.40	4.25	3.67	4.15	3.69	4.24	3.92	3.44
K_2O	4.53	2.30	4.74	4.04	4.59	3.66	4.42	5.80
P_2O_5	0.04	0.05	0.04	0.07	0.07	0.03	0.03	0.03
LOI	0.59	0.39	2.63	0.19	0.77	0.54	0.88	0.13
Total	100.13	99.83	99.35	100.37	99.71	99.50	99.67	100.17
V	14	22	14	17	15	14	14	16
Cr	3	5	5	5	3	3	3	5
Ni	7	3	3	3	6	7	3	3
Zn	15	27	18	26	31	22	16	16
Ga	23	19	14	22	21	16	10	19
Rb	118	45	210	117	205	93	258	239
Sr	93	159	149	222	48	94	196	68
Y	10	15	23	13	25	27	21	20
Zr	37	91	70	57	121	155	95	39
Nb	9	8	10	9	10	6	13	8
Ba	426	706	4255	1009	397	1134	5452	1004
La	16	12	7	10	50	31	17	5
Ce	7	23	17	23	107	67	39	10
Nd	20	37	17	30	58	36	16	26
Pb	34	12	27	22	26	18	22	26
Th	2	7	18	7	27	15	39	12
SiO_2	74.91	77.75	76.55	75.79	77.13	76.93	77.71	75.90
TiO_2	0.09	0.13	0.08	0.09	0.16	0.10	0.09	0.13
Al_2O_3	14.57	12.64	13.37	13.89	12.67	13.02	12.25	13.40
Fe_2O_3	0.45	1.24	0.52	0.82	1.07	1.01	0.71	0.66
MnO	0.02	0.02	0.01	0.03	0.01	0.01	0.02	0.01
MgO	0.05	0.24	0.05	0.12	0.05	0.05	0.07	0.05
CaO	0.89	1.35	0.68	1.02	0.48	0.87	0.68	0.58
Na_2O	4.42	4.27	3.79	4.14	3.73	4.28	3.97	3.44
K_2O	4.55	2.31	4.90	4.03	4.64	3.70	4.47	5.80
P_2O_5	0.04	0.05	0.04	0.07	0.07	0.03	0.03	0.03
Total	100.00	100.00	100.00	100.00	100.00	100.00	100.00	100.00
Q	29.74	40.41	34.10	33.74	36.37	35.58	35.90	32.24
or	26.89	13.67	28.96	23.83	27.42	21.86	26.44	34.26
ab	37.40	36.17	32.11	35.05	31.56	36.26	33.58	29.10
an	4.17	6.36	3.12	4.59	1.89	4.11	2.40	2.68
C	0.84	0.78	0.68	1.02	0.82	0.46	0.00	0.49
di	0.00	0.00	0.00	0.00	0.00	0.00	0.66	0.00
hy	0.50	1.74	0.56	1.08	1.02	1.06	0.48	0.63
mt	0.15	0.42	0.18	0.28	0.37	0.35	0.24	0.23
il	0.17	0.25	0.16	0.17	0.31	0.19	0.17	0.25
ap	0.09	0.12	0.10	0.16	0.16	0.07	0.07	0.07

Sample	23992	23993	23994	23995	24085	23996	23997	23998
SiO_2	77.35	77.18	76.24	70.66	75.69	74.16	71.97	77.23
TiO_2	0.07	0.17	0.10	0.17	0.05	0.15	0.17	0.09
Al_2O_3	12.55	13.06	14.70	11.54	12.83	14.51	13.24	12.61
Fe_2O_3	0.75	0.78	0.53	1.24	0.30	0.69	1.05	0.40
MnO	0.01	0.01	0.02	0.01	0.01	0.01	0.03	0.01
MgO	0.05	0.05	0.09	0.11	0.05	0.11	0.23	0.05
CaO	0.57	0.92	0.83	0.74	1.04	1.21	2.17	0.42
Na_2O	3.84	4.05	2.34	3.25	3.24	4.37	2.76	3.93
K_2O	4.45	3.70	3.46	4.02	5.54	3.83	5.29	4.64
P_2O_5	0.04	0.04	0.11	0.02	0.03	0.05	0.24	0.05
LOI	0.69	0.49	1.28	8.08	1.01	0.33	2.08	0.93
Total	100.37	100.45	99.70	99.84	99.79	99.42	99.23	100.36
V	15	12	18	18	17	18	15	15
Cr	6	3	3	8	6	9	3	4
Ni	3	6	6	3	5	3	8	3
Zn	19	25	13	19	43	31	25	22
Ga	18	22	23	18	22	20	9	21
Rb	210	145	102	161	196	138	196	271
Sr	47	72	99	42	150	513	188	47
Y	28	27	14	25	22	11	22	34
Zr	72	133	34	117	71	65	65	110
Nb	8	2	10	11	16	13	8	16
Ba	840	676	302	642	213	1063	3796	477
La	24	26	5	22	13	17	7	28
Ce	44	56	11	53	18	32	23	51
Nd	40	47	17	43	38	38	17	59
Pb	30	11	23	15	31	44	27	20
Th	28	21	5	29	12	10	1	41
SiO_2	77.60	77.21	77.46	77.01	76.62	74.84	74.08	77.67
TiO_2	0.07	0.17	0.10	0.19	0.05	0.15	0.17	0.09
Al_2O_3	12.59	13.07	14.94	12.58	12.99	14.64	13.63	12.68
Fe_2O_3	0.75	0.78	0.54	1.35	0.30	0.70	1.08	0.40
MnO	0.01	0.01	0.02	0.01	0.01	0.01	0.03	0.01
MgO	0.05	0.05	0.09	0.12	0.05	0.11	0.24	0.05
CaO	0.57	0.92	0.84	0.81	1.05	1.22	2.23	0.42
Na_2O	3.85	4.05	2.38	3.54	3.28	4.41	2.84	3.95
K_2O	4.46	3.70	3.52	4.38	5.61	3.87	5.45	4.67
P_2O_5	0.04	0.04	0.11	0.02	0.03	0.05	0.25	0.05
Total	100.00	100.00	100.00	100.00	100.00	100.00	100.00	100.00
Q	36.59	37.28	48.35	37.26	33.90	31.52	32.09	35.85
or	26.38	21.87	20.78	25.89	33.14	22.84	32.18	27.58
ab	32.60	34.28	20.12	29.97	27.75	37.32	24.04	33.45
an	2.57	4.30	3.45	3.86	4.15	5.73	8.35	1.77
C	0.48	0.82	5.95	0.59	0.00	1.11	0.00	0.48
di	0.00	0.00	0.00	0.00	0.74	0.00	0.94	0.00
hy	0.83	0.70	0.67	1.46	0.01	0.79	1.04	0.42
mt	0.26	0.27	0.18	0.46	0.10	0.24	0.37	0.14
il	0.13	0.32	0.19	0.35	0.10	0.29	0.33	0.17
ap	0.09	0.09	0.26	0.05	0.07	0.12	0.57	0.12

Sample	23999	24000	24005	24006	24007	24008	24009	24010
SiO_2	77.35	71.37	75.15	74.31	75.99	74.75	73.09	76.24
TiO_2	0.05	0.32	0.19	0.13	0.30	0.29	0.32	0.09
Al_2O_3	12.96	15.33	13.36	13.35	12.21	12.49	13.84	12.91
Fe_2O_3	0.38	1.66	0.94	1.40	2.72	2.46	1.61	0.77
MnO	0.02	0.02	0.02	0.02	0.05	0.03	0.02	0.02
MgO	0.05	0.43	0.26	0.26	0.24	0.43	0.33	0.05
CaO	1.05	2.33	1.10	1.00	1.11	1.60	1.54	0.17
Na_2O	4.10	4.52	4.33	3.89	4.77	4.24	4.33	4.88
K_2O	3.62	2.59	3.45	4.11	2.03	2.01	3.06	4.23
P_2O_5	0.02	0.12	0.06	0.03	0.06	0.07	0.13	0.02
LOI	0.25	0.81	0.43	0.80	0.69	1.43	0.58	0.37
Total	99.85	99.50	99.29	99.30	100.17	99.80	98.85	99.75
V	17	28	17	20	12	29	32	13
Cr	4	8	5	6	3	6	8	3
Ni	3	3	3	3	11	6	28	7
Zn	22	39	22	41	49	40	52	80
Ga	22	21	18	24	18	18	20	32
Rb	105	74	102	130	35	39	67	401
Sr	167	558	215	102	162	155	239	8
Y	11	11	15	36	42	37	22	46
Zr	44	125	95	142	157	146	162	149
Nb	7	11	12	10	2	5	7	36
Ba	924	1366	913	1326	628	693	765	362
La	11	29	28	7	6	21	26	24
Ce	19	49	48	19	24	45	55	67
Nd	34	43	44	32	25	35	39	42
Pb	26	20	21	20	7	9	12	24
Th	7	12	14	12	8	10	13	53
SiO_2	77.66	72.32	76.02	75.44	76.39	75.99	74.38	76.72
TiO_2	0.05	0.32	0.19	0.13	0.30	0.29	0.33	0.09
Al_2O_3	13.01	15.53	13.51	13.55	12.27	12.70	14.08	12.99
Fe_2O_3	0.38	1.68	0.95	1.42	2.73	2.50	1.64	0.77
MnO	0.02	0.02	0.02	0.02	0.05	0.03	0.02	0.02
MgO	0.05	0.44	0.26	0.26	0.24	0.44	0.34	0.05
CaO	1.05	2.36	1.11	1.02	1.12	1.63	1.57	0.17
Na_2O	4.12	4.58	4.38	3.95	4.79	4.31	4.41	4.91
K_2O	3.63	2.62	3.49	4.17	2.04	2.04	3.11	4.26
P_2O_5	0.02	0.12	0.06	0.03	0.06	0.07	0.13	0.02
Total	100.00	100.00	100.00	100.00	100.00	100.00	100.00	100.00
Q	37.36	29.67	34.24	33.41	36.96	38.14	32.77	31.15
or	21.48	15.51	20.62	24.66	12.06	12.08	18.40	25.15
ab	34.83	38.76	37.06	33.42	40.57	36.47	37.28	41.55
an	5.10	10.92	5.12	4.84	5.14	7.60	6.91	0.72
C	0.44	1.16	0.65	0.77	0.29	0.61	0.93	0.04
hy	0.49	2.38	1.39	1.99	3.12	3.33	2.09	0.84
mt	0.13	0.58	0.33	0.49	0.94	0.86	0.56	0.27
il	0.10	0.62	0.37	0.25	0.57	0.56	0.62	0.17
ap	0.05	0.28	0.14	0.07	0.14	0.16	0.31	0.05

Sample	24011	24012	24013	24014	24015	24016	24017	24018
SiO_2	74.39	68.96	76.68	71.06	77.64	76.08	78.85	77.48
TiO_2	0.28	0.17	0.10	0.23	0.12	0.16	0.15	0.14
Al_2O_3	14.00	13.59	12.69	13.95	12.28	12.61	12.86	12.27
Fe_2O_3	1.66	1.12	0.62	1.69	0.77	0.81	0.96	0.73
MnO	0.07	0.03	0.01	0.04	0.01	0.01	0.01	0.01
MgO	0.27	0.27	0.05	0.33	0.05	0.05	0.05	0.05
CaO	0.72	1.73	0.20	2.63	0.16	0.72	0.75	0.06
Na_2O	4.48	3.93	4.38	3.56	3.83	3.09	6.07	4.59
K_2O	3.66	3.06	4.58	4.84	4.81	5.59	0.71	4.12
P_2O_5	0.06	0.07	0.03	0.17	0.04	0.03	0.03	0.03
LOI	0.73	6.27	0.20	1.64	0.57	0.54	0	0.42
Total	100.32	99.20	99.54	100.14	100.28	99.69	100.44	99.90
V	17	21	10	21	13	10	13	10
Cr	6	5	4	7	6	5	3	5
Ni	3	3	3	3	4	3	8	3
Zn	46	31	26	40	29	27	16	22
Ga	20	19	25	20	23	22	21	28
Rb	140	119	194	128	116	160	24	464
Sr	178	412	19	158	79	120	91	22
Y	13	12	28	19	30	26	22	49
Zr	202	85	239	144	201	217	153	406
Nb	13	9	19	9	20	12	6	34
Ba	979	1057	1011	475	380	1235	581	256
La	41	23	49	16	48	73	37	43
Ce	65	46	97	39	99	154	75	97
Nd	46	40	77	45	70	97	46	76
Pb	18	21	20	19	11	16	9	14
Th	16	7	28	6	19	27	15	44
SiO_2	74.70	74.21	77.19	72.14	77.87	76.73	78.50	77.89
TiO_2	0.28	0.18	0.10	0.23	0.12	0.16	0.15	0.14
Al_2O_3	14.06	14.62	12.77	14.16	12.32	12.72	12.80	12.33
Fe_2O_3	1.67	1.21	0.62	1.72	0.77	0.82	0.96	0.73
MnO	0.07	0.03	0.01	0.04	0.01	0.01	0.01	0.01
MgO	0.27	0.29	0.05	0.34	0.05	0.05	0.05	0.05
CaO	0.72	1.86	0.20	2.67	0.16	0.73	0.75	0.06
Na_2O	4.50	4.23	4.41	3.61	3.84	3.12	6.04	4.61
K_2O	3.68	3.29	4.61	4.91	4.82	5.64	0.71	4.14
P_2O_5	0.06	0.08	0.03	0.17	0.04	0.03	0.03	0.03
Total	100.00	100.00	100.00	100.00	100.00	100.00	100.00	100.00
Q	32.02	32.32	33.24	26.79	36.46	35.20	38.69	34.82
or	21.72	19.46	27.25	29.04	28.51	33.32	4.18	24.48
ab	38.06	35.78	37.31	30.58	32.50	26.37	51.14	39.04
an	3.19	8.74	0.80	7.91	0.53	3.40	3.51	0.10
C	1.51	0.90	0.24	0.00	0.58	0.24	0.81	0.22
di	0.00	0.00	0.00	3.55	0.00	0.00	0.00	0.00
hy	2.12	1.77	0.64	0.56	0.77	0.75	0.92	0.69
mt	0.57	0.41	0.21	0.59	0.26	0.28	0.33	0.25
il	0.53	0.35	0.19	0.44	0.23	0.31	0.28	0.27
ap	0.14	0.17	0.07	0.40	0.09	0.07	0.07	0.07

Sample	24019	24020	24021	24022	24086	24023	24024	24025
SiO_2	77.84	77.31	76.72	76.07	73.32	75.79	74.34	75.95
TiO_2	0.13	0.11	0.08	0.11	0.07	0.16	0.02	0.10
Al_2O_3	12.73	12.58	13.19	13.28	14.86	13.28	15.11	13.21
Fe_2O_3	0.19	0.32	0.12	1.07	0.53	0.54	0.98	1.05
MnO	0.01	0.01	0.01	0.01	0.02	0.01	0.12	0.01
MgO	0.05	0.05	0.05	0.14	0.05	0.05	0.05	0.05
CaO	0.16	0.42	0.68	0.56	0.25	0.45	0.25	0.37
Na_2O	4.16	3.80	4.29	4.20	4.74	4.37	5.93	3.59
K_2O	4.84	4.70	4.24	3.74	4.04	4.51	2.42	4.78
P_2O_5	0.02	0.02	0.02	0.07	0.21	0.05	0.29	0.06
LOI	0.20	0.46	0.32	0.94	0.67	0.41	0.76	0.68
Total	100.33	99.78	99.72	100.19	98.76	99.62	100.27	99.85
V	9	18	15	24	16	13	19	15
Cr	3	3	6	13	6	5	3	3
Ni	6	8	3	5	5	3	10	12
Zn	10	6	10	20	46	14	47	18
Ga	24	22	21	18	20	20	22	18
Rb	235	243	171	63	171	186	185	175
Sr	7	40	135	54	152	47	22	67
Y	21	17	25	20	22	41	9	28
Zr	197	73	51	68	13	237	10	118
Nb	16	12	7	10	65	15	8	13
Ba	123	228	66	466	140	1575	88	799
La	49	20	5	18	5	50	5	46
Ce	95	42	12	29	8	87	5	89
Nd	60	25	35	38	33	59	16	42
Pb	17	16	15	8	29	10	15	14
Th	35	33	24	14	17	25	1	29
SiO_2	77.74	77.84	77.18	76.64	74.75	76.39	74.71	76.59
TiO_2	0.13	0.11	0.08	0.11	0.07	0.16	0.02	0.10
Al_2O_3	12.71	12.67	13.27	13.38	15.15	13.39	15.18	13.32
Fe_2O_3	0.19	0.32	0.12	1.08	0.54	0.54	0.98	1.06
MnO	0.01	0.01	0.01	0.01	0.02	0.01	0.12	0.01
MgO	0.05	0.05	0.05	0.14	0.05	0.05	0.05	0.05
CaO	0.16	0.42	0.68	0.56	0.25	0.45	0.25	0.37
Na_2O	4.15	3.83	4.32	4.23	4.83	4.40	5.96	3.62
K_2O	4.83	4.73	4.27	3.77	4.12	4.55	2.43	4.82
P_2O_5	0.02	0.02	0.02	0.07	0.21	0.05	0.29	0.06
Total	100.00	100.00	100.00	100.00	100.00	100.00	100.00	100.00
q	34.71	36.47	34.26	35.94	30.63	32.32	30.38	35.93
or	28.57	27.97	25.21	22.27	24.34	26.87	14.37	28.49
ab	35.16	32.38	36.52	35.81	40.89	37.27	50.43	30.63
an	0.66	1.97	3.26	2.34	-0.13	1.92	-0.66	1.46
c	0.40	0.53	0.36	1.48	2.79	0.52	2.99	1.62
hy	0.13	0.31	0.14	1.34	0.62	0.46	1.37	1.11
mt	0.06	0.11	0.04	0.37	0.18	0.19	0.34	0.36
il	0.25	0.21	0.15	0.21	0.14	0.31	0.04	0.19
ap	0.05	0.05	0.05	0.16	0.50	0.12	0.68	0.14

Sample	24026	24033
SiO_2	74.74	74.76
TiO_2	0.29	0.14
Al_2O_3	13.85	14.43
Fe_2O_3	0.59	0.72
MnO	0.01	0.04
MgO	0.05	0.09
CaO	0.30	1.18
Na_2O	5.00	4.17
K_2O	3.60	4.18
P_2O_5	0.03	0.06
LOI	0.76	0.42
Total	99.22	100.19
V	12	18
Cr	7	5
Ni	3	3
Zn	18	20
Ga	22	20
Rb	139	157
Sr	238	163
Y	21	21
Zr	278	94
Nb	14	16
Ba	745	788
La	23	14
Ce	54	21
Nd	54	35
Pb	16	26
Th	24	17
SiO_2	75.91	74.93
TiO_2	0.29	0.14
Al_2O_3	14.07	14.46
Fe_2O_3	0.60	0.72
MnO	0.01	0.04
MgO	0.05	0.09
CaO	0.30	1.18
Na_2O	5.08	4.18
K_2O	3.66	4.19
P_2O_5	0.03	0.06
Total	100.00	100.00
Q	31.65	31.81
or	21.61	24.76
ab	42.97	35.37
an	1.31	5.47
C	1.27	1.05
hy	0.30	0.84
mt	0.21	0.25
il	0.56	0.27
ap	0.07	0.14

CHATHAM ISLANDS - VOLCANIC CLASTS

Sample	24001	24002	24003	24004	24027	24028	24029	24030	24031	24032
SiO_2	75.15	72.43	76.03	67.57	76.29	78.93	72.54	74.88	75.54	78.45
TiO_2	0.24	0.24	0.13	0.51	0.16	0.10	0.37	0.15	0.20	0.08
Al_2O_3	12.90	14.25	12.43	16.04	12.72	11.47	15.03	13.34	13.18	11.80
Fe_2O_3	1.53	2.53	0.94	3.57	1.48	1.29	2.35	1.98	2.15	0.39
MnO	0.02	0.05	0.02	0.05	0.01	0.01	0.04	0.03	0.03	0.01
MgO	0.05	0.28	0.05	0.66	0.05	0.05	0.25	0.17	0.30	0.05
CaO	0.49	0.68	0.36	2.06	0.55	0.10	1.52	0.77	0.32	0.10
Na_2O	3.85	4.21	3.44	4.21	3.76	1.29	4.66	4.11	5.22	2.98
K_2O	5.13	4.22	5.36	3.51	4.02	6.09	2.86	4.17	2.62	5.60
P_2O_5	0.06	0.05	0.03	0.16	0.03	0.02	0.08	0.05	0.04	0.02
LOI	0.17	0.43	0.46	0.33	0.42	0.47	0.71	0.58	0.09	0.68
Total	99.59	99.37	99.25	98.67	99.49	99.82	100.41	100.23	99.69	100.16
V	9	19	20	45	12	14	17	17	24	15
Cr	6	4	3	6	6	5	3	6	5	5
Ni	4	3	6	11	3	3	7	3	3	3
Zn	59	46	51	74	31	25	56	26	32	12
Ga	25	23	20	19	20	32	25	21	20	24
Rb	172	181	228	138	218	851	82	160	125	158
Sr	45	128	94	486	56	10	259	174	526	304
Y	72	17	42	21	19	32	29	26	23	20
Zr	378	244	158	206	221	120	299	121	149	132
Nb	27	12	16	4	19	23	9	13	9	13
Ba	355	989	871	793	977	289	952	756	527	604
La	118	40	67	31	57	45	42	34	33	8
Ce	210	73	135	65	110	85	94	57	64	15
Nd	138	55	71	35	91	91	40	46	54	45
Pb	21	10	71	13	49	17	33	25	12	17
Th	34	25	37	26	15	9	17	17	4	19
SiO_2	75.59	73.21	76.96	68.71	77.01	79.45	72.76	75.14	75.84	78.86
TiO_2	0.24	0.24	0.13	0.52	0.16	0.10	0.37	0.15	0.20	0.08
Al_2O_3	12.98	14.40	12.58	16.31	12.84	11.55	15.08	13.39	13.23	11.86
Fe_2O_3	1.54	2.56	0.95	3.63	1.49	1.30	2.36	1.99	2.16	0.39
MnO	0.02	0.05	0.02	0.05	0.01	0.01	0.04	0.03	0.03	0.01
MgO	0.05	0.28	0.05	0.67	0.05	0.05	0.25	0.17	0.30	0.05
CaO	0.49	0.69	0.36	2.09	0.56	0.10	1.52	0.77	0.32	0.10
Na_2O	3.87	4.26	3.48	4.28	3.80	1.30	4.67	4.12	5.24	3.00
K_2O	5.16	4.27	5.43	3.57	4.06	6.13	2.87	4.18	2.63	5.63
P_2O_5	0.06	0.05	0.03	0.16	0.03	0.02	0.08	0.05	0.04	0.02
Total	100.00	100.00	100.00	100.00	100.00	100.00	100.00	100.00	100.00	100.00
Q	31.77	29.27	34.79	23.70	37.61	47.63	30.28	32.49	33.34	39.52
or	30.49	25.21	32.06	21.09	23.98	36.23	16.95	24.73	15.55	33.27
ab	32.77	36.01	29.47	36.23	32.12	10.99	39.55	34.90	44.35	25.35
an	2.05	3.08	1.61	9.33	2.56	0.37	7.04	3.51	1.33	0.37
C	0.27	1.66	0.39	1.99	1.27	2.64	1.70	0.79	1.28	0.71
hy	1.41	3.13	0.96	4.79	1.47	1.36	2.60	2.35	2.78	0.43
mt	0.53	0.87	0.33	1.24	0.51	0.44	0.81	0.68	0.74	0.13
il	0.46	0.46	0.25	0.98	0.31	0.19	0.70	0.29	0.38	0.15
ap	0.14	0.12	0.07	0.38	0.07	0.05	0.19	0.12	0.09	0.05

ETHELTON - GRANITOID CLASTS

Sample	24034	24035	24036	24037	24038	24040	24041	24042
SiO_2	77.32	76.51	69.98	76.10	69.35	71.80	78.15	74.89
TiO_2	0.06	0.19	0.37	0.14	0.44	0.28	0.06	0.14
Al_2O_3	12.49	12.45	15.01	13.13	15.31	13.95	12.13	13.62
Fe_2O_3	0.29	0.71	1.92	0.85	2.51	1.57	0.54	0.86
MnO	0.01	0.02	0.04	0.03	0.05	0.04	0.01	0.02
MgO	0.05	0.05	0.50	0.19	0.81	0.34	0.05	0.27
CaO	0.54	0.82	3.21	0.83	2.64	2.76	0.53	0.82
Na_2O	4.53	4.33	4.80	4.40	4.60	4.52	4.51	2.83
K_2O	4.00	3.68	2.31	3.70	2.97	3.01	3.68	5.49
P_2O_5	0.02	0.03	0.12	0.05	0.13	0.09	0.01	0.06
LOI	0.74	0.96	1.79	0.21	1.15	1.65	0.75	1.03
Total	100.05	99.75	100.05	99.63	99.96	100.01	100.42	100.03
V	10	11	33	12	53	27	11	20
Cr	4	3	6	5	12	6	4	5
Ni	3	4	3	3	5	3	5	4
Zn	25	45	47	43	57	44	55	22
Ga	21	20	20	19	20	21	22	17
Rb	167	139	65	145	109	108	134	115
Sr	21	68	255	94	259	187	23	587
Y	23	25	17	22	26	19	25	5
Zr	133	111	164	81	179	121	138	58
Nb	10	8	6	7	8	7	9	3
Ba	430	584	654	422	696	628	359	1931
La	17	32	19	21	22	22	16	9
Ce	50	69	44	51	54	42	48	26
Nd	29	26	30	32	27	29	23	10
Pb	22	27	21	23	24	23	40	35
Th	18	17	14	18	14	13	22	1
SiO_2	77.86	77.45	71.22	76.54	70.19	73.00	78.41	75.65
TiO_2	0.06	0.19	0.38	0.14	0.45	0.28	0.06	0.14
Al_2O_3	12.58	12.60	15.28	13.21	15.49	14.18	12.17	13.76
Fe_2O_3	0.29	0.72	1.95	0.85	2.54	1.60	0.54	0.87
MnO	0.01	0.02	0.04	0.03	0.05	0.04	0.01	0.02
MgO	0.05	0.05	0.51	0.19	0.82	0.35	0.05	0.27
CaO	0.54	0.83	3.27	0.83	2.67	2.81	0.53	0.83
Na_2O	4.56	4.38	4.88	4.43	4.66	4.60	4.52	2.86
K_2O	4.03	3.73	2.35	3.72	3.01	3.06	3.69	5.55
P_2O_5	0.02	0.03	0.12	0.05	0.13	0.09	0.01	0.06
Total	100.00	100.00	100.00	100.00	100.00	100.00	100.00	100.00
Q	34.75	35.75	26.25	34.29	24.08	28.61	36.67	35.45
or	23.80	22.01	13.89	21.99	17.76	18.08	21.82	32.77
ab	38.60	37.09	41.34	37.45	39.39	38.89	38.29	24.19
an	1.95	3.71	12.81	3.81	12.40	9.03	1.99	3.71
C	0.00	0.00	0.00	0.50	0.04	0.00	0.00	1.69
di	0.52	0.18	2.16	0.00	0.00	3.60	0.50	0.00
hy	0.09	0.52	1.73	1.21	4.11	0.36	0.36	1.41
mt	0.10	0.25	0.67	0.29	0.87	0.55	0.19	0.30
il	0.11	0.37	0.72	0.27	0.85	0.54	0.11	0.27
ap	0.05	0.07	0.28	0.12	0.30	0.21	0.02	0.14

Sample	24043	24044	24045	24046	24047	24048	24049	24053
SiO_2	74.35	77.09	70.36	66.45	74.34	72.88	71.46	69.14
TiO_2	0.25	0.09	0.27	0.39	0.14	0.08	0.36	0.36
Al_2O_3	13.81	12.17	15.04	15.97	12.67	14.70	14.34	15.20
Fe_2O_3	1.43	0.47	1.34	2.03	0.30	0.56	2.02	3.36
MnO	0.04	0.01	0.03	0.06	0.01	0.02	0.04	0.05
MgO	0.32	0.05	0.22	0.17	0.05	0.05	0.64	0.75
CaO	1.67	0.83	2.63	3.97	2.22	1.04	1.88	1.83
Na_2O	4.44	4.67	4.59	5.65	5.03	4.53	4.10	4.50
K_2O	2.98	3.78	3.36	2.18	3.39	4.44	3.42	3.00
P_2O_5	0.07	0.02	0.09	0.07	0.02	0.11	0.09	0.10
LOI	0.88	0.83	1.17	2.50	1.67	0.95	1.55	0.96
Total	100.24	100.01	99.10	99.44	99.84	99.36	99.90	99.25
V	13	10	15	5	9	13	34	39
Cr	4	4	5	7	4	5	10	10
Ni	3	3	4	3	3	6	8	5
Zn	56	62	33	64	26	32	31	49
Ga	20	21	20	21	19	18	20	21
Rb	87	123	120	57	112	82	114	92
Sr	161	10	192	266	38	242	220	191
Y	22	20	17	10	29	9	21	24
Zr	146	238	140	326	230	66	162	192
Nb	7	10	9	10	8	7	6	8
Ba	776	502	563	729	728	1476	611	712
La	19	15	23	19	27	11	23	25
Ce	37	35	47	35	66	34	52	49
Nd	21	20	27	19	34	10	23	26
Pb	27	18	25	16	26	35	24	22
Th	14	17	17	10	16	1	20	13
SiO_2	74.83	77.73	71.85	68.55	75.73	74.06	72.66	70.34
TiO_2	0.25	0.09	0.28	0.40	0.14	0.08	0.37	0.37
Al_2O_3	13.90	12.27	15.36	16.47	12.91	14.94	14.58	15.46
Fe_2O_3	1.44	0.47	1.37	2.09	0.31	0.57	2.05	3.42
MnO	0.04	0.01	0.03	0.06	0.01	0.02	0.04	0.05
MgO	0.32	0.05	0.22	0.18	0.05	0.05	0.65	0.76
CaO	1.68	0.84	2.69	4.10	2.26	1.06	1.91	1.86
Na_2O	4.47	4.71	4.69	5.83	5.12	4.60	4.17	4.58
K_2O	3.00	3.81	3.43	2.25	3.45	4.51	3.48	3.05
P_2O_5	0.07	0.02	0.09	0.07	0.02	0.11	0.09	0.10
Total	100.00	100.00	100.00	100.00	100.00	100.00	100.00	100.00
Q	32.93	34.40	25.57	18.10	29.75	27.76	29.53	25.76
or	17.72	22.52	20.28	13.29	20.41	26.66	20.55	18.04
ab	37.81	39.84	39.66	49.32	43.36	38.95	35.28	38.74
an	7.88	1.09	10.74	12.15	2.02	4.51	8.89	8.57
C	0.41	0.00	0.00	0.00	0.00	0.83	0.70	1.49
di	0.00	0.98	1.68	4.11	0.48	0.00	0.00	0.00
hy	2.00	0.00	0.77	0.00	0.00	0.64	3.28	5.04
wo	0.00	0.75	0.00	1.22	3.54	0.00	0.00	0.00
mt	0.49	0.16	0.47	0.72	0.10	0.19	0.70	1.17
il	0.48	0.17	0.52	0.76	0.27	0.15	0.70	0.70
ap	0.16	0.05	0.21	0.17	0.05	0.26	0.21	0.24

Sample	24055	24056	24057	24059	24077	24078	24079	24080	24081	24082
SiO_2	72.36	74.98	77.17	75.73	73.55	75.92	72.04	72.18	72.08	75.50
TiO_2	0.23	0.06	0.16	0.20	0.07	0.11	0.05	0.06	0.26	0.16
Al_2O_3	14.38	12.01	12.83	12.69	14.43	13.13	14.54	15.47	15.42	13.49
Fe_2O_3	2.23	0.26	0.83	1.01	0.89	1.20	0.49	0.42	1.26	1.16
MnO	0.04	0.02	0.03	0.03	0.03	0.03	0.02	0.02	0.03	0.02
MgO	0.66	0.05	0.08	0.26	0.07	0.19	0.05	0.05	0.39	0.07
CaO	0.72	2.27	0.79	1.07	0.71	1.11	3.27	1.38	1.82	0.92
Na_2O	4.01	3.81	3.95	3.36	4.33	3.87	4.67	3.86	4.47	4.87
K_2O	4.14	4.34	4.28	4.90	4.65	3.45	3.19	6.02	3.48	3.49
P_2O_5	0.09	0.01	0.03	0.06	0.17	0.06	0.03	0.02	0.09	0.04
LOI	1.30	1.93	-0.29	0.39	1.16	0.07	1.70	0.82	0.06	0.56
Total	100.16	99.74	99.86	99.70	100.06	99.14	100.05	100.30	99.36	100.28
V	24	12	11	17	14	13	12	10	26	11
Cr	21	5	4	4	3	5	4	5	5	4
Ni	11	5	3	3	6	6	3	3	8	3
Zn	38	16	20	31	43	32	45	21	42	48
Ga	19	20	20	18	23	19	22	22	20	22
Rb	177	166	160	169	162	71	139	178	76	114
Sr	120	26	49	152	45	237	184	95	789	90
Y	27	26	24	12	17	11	6	14	9	34
Zr	100	72	74	79	37	43	41	41	88	199
Nb	11	7	6	4	9	8	8	12	3	9
Ba	583	100	539	657	117	1072	284	181	1540	665
La	22	10	21	20	5	20	5	5	12	26
Ce	46	36	39	30	21	44	8	12	36	61
Nd	31	25	29	27	11	24	14	15	19	29
Pb	28	26	22	18	31	30	40	66	37	46
Th	10	22	19	17	2	6	3	8	5	12
SiO_2	73.19	76.66	77.05	76.26	74.37	76.63	73.25	72.56	72.59	75.71
TiO_2	0.23	0.06	0.16	0.20	0.07	0.11	0.05	0.06	0.26	0.16
Al_2O_3	14.55	12.28	12.81	12.78	14.59	13.25	14.78	15.55	15.53	13.53
Fe_2O_3	2.26	0.27	0.83	1.02	0.90	1.21	0.50	0.42	1.27	1.16
MnO	0.04	0.02	0.03	0.03	0.03	0.03	0.02	0.02	0.03	0.02
MgO	0.67	0.05	0.08	0.26	0.07	0.19	0.05	0.05	0.39	0.07
CaO	0.73	2.32	0.79	1.08	0.72	1.12	3.32	1.39	1.83	0.92
Na_2O	4.06	3.90	3.94	3.38	4.38	3.91	4.75	3.88	4.50	4.88
K_2O	4.19	4.44	4.27	4.93	4.70	3.48	3.24	6.05	3.50	3.50
P_2O_5	0.09	0.01	0.03	0.06	0.17	0.06	0.03	0.02	0.09	0.04
Total	100.00	100.00	100.00	100.00	100.00	100.00	100.00	100.00	100.00	100.00
Q	30.32	33.74	35.72	34.79	29.34	37.53	27.36	23.66	28.29	31.48
or	24.75	26.22	25.26	29.16	27.79	20.58	19.17	35.76	20.71	20.68
ab	34.32	32.96	33.37	28.63	37.05	33.05	40.18	32.83	38.09	41.32
an	3.02	2.92	3.72	4.95	2.44	5.16	9.45	6.75	8.50	4.32
C	2.23	0.00	0.33	0.06	1.41	1.17	0.00	0.14	1.22	0.12
di	0.00	0.69	0.00	0.00	0.00	0.00	1.19	0.00	1.96	1.19
hy	3.76	0.00	0.88	1.46	1.08	1.64	0.00	0.51	0.43	0.40
wo	0.00	3.22	0.00	0.00	0.00	0.00	2.29	0.00	0.50	0.30
mt	0.77	0.09	0.28	0.35	0.31	0.41	0.17	0.14	0.21	0.09
il	0.44	0.12	0.30	0.38	0.13	0.21	0.10	0.11		
ap	0.21	0.02	0.07	0.14	0.40	0.14	0.07	0.05		

ETHELTON - VOLCANIC CLASTS

Sample	24039	24050	24051	24052	24054	24058	24060	24061
SiO_2	74.40	71.91	71.46	69.44	68.47	74.22	70.83	71.59
TiO_2	0.18	0.31	0.29	0.38	0.42	0.25	0.36	0.38
Al_2O_3	13.56	14.09	13.95	14.93	14.22	13.64	14.76	14.89
Fe_2O_3	0.94	2.22	2.75	2.93	2.89	1.87	2.69	2.55
MnO	0.03	0.05	0.06	0.08	0.06	0.04	0.06	0.06
MgO	0.11	0.48	0.66	0.63	0.83	0.37	0.80	0.72
CaO	1.13	1.84	1.75	2.28	2.74	1.19	1.87	1.81
Na_2O	4.64	4.36	3.69	4.48	4.53	4.23	4.43	4.58
K_2O	3.85	3.14	3.72	2.79	2.67	3.44	2.85	2.79
P_2O_5	0.04	0.09	0.09	0.09	0.13	0.07	0.10	0.10
LOI	0.68	1.03	1.19	1.40	2.07	0.91	0.88	1.03
Total	99.56	99.52	99.61	99.43	99.03	100.23	99.63	100.50
V	12	27	42	37	55	23	41	36
Cr	4	6	9	8	6	6	13	8
Ni	3	7	4	7	6	4	6	5
Zn	51	45	47	53	43	35	55	59
Ga	20	19	20	21	19	19	19	21
Rb	160	115	170	110	113	182	110	112
Sr	110	189	153	240	220	168	210	225
Y	34	24	27	23	12	20	24	23
Zr	161	135	118	140	115	144	149	159
Nb	9	3	9	6	5	8	7	7
Ba	606	621	530	613	614	585	564	580
La	29	26	22	25	18	25	27	25
Ce	66	59	45	59	47	54	57	56
Nd	35	27	25	26	16	31	33	31
Pb	29	15	30	19	17	22	29	29
Th	21	22	25	14	14	30	15	15
SiO_2	75.24	73.01	72.61	70.84	70.62	74.73	71.73	71.97
TiO_2	0.18	0.31	0.29	0.39	0.43	0.25	0.36	0.38
Al_2O_3	13.71	14.31	14.17	15.23	14.67	13.73	14.95	14.97
Fe_2O_3	0.95	2.25	2.79	2.99	2.98	1.88	2.72	2.56
MnO	0.03	0.05	0.06	0.08	0.06	0.04	0.06	0.06
MgO	0.11	0.49	0.67	0.64	0.86	0.37	0.81	0.72
CaO	1.14	1.87	1.78	2.33	2.83	1.20	1.89	1.82
Na_2O	4.69	4.43	3.75	4.57	4.67	4.26	4.49	4.60
K_2O	3.89	3.19	3.78	2.85	2.75	3.46	2.89	2.80
P_2O_5	0.04	0.09	0.09	0.09	0.13	0.07	0.10	0.10
Total	100.00	100.00	100.00	100.00	100.00	100.00	100.00	100.00
Q	30.31	29.69	30.59	26.45	25.25	33.01	28.50	28.75
or	23.01	18.84	22.34	16.82	16.27	20.47	17.06	16.58
ab	39.71	37.46	31.73	38.67	39.53	36.04	37.96	38.96
an	4.86	8.67	8.22	10.94	10.91	5.48	8.73	8.37
C	0.00	0.40	0.90	0.62	0.00	0.97	1.24	1.29
di	0.47	0.00	0.00	0.00	1.86	0.00	0.00	0.00
hy	0.81	3.19	4.28	4.30	3.79	2.60	4.44	4.02
mt	0.33	0.77	0.96	1.02	1.02	0.64	0.93	0.88
il	0.35	0.60	0.56	0.74	0.82	0.48	0.69	0.73
ap	0.09	0.21	0.21	0.21	0.31	0.16	0.23	0.23

Sample	24062	24063	24064	24065	24066	24067	24068	24069
SiO_2	72.25	72.95	70.37	71.35	74.32	71.96	65.63	74.71
TiO_2	0.34	0.29	0.37	0.35	0.20	0.26	0.57	0.15
Al_2O_3	13.53	14.19	14.31	14.45	13.67	14.15	16.11	12.54
Fe_2O_3	1.31	2.08	2.90	2.58	1.80	2.07	4.01	1.50
MnO	0.03	0.05	0.07	0.06	0.04	0.04	0.08	0.04
MgO	0.28	0.39	0.68	0.60	0.05	0.31	1.02	0.05
CaO	1.56	1.77	2.29	1.48	0.81	1.24	3.36	2.04
Na_2O	4.21	3.33	4.45	4.61	4.74	4.04	4.52	4.53
K_2O	3.84	4.05	2.87	3.37	3.90	4.13	2.30	2.90
P_2O_5	0.04	0.08	0.11	0.09	0.03	0.07	0.16	0.02
LOI	1.28	0.65	1.81	0.73	0.13	0.56	1.86	1.13
Total	98.67	99.83	100.23	99.67	99.69	98.83	99.62	99.61
V	16	27	36	34	8	21	61	8
Cr	5	8	8	6	5	4	7	4
Ni	4	4	4	7	3	3	6	3
Zn	34	47	81	53	29	49	67	62
Ga	20	20	19	20	19	18	21	18
Rb	151	196	118	141	141	185	63	111
Sr	116	132	202	188	97	158	290	57
Y	29	42	23	32	33	31	22	34
Zr	255	155	151	221	324	153	170	225
Nb	10	10	7	6	11	9	7	10
Ba	686	586	571	596	739	734	734	717
La	23	29	20	28	30	26	25	31
Ce	67	70	52	68	69	66	62	66
Nd	32	34	23	27	30	27	23	34
Pb	32	27	27	29	26	32	20	28
Th	22	28	15	20	19	23	15	20
SiO_2	74.19	73.55	71.50	72.11	74.65	73.23	67.13	75.86
TiO_2	0.35	0.29	0.38	0.35	0.20	0.26	0.58	0.15
Al_2O_3	13.89	14.31	14.54	14.60	13.73	14.40	16.48	12.73
Fe_2O_3	1.35	2.10	2.95	2.61	1.81	2.11	4.10	1.52
MnO	0.03	0.05	0.07	0.06	0.04	0.04	0.08	0.04
MgO	0.29	0.39	0.69	0.61	0.05	0.32	1.04	0.05
CaO	1.60	1.78	2.33	1.50	0.81	1.26	3.44	2.07
Na_2O	4.32	3.36	4.52	4.66	4.76	4.11	4.62	4.60
K_2O	3.94	4.08	2.92	3.41	3.92	4.20	2.35	2.94
P_2O_5	0.04	0.08	0.11	0.09	0.03	0.07	0.16	0.02
Total	100.00	100.00	100.00	100.00	100.00	100.00	100.00	100.00
Q	29.96	33.37	27.14	27.07	29.47	29.39	21.15	33.74
or	23.30	24.13	17.23	20.13	23.15	24.84	13.90	17.40
ab	36.58	28.41	38.26	39.43	40.29	34.79	39.12	38.92
an	6.86	8.33	10.77	6.83	3.84	5.79	15.98	5.40
C	0.00	1.31	0.00	0.75	0.25	0.96	0.47	0.00
di	0.68	0.00	0.04	0.00	0.00	0.00	0.00	3.00
hy	1.29	2.83	4.36	3.82	1.80	2.67	6.17	0.00
wo	0.00	0.00	0.00	0.00	0.00	0.00	0.00	0.56
mt	0.46	0.72	1.01	0.89	0.62	0.72	1.40	0.52
il	0.66	0.56	0.71	0.67	0.38	0.50	1.11	0.29
ap	0.10	0.19	0.26	0.21	0.07	0.17	0.38	0.05

Sample	24070	24071	24072	24073	24074	24075	24076	24083
SiO_2	74.00	75.47	78.91	77.06	77.04	73.99	76.88	69.77
TiO_2	0.22	0.18	0.07	0.08	0.11	0.21	0.09	0.37
Al_2O_3	13.46	13.32	11.66	12.57	12.25	13.73	12.47	14.85
Fe_2O_3	1.75	1.81	0.42	0.98	0.75	1.85	1.10	2.82
MnO	0.03	0.04	0.01	0.02	0.02	0.05	0.02	0.07
MgO	0.05	0.25	0.05	0.05	0.05	0.25	0.05	0.76
CaO	0.56	1.38	0.25	0.28	1.11	1.38	0.92	2.03
Na_2O	5.13	4.10	4.35	3.92	4.08	4.25	3.29	4.59
K_2O	3.49	3.09	3.79	4.43	3.89	3.53	4.26	2.65
P_2O_5	0.03	0.06	0.01	0.02	0.03	0.06	0.02	0.09
LOI	0.86	0.78	0.99	0.39	0.96	1.05	0.75	1.12
Total	99.58	100.48	100.51	99.80	100.29	100.35	99.85	99.12
V	9	20	10	9	12	17	14	38
Cr	4	7	3	4	3	5	5	11
Ni	3	6	3	3	6	3	5	5
Zn	42	38	30	29	32	44	37	60
Ga	17	22	22	20	20	20	19	20
Rb	116	88	139	182	151	145	195	103
Sr	43	123	15	17	62	143	78	207
Y	27	23	44	28	28	28	35	25
Zr	303	151	401	149	199	133	106	163
Nb	6	8	11	14	7	10	7	7
Ba	2566	606	290	312	885	614	648	605
La	25	24	30	22	22	28	25	28
Ce	62	65	75	53	71	62	61	59
Nd	26	25	37	32	27	23	28	22
Pb	18	26	10	18	34	17	31	22
Th	9	19	20	19	18	14	24	14
SiO_2	74.96	75.70	79.29	77.52	77.56	74.51	77.58	71.19
TiO_2	0.22	0.18	0.07	0.08	0.11	0.21	0.09	0.38
Al_2O_3	13.63	13.36	11.72	12.64	12.33	13.83	12.58	15.15
Fe_2O_3	1.77	1.82	0.42	0.99	0.76	1.86	1.11	2.88
MnO	0.03	0.04	0.01	0.02	0.02	0.05	0.02	0.07
MgO	0.05	0.25	0.05	0.05	0.05	0.25	0.05	0.78
CaO	0.57	1.38	0.25	0.28	1.12	1.39	0.93	2.07
Na_2O	5.20	4.11	4.37	3.94	4.11	4.28	3.32	4.68
K_2O	3.54	3.10	3.81	4.46	3.92	3.55	4.30	2.70
P_2O_5	0.03	0.06	0.01	0.02	0.03	0.06	0.02	0.09
Total	100.00	100.00	100.00	100.00	100.00	100.00	100.00	100.00
q	29.28	35.96	38.56	36.47	36.36	32.04	39.32	27.09
or	20.89	18.32	22.51	26.34	23.14	21.01	25.40	15.98
ab	43.97	34.80	36.99	33.37	34.76	36.22	28.09	39.63
an	2.62	6.47	1.10	1.27	3.65	6.50	4.47	9.68
c	0.30	0.87	0.00	0.87	0.00	0.56	0.83	0.98
di	0.00	0.00	0.07	0.00	1.48	0.00	0.00	0.00
hy	1.71	2.34	0.44	1.08	0.02	2.36	1.20	4.51
mt	0.61	0.62	0.14	0.34	0.26	0.64	0.38	0.98
il	0.42	0.34	0.13	0.15	0.21	0.40	0.17	0.72
ap	0.07	0.14	0.02	0.05	0.07	0.14	0.05	0.21

MOUNT SAUL - GRANITOID CLASTS

Sample	24397	24398	24399	24400	24401	24402	24403	24404
SiO_2	76.06	68.86	75.16	77.77	78.32	75.47	73.55	72.75
TiO_2	0.03	0.50	0.22	0.15	0.08	0.19	0.30	0.21
Al_2O_3	12.97	15.74	13.19	12.29	12.46	13.18	13.56	13.08
Fe_2O_3	0.41	2.70	1.02	0.45	0.50	0.96	1.67	0.94
MnO	0.01	0.06	0.02	0.01	0.01	0.03	0.02	0.04
MgO	0.05	0.43	0.19	0.05	0.05	0.12	0.21	0.11
CaO	2.18	2.09	0.96	0.42	0.25	0.84	0.78	2.20
Na_2O	3.59	4.71	3.98	3.81	4.24	4.13	3.70	4.54
K_2O	3.75	3.98	3.94	4.46	4.28	3.83	4.95	3.87
P_2O_5	0.05	0.13	0.05	0.03	0.03	0.04	0.06	0.04
LOI	1.36	-0.16	0	0.60	0.26	0.63	0.66	1.95
Total	100.46	99.04	98.73	100.04	100.48	99.42	99.46	99.73
V	14	49	19	13	15	14	27	14
Cr	4	7	5	4	4	5	5	4
Ni	6	7	5	5	6	5	6	6
Zn	14	28	23	13	13	20	21	25
Ga	18	20	20	20	21	18	20	20
Rb	62	150	121	134	210	94	165	123
Sr	543	291	179	45	52	156	191	97
Y	5	21	11	21	19	11	14	16
Zr	41	243	81	57	46	72	212	201
Nb	3	7	2	2	14	4	4	14
Ba	1263	635	652	644	241	767	598	574
La	5	21	10	14	6	14	16	19
Ce	14	53	30	33	26	41	37	50
Nd	10	27	11	14	15	10	15	15
Pb	30	26	19	12	9	27	24	13
Th	4	22	18	16	28	17	26	18
SiO_2	76.75	69.42	76.13	78.21	78.15	76.39	74.44	74.40
TiO_2	0.03	0.50	0.22	0.15	0.08	0.19	0.30	0.21
Al_2O_3	13.09	15.87	13.36	12.36	12.43	13.34	13.72	13.38
Fe_2O_3	0.41	2.72	1.03	0.45	0.50	0.97	1.69	0.96
MnO	0.01	0.06	0.02	0.01	0.01	0.03	0.02	0.04
MgO	0.05	0.43	0.19	0.05	0.05	0.12	0.21	0.11
CaO	2.20	2.11	0.97	0.42	0.25	0.85	0.79	2.25
Na_2O	3.62	4.75	4.03	3.83	4.23	4.18	3.74	4.64
K_2O	3.78	4.01	3.99	4.49	4.27	3.88	5.01	3.96
P_2O_5	0.05	0.13	0.05	0.03	0.03	0.04	0.06	0.04
Total	100.00	100.00	100.00	100.00	100.00	100.00	100.00	100.00
Q	36.86	20.65	34.82	37.74	36.48	35.00	31.04	28.53
or	22.36	23.71	23.58	26.51	25.24	22.91	29.61	23.39
ab	30.65	40.18	34.11	32.42	35.80	35.38	31.69	39.29
an	8.28	9.60	4.49	1.90	1.04	3.95	3.52	3.97
C	0.00	0.20	0.76	0.51	0.47	0.82	0.85	0.00
di	1.04	0.00	0.00	0.00	0.00	0.00	0.00	2.01
hy	0.00	3.27	1.25	0.38	0.54	1.08	1.87	0.00
wo	0.46	0.00	0.00	0.00	0.00	0.00	0.00	1.91
mt	0.14	0.93	0.35	0.15	0.17	0.33	0.58	0.33
il	0.06	0.96	0.42	0.29	0.15	0.37	0.58	0.41
ap	0.12	0.30	0.12	0.07	0.07	0.09	0.14	0.09

Sample	24405	24406	24407	24408	24428	24431	24432	24433
SiO_2	77.16	77.51	75.76	74.78	73.11	71.27	70.00	75.64
TiO_2	0.15	0.08	0.25	0.23	0.33	0.37	0.44	0.16
Al_2O_3	12.10	12.68	12.89	13.38	14.25	14.90	15.51	13.18
Fe_2O_3	0.80	0.61	0.64	1.17	1.70	2.13	2.79	0.74
MnO	0.02	0.02	0.03	0.04	0.06	0.07	0.07	0.05
MgO	0.05	0.05	0.18	0.25	0.25	0.23	0.46	0.09
CaO	0.47	0.57	0.73	0.98	1.27	0.97	1.86	0.40
Na_2O	3.70	2.95	4.02	3.43	4.19	5.54	4.39	4.63
K_2O	4.70	5.64	4.59	4.76	4.35	3.65	4.09	4.34
P_2O_5	0.02	0.02	0.04	0.05	0.07	0.11	0.12	0.04
LOI	0.17	0.36	0.43	0.60	0.76	0.20	0.76	0.77
Total	99.34	100.49	99.56	99.67	100.34	99.44	100.49	100.04
V	11	18	13	23	33	21	47	12
Cr	3	5	4	5	6	4	6	5
Ni	6	6	5	5	6	5	7	5
Zn	21	15	23	55	27	53	34	40
Ga	20	19	20	19	19	20	19	20
Rb	142	207	159	177	147	117	160	109
Sr	70	45	95	164	196	187	278	65
Y	16	18	21	14	14	22	16	22
Zr	87	60	135	75	180	314	206	132
Nb	10	3	6	5	4	17	7	15
Ba	598	126	590	565	616	765	597	447
La	25	13	22	25	19	42	22	29
Ce	61	35	50	56	52	81	55	67
Nd	23	14	21	27	23	39	25	29
Pb	21	41	26	56	17	21	29	15
Th	27	38	22	24	27	17	24	17
SiO_2	77.81	77.41	76.42	75.48	73.42	71.82	70.19	76.20
TiO_2	0.15	0.08	0.25	0.23	0.33	0.37	0.44	0.16
Al_2O_3	12.20	12.66	13.00	13.51	14.31	15.01	15.55	13.28
Fe_2O_3	0.81	0.61	0.65	1.18	1.71	2.15	2.80	0.75
MnO	0.02	0.02	0.03	0.04	0.06	0.07	0.07	0.05
MgO	0.05	0.05	0.18	0.25	0.25	0.23	0.46	0.09
CaO	0.47	0.57	0.74	0.99	1.28	0.98	1.87	0.40
Na_2O	3.73	2.95	4.06	3.46	4.21	5.58	4.40	4.66
K_2O	4.74	5.63	4.63	4.80	4.37	3.68	4.10	4.37
P_2O_5	0.02	0.02	0.04	0.05	0.07	0.11	0.12	0.04
Total	100.00	100.00	100.00	100.00	100.00	100.00	100.00	100.00
Q	36.63	37.22	33.23	34.17	28.68	22.32	23.46	31.16
or	28.01	33.29	27.36	28.39	25.82	21.74	24.24	25.84
ab	31.57	24.93	34.32	29.30	35.60	47.24	37.25	39.47
an	2.22	2.69	3.39	4.58	5.87	4.12	8.47	1.74
C	0.12	0.73	0.08	0.93	0.51	0.34	0.77	0.24
hy	0.77	0.68	0.78	1.58	2.01	2.38	3.54	0.85
mt	0.28	0.21	0.22	0.40	0.58	0.73	0.96	0.26
il	0.29	0.15	0.48	0.44	0.63	0.71	0.84	0.31
ap	0.05	0.05	0.09	0.12	0.16	0.26	0.28	0.09

Sample	24435	24436	24437	24438
SiO_2	76.22	74.31	72.48	70.12
TiO_2	0.06	0.05	0.09	0.03
Al_2O_3	12.44	14.70	14.85	13.84
Fe_2O_3	0.60	0.72	0.63	0.44
MnO	0.01	0.02	0.02	0.03
MgO	0.05	0.05	0.05	0.05
CaO	0.38	1.14	0.85	4.04
Na_2O	3.11	3.73	3.62	3.96
K_2O	5.83	5.00	6.00	4.46
P_2O_5	0.02	0.07	0.12	0.01
LOI	0.27	0.33	0.58	2.81
Total	98.99	100.12	99.29	99.79
V	14	13	13	15
Cr	4	4	4	4
Ni	5	6	6	5
Zn	13	17	20	13
Ga	20	19	19	20
Rb	210	140	132	104
Sr	30	246	191	122
Y	8	9	10	6
Zr	82	52	35	35
Nb	2	2	4	2
Ba	64	1254	692	175
La	5	9	5	5
Ce	21	27	18	7
Nd	10	10	10	10
Pb	35	49	58	33
Th	42	3	4	1
SiO_2	77.21	74.47	73.43	72.30
TiO_2	0.06	0.05	0.09	0.03
Al_2O_3	12.60	14.73	15.04	14.27
Fe_2O_3	0.61	0.72	0.64	0.45
MnO	0.01	0.02	0.02	0.03
MgO	0.05	0.05	0.05	0.05
CaO	0.38	1.14	0.86	4.17
Na_2O	3.15	3.74	3.67	4.08
K_2O	5.91	5.01	6.08	4.60
P_2O_5	0.02	0.07	0.12	0.01
Total	100.00	100.00	100.00	100.00
Q	35.18	30.89	26.99	24.68
or	34.90	29.61	35.92	27.18
ab	26.66	31.63	31.03	34.55
an	1.78	5.21	3.48	7.03
C	0.38	1.25	1.16	0.00
di	0.00	0.00	0.00	1.20
hy	0.69	0.85	0.69	0.00
wo	0.00	0.00	0.00	5.09
mt	0.21	0.25	0.22	0.16
il	0.12	0.10	0.17	0.06
ap	0.05	0.16	0.28	0.02

MOUNT SAUL - VOLCANIC CLASTS

Sample	24395	24396	24409	24410	24411	24412	24413	24414
SiO_2	70.60	70.45	71.84	70.83	71.37	69.54	71.28	66.46
TiO_2	0.26	0.35	0.31	0.45	0.23	0.58	0.36	0.62
Al_2O_3	13.97	15.03	14.12	14.04	14.30	15.03	14.41	15.29
Fe_2O_3	2.32	2.80	2.45	2.69	1.76	2.54	2.05	3.63
MnO	0.07	0.08	0.08	0.06	0.07	0.07	0.06	0.10
MgO	0.46	0.59	0.27	0.53	0.32	0.62	0.44	1.06
CaO	2.81	2.17	0.94	1.40	1.15	1.15	2.32	2.40
Na_2O	4.99	4.11	5.09	4.83	4.51	4.79	4.06	5.16
K_2O	2.58	3.39	3.63	3.19	4.32	4.26	3.71	2.56
P_2O_5	0.08	0.11	0.08	0.11	0.07	0.14	0.08	0.16
LOI	2.30	0.82	0.76	0.78	0.74	0.85	0.83	1.58
Total	100.44	99.90	99.57	98.91	98.84	99.57	99.60	99.02
V	25	37	12	32	24	40	35	34
Cr	7	6	3	6	6	4	4	13
Ni	6	6	5	6	6	3	6	9
Zn	41	44	53	64	32	52	25	56
Ga	19	19	19	21	19	20	19	19
Rb	69	96	103	95	132	169	66	76
Sr	223	284	149	212	364	285	322	311
Y	26	16	26	28	16	29	17	26
Zr	195	119	242	239	130	236	197	229
Nb	8	4	7	8	13	13	8	5
Ba	525	587	882	738	698	759	749	640
La	23	16	26	23	26	14	20	28
Ce	58	44	65	61	55	94	48	69
Nd	23	16	24	29	20	71	20	45
Pb	18	20	30	30	18	36	32	29
Th	10	18	13	15	21	20	12	12
SiO_2	71.94	71.10	72.71	72.18	72.75	70.44	72.17	68.21
TiO_2	0.26	0.35	0.31	0.46	0.23	0.59	0.36	0.64
Al_2O_3	14.23	15.17	14.29	14.31	14.58	15.22	14.59	15.69
Fe_2O_3	2.36	2.83	2.48	2.74	1.79	2.57	2.08	3.73
MnO	0.07	0.08	0.08	0.06	0.07	0.07	0.06	0.10
MgO	0.47	0.60	0.27	0.54	0.33	0.63	0.45	1.09
CaO	2.86	2.19	0.95	1.43	1.17	1.16	2.35	2.46
Na_2O	5.08	4.15	5.15	4.92	4.60	4.85	4.11	5.30
K_2O	2.63	3.42	3.67	3.25	4.40	4.32	3.76	2.63
P_2O_5	0.08	0.11	0.08	0.11	0.07	0.14	0.08	0.16
Total	100.00	100.00	100.00	100.00	100.00	100.00	100.00	100.00
Q	25.85	27.44	25.42	26.52	25.60	21.80	27.81	19.49
or	15.54	20.22	21.71	19.21	26.02	25.50	22.20	15.53
ab	43.02	35.10	43.59	41.65	38.90	41.06	34.78	44.81
an	8.25	10.14	4.19	6.35	5.35	4.85	10.27	11.15
C	0.00	0.93	0.30	0.37	0.29	0.79	0.00	0.05
di	4.58	0.00	0.00	0.00	0.00	0.00	0.72	0.00
hy	1.07	4.07	2.96	3.63	2.47	3.47	2.47	5.83
mt	0.81	0.97	0.85	0.94	0.61	0.88	0.71	1.27
il	0.50	0.67	0.60	0.87	0.45	1.12	0.69	1.21
ap	0.19	0.26	0.19	0.26	0.17	0.33	0.19	0.38

Sample	24415	24416	24417	24418	24419	24420	24421	24422
SiO_2	68.20	76.44	75.92	72.30	69.91	73.91	75.73	74.03
TiO_2	0.55	0.40	0.26	0.34	0.36	0.20	0.29	0.20
Al_2O_3	16.14	11.27	11.92	13.96	15.69	14.18	12.79	13.85
Fe_2O_3	2.39	2.39	1.96	2.44	3.29	2.12	1.03	1.55
MnO	0.09	0.02	0.14	0.04	0.02	0.02	0.01	0.07
MgO	0.39	0.05	0.05	0.25	0.05	0.20	0.05	0.18
CaO	1.41	0.09	0.14	0.65	0.12	0.93	0.07	0.82
Na_2O	5.67	3.18	4.75	4.89	6.96	4.44	4.30	4.73
K_2O	4.24	5.26	4.41	3.89	3.23	3.98	5.24	3.81
P_2O_5	0.15	0.03	0.02	0.07	0.06	0.06	0.03	0.06
LOI	0.36	0.54	0.48	0.82	0.64	0.47	0.69	0.74
Total	99.59	99.67	100.05	99.65	100.33	100.51	100.23	100.04
V	24	22	18	21	5	15	14	12
Cr	4	5	4	5	4	5	4	4
Ni	6	6	5	7	5	5	5	5
Zn	56	22	85	47	52	14	58	38
Ga	20	23	22	21	26	20	22	21
Rb	175	122	108	92	43	129	129	120
Sr	371	12	5	158	52	105	8	172
Y	26	53	76	25	87	29	71	17
Zr	437	706	688	314	877	186	689	142
Nb	13	22	20	7	48	11	20	8
Ba	1154	87	93	981	417	915	90	852
La	33	40	52	20	67	40	76	32
Ce	90	99	112	50	146	84	171	65
Nd	46	47	52	20	66	36	78	28
Pb	40	26	20	24	22	13	50	27
Th	23	17	20	13	9	20	22	24
SiO_2	68.73	77.11	76.25	73.16	70.13	73.88	76.08	74.55
TiO_2	0.55	0.40	0.26	0.34	0.36	0.20	0.29	0.20
Al_2O_3	16.27	11.37	11.97	14.13	15.74	14.17	12.85	13.95
Fe_2O_3	2.41	2.41	1.97	2.47	3.30	2.12	1.03	1.56
MnO	0.09	0.02	0.14	0.04	0.02	0.02	0.01	0.07
MgO	0.39	0.05	0.05	0.25	0.05	0.20	0.05	0.18
CaO	1.42	0.09	0.14	0.66	0.12	0.93	0.07	0.83
Na_2O	5.71	3.21	4.77	4.95	6.98	4.44	4.32	4.76
K_2O	4.27	5.31	4.43	3.94	3.24	3.98	5.26	3.84
P_2O_5	0.15	0.03	0.02	0.07	0.06	0.06	0.03	0.06
Total	100.00	100.00	100.00	100.00	100.00	100.00	100.00	100.00
Q	15.10	37.07	31.74	26.75	15.60	29.82	30.38	29.62
or	25.25	31.36	26.17	23.26	19.15	23.51	31.11	22.67
ab	48.35	27.14	36.92	41.87	59.08	37.56	36.55	40.31
an	6.06	0.25	0.00	2.80	0.20	4.22	0.12	3.70
C	0.02	0.26	0.00	0.70	0.67	1.02	0.00	0.60
di	0.00	0.00	0.50	0.00	0.00	0.00	0.03	0.00
hy	2.80	2.07	2.18	2.77	3.09	2.47	0.75	1.92
ac	0.00	0.00	1.34	0.00	0.00	0.00	0.00	0.00
mt	0.82	0.82	0.00	0.84	1.13	0.73	0.35	0.53
il	1.05	0.77	0.50	0.65	0.69	0.38	0.55	0.38
ap	0.35	0.07	0.05	0.16	0.14	0.14	0.07	0.14
NNS	0.00	0.00	0.45	0.00	0.00	0.00	0.00	0.00

Sample	24423	24424	24425	24426	24427	24429	24430	24434
SiO_2	73.21	66.62	76.64	75.23	66.88	73.10	77.90	71.19
TiO_2	0.27	0.82	0.25	0.32	0.49	0.30	0.09	0.47
Al_2O_3	14.66	15.55	11.62	12.34	17.17	14.57	12.67	15.12
Fe_2O_3	1.24	4.23	1.93	1.78	3.08	0.49	0.56	1.24
MnO	0.05	0.06	0.07	0.03	0.17	0.01	0.01	0.07
MgO	0.17	0.58	0.05	0.05	0.34	0.05	0.05	0.08
CaO	0.41	2.67	0.22	0.28	0.37	0.24	0.16	0.54
Na_2O	3.85	4.84	4.28	4.14	5.71	5.58	3.10	6.31
K_2O	4.89	3.92	3.94	4.50	4.20	4.86	5.03	3.60
P_2O_5	0.04	0.22	0.02	0.02	0.18	0.05	0.03	0.05
LOI	0.63	0.95	0.73	1.20	1.16	0.59	0.63	0.62
Total	99.42	100.46	99.75	99.89	99.75	99.84	100.23	99.29
V	12	58	15	17	7	9	14	5
Cr	4	9	5	4	5	3	4	4
Ni	5	9	5	6	5	5	5	6
Zn	33	45	19	53	45	21	20	68
Ga	21	20	22	24	22	20	20	19
Rb	146	119	100	116	65	181	199	70
Sr	145	314	35	35	74	63	44	74
Y	19	32	54	75	39	23	23	44
Zr	233	320	632	776	918	292	93	414
Nb	18	6	21	26	42	17	11	16
Ba	760	659	63	25	764	793	775	1675
La	34	28	41	78	66	42	5	45
Ce	72	64	95	166	132	95	26	106
Nd	21	25	48	86	64	43	11	49
Pb	62	31	15	37	11	20	14	31
Th	14	16	17	23	4	23	22	16
SiO_2	74.11	66.95	77.40	76.23	67.84	73.65	78.21	72.15
TiO_2	0.27	0.82	0.25	0.32	0.50	0.30	0.09	0.48
Al_2O_3	14.84	15.63	11.73	12.50	17.42	14.68	12.72	15.32
Fe_2O_3	1.26	4.25	1.95	1.80	3.12	0.49	0.56	1.26
MnO	0.05	0.06	0.07	0.03	0.17	0.01	0.01	0.07
MgO	0.17	0.58	0.05	0.05	0.34	0.05	0.05	0.08
CaO	0.42	2.68	0.22	0.28	0.38	0.24	0.16	0.55
Na_2O	3.90	4.86	4.32	4.19	5.79	5.62	3.11	6.40
K_2O	4.95	3.94	3.98	4.56	4.26	4.90	5.05	3.65
P_2O_5	0.04	0.22	0.02	0.02	0.18	0.05	0.03	0.05
Total	100.00	100.00	100.00	100.00	100.00	100.00	100.00	100.00
q	31.01	16.67	35.74	33.09	15.75	21.85	40.23	19.53
or	29.25	23.28	23.51	26.95	25.18	28.94	29.85	21.56
ab	32.98	41.16	36.57	35.50	49.01	47.57	26.34	54.11
an	1.79	9.17	0.87	1.28	0.67	0.36	0.60	2.33
c	2.41	0.00	0.00	0.20	3.03	0.00	1.91	0.00
di	0.00	2.29	0.09	0.00	0.00	0.36	0.00	0.04
hy	1.41	3.58	1.87	1.57	3.69	0.00	0.59	0.87
wo	0.00	0.00	0.00	0.00	0.00	0.03	0.00	0.00
mt	0.43	1.45	0.67	0.62	1.07	0.17	0.19	0.43
il	0.52	1.57	0.48	0.62	0.94	0.57	0.17	0.90
ap	0.09	0.51	0.05	0.05	0.42	0.12	0.07	0.12

Sample	24439	24440	24441	24442	24443
SiO_2	75.59	64.14	72.13	71.77	68.62
TiO_2	0.12	0.70	0.61	0.66	0.74
Al_2O_3	12.81	15.31	13.04	13.10	15.03
Fe_2O_3	1.74	4.89	3.64	3.63	3.47
MnO	0.03	0.12	0.13	0.14	0.11
MgO	0.05	1.31	0.25	0.25	0.66
CaO	0.26	3.71	0.42	0.41	1.14
Na_2O	4.69	4.58	4.11	4.12	5.96
K_2O	4.11	2.40	5.11	5.14	3.01
P_2O_5	0.01	0.17	0.16	0.16	0.17
LOI	0.13	1.25	0.33	0.84	1.24
Total	99.54	98.58	99.93	100.22	100.15
V	8	78	18	6	55
Cr	4	10	7	4	9
Ni	6	7	9	6	11
Zn	70	48	34	80	116
Ga	22	21	22	18	20
Rb	168	61	132	118	73
Sr	9	380	37	65	167
Y	53	23	68	55	52
Zr	369	145	1002	472	382
Nb	11	4	46	20	14
Ba	196	580	141	1894	789
La	48	33	35	54	43
Ce	106	69	83	120	95
Nd	53	25	34	50	47
Pb	46	23	23	14	31
Th	29	5	19	16	13
SiO_2	76.04	65.90	72.42	72.22	69.38
TiO_2	0.12	0.72	0.61	0.66	0.75
Al_2O_3	12.89	15.73	13.09	13.18	15.20
Fe_2O_3	1.75	5.02	3.65	3.65	3.51
MnO	0.03	0.12	0.13	0.14	0.11
MgO	0.05	1.35	0.25	0.25	0.67
CaO	0.26	3.81	0.42	0.41	1.15
Na_2O	4.72	4.71	4.13	4.15	6.03
K_2O	4.13	2.47	5.13	5.17	3.04
P_2O_5	0.01	0.17	0.16	0.16	0.17
Total	100.00	100.00	100.00	100.00	100.00
Q	31.38	18.10	26.53	26.11	18.46
or	24.43	14.57	30.32	30.57	17.98
ab	39.92	39.82	34.92	35.08	50.99
an	1.23	14.52	1.04	0.99	4.60
C	0.20	0.00	0.37	0.40	0.31
di	0.00	2.72	0.00	0.00	0.00
hy	1.85	6.40	3.76	3.69	4.38
mt	0.60	1.72	1.25	1.25	1.20
il	0.23	1.37	1.16	1.26	1.42
ap	0.02	0.40	0.37	0.37	0.40

LAKE HILL - GRANITOID CLASTS

Sample	24445	24446	24447	24448	24449	24450	24451	24452
SiO_2	73.93	75.82	78.26	69.96	72.69	71.86	72.10	73.30
TiO_2	0.32	0.15	0.20	0.33	0.37	0.36	0.19	0.20
Al_2O_3	13.55	12.70	12.37	16.18	14.07	14.73	15.24	14.39
Fe_2O_3	2.49	1.51	0.69	2.18	2.15	1.89	1.65	1.79
MnO	0.03	0.02	0.01	0.03	0.04	0.05	0.03	0.03
MgO	0.70	0.16	0.10	0.55	0.62	0.42	0.47	0.58
CaO	1.30	0.61	0.84	2.29	1.71	1.50	1.67	2.36
Na_2O	5.32	3.39	5.83	5.40	3.98	4.60	4.43	4.21
K_2O	1.14	4.84	1.07	1.82	3.28	3.03	3.22	1.06
P_2O_5	0.09	0.05	0.05	0.13	0.08	0.06	0.08	0.03
LOI	1.13	0.76	0.55	0.48	1.18	0.91	0.83	1.01
Total	100.00	100.01	99.97	99.35	100.17	99.41	99.91	98.96
V	37	16	12	29	34	17	28	34
Cr	14	5	5	6	10	4	8	17
Ni	11	7	4	6	7	5	7	9
Zn	35	18	18	46	33	38	28	29
Ga	20	21	19	23	19	21	23	18
Rb	49	179	26	51	72	83	77	30
Sr	308	75	280	715	345	311	565	429
Y	27	42	12	12	20	16	12	6
Zr	137	111	124	165	177	217	52	101
Nb	8	13	3	7	7	8	7	2
Ba	251	432	198	726	823	919	868	368
La	22	39	43	26	37	37	8	5
Ce	53	84	93	60	73	78	27	16
Nd	26	40	44	21	26	27	13	10
Pb	21	28	35	28	20	25	30	22
Th	20	28	25	5	17	21	3	1
SiO_2	74.77	76.39	78.72	70.76	73.43	72.95	72.77	74.83
TiO_2	0.32	0.15	0.20	0.33	0.37	0.37	0.19	0.20
Al_2O_3	13.70	12.80	12.44	16.36	14.21	14.95	15.38	14.69
Fe_2O_3	2.52	1.52	0.69	2.20	2.17	1.92	1.67	1.83
MnO	0.03	0.02	0.01	0.03	0.04	0.05	0.03	0.03
MgO	0.71	0.16	0.10	0.56	0.63	0.43	0.47	0.59
CaO	1.31	0.61	0.84	2.32	1.73	1.52	1.69	2.41
Na_2O	5.38	3.42	5.86	5.46	4.02	4.67	4.47	4.30
K_2O	1.15	4.88	1.08	1.84	3.31	3.08	3.25	1.08
P_2O_5	0.09	0.05	0.05	0.13	0.08	0.06	0.08	0.03
Total	100.00	100.00	100.00	100.00	100.00	100.00	100.00	100.00
Q	34.44	35.80	38.47	25.68	32.15	29.59	29.54	38.97
or	6.81	28.82	6.36	10.88	19.58	18.18	19.21	6.40
ab	45.53	28.90	49.62	46.22	34.02	39.52	37.83	36.37
an	5.93	2.72	3.86	10.63	8.04	7.16	7.83	11.75
C	1.43	0.90	0.22	1.49	1.07	1.32	1.64	2.14
hy	3.97	1.81	0.68	3.24	3.34	2.60	2.70	3.15
mt	0.86	0.52	0.24	0.75	0.74	0.66	0.57	0.63
il	0.61	0.29	0.38	0.63	0.71	0.69	0.36	0.39
ap	0.21	0.12	0.12	0.30	0.19	0.14	0.19	0.07

Sample	24453	24454	24455	24456	24457	24458	24459	24460
SiO_2	73.07	74.99	78.36	73.12	76.04	76.05	76.47	76.10
TiO_2	0.18	0.26	0.18	0.08	0.09	0.06	0.23	0.11
Al_2O_3	14.99	12.97	11.78	16.07	13.76	14.50	13.10	13.88
Fe_2O_3	1.57	3.06	0.80	0.53	0.51	0.68	1.39	0.86
MnO	0.05	0.04	0.01	0.01	0.02	0.03	0.05	0.01
MgO	0.38	0.24	0.09	0.06	0.06	0.07	0.21	0.13
CaO	1.51	1.15	0.48	1.80	0.89	0.92	0.99	1.44
Na_2O	4.00	4.82	3.80	6.58	3.88	5.67	6.33	5.06
K_2O	3.33	0.64	3.69	0.63	4.43	1.46	0.20	1.50
P_2O_5	0.06	0.04	0.03	0.03	0.03	0.07	0.03	0.02
LOI	0.73	0.92	0.70	0.42	0.46	0.72	0.98	0.59
Total	99.87	99.13	99.92	99.33	100.17	100.23	99.98	99.70
V	18	23	15	18	17	15	16	20
Cr	9	6	5	4	4	4	6	6
Ni	6	6	5	5	6	5	6	6
Zn	23	33	12	15	21	19	17	17
Ga	17	22	18	21	20	23	21	19
Rb	67	34	70	15	108	45	6	31
Sr	501	186	127	1038	429	291	132	261
Y	14	43	9	4	16	14	37	37
Zr	57	151	138	19	42	5	247	27
Nb	2	6	2	2	5	4	9	7
Ba	970	227	289	264	974	203	63	403
La	29	20	60	5	12	5	16	5
Ce	27	55	115	12	33	27	42	20
Nd	19	31	36	10	12	13	36	15
Pb	33	8	16	27	40	28	5	38
Th	9	12	45	1	5	3	5	16
SiO_2	73.70	76.36	78.98	73.93	76.26	76.42	77.24	76.78
TiO_2	0.18	0.26	0.18	0.08	0.09	0.06	0.23	0.11
Al_2O_3	15.12	13.21	11.87	16.25	13.80	14.57	13.23	14.00
Fe_2O_3	1.58	3.12	0.81	0.54	0.51	0.68	1.40	0.87
MnO	0.05	0.04	0.01	0.01	0.02	0.03	0.05	0.01
MgO	0.38	0.24	0.09	0.06	0.06	0.07	0.21	0.13
CaO	1.52	1.17	0.48	1.82	0.89	0.92	1.00	1.45
Na_2O	4.03	4.91	3.83	6.65	3.89	5.70	6.39	5.11
K_2O	3.36	0.65	3.72	0.64	4.44	1.47	0.20	1.51
P_2O_5	0.06	0.04	0.03	0.03	0.03	0.07	0.03	0.02
Total	100.00	100.00	100.00	100.00	100.00	100.00	100.00	100.00
Q	33.04	41.21	41.11	28.68	34.51	35.46	36.35	37.69
or	19.85	3.85	21.98	3.76	26.26	8.67	1.19	8.94
ab	34.14	41.53	32.41	56.29	32.93	48.21	54.10	43.20
an	7.16	5.54	2.20	8.83	4.23	4.13	4.76	7.08
C	2.22	2.40	0.74	1.38	1.04	2.10	0.75	1.37
hy	2.44	3.57	0.81	0.61	0.58	0.86	1.74	1.09
mt	0.54	1.07	0.28	0.18	0.18	0.23	0.48	0.30
il	0.34	0.50	0.34	0.15	0.17	0.11	0.44	0.21
ap	0.14	0.09	0.07	0.07	0.07	0.16	0.07	0.05

Sample	24461	24462	24463	24464	24465	24466	24467	24468
SiO_2	78.64	71.60	77.18	75.43	75.08	74.30	76.96	75.44
TiO_2	0.11	0.22	0.14	0.17	0.14	0.21	0.15	0.03
Al_2O_3	11.61	15.52	12.39	13.28	14.38	13.33	12.35	13.76
Fe_2O_3	1.28	1.43	0.83	1.00	0.93	1.51	1.57	0.55
MnO	0.02	0.02	0.02	0.03	0.02	0.03	0.02	0.14
MgO	0.10	0.37	0.05	0.23	0.35	0.27	0.05	0.05
CaO	0.27	1.91	0.49	1.25	2.14	1.17	1.00	0.18
Na_2O	3.32	4.76	3.79	3.99	5.37	3.76	4.70	4.70
K_2O	4.36	2.74	4.47	3.26	0.55	4.19	2.12	3.71
P_2O_5	0.03	0.08	0.03	0.04	0.03	0.04	0.03	0.03
LOI	0.23	1.06	0.52	0.84	1.07	0.58	0.47	0.81
Total	99.97	99.71	99.91	99.52	100.06	99.39	99.42	99.40
V	17	21	13	18	19	19	14	16
Cr	5	7	5	5	7	6	4	4
Ni	7	6	5	6	5	6	7	5
Zn	17	25	16	24	24	26	14	16
Ga	24	19	23	17	19	16	19	28
Rb	339	49	304	97	15	153	41	304
Sr	21	769	28	234	524	200	83	23
Y	75	9	35	11	14	20	41	37
Zr	77	93	80	64	91	146	241	21
Nb	13	3	5	7	2	10	4	36
Ba	53	1124	83	567	157	775	415	175
La	26	13	14	23	13	35	16	8
Ce	76	40	43	51	37	72	49	42
Nd	37	11	25	18	12	29	22	36
Pb	18	29	21	27	35	28	8	19
Th	33	2	37	18	12	37	11	13
SiO_2	78.84	72.58	77.65	76.44	75.85	75.19	77.78	76.52
TiO_2	0.11	0.22	0.14	0.17	0.14	0.21	0.15	0.03
Al_2O_3	11.64	15.73	12.47	13.46	14.53	13.49	12.48	13.96
Fe_2O_3	1.28	1.45	0.84	1.01	0.94	1.53	1.59	0.56
MnO	0.02	0.02	0.02	0.03	0.02	0.03	0.02	0.14
MgO	0.10	0.38	0.05	0.23	0.35	0.27	0.05	0.05
CaO	0.27	1.94	0.49	1.27	2.16	1.18	1.01	0.18
Na_2O	3.33	4.83	3.81	4.04	5.42	3.81	4.75	4.77
K_2O	4.37	2.78	4.50	3.30	0.56	4.24	2.14	3.76
P_2O_5	0.03	0.08	0.03	0.04	0.03	0.04	0.03	0.03
Total	100.00	100.00	100.00	100.00	100.00	100.00	100.00	100.00
Q	41.55	28.85	36.90	36.94	36.72	33.39	39.12	33.64
or	25.83	16.41	26.58	19.52	3.28	25.06	12.66	22.24
ab	28.17	40.83	32.27	34.21	45.90	32.20	40.19	40.34
an	1.15	9.08	2.25	6.02	10.53	5.61	4.82	0.71
C	1.01	1.46	0.50	1.02	1.14	0.59	0.58	1.78
hy	1.48	2.15	0.82	1.43	1.69	2.02	1.61	0.94
mt	0.44	0.50	0.29	0.35	0.32	0.52	0.54	0.19
il	0.21	0.42	0.27	0.33	0.27	0.40	0.29	0.06
ap	0.07	0.19	0.07	0.09	0.07	0.09	0.07	0.07

Sample	24469	24470	24471	24475	24479	24482	24483	24484
SiO_2	74.63	73.94	74.72	72.50	77.27	77.45	75.51	73.71
TiO_2	0.17	0.13	0.05	0.25	0.09	0.24	0.06	0.18
Al_2O_3	13.84	14.16	14.49	13.84	12.39	12.28	14.25	14.64
Fe_2O_3	1.14	0.77	0.29	2.21	1.18	0.92	0.44	1.17
MnO	0.02	0.02	0.01	0.04	0.01	0.02	0.02	0.02
MgO	0.18	0.19	0.05	0.46	0.08	0.22	0.05	0.27
CaO	0.87	0.94	0.90	1.07	0.24	1.09	1.14	1.49
Na_2O	3.32	3.55	3.86	4.18	4.55	5.87	4.36	4.32
K_2O	5.44	5.43	5.25	3.58	3.23	0.60	3.83	3.66
P_2O_5	0.04	0.09	0.02	0.04	0.03	0.05	0.05	0.05
LOI	0.63	0.75	0.86	1.61	0.78	0.89	0.52	0.56
Total	100.28	99.97	100.50	99.78	99.85	99.63	100.23	100.07
V	17	29	14	23	17	12	14	22
Cr	6	8	5	8	5	6	4	6
Ni	6	7	5	7	9	6	5	6
Zn	25	14	14	37	27	28	11	25
Ga	20	21	16	17	19	21	17	20
Rb	119	133	84	130	164	40	82	62
Sr	306	338	275	205	78	281	380	646
Y	15	20	11	23	29	38	16	7
Zr	42	42	31	178	79	149	6	60
Nb	9	7	2	9	9	10	2	3
Ba	845	688	1011	815	332	133	783	932
La	10	21	5	32	22	51	6	7
Ce	30	45	21	74	91	114	22	22
Nd	17	18	10	24	31	53	10	10
Pb	32	11	37	20	17	19	40	26
Th	4	7	2	23	38	39	2	1
SiO_2	74.89	74.52	74.99	73.85	78.00	78.44	75.73	74.07
TiO_2	0.17	0.13	0.05	0.25	0.09	0.24	0.06	0.18
Al_2O_3	13.89	14.27	14.54	14.10	12.51	12.44	14.29	14.71
Fe_2O_3	1.14	0.78	0.29	2.25	1.19	0.93	0.44	1.18
MnO	0.02	0.02	0.01	0.04	0.01	0.02	0.02	0.02
MgO	0.18	0.19	0.05	0.47	0.08	0.22	0.05	0.27
CaO	0.87	0.95	0.90	1.09	0.24	1.10	1.14	1.50
Na_2O	3.33	3.58	3.87	4.26	4.59	5.94	4.37	4.34
K_2O	5.46	5.47	5.27	3.65	3.26	0.61	3.84	3.68
P_2O_5	0.04	0.09	0.02	0.04	0.03	0.05	0.05	0.05
Total	100.00	100.00	100.00	100.00	100.00	100.00	100.00	100.00
Q	32.15	30.41	30.22	31.27	37.73	38.69	33.02	30.82
or	32.26	32.34	31.14	21.55	19.27	3.59	22.70	21.74
ab	28.19	30.28	32.78	36.03	38.86	50.30	37.00	36.74
an	4.07	4.11	4.35	5.14	1.00	5.15	5.34	7.10
C	1.01	0.96	0.87	1.26	1.05	0.11	0.98	0.99
hy	1.43	1.13	0.37	3.23	1.34	1.19	0.53	1.67
mt	0.39	0.27	0.10	0.77	0.41	0.32	0.15	0.40
il	0.32	0.25	0.10	0.48	0.17	0.46	0.11	0.34
ap	0.09	0.21	0.05	0.09	0.07	0.12	0.12	0.12

Sample	24485	24486	24487	24488	24489	24490	24491
SiO_2	76.79	75.88	76.49	69.89	74.34	77.93	76.33
TiO_2	0.09	0.10	0.14	0.38	0.08	0.12	0.15
Al_2O_3	13.61	13.97	12.80	14.86	14.35	12.77	13.39
Fe_2O_3	0.45	0.67	1.02	3.56	0.49	0.94	1.20
MnO	0.02	0.02	0.03	0.04	0.02	0.02	0.02
MgO	0.05	0.09	0.05	1.19	0.05	0.20	0.28
CaO	1.11	1.06	1.09	3.40	1.14	1.25	1.29
Na_2O	6.12	6.38	4.26	4.15	4.09	5.55	5.57
K_2O	0.94	0.75	3.33	1.00	4.25	0.62	1.15
P_2O_5	0.04	0.04	0.03	0.15	0.02	0.03	0.07
LOI	0.59	1.25	0.45	1.22	0.33	0.39	0.49
Total	99.81	100.21	99.69	99.84	99.16	99.82	99.94
V	15	19	11	56	16	16	23
Cr	4	5	4	19	5	5	6
Ni	6	5	5	11	6	5	5
Zn	15	14	23	54	14	22	23
Ga	16	18	19	20	20	17	21
Rb	25	18	90	27	72	20	23
Sr	328	398	164	442	516	263	472
Y	7	7	35	11	8	9	6
Zr	19	32	183	116	8	62	55
Nb	2	2	10	6	2	4	2
Ba	203	222	700	340	891	116	305
La	5	5	51	41	5	13	10
Ce	12	15	116	78	19	44	35
Nd	13	10	47	32	10	19	14
Pb	35	29	17	13	35	19	35
Th	1	1	15	9	4	10	2
SiO_2	77.39	76.68	77.08	70.87	75.22	78.38	76.75
TiO_2	0.09	0.10	0.14	0.39	0.08	0.12	0.15
Al_2O_3	13.72	14.12	12.90	15.07	14.52	12.84	13.46
Fe_2O_3	0.45	0.68	1.03	3.61	0.50	0.95	1.21
MnO	0.02	0.02	0.03	0.04	0.02	0.02	0.02
MgO	0.05	0.09	0.05	1.21	0.05	0.20	0.28
CaO	1.12	1.07	1.10	3.45	1.15	1.26	1.30
Na_2O	6.17	6.45	4.29	4.21	4.14	5.58	5.60
K_2O	0.95	0.76	3.36	1.01	4.30	0.62	1.16
P_2O_5	0.04	0.04	0.03	0.15	0.02	0.03	0.07
Total	100.00	100.00	100.00	100.00	100.00	100.00	100.00
Q	35.36	33.69	36.50	32.25	32.00	40.23	36.26
or	5.60	4.48	19.83	5.99	25.41	3.69	6.83
ab	52.19	54.55	36.32	35.61	35.02	47.23	47.39
an	5.29	5.05	5.25	16.11	5.59	6.04	5.98
C	0.61	0.84	0.28	1.14	1.01	0.77	0.81
hy	0.50	0.82	1.05	6.30	0.56	1.35	1.78
mt	0.16	0.23	0.35	1.24	0.17	0.32	0.41
il	0.17	0.19	0.27	0.73	0.15	0.23	0.29
ap	0.09	0.09	0.07	0.35	0.05	0.07	0.16

LAKE HILL - VOLCANIC CLASTS

Sample	24472	24473	24474	24476	24477	24478	24480
SiO_2	68.61	75.00	71.29	70.11	70.44	80.77	76.57
TiO_2	0.35	0.32	0.27	0.38	0.45	0.27	0.19
Al_2O_3	15.48	12.45	14.44	14.74	14.32	9.21	11.72
Fe_2O_3	3.09	2.15	1.99	2.99	3.08	2.04	1.40
MnO	0.07	0.03	0.05	0.05	0.04	0.02	0.02
MgO	1.43	0.36	0.46	0.68	0.69	0.13	0.12
CaO	2.44	0.71	1.33	1.55	1.24	1.03	0.45
Na_2O	4.46	3.40	3.95	4.77	3.77	2.34	3.56
K_2O	2.89	4.29	4.00	2.50	4.32	1.73	4.48
P_2O_5	0.18	0.08	0.08	0.10	0.13	0.35	0.05
LOI	1.44	0.79	1.56	1.25	1.05	1.07	0.92
Total	100.44	99.58	99.42	99.12	99.53	98.96	99.48
V	68	30	25	31	43	19	25
Cr	88	9	6	7	12	9	6
Ni	22	9	6	6	10	7	7
Zn	45	36	27	47	45	50	40
Ga	21	16	19	19	19	16	17
Rb	62	180	156	92	173	109	133
Sr	637	93	299	327	220	139	155
Y	13	35	22	25	39	52	23
Zr	99	172	160	136	244	168	94
Nb	8	12	12	11	13	10	14
Ba	825	529	780	802	656	570	566
La	19	35	39	34	42	47	23
Ce	45	78	80	79	92	89	64
Nd	19	34	30	33	40	44	27
Pb	29	23	10	15	20	27	17
Th	4	26	18	21	27	17	15
SiO_2	69.30	75.92	72.85	71.64	71.53	82.51	77.69
TiO_2	0.35	0.32	0.28	0.39	0.46	0.28	0.19
Al_2O_3	15.64	12.60	14.76	15.06	14.54	9.41	11.89
Fe_2O_3	3.12	2.18	2.03	3.06	3.13	2.08	1.42
MnO	0.07	0.03	0.05	0.05	0.04	0.02	0.02
MgO	1.44	0.36	0.47	0.69	0.70	0.13	0.12
CaO	2.46	0.72	1.36	1.58	1.26	1.05	0.46
Na_2O	4.51	3.44	4.04	4.87	3.83	2.39	3.61
K_2O	2.92	4.34	4.09	2.55	4.39	1.77	4.55
P_2O_5	0.18	0.08	0.08	0.10	0.13	0.36	0.05
Total	100.00	100.00	100.00	100.00	100.00	100.00	100.00
Q	23.69	36.58	29.52	28.13	27.89	59.58	37.70
or	17.25	25.66	24.16	15.10	25.92	10.44	26.86
ab	38.12	29.12	34.16	41.24	32.39	20.23	30.56
an	11.04	3.04	6.21	7.19	5.38	2.88	1.93
C	1.02	1.13	1.42	1.64	1.52	2.51	0.32
hy	6.48	2.75	2.98	4.45	4.41	2.14	1.54
mt	1.07	0.74	0.70	1.05	1.07	0.71	0.49
il	0.67	0.62	0.52	0.74	0.87	0.52	0.37
ap	0.42	0.19	0.19	0.24	0.31	0.83	0.12

BOUNTY ISLANDS

Sample	24099	24100	24101	24102	24103	24104	24105	24106
SiO_2	73.87	73.69	54.00	76.42	70.64	74.55	73.91	75.07
TiO_2	0.20	0.26	0.81	0.10	0.37	0.16	0.21	0.22
Al_2O_3	14.17	14.12	15.39	12.76	14.73	14.31	13.87	13.97
Fe_2O_3	1.60	2.01	7.40	0.51	2.60	1.26	1.53	1.58
MnO	0.03	0.04	0.16	0.01	0.03	0.01	0.03	0.03
MgO	0.27	0.36	7.15	0.05	0.79	0.20	0.30	0.22
CaO	1.57	1.58	6.39	0.43	2.40	1.45	1.27	1.39
Na_2O	3.90	3.74	2.92	3.42	3.78	3.99	3.63	3.86
K_2O	3.89	3.87	2.15	5.31	3.60	3.68	4.30	3.86
P_2O_5	0.08	0.09	0.19	0.03	0.13	0.06	0.13	0.11
LOI	0.44	0.46	3.71	0.34	0.14	0.34	0.67	-0.16
Total	100.02	100.22	100.27	99.38	99.21	100.01	99.85	100.15
V	21	23	190	17	45	22	22	23
Cr	6	3	259	3	8	6	8	6
Ni	3	7	71	6	3	3	3	3
Zn	31	34	68	56	41	25	31	34
Ga	21	23	19	25	18	20	21	21
Rb	165	170	153	188	152	158	197	172
Sr	182	156	173	71	191	166	151	154
Y	20	22	13	35	20	23	20	21
Zr	123	124	130	72	138	109	111	128
Nb	13	12	7	15	13	12	12	11
Ba	678	534	1050	289	622	597	623	599
La	30	26	15	8	24	26	15	31
Ce	52	57	31	19	48	53	25	51
Nd	54	33	35	16	46	49	30	44
Pb	19	38	23	29	23	36	31	32
Th	14	23	18	29	19	20	14	19
SiO_2	74.18	73.87	55.92	77.16	71.30	74.80	74.52	74.84
TiO_2	0.20	0.26	0.84	0.10	0.37	0.16	0.21	0.22
Al_2O_3	14.23	14.15	15.94	12.88	14.87	14.36	13.98	13.93
Fe_2O_3	1.61	2.01	7.66	0.51	2.62	1.26	1.54	1.58
MnO	0.03	0.04	0.17	0.01	0.03	0.01	0.03	0.03
MgO	0.27	0.36	7.40	0.05	0.80	0.20	0.30	0.22
CaO	1.58	1.58	6.62	0.43	2.42	1.45	1.28	1.39
Na_2O	3.92	3.75	3.02	3.45	3.82	4.00	3.66	3.85
K_2O	3.91	3.88	2.23	5.36	3.63	3.69	4.34	3.85
P_2O_5	0.08	0.09	0.20	0.03	0.13	0.06	0.13	0.11
Total	100.00	100.00	100.00	100.00	100.00	100.00	100.00	100.00
Q	32.24	32.72	3.69	35.45	28.17	33.63	33.20	34.11
or	23.09	22.93	13.16	31.69	21.47	21.82	25.62	22.74
ab	33.14	31.72	25.59	29.22	32.29	33.87	30.97	32.56
an	7.30	7.27	23.34	1.96	11.16	6.82	5.50	6.16
C	0.88	1.12	0.00	0.68	0.57	1.27	1.26	1.17
di	0.00	0.00	6.60	0.00	0.00	0.00	0.00	0.00
hy	2.12	2.69	22.37	0.53	4.23	1.60	2.11	1.92
mt	0.55	0.69	2.62	0.18	0.90	0.43	0.53	0.54
il	0.38	0.49	1.59	0.19	0.71	0.30	0.40	0.42
ap	0.19	0.21	0.46	0.07	0.30	0.14	0.30	0.25

Sample	24107	24108	24109	24110
SiO_2	73.38	74.86	72.62	73.83
TiO_2	0.20	0.26	0.26	0.19
Al_2O_3	14.57	14.11	14.59	13.64
Fe_2O_3	1.73	1.12	1.73	1.44
MnO	0.03	0.02	0.03	0.03
MgO	0.31	0.18	0.34	0.27
CaO	1.54	1.26	1.54	1.16
Na_2O	4.05	3.66	3.69	3.64
K_2O	3.81	3.87	4.00	3.82
P_2O_5	0.11	0.10	0.05	0.11
LOI	0.43	0.33	0.31	1.16
Total	100.16	99.77	99.16	99.29
V	23	25	27	23
Cr	8	9	9	3
Ni	3	3	3	6
Zn	37	36	34	30
Ga	21	24	19	19
Rb	168	154	156	167
Sr	181	171	190	163
Y	18	17	21	19
Zr	126	119	127	125
Nb	15	13	13	9
Ba	619	694	760	601
La	22	24	31	23
Ce	34	44	50	46
Nd	34	37	29	26
Pb	22	25	24	30
Th	16	19	19	16
SiO_2	73.58	75.28	73.46	75.24
TiO_2	0.20	0.26	0.26	0.19
Al_2O_3	14.61	14.19	14.76	13.90
Fe_2O_3	1.73	1.13	1.75	1.47
MnO	0.03	0.02	0.03	0.03
MgO	0.31	0.18	0.34	0.28
CaO	1.54	1.27	1.56	1.18
Na_2O	4.06	3.68	3.73	3.71
K_2O	3.82	3.89	4.05	3.89
P_2O_5	0.11	0.10	0.05	0.11
Total	100.00	100.00	100.00	100.00
Q	31.16	35.91	31.88	35.54
or	22.58	23.00	23.91	23.01
ab	34.36	31.14	31.59	31.39
an	6.94	5.63	7.40	5.13
C	1.25	1.86	1.53	1.70
hy	2.35	1.26	2.35	1.99
mt	0.59	0.39	0.60	0.50
il	0.38	0.50	0.50	0.37
ap	0.26	0.23	0.12	0.26

WESTERN PROVINCE GRANITOIDS

Sample	RNZ20	RNZ120	RNZ119	JS83
SiO_2	68.25	72.73	73.29	72.23
TiO_2	0.35	0.31	0.11	0.27
Al_2O_3	16.18	14.54	15.12	14.19
Fe_2O_3	1.63	1.42	0.86	2.24
FeO	0.63	0.55	0.33	0.86
MnO	0.03	0.02	0.03	0.04
MgO	0.58	0.52	0.14	0.19
CaO	2.33	0.96	0.95	1.19
Na_2O	5.77	2.88	4.25	3.08
K_2O	2.58	5.31	4.05	4.81
P_2O_5	0.20	0.25	0.07	0.30
Total	98.53	99.49	99.20	99.40
LOI	0.54	0.80	0.56	0.65
Mg #	33.02	33.66	18.39	10.52
Cr	7	13	7	9
Ni	3	7	3	4
V	32	16	13	6
Pb	18	28	28	28
Zn	50	67	46	96
Rb	77	323	166	223
Ba	880	356	1054	376
Sr	1082	84	453	82
Ga	19	25	19	22
Nb	8	13	7	42
Zr	130	140	95	379
Y	8	21	16	31
Th	8	23	8	9
La	19	27	27	48
Ce	40	75	43	121
Nd	20	39	23	53
Density	2.35	2.33	2.32	2.34

Cape Foulwind Granite = JS83
O'Sullivans Granite = RNZ120
Separation Point Granite = RNZ20
Bucklands Granite = RNZ119

APPENDIX 2 ANALYTICAL PRECISION

Estimate of XRF precision for all elements expressed as the standard deviation: (Weaver et al.,1990)(S.D. Weaver, pers.comm.)

Oxide(wt%)/ Element (ppm)	Standard Deviation
SiO_2	0.210
TiO_2	0.004
Al_2O_3	0.078
Fe_2O_3	0.036
MnO	0.018
MgO	0.020
CaO	0.005
Na_2O	0.074
K_2O	0.033
P_2O_5	0.007
LOI	0.105
V	1.1
Cr	0.8
Ni	1.1
Zn	4.7
Ga	0.9
Rb	1.6
Sr	0.5
Y	2.7
Zr	10
Nb	1.0
Ba	20
La	2.5
Ce	4.0
Nd	4.0
Pb	1.7
Th	2.5

XRF detection limits for major and trace element determinations:

MAJOR ELEMENTS	
Oxides	**%**
SiO_2	0.2
TiO_2	0.01
Al_2O_3	0.2
Fe_2O_3	0.01
MnO	0.01
MgO	0.05
CaO	0.01
Na_2O	0.1
K_2O	0.01
P_2O_5	0.01

TRACE ELEMENTS	
Element	**ppm**
V	3
Cr	3
Ni	3
Zn	3
Zr	2
Nb	2
Ba	20
La	5
Ce	5
Nd	10
Ga	2
Pb	1
Rb	1
Sr	1
Th	1
Y	1

APPENDIX 3 RECALCULATED MODAL ANALYSES FOR GRANITOID SAMPLES FROM POINT COUNT DATA

Chatham Islands					
Modal Analyses %					
Field No.	Lab.No.	Quartz	Plag	Kspar	P:K
WB1	23984	25.8	9.0	65.2	13:87
WB2	23985	31.0	14.9	54.1	22:78
WB3	23986	37.2	12.5	50.3	20:80
WB4	23987	26.4	15.1	58.5	21:79
WB5	23988	46.1	7.8	46.1	15:85
WB6	23989	50.4	23.2	26.4	47:53
WB7	23990	40.0	18.7	40.5	32:68
WB8	23991	27.0	8.3	64.7	12:88
WB9	23992	37.8	13.3	48.9	22:78
WB10	23993	30.8	13.7	55.5	19:81
WB11	23994	54.1	8.6	37.3	19:81
WB12	23995	43.6	8.6	47.8	15:85
WB13	24085	32.1	12.9	55.0	19:81
WB14	23996	31.4	21.6	47.0	32:68
WB15	23997	28.0	19.2	52.8	27:73
WB16	23998	36.8	12.4	50.8	20:80
WB17	23999	38.1	12.0	49.9	20:80
WB18	24000	41.1	18.7	40.2	32:68
WB23	24005	43.4	23.0	33.6	40:60
WB24	24006	36.2	18.7	45.1	30:70
WB27	24007	44.9	21.4	33.6	39:61
WB28	24008	48.2	29.8	22.0	58:42
WB29	24009	34.3	20.7	45.0	30:70
PD1	24010	24.6	21.8	53.5	29:71
PD2	24011	42.8	14.0	43.2	25:75
PD3	24012	30.2	33.8	36.0	48:52
PD4	24013	47.6	14.8	37.6	28:72
PD5	24014	19.9	17.7	62.4	22:78
PD6	24015	34.5	13.9	51.5	22:78
PD7	24016	42.0	12.7	45.3	22:78
PD8	24017	58.5	0	41.5	100:1
PD9	24018	48.1	8.7	42.9	17:83
PD10	24019	41.7	21.5	36.7	36:64
PD11	24020	35.9	23.3	40.8	36:64
PD12	24021	38.0	20.7	41.3	34:66
PD13	24022	38.2	21.6	40.2	34:66
PD14	24086	40.2	39.8	20.0	66:34
PD15	24023	37.6	41.8	20.6	67:33
PD16	24024	49.4	33.0	17.6	66:34
PD17	24025	43.4	28.5	28.1	50:50
PD18	24026	27.6	34.0	38.4	53:47
PD25	24033	45.3	24.9	29.8	54:46

Ethelton					
Modal Analyses %					
Field No.	Lab.No.	Quartz	Plag	Kspar	P:K
ETH1	24034	53.0	12.9	34.1	27:73
ETH2	24035	33.1	25.2	41.6	37:63
ETH3	24036	25.3	48.7	26.0	66:34
ETH4	24037	31.4	35.8	32.6	52:48
ETH5	24038	21.5	43.8	34.7	55:45
ETH7	24040	32.1	45.8	22.1	67:33
ETH8	24041	42.1	17.0	40.9	29:71
ETH9	24042	35.2	21.1	43.7	32:68
ETH10	24043	34.5	35.8	29.6	54:46
ETH11	24044	41.5	13.9	45.3	24:76
ETH12	24045	34.2	37.5	28.2	56:44
ETH13	24046	32.5	50.1	17.3	74:26
ETH14	24047	40.2	8.4	51.4	86:14
ETH15	24048	31.2	50.9	17.8	74:26
ETH16	24049	26.1	54.7	19.2	74:26
ETH20	24053	29.2	55.2	15.6	78:22
ETH22	24055	39.5	41.0	19.5	67:33
ETH23	24056	47.1	28.2	24.7	53:47
ETH24	24057	56.1	17.7	26.2	41:59
ETH26	24059	39.0	26.3	34.7	43:57
ETH44	24077	43.4	46.6	10.0	82:18
ETH45	24078	38.5	45.3	16.0	73:27
ETH46	24079	42.8	44.3	12.8	77:23
ETH47	24080	38.2	43.8	18.0	70:30
ETH48	24081	39.0	47.9	13.1	78:22
ETH49	24082	48.5	37.8	13.7	73:27

Mount Saul					
Modal Analyses %					
Field No.	Lab.No.	Quartz	Plag	Kspar	P:K
MS3	24397	34.2	16.6	49.2	25:75
MS4	24398	31.9	40.6	27.5	59:41
MS5	24399	25.1	55.3	19.6	74:26
MS6	24400	34.7	21.8	43.5	33:67
MS7	24401	39.6	28.7	31.7	47:53
MS8	24402	40.2	38.5	21.2	64:36
MS9	24403	41.0	35.0	24.0	59:41
MS10	24404	25.8	37.6	36.6	50:50
MS11	24405	52.4	22.2	25.4	46:54
MS12	24406	39.2	43.8	17.0	72:28
MS13	24407	34.9	24.6	40.4	38:62
MS14	24408	33.2	42.0	24.8	63:37
MS34	24428	34.0	38.2	27.8	58:42
MS37	24431	20.6	34.0	45.4	42:58
MS38	24432	24.5	50.1	25.3	66:34
MS39	24433	33.5	18.7	47.7	28:72
MS41	24435	45.2	20.1	34.6	36:64
MS42	24436	40.4	35.4	24.1	59:41
MS43	24437	34.3	27.3	38.3	58:42
MS44	24438	39.4	28.7	31.8	47:53

Lake Hill					
Modal Analyses %					
Field No.	Lab.No.	Quartz	Plag	Kspar	P:K
LH1	24445	33.9	58.8	7.3	89:11
LH2	24446	34.7	28.6	36.7	43:57
LH3	24447	38.7	30.8	30.5	50:50
LH4	24448	29.3	65.2	5.5	92:8
LH5	24449	39.6	41.6	18.8	69:31
LH6	24450	38.7	45.9	15.4	74:26
LH7	24451	42.6	42.4	15.0	74:26
LH8	24452	46.0	53.0	0.0	100:1
LH9	24453	36.7	48.0	15.3	76:24
LH10	24454	50.1	49.0	0.0	100:1
LH11	24455	43.6	37.4	19.0	66:34
LH12	24456	30.1	68.3	1.6	97:3
LH13	24457	37.2	42.5	20.3	68:32
LH14	24458	26.8	61.4	11.8	84:16
LH15	24459	40.5	48.0	11.4	80:20
LH16	24460	44.6	37.5	17.9	68:32
LH17	24461	37.0	44.0	19.0	70:30
LH18	24462	26.4	44.7	28.8	60:40
LH19	24463	39.1	31.1	29.7	51:49
LH20	24464	37.4	48.2	14.3	77:23
LH21	24465	35.5	51.5	13.0	80:20
LH22	24466	35.6	43.0	21.4	67:33
LH23	24467	39.0	52.9	8.1	87:13
LH24	24468	38.8	39.1	22.1	64:36
LH25	24469	36.7	35.3	28.0	55:45
LH26	24470	30.9	33.3	35.7	48:52
LH27	24471	34.6	34.8	30.6	53:47
LH31	24475	38.3	50.3	11.4	81:19
LH35	24479	37.6	27.3	35.1	43:57
LH38	24482	46.8	42.7	10.5	80:20
LH39	24483	28.2	41.0	30.8	57:43
LH40	24484	41.7	48.1	10.2	82:18
LH41	24485	37.6	42.8	19.5	69:31
LH42	24486	32.2	54.6	13.2	80:20
LH43	24487	51.6	29.0	19.2	60:40
LH44	24488	41.1	42.7	16.2	72:28
LH45	24489	27.1	42.1	30.8	58:42
LH46	24490	42.6	43.2	14.2	75:25
LH47	24491	51.6	41.2	7.2	85:15

APPENDIX 4 TERMINOLOGY, ABBREVIATIONS AND MISCELLANEOUS INFORMATION

Key to Geochemical Diagrams	
▲	Waihere Bay Granitoid
△	Waihere Bay Volcanic
▼	Parran Dam Granitoid
▽	Parran Dam Volcanic
■	Ethelton Granitoid
□	Ethelton Volcanic
●	Mount Saul Granitoid
○	Mount Saul Volcanic
♦	Lake Hill Granitoid
◊	Lake Hill Volcanic
✳	Bounty Islands

Group Abbreviations	
CIG	Chatham Island Granitoid
CIV	Chatham Island Volcanic
ETHG	Ethelton Granitoid
ETHV	Ethelton Volcanic
MSG	Mount Saul Granitoid
MSV	Mount Saul Volcanic
LHG	Lake Hill Granitoid
LHV	Lake Hill Volcanic

Size Determinations (petrographic descriptions)

Coarse = >2.5mm

Medium = 1.0 - 2.5mm

Fine = <1.0mm

Alkali-Lime Index

The alkali-lime index represents the silica value (wt%) where log Na_2O + K_2O/CaO (wt%) equals 0 (after Peacock,1931 with modifications by Brown,1982 and Maniar and Piccoli,1989).

SiO_2 (wt%)	Alkali-lime Index
<51.0	Alkalic
51.0 - 56.0	Alkali-calcic
56.0 - 61.0	Calc-alkalic
>61.0	Calcic

Thin Section Symbols

q = quartz	amp = amphibole
k = alkali feldspar	b = biotite
p = plagioclase	cl = chlorite
ep = epidote	z = zircon
mu = muscovite	g = garnet
sp = spherulites	t = tourmaline

APPENDIX 5 ALUMINIUM SATURATION INDICES

All ratios are molar ratios with;

A/CNK = $Al_2O_3/CaO+Na_2O+K_2O$ (standard index applied, abbreviated to ASI)

A/NK = Al_2O_3/Na_2O+K_2O (used to supplement initial evaluation)

peraluminous: A/CNK >1.0

metaluminous: A/CNK <1.0 and A/NK >1.0

peralkaline: A/CNK and A/NK <1.0

ASI values are sensitive to hydrothermal alteration. The destruction or alteration of feldspars can occur due to a mobilization of Na^+, K^+ and Ca^+ with modification and consequent changes in ASI. The freshest samples were chosen to lessen this effect.

Chatham Islands			
Field No.	Lab No.	A/CNK	A/NK
WB1	23984	1.0538	1.1943
WB2	23985	1.0548	1.3258
WB3	23986	1.0455	1.1578
WB4	23987	1.0656	1.2420
WB5	23988	1.0536	1.1351
WB6	23989	1.0304	1.1777
WB7	23990	0.9718	1.0772
WB8	23991	1.0322	1.1234
WB9	23992	1.0312	1.1272
WB10	23993	1.0584	1.2243
WB11	23994	1.6148	1.9356
WB12	23995	1.0545	1.1900
WB13	24085	0.9707	1.1328
WB14	23996	1.0721	1.2802
WB15	23997	0.9316	1.2897
WB16	23998	1.0293	1.0977
WB17	23999	1.0309	1.2154
WB18	24000	1.0591	1.4972
WB19	24001	1.0494	1.1286
WB20	24002	1.1194	1.2399
WB21	24003	1.0260	1.0846
WB22	24004	1.1085	1.4956
WB23	24005	1.0391	1.2305
WB24	24006	1.0540	1.2307
WB27	24007	1.0457	1.3263
WB28	24008	0.9996	1.0241
WB29	24009	1.0457	1.3263
PD1	24010	1.1076	1.2355
PD2	24011	1.0517	1.3900
PD3	24012	1.0131	1.0434
PD4	24013	0.8786	1.2573
PD5	24014	1.0409	1.0672
PD6	24015	1.0134	1.1326
PD7	24016	1.0613	1.1958
PD8	24017	1.0124	1.0216
PD9	24018	1.0289	1.0536
PD10	24019	1.0395	1.1095
PD11	24020	1.0238	1.1325
PD12	24021	1.1089	1.2120
PD13	24022	1.1770	1.2210
PD14	24086	1.0304	1.1002
PD15	24023	1.1778	1.2211
PD16	24024	1.1240	1.1923
PD17	24025	1.0934	1.1426
PD18	24026	1.1026	1.2072
PD19	24027	1.3198	1.3473
PD20	24028	1.1113	1.3966
PD21	24029	1.0525	1.1832
PD22	24030	1.0979	1.1538
PD23	24031	1.0587	1.0763
PD24	24032	1.0667	1.2677
PD25	24033	1.0666	1.2675

Ethelton			
Field No.	Lab No.	A/CNK	A/NK
ETH1	24034	0.9786	1.0601
ETH2	34035	0.9883	1.1210
ETH3	24036	0.9247	1.4438
ETH4	24037	1.0296	1.1178
ETH5	24038	0.9826	1.4200
ETH6	24039	0.9787	1.1491
ETH7	24040	0.8879	1.3045
ETH8	24041	0.9809	1.0638
ETH9	24042	1.1267	1.2852
ETH10	24043	1.0180	1.3116
ETH11	24044	0.9162	1.0337
ETH12	24045	0.9418	1.3444
ETH13	24046	0.8462	1.3703
ETH14	24047	0.7929	1.0608
ETH15	24048	1.0390	1.1992
ETH16	24049	1.0343	1.3727
ETH17	24050	1.0125	1.3329
ETH18	24051	1.0506	1.3816
ETH19	24052	1.0272	1.4370
ETH20	24053	1.0875	1.4273
ETH21	24054	0.9280	1.3750
ETH22	24055	1.1609	1.2981
ETH23	24056	0.7958	1.0953
ETH24	24057	1.0209	1.1527
ETH25	24058	1.0619	1.2769
ETH26	24059	0.9932	1.1716
ETH27	24060	1.0717	1.4230
ETH28	24061	1.0755	1.4108
ETH29	24062	0.9721	1.2209
ETH30	24063	1.0849	1.4387
ETH31	24064	0.9808	1.3724
ETH32	24065	1.0379	1.2866
ETH33	24066	1.0132	1.1374
ETH34	24067	1.0583	1.2729
ETH35	24068	1.0047	1.6232
ETH36	24069	0.8769	1.1840
ETH37	24070	1.0170	1.1018
ETH38	24071	1.0573	1.3202
ETH39	24072	0.9955	1.0357
ETH40	24073	1.0696	1.1180
ETH41	24074	0.9467	1.1216
ETH42	24075	1.0307	1.2699
ETH43	24076	1.0662	1.2441
ETH44	24077	1.0731	1.1871
ETH45	24078	1.0835	1.2999
ETH46	24079	0.8513	1.3058
ETH47	24080	1.0062	1.2024
ETH48	24081	1.0687	1.3867
ETH49	24082	1.0021	1.1443
ETH50	24083	1.0525	1.4253

Mount Saul			
Field No.	Lab No.	A/CNK	A/NK
MS1	24395	0.8672	1.2698
MS2	24396	1.0455	1.4410
MS3	24397	0.9312	1.3016
MS4	24398	0.9927	1.3056
MS5	24399	1.0504	1.2200
MS6	24400	1.0364	1.1077
MS7	24401	1.0330	1.0734
MS8	24402	1.0572	1.2048
MS9	24403	1.0542	1.1849
MS10	24404	0.8354	1.1220
MS11	24405	1.0060	1.0829
MS12	24406	1.0572	1.1572
MS13	24407	0.9986	1.1130
MS14	24408	1.0639	1.2395
MS15	24409	1.0078	1.1478
MS16	24410	1.0069	1.2318
MS17	24411	1.0080	1.1823
MS18	24412	1.0308	1.2033
MS19	24413	0.9663	1.3474
MS20	24414	0.9787	1.3580
MS21	24415	0.9794	1.1598
MS22	24416	1.0164	1.0316
MS23	24417	0.9282	0.9470
MS24	24418	1.0390	1.1392
MS25	24419	1.0347	1.0498
MS26	24420	1.0659	1.2212
MS27	24421	0.9936	1.0035
MS28	24422	1.0339	1.1634
MS29	24423	1.1850	1.2609
MS30	24424	0.9115	1.2741
MS31	24425	0.9927	1.0278
MS32	24426	1.0123	1.0564
MS33	24427	1.1751	1.2318
MS34	24428	1.0244	1.2283
MS35	24429	0.9794	1.0090
MS36	24430	1.1694	1.2016
MS37	24431	1.0049	1.1405
MS38	24432	1.0319	1.3315
MS39	24433	1.0106	1.0703
MS40	24434	0.9909	1.0591
MS41	24435	1.0266	1.0887
MS42	24436	1.0793	1.2730
MS43	24437	1.0611	1.1928
MS44	24438	0.7406	1.2203
MS45	24439	1.0137	1.0531
MS46	24440	0.9071	1.5111
MS47	24441	0.9988	1.0608
MS48	24442	1.0010	1.0615
MS49	24443	0.9931	1.1506

Lake Hill			
Field No.	Lab No.	A/CNK	A/NK
LH1	24445	1.0972	1.3570
LH2	24446	1.0650	1.1742
LH3	24447	1.0077	1.1508
LH4	24448	1.0775	1.4908
LH5	24449	1.0654	1.3934
LH6	24450	1.0852	1.3580
LH7	24451	1.1036	1.4147
LH8	24452	1.1639	1.7825
LH9	24453	1.1593	1.4718
LH10	24454	1.2107	1.5043
LH11	24455	1.0596	1.1498
LH12	24456	1.0874	1.3966
LH13	24457	1.0753	1.2310
LH14	24458	1.1526	1.3293
LH15	24459	1.0539	1.2324
LH16	24460	1.1046	1.3953
LH17	24461	1.0879	1.1404
LH18	24462	1.0877	1.4376
LH19	24463	1.0356	1.1189
LH20	24464	1.0740	1.3159
LH21	24465	1.0796	1.5250
LH22	24466	1.0375	1.2434
LH23	24467	1.0427	1.2318
LH24	24468	1.1396	1.1713
LH25	24469	1.0703	1.2194
LH26	24470	1.0546	1.2085
LH27	24471	1.0601	1.2043
LH28	24472	1.0388	1.4792
LH29	24473	1.0800	1.2162
LH30	24474	1.0902	1.3336
LH31	24475	1.0901	1.2873
LH32	24476	1.1024	1.3968
LH33	24477	1.0905	1.3165
LH34	24478	1.2127	1.6096
LH35	24479	1.0852	1.1283
LH36	24480	1.0170	1.0948
LH38	24482	0.9994	1.1916
LH39	24483	1.0642	1.2591
LH40	24484	1.0626	1.3227
LH41	24485	1.0387	1.2278
LH42	24486	1.0556	1.2355
LH43	24487	1.0164	1.2062
LH44	24488	1.0546	1.8788
LH45	24489	1.0708	1.2667
LH46	24490	1.0577	1.3029
LH47	24491	1.0499	1.2866

APPENDIX 6 MICROPROBE ANALYSES

Mineral analyses were carried out using a JEOL Superprobe JXA-8600 electron probe micro-analyzer at the Geology Department, University of Otago. Probe current was 2.0 x 10^{-8}A, with an electron gun accelerating voltage of 15kV. Probe diameter was $< 5\mu$m. A 2AF correction programme was used, developed by Y. Kawachi and M.W. Trinder at Otago University.

The optical properties of the mineral analyzed were equivocal and indicated that it was either allanite, katophorite or astrophyllite. Microprobe analyses discounted katophorite and astrophyllite. Although not a perfect match, the most likely mineral is allanite, probably with a high trace element content.

	MS1	MS1[3]	H12[4]	H12[1]	MS1[2]
SiO2	28.50	28.75	27.84	28.94	28.50
TiO2	2.28	1.90	2.21	1.89	2.28
Al2O3	9.98	10.52	9.91	11.32	9.98
Fe2O3	-	-	-	-	-
FeO	18.09	18.25	17.82	13.72	18.09
MnO	0.29	0.40	0.29	0.50	0.29
MgO	0.97	0.83	0.87	0.63	0.97
CaO	9.13	9.57	9.23	9.18	9.13
Na2O	-	-	-	0.16	-
K2O	0.02	0.02	0.01	0.08	0.02
P2O5	-	-	-	-	-
H2O+	-	-	-	-	-
H2O-	-	-	-	-	-
Cr2O3	-	-	-	-	-